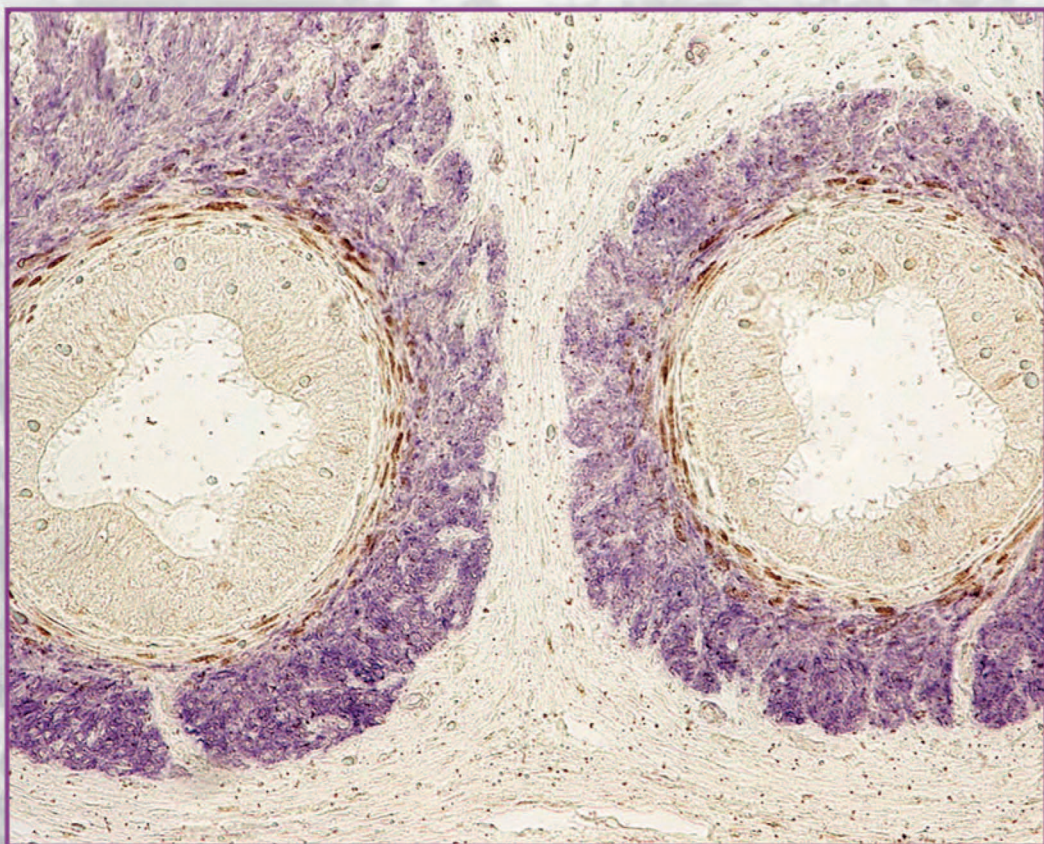


Acta Morphologica et Anthropologica 32 (1-2)



Prof. Marin Drinov Publishing House
of Bulgarian Academy of Sciences

Acta Morphologica et Anthropologica

is the continuation of Acta cytobiologica et morphologica

Indexed in:



WEB OF SCIENCE



Editorial Correspondence

Institute of Experimental Morphology, Pathology and Anthropology with Museum
Bulgarian Academy of Sciences
Acta Morphologica et Anthropologica
Acad. Georgi Bonchev Str., Bl. 25
1113 Sofia, Bulgaria

E-mail: ama.journal@iempam.bas.bg; yordanka.gluhcheva@iempam.bas.bg;
ygluhcheva@hotmail.com

Tel.: +359 2 979 2344

Издаването на настоящия том 32, книжки 1 и 2 е осъществено с финансовата подкрепа на Фонд „Научни изследвания“ по Договор КП-06-НП6/16 от 02.12.2024 г. Фонд „Научни изследвания“ не носи отговорност за съдържанието на материалите

©БАН, Bulgarian Academy of Sciences, Institute of Experimental Morphology, Pathology and Anthropology with Museum, 2025

Prof. Marin Drinov Publishing House of Bulgarian Academy of Sciences
Bulgaria, 1113 Sofia, Acad. Georgi Bonchev Str., Bl. 6

Graphic designer: Veronika Tomcheva.
Format 70×100/16 Printed sheets 10,50

Printing Office of Prof. Marin Drinov Publishing House of Bulgarian Academy of Sciences
Bulgaria, 1113 Sofia, Acad. Georgi Bonchev Str., Bl. 5

Acta Morphologica et Anthropologica

Editorial Board

Editor-in-Chief: Prof. Nina Atanassova (Institute of Experimental Morphology, Pathology and Anthropology with Museum, Bulgarian Academy of Sciences, Sofia, Bulgaria)
e-mail: ninaatanassova@bas.bg; ninaatanassova@yahoo.com
+359 2 979 2342

Deputy Editor-in-Chief: Prof. Dimitar Kadiysky (Institute of Experimental Morphology, Pathology and Anthropology with Museum, Bulgarian Academy of Sciences, Sofia, Bulgaria)
e-mail: dimkad@bas.bg; dkadiysky@yahoo.com
+359 2 979 2340

Managing Editor: Assoc. Prof. Yordanka Gluhcheva (Institute of Experimental Morphology, Pathology and Anthropology with Museum, Bulgarian Academy of Sciences, Sofia, Bulgaria)
e-mail: yordanka.gluhcheva@iempam.bas.bg; ygluhcheva@hotmail.com
+359 2 979 2344

Web Management: Assoc. Prof. Ivelin Vladov (Institute of Experimental Morphology, Pathology and Anthropology with Museum, Bulgarian Academy of Sciences, Sofia, Bulgaria)
e-mail: ivelin.vladov@iempam.bas.bg; iepparazit@yahoo.com
+359 2 979 2326

Members

Prof. Doychin Angelov (Center of Anatomy, University of Cologne, Germany)

Prof. Radostina Alexandrova (Institute of Experimental Morphology, Pathology and Anthropology with Museum, Bulgarian Academy of Sciences, Sofia, Bulgaria)

Prof. Osama Azmy (National Research Centre, Cairo, Egypt)

Prof. Barbara Bilinska (Jagiellonian University, Krakow, Poland)

Prof. Alexandra Buzhilova (Research Institute and Museum of Anthropology, Moscow State University, Russia)

Assoc. Prof. Alexandra Comsa („Vasile Pârvan” Institute of Archaeology, Romanian Academy, Bucharest, Romania)

Assoc. Prof. Natasha Davceva (Institute of Forensic Medicine and Criminalistics, Ss. Cyril and Methodius University, Scopje, North Macedonia)

Prof. Valentin Djonov (Institute of Anatomy, University of Bern, Switzerland)

Prof. Mashenka Dimitrova ((Institute of Experimental Morphology, Pathology and Anthropology with Museum, Bulgarian Academy of Sciences, Sofia, Bulgaria)

Prof. Milena Fini (Rizzoli Orthopedic Institute, Bologna, Italy)

Prof. Mary Gantcheva ((Institute of Experimental Morphology, Pathology and Anthropology with Museum, Bulgarian Academy of Sciences, Sofia, Bulgaria)

Prof. Volodia Georgiev (Department of Biology, Manhattanville College, New York, USA)

Prof. Elena Godina (Research Institute and Museum of Anthropology, Moscow State University, Russia)

Assoc. Prof. Manana Kakabadze („Alexandre Natishvili“ Institute of Morphology, Tbilisi State University, Georgia)

Acad. Vladimir Kolchitsky (Institute of Physiology, National Academy of Sciences, Minsk, Belarus)

Prof. Dimitri Kordzaia („Ivane Javakhishvili“ Tbilisi State University, Georgia)

Prof. Nikolai Lazarov (Medical University Sofia, Bulgaria)

Prof. Tsvetanka Marinova (Faculty of Medicine, Sofia University “St. Kliment Ohridski”, Bulgaria)

Prof. Ralf Middendorff (Institute of Anatomy and Cell Biology, Justus Liebig University, Gießen, Germany)

Prof. Modra Murovska (Institute of Microbiology and Virology, Riga Stradins University, Latvia)

Acad. Wladimir Ovtscharoff (Medical University Sofia, Bulgaria)

Prof. Svetlozara Petkova ((Institute of Experimental Morphology, Pathology and Anthropology with Museum, Bulgarian Academy of Sciences, Sofia, Bulgaria)

Assoc. Prof. Marina Quartu (University of Cagliari, Monserrato, Italy)

Prof. Gorana Rancic (School of Medicine, University of Niš, Serbia)

Prof. Stefan Sivkov (Medical University Plovdiv, Bulgaria)

Assoc. Prof. Racho Stoev ((Institute of Experimental Morphology, Pathology and Anthropology with Museum, Bulgarian Academy of Sciences, Sofia, Bulgaria)

Assoc. Prof. Katja Teerds (Wageningen University, Netherlands)

Prof. Angel Vodenicharov (Faculty of Veterinary Medicine, Trakia University, Stara Zagora, Bulgaria)

C o n t e n t s

MORPHOLOGY 32 (1)

Original Articles

O. K. Ijomone, O. M. Ijomone – Region- and Sex-specific Differences of Brain Parvalbumin Distribution and Expression in Rats	5
T. Kirov, V. Ivanova, T. Dikov, R. Todorov, L. Malinova – Histopathological Changes in the Enteric Nervous System of Patients Undergoing Surgical Treatment for Intestinal Pseudo-Obstruction	14
R. Spasov, D. Stoyanov, I. Ivanov, A. B. Tonchev – Histomorphological Evaluation of Medio-Lateral Asymmetry in the Adult Murine Cerebellar Cortex	22
N. Genov, N. Dimitrov, D. Atanasova – Aging of the Myenteric Plexus in the Rat Colorectal Region	31
A. Ilvaska, Y. Gluhcheva – Alterations in the Expression of TfR1, DMT-1 and Hepsidin in Immature Mice Liver after Chronic Exposure to Cobalt Chloride	37
M. Gantcheva, V. Broshtilova – Pathogenesis and Diagnostic Complexities of Granuloma Faciale	45

Review Articles

M. Guarino – Palatogenesis and Palatoschisis. A Review on the Cellular and Molecular Mechanisms of Development	50
M. Markova – Keep Your Head Attached: The Sperm Connecting Piece	76

ANTHROPOLOGY AND ANATOMY 32 (2)

Original Articles

S. Panda, P. Das, M. Goswami – Do Foot Dimensions Influence Stature Estimation: A Study among the Bhumij Tribal Population of Northern Odisha, India	83
A. Dimitrova - Morphofunctional Limb Asymmetry in Adolescent Tennis Players	98
M. Hristova, N. Stefanova, M. Tzaneva, A. Hachmeriyan, G. Bekyarova – Morphometric Analysis of Burned Induced Gastric Mucosal Injury and Effect of Melatonin	107
N. Davceva, B. Krsteska, G. Popova – A Case of Sarcoidosis in a Forensic Setting: What Has Been Found as Cause of Death	118
N. Atanassova, E. Vasileva – Preliminary Anthropological Data of Inhumated Bone Remains from Late Medieval (Ottoman period) Necropolis from Object No. 7, along the Route of Road I-1 (E79) “Vidin-Ruzhints-Montana”, Near the Village of Turnyane, Vidin Region, Bulgaria	125

Review Articles

A. Fasova, M. Sotirova, T. Gudelova, A. Topalidis, S. Delchev – Advantages and Disadvantages of Virtual Autopsy in the Field of Forensic Medicine	143
R. Gatsin – Longevity in the Exhibition “Codes of Identity” of the National Anthropological Museum at the Institute of Experimental Morphology, Pathology and Anthropology with Museum, Bulgarian Academy of Sciences	150
Prof. Stefan Mutafov Commemorate 100 Years since His Birth	157
Prof. Anna Bojadjieva-Mihailova Commemorate 100 Years since Her Birth	161

Region- and Sex-Specific Differences of Cerebral Parvalbumin Distribution and Expression in Rats.

Olayemi K. Ijomone^{1,2}, Omamuyovwi M. Ijomone^{1,2,3}*

¹*Laboratory for Experimental and Translational Neurobiology, University of Medical Sciences, Ondo, Nigeria*

²*Department of Anatomy, Faculty of Basic Medical Sciences, University of Medical Sciences, Ondo, Nigeria*

³*Department of Molecular, Pharmacology Albert Einstein College of Medicine, New York, USA*

*Corresponding author e-mail: omijomone@unimed.edu.ng

Parvalbumin-expressing interneurons in the brain play key roles in the modulation of various neuronal communications and their dysfunction is implicated in multiple neurological disorders. Understanding their anatomical distribution across the brain and potential sex-specific differences holds significance in neuroscience. Here we used immunohistochemistry methods and digital image analysis to evaluate parvalbumin distribution and expression across selected brain regions. The study showed a higher number of parvalbumin-positive cells in the cerebral cortex (frontal and parietal) compared to subcortical regions (midbrain, thalamus, hippocampus, striatum). However, parvalbumin immunoreactivity was similar across regions examined except the striatum. Furthermore, we observed a significant sex-specific difference in the number of parvalbumin-positive cells only in the parietal cortex. The study thus suggests strong parvalbumin expressions across the brain even in regions with a smaller number of parvalbumin-positive cells, indicative of extensive parvalbumin neuronal connections. Additionally, the study notes the potential effect of sexual dimorphism in parvalbumin distribution.

Key words: Parvalbumin; Immunoreactivity; Cerebrum; Sex dimorphism; Rats

Introduction

In the brain, many activities are influenced by intracellular calcium (Ca) changes; these include neuronal excitation, and synaptic modulation, amongst others. Parvalbumin is a Ca-binding protein which plays an important role in the regulation of intracellular Ca concentrations [2,11]. A group of interneurons express parvalbumin. Key characteristics of this class of interneurons are fast responses and effective inhibition of neighbouring primary neurons [10]. These parvalbumin-expressing neurons are mostly GABAergic interneurons and have been reported to perform vital functions in neuronal

communications [18]. For example, parvalbumin interneurons in the parahippocampal domains are key modulators of the characteristic grid cells in the medial entorhinal cortex, where they serve as how the primary neurons communicate [3, 17]. Similar inhibitory connectedness has also been reported in the lateral entorhinal cortex, where the inhibitory interneurons are involved in tuning of primary neurons [19, 24].

Obviously, parvalbumin interneurons are hugely important across the brain, as their dysfunction is implicated in a variety of brain disorders including neurodegenerative diseases, neuropsychiatric and developmental disorders [5, 18]. Disturbances in parvalbumin interneurons are reported to be a hallmark of the progression of schizophrenia, where such disruptions trigger dopaminergic and glutamatergic dysfunctions [7, 9]. Additionally, the reduction of GABAergic interneurons that have been reported in the hippocampus of human schizophrenia patients has been linked to lowered parvalbumin expression [30]. Similarly, decreased parvalbumin expression and loss of parvalbumin interneurons have been reported in transgenic mice models of Alzheimer's diseases [29]. Furthermore, the downregulation of parvalbumin in interneurons has been indicated to trigger autistic phenotypes in rodent models [6, 16]. Interestingly, parvalbumin expression in the brain may be sexually dimorphic, and such sex-specific differences may provide vital insights into disorders in which parvalbumin disruptions are implicated. Curiously, an earlier report has shown a greater deficit in the relative density of hippocampal parvalbumin-positive neurons in male schizophrenic patients compared to their female counterparts [30].

Given the hugely important role of parvalbumin interneurons in various brain functions and implications in a wide variety of brain disorders, understanding their anatomical distribution in the brain, as well potential variabilities across the sexes, will prove hugely useful resources and of high interest in the neurosciences. Hence, the present study utilized immunohistochemical methods to evaluate parvalbumin distribution and expression across selected brain regions, as well as evaluating potential sexual dimorphic differences in brain parvalbumin expression.

Materials and Methods

Animals

Adult Sprague Dawley rats of both sexes [$n = 6/\text{sex}$; average weight: males = 339 ± 4.84 g, females = 215 ± 4.59 g], aged 10 weeks were procured from Charles Rivers Laboratories, USA, for the study. All animal experimental protocols were performed in strict accordance to the guidelines of the National Institute of Health for the care and use of laboratory animals and approved by the Institutional Animal Care and Use Committee. Animals were kept under 12-hour light-dark cycle with free access to regular food and water. Three weeks post-procurement, rats were euthanized via isoflurane inhalation, brains were rapidly excised, fixed by immersion in 10% neutral buffered formalin and processed for immunohistochemistry.

Immunohistochemistry

Brain tissues were processed for routine paraffin wax embedding. Using The Rat Brain Atlas [22] as guide, serial mid-sagittal (2-3 mm lateral to midline) sections of 5 μm thin sections were obtained. Immunohistochemistry followed protocols we have

previously established [13,21]. Sections were deparaffinized and heat mediated antigen retrieval performed in citrate-based antigen unmasking solution, pH 6.0 (Vector®, USA; #H3300). Sections were then treated for 10 min in hydrogen peroxide solution (0.3% in Tris Buffered Saline) for endogenous peroxidase blocking. Protein block was performed for 30 min in 2.5% normal horse serum (Vector® #MP-7401). Sections were then incubated in anti-parvalbumin (Novus Biologicals, USA; NB120-11427) at 1:1000 dilution, for 1 h at room temperature. Secondary incubation was performed using ImmPRESS™ (Peroxidase) Polymer Anti-Rabbit IgG Reagent (Vector® #MP-7401). DAB Peroxidase (HRP) Substrate Kit (Vector® #SK-4100) was used to reveal antibody immunoreactivity, after which sections were counter-stained in haematoxylin.

Imaging and Quantification

Digital imaging was performed using the Panoramic 250 Flash II slide scanner (3D Hitech, Budapest, Hungary) at 20x objective. Random non-overlapping images were obtained at x200 magnification (area size = $\approx 2.5 \times 10^5 \mu\text{m}^2$) from each animal. Ten random non-overlapping images were obtained from the frontal cortex, parietal cortex, midbrain region, thalamus and striatum. Four to five images were obtained from hippocampal CA3 region, and 5-7 from the hippocampal dentate gyrus (DG). Quantification of immunostained images were performed using the Image Analysis and Processing for Java (ImageJ), a public domain software sponsored by the National Institute of Health (USA). To quantify number of parvalbumin positive cells, Image J Cell Counter tool was used to identify and count positive cells as previously established [12]. To determine immunoreactivity of parvalbumin expression, images were analysed using the ImmunoRatio plugin on Image J, which separates and quantifies the percentage of DAB (positive immunoreactivity) by digital colour deconvolution [4]. Data for subsequent statistical analysis were averages obtained from each animal.

Statistics

Data are presented as mean \pm SEM. Data were analysed on GraphPad Prism 8 software (GraphPad Inc, USA) by two-way analysis of variance (ANOVA) followed by Bonferroni's *post-hoc* tests. Significant difference between sexes were further confirmed by t-test. Values of $p < 0.05$ were considered statistically significant.

Results

Immunostaining for parvalbumin shows marked expression across many brain regions in both male and female rats. Specifically, parvalbumin distribution across the cerebrum is most prominent in the cortex compared to subcortical regions (**Fig. 1** and **Fig. 2**).

Further analysis to quantify number of parvalbumin cells across selected brain regions was performed with Cell counter tool in Image J software. Two-ANOVA analysis of data obtained revealed no significant interaction ($p = 0.3357$; $F_{(6,69)} = 1.16$) between sex and brain regions. However, analysis revealed significant sex ($p < 0.01$; $F_{(1,69)} = 4.78$) and region ($p < 0.001$; $F_{(6,69)} = 19.94$) specific effects. Further Bonferroni's *post-hoc* test showed significantly higher number of parvalbumin cells in frontal cortex of males compared to other regions examined (parietal cortex, midbrain, thalamus, hippocampus (CA3 and DG), and striatum). Similarly for females, number

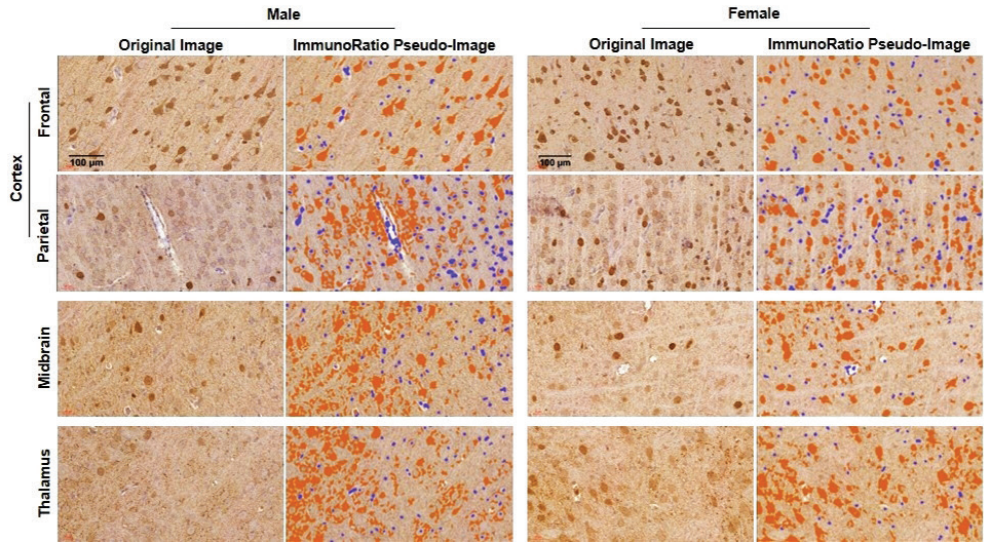


Fig. 1. Representative photomicrographs of parvalbumin expression and positive cells in the cortex (frontal and parietal), midbrain, and thalamus of male and female rats. Original images are accompanied by Pseudo-Image generated with ImmunoRatio plugin in Image J software.

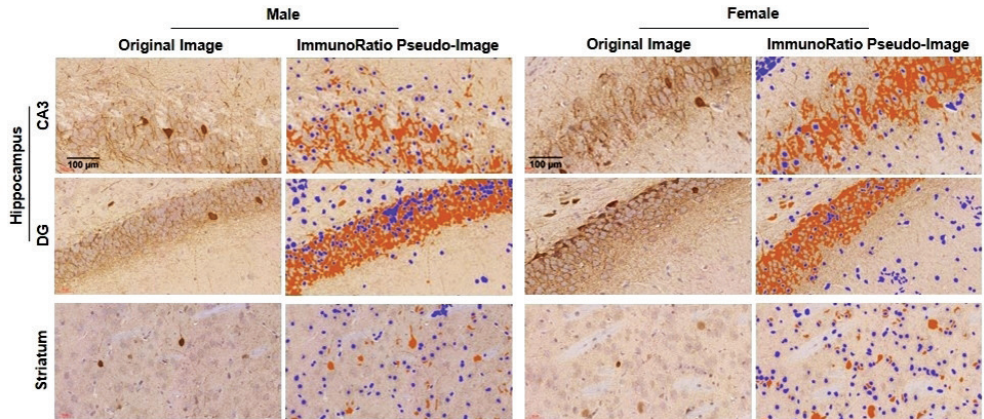


Fig. 2. Representative photomicrographs of parvalbumin expression and positive cells in the hippocampus (CA3 and DG), and striatum of male and female rats. Original images are accompanied by Pseudo-Image generated with ImmunoRatio plugin in Image J software.

of parvalbumin cells in the frontal cortex was significantly higher compared to other regions except for the parietal cortex which showed no significant difference. However, the parietal cortex had significantly higher number of parvalbumin cells compared to the hippocampus CA3 and DG, and the striatum. Bonferroni's post-hoc test showed no difference between sex for all regions, however further confirmation using t-test

revealed that in the parietal cortex, the number of parvalbumin cells is significantly higher ($p < 0.05$) compared to males (Fig. 3).

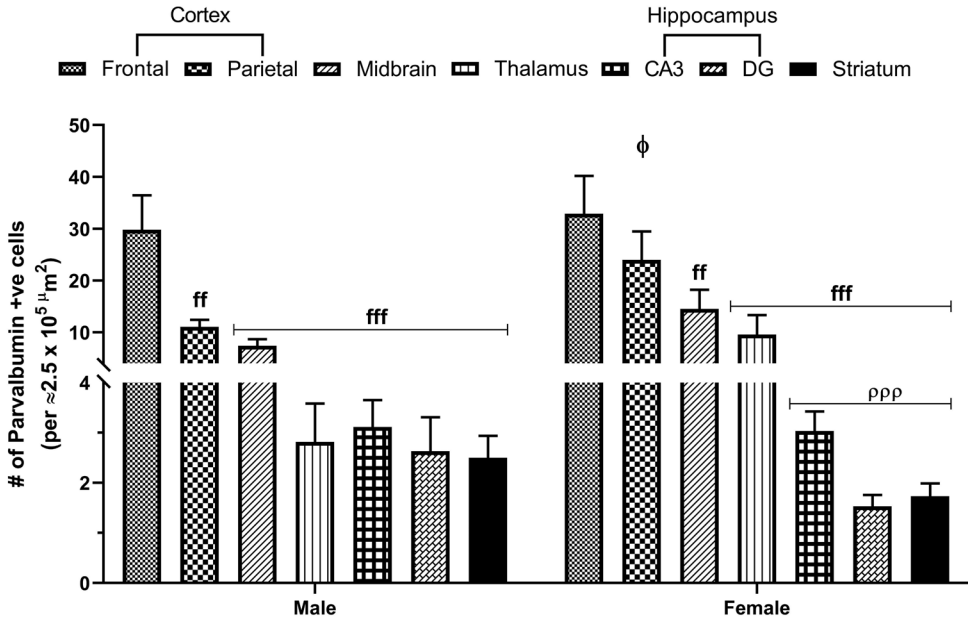


Fig. 3. Image J cell count of parvalbumin positive cells in the selected regions of the brain. Data were analyzed by two-way ANOVA followed by Bonferroni's post-hoc tests. Significant difference between sex was further confirmed by t-test. # $p < 0.01$, ### $p < 0.001$ compared to frontal cortex; ppp $p < 0.001$ compared to parietal cortex; φ $p < 0.01$ between male and female for same region.

The ImmunoRatio plugin on Image J software was used to quantify immunoreactivity of parvalbumin expression. Two-ANOVA analysis of data obtained revealed no significant interaction ($p = 0.4938$; $F_{(6,69)} = 0.91$) between sex and brain regions, as well as no sex effect ($p = 0.5373$; $F_{(1,69)} = 0.38$). However, analysis revealed significant region specific effect ($p < 0.001$; $F_{(6,69)} = 64.22$). Bonferroni's post-hoc test revealed significantly lower ($p < 0.001$) parvalbumin expression in striatum compared to the other regions examined in male rats. Additionally, both regions of hippocampus examined, the CA3 and DG, showed significantly lower ($p < 0.01$) expression compared to thalamus, while only the DG showed significant lower ($p < 0.05$) expression compared to the frontal cortex. In the female rats, the parvalbumin expression in the striatum is also significantly lower ($p < 0.001$) compared to other regions. No other significant difference is seen. Similarly, no significant differences between the sexes are revealed (Fig. 4).

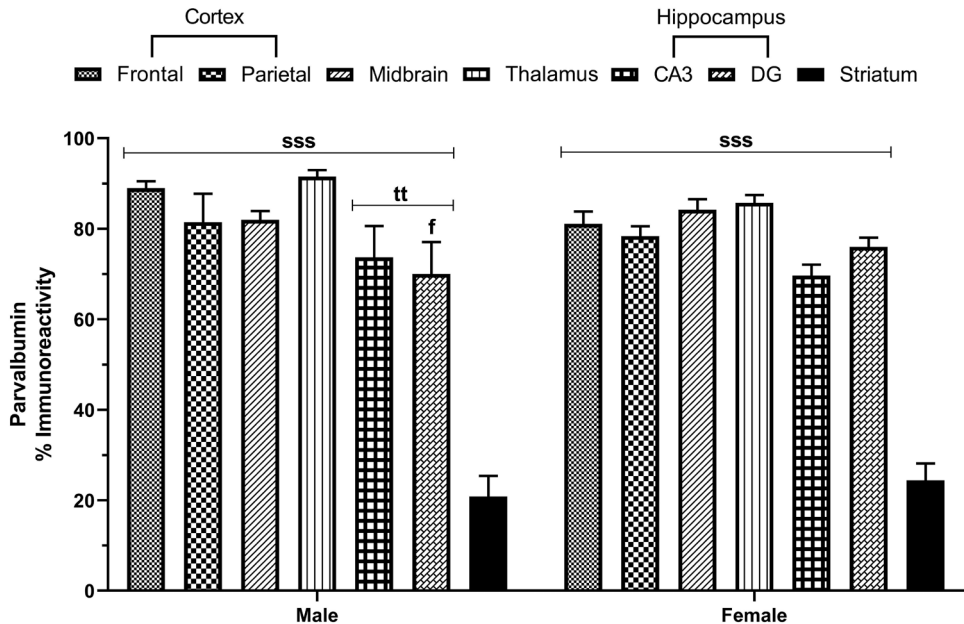


Fig. 4. ImmunoRatio analysis of parvalbumin immunoreactivity in the selected regions of the brain. Data were analyzed by two-way ANOVA followed by Bonferroni's post-hoc tests. ^f $p < 0.01$ compared to frontal cortex; ^{tt} $p < 0.01$ compared to thalamus; ^{sss} $p < 0.001$ compared to striatum.

Discussion

The current study evaluated parvalbumin distribution across several brain regions (frontal and parietal cortex, midbrain, thalamus, hippocampal CA3 and DG, and striatum), as well as examined the sexual dimorphism on the neuroanatomical distribution pattern of parvalbumin-expressing cells in the cerebrum.

The study demonstrates the differential distribution of parvalbumin-expressing cells across the above brain regions. Previous reports provide evidence that neuron and neurotransmitter distribution and axonal connection vary substantially across different cortical and subcortical areas [1,27]. In line with this, the findings here showed that parvalbumin-expressing neurons are more abundant in the frontal cortex, an area known for its immense importance in sensorimotor functions. Unsurprisingly, Kim and colleagues [15] highlighted the importance of parvalbumin neurons in sensory-motor cortical areas. They also noted that parvalbumin neurons appear to be dominant in these areas, which is similar to an earlier observation by an earlier study [14].

Interestingly, our results show a similar level of parvalbumin immunoreactivity in the subcortical regions (except for the striatum) compared to the cerebral cortex, despite the lower number of parvalbumin-expressing cells in the subcortical regions. Particularly, the thalamus, which showed a less parvalbumin-expressing cells compared to the cortex in both males and females, had higher parvalbumin immunoreactivity

compared to other groups, including the cortex, albeit not significant. This is indicative of strong parvalbumin-neuronal connections in these regions. For instance, although parvalbumin cells make up a small percentage of neurons in the hippocampus, they have the strongest inhibitory effect on the population of projection neurons [20], by forming a vast number of synapses amongst themselves and other neurons [8]. Likewise, these parvalbumin-expressing cells are characterized by their ability to form long-distance projections [28]. Therefore, it is possible that the regions with fewer soma of parvalbumin-expressing neurons might be receiving several axonal projections from other regions and exhibiting numerous synaptic connections.

Finally, the study examined the effect of sex dimorphism on parvalbumin distribution in the cerebrum. This is imperative to better understand the sex-related differences in the progression of some neurologic disorders. For instance, an earlier report showed a larger reduction of hippocampal parvalbumin-positive neurons in male schizophrenic patients compared to their female counterparts [30]. Further, a study in juvenile rats has shown that males generally had higher parvalbumin-positive interneurons in the upper part of the frontal cortex, but lower numbers in the dorsal hippocampus, compared to age-matched females [25]. Other preclinical studies indicate decreased parvalbumin-positive cells in males after prenatal stress, whereas females show more deficits after neonatal and adult stress [26]. In the present study, only in the parietal cortex did we observe a significant difference in parvalbumin distribution between the sexes, with females exhibiting a significantly higher number of parvalbumin-positive cells compared to males. Overall, these indicate sex-specific differences in parvalbumin distribution that could impact its role in the pathogenesis of brain disorders. Perturbations to parvalbumin interneurons have been linked to the pathophysiology of various neuropsychiatric, neurodevelopmental and/or neurodegenerative disorders, including autism, schizophrenia, bipolar disorders, Alzheimer's disease, among others [23]. Hence, understanding sex differences in parvalbumin distribution holds translational value to unravel sex-linked phenomena in the impact, distribution and severity of these brain disorders.

Conclusions

The study demonstrates that parvalbumin-expressing cells distribution is widespread across the cerebrum, with a higher population in the cortex compared to subcortical regions. However, levels of expression are similar across most major brain regions (except for the striatum), suggesting extensive connections of parvalbumin neurons. Also, the study indicates potentially sex differences in parvalbumin distribution in the cerebrum.

Limitations of the study: The study, however, highlights some limitations. Firstly, though the study sample size is based on PS Power analysis that indicates $n = 6$ is adequate, we do acknowledge that inter-individual variability could impact the findings. Further, immunostaining used here reveals broad types of parvalbumin-positive cells and could not account for the identification of subtypes. Also, we have not used sections from the whole brain, but serial sections were obtained from 2-3 mm lateral to midline as already described in methods, hence certain cerebral subregions might not have been fully represented. Finally, the use of immunohistochemistry may

produce results slightly different to other methods of cell visualization such as utilizing transgenic models.

Acknowledgements. OMI acknowledges the support of the International Brain Research Organization (IBRO) and the International Society for Neurochemistry (ISN).

References

1. **Awasthi, J. R., K. Tamada, E. T. Overton, T. Takumi.** Comprehensive topographical map of the serotonergic fibers in the male mouse brain. – *J. Comp. Neurol.*, **529**, 2021, 1391-1429.
2. **Caillard, O., H. Moreno, B. Schwaller, I. Llano, M. R. Celio, A. Marty.** Role of the calcium-binding protein parvalbumin in short-term synaptic plasticity. – *Proceedings of the National Academy of Sciences*, **97**, 2000, 13372-13377.
3. **Couey, J. J., A. Witoelar, S.-J. Zhang, K. Zheng, J. Ye, B. Dunn, R. Czajkowski, M.-B. Moser, E. I. Moser, Y. Roudi.** Recurrent inhibitory circuitry as a mechanism for grid formation. – *Nat. Neurosci.*, **16**, 2013, 318-324.
4. **Erukainure, O. L., O. M. Ijomone, O. Sanni, M. Aschner, M. S. Islam.** Type 2 diabetes induced oxidative brain injury involves altered cerebellar neuronal integrity and elemental distribution, and exacerbated Nrf2 expression: therapeutic potential of raffia palm (*Raphia hookeri*) wine. – *Metab. Brain Dis.*, **34**, 2019, 1385-1399.
5. **Ferguson, B. R., W.-J. Gao.** PV interneurons: critical regulators of E/I balance for prefrontal cortex-dependent behavior and psychiatric disorders. – *Frontiers in Neural Circuits*, **12**, 2018, 37.
6. **Filice, F., B. Schwaller, T. M. Michel, E. Grünblatt.** Profiling parvalbumin interneurons using iPSC: challenges and perspectives for Autism Spectrum Disorder (ASD). – *Mol. Autism*, **11**, 2020, 1-5.
7. **Frohlich, J., J. D. Van Horn.** Reviewing the ketamine model for schizophrenia. – *Journal of Psychopharmacology*, **28**, 2014, 287-302.
8. **Fukuda, T., T. Kosaka.** Gap junctions linking the dendritic network of GABAergic interneurons in the hippocampus. – *J. Neurosci.*, **20**, 2000, 1519-1528.
9. **Howes, O. D., J. Kambeitz, E. Kim, D. Stahl, M. Slifstein, A. Abi-Dargham, S. Kapur.** The nature of dopamine dysfunction in schizophrenia and what this means for treatment: meta-analysis of imaging studies. – *Arch. Gen. Psychiatry*, **69**, 2012, 776-786.
10. **Hu, H., J. Gan, P. Jonas.** Fast-spiking, parvalbumin+ GABAergic interneurons: From cellular design to microcircuit function. – *Science*, **345**, 2014, 1255-1263.
11. **Ijomone, O. M., O. M. Aluko, C. O. Okoh, A. C. Martins Jr, M. Aschner.** Role for calcium signaling in manganese neurotoxicity. – *J. Trace Elem. Med. Biol.*, **56**, 2019, 146-155.
12. **Ijomone, O. M., P. U. Nwoha.** Nicotine inhibits hippocampal and striatal acetylcholinesterase activities, and demonstrates dual action on adult neuronal proliferation and maturation. – *Pathophysiology*, **22**, 2015, 231-239.
13. **Ijomone, O. M., S. Y. Olatunji, J. O. Owolabi, T. Naicker, M. Aschner.** Nickel-induced neurodegeneration in the hippocampus, striatum and cortex; an ultrastructural insight, and the role of caspase-3 and α -synuclein. – *J. Trace Elem. Med. Biol.*, **50**, 2018, 16-23.
14. **Kawaguchi, Y., Y. Kubota.** GABAergic cell subtypes and their synaptic connections in rat frontal cortex. – *Cerebral cortex (New York, NY: 1991)*, **7**, 1997, 476-486.

15. **Kim, H., S. Ährlund-Richter, X. Wang, K. Deisseroth, M. Carlén.** Prefrontal parvalbumin neurons in control of attention. – *Cell*, **164**, 2016, 208-218.
16. **Lauber, E., F. Filice, B. Schwaller.** Dysregulation of parvalbumin expression in the *Cntnap2*^{-/-} mouse model of autism spectrum disorder. – *Front. Mol. Neurosci.*, **11**, 2018, 262.
17. **Miao, C., Q. Cao, M.-B. Moser, E. I. Moser.** Parvalbumin and somatostatin interneurons control different space-coding networks in the medial entorhinal cortex. – *Cell*, **171**, 2017, 507-521. e517.
18. **Nahar, L., B. M. Delacroix, H. W. Nam.** The role of parvalbumin interneurons in neurotransmitter balance and neurological disease. – *Frontiers in Psychiatry*, **12**, 2021, 985.
19. **Nilssen, E. S., B. Jacobsen, G. Fjeld, R. R. Nair, S. Blankvoort, C. Kentros, M. P. Witter.** Inhibitory connectivity dominates the fan cell network in layer II of lateral entorhinal cortex. – *J. Neurosci.*, **38**, 2018, 9712-9727.
20. **Ognjanovski, N., S. Schaeffer, J. Wu, S. Mofakham, D. Maruyama, M. Zochowski, S. J. Aton.** Parvalbumin-expressing interneurons coordinate hippocampal network dynamics required for memory consolidation. – *Nature Communications*, **8**, 2017, 1-14.
21. **Okeowo, O. M., O. O. Oke, G. O. David, O. M. Ijomone.** Caffeine administration mitigates chronic stress-induced behavioral deficits, neurochemical alterations, and glial disruptions in rats. – *Brain Sciences*, **13**, 2023, 1663.
22. **Paxinos, G., C. Watson.** *The rat brain in stereotaxic coordinates*, 6th Edition, Academic Press, 2007, pp. 456
23. **Ruden, J. B., L. L. Dugan, C. Konradi.** Parvalbumin interneuron vulnerability and brain disorders. – *Neuropsychopharmacology*, **46**, 2021, 279-287.
24. **Tsao, A., M.-B. Moser, E. I. Moser.** Traces of experience in the lateral entorhinal cortex. – *Curr. Biol.*, **23**, 2013, 399-405.
25. **Vojtechova, I., K. Maleninska, V. Kutna, O. Klovrcza, K. Tuckova, T. Petrasek, A. Stuchlik.** Behavioral alterations and decreased number of parvalbumin-positive interneurons in wistar rats after maternal immune activation by lipopolysaccharide: sex matters. – *Int. J. Mol. Sci.*, **22**, 2021, 3274.
26. **Woodward, E. M., L. Coutellier.** Age- and sex-specific effects of stress on parvalbumin interneurons in preclinical models: Relevance to sex differences in clinical neuropsychiatric and neurodevelopmental disorders. – *Neurosci. Biobehav. Rev.*, **131**, 2021, 1228-1242.
27. **Yu, Q., Y.-Z. Liu, Y.-B. Zhu, Y.-Y. Wang, Q. Li, D.-M. Yin.** Genetic labeling reveals temporal and spatial expression pattern of D2 dopamine receptor in rat forebrain. – *Brain Structure and Function*, **224**, 2019, 1035-1049.
28. **Yuan, K., K. L. Fink, J. A. Winer, C. E. Schreiner.** Local connection patterns of parvalbumin-positive inhibitory interneurons in rat primary auditory cortex. – *Hear. Res.*, **274**, 2011, 121-128.
29. **Zallo, F., E. Gardenal, A. Verkhatsky, J. J. Rodríguez.** Loss of calretinin and parvalbumin positive interneurons in the hippocampal CA1 of aged Alzheimer's disease mice. – *Neurosci. Lett.*, **681**, 2018, 19-25.
30. **Zhang, Z. J., G. P. Reynolds.** A selective decrease in the relative density of parvalbumin-immunoreactive neurons in the hippocampus in schizophrenia. – *Schizophr. Res.*, **55**, 2002, 1-10.

Histopathological Changes in the Enteric Nervous System of Patients Undergoing Surgical Treatment for Intestinal Pseudo-Obstruction

Todor Kirov^{1}, Vesela Ivanova², Tihomir Dikov², Radoslav Todorov³, Lina Malinova¹*

¹ Dept. of Anatomy, Histology and Embryology, Medical University of Sofia, Sofia, Bulgaria;

² Dept. of General and Clinical Pathology, Medical University of Sofia, Sofia, Bulgaria;

³ Dept. of General and Operative Surgery, Medical University of Sofia, Sofia, Bulgaria

*Corresponding author e-mail: tkirov@medfac.mu-sofia.bg

This study addresses congenital colorectal neural disorders that mimic Hirschsprung's disease (HD), and which present with severe bowel motility issues. We analyzed full-thickness colorectal biopsies from eight adult patients with symptoms resembling HD to investigate expression patterns of PTEN, calretinin, and NOS1 in the enteric nervous system. Immunohistochemical findings revealed that while PTEN and calretinin staining was markedly reduced, NOS1 expression remained relatively stable. The reduced PTEN expression aligns with its established role in regulation of neuronal growth and suggests dysregulated PTEN pathways in the pathogenesis of HD-related conditions, like intestinal neuronal dysplasia. Likewise, diminished calretinin staining suggests altered intracellular calcium-buffering mechanisms, though overall neuronal numbers were not significantly altered. However, NOS1 findings pointed to relatively intact nitric oxide-mediated pathways. These observations highlight the need for refined diagnostic criteria and may guide future targeted therapeutic strategies.

Key words: Hirschsprung's disease, intestinal neuronal dysplasia, PTEN, NOS1, calretinin

Introduction

The ENS, often described as the “second brain,” comprises a complex network of neurons and glial cells that regulate essential gastrointestinal functions, including motility, secretion, and blood flow. Disruptions in ENS development or function underlie the pathophysiology of a range of pathologies, head example of which is Hirschsprung's disease (HD). It presents with severe chronic constipation and other motility issues that predominantly affect children, though adults can also present with these conditions [7]. From the conditions that resemble HD in terms

of manifestation, with highest occurrence is the intestinal neuronal dysplasia type B (IND-B). It is characterized morphologically by hyperplasia of the submucosal ganglia and immaturity of ganglion cells [4]. In contrast with this, HD involves complete absence of ganglion cells in the affected bowel segments, resulting in functional obstruction [7]. Another related condition, the internal anal sphincter achalasia (IASA), though less well understood, is associated with impaired neural regulation of the internal anal sphincter [1]. HD is the most common, occurring in approximately 1 in 5,000 live births, while IND-B and IASA are less prevalent but clinically significant due to their diagnostic and therapeutic challenges [5]. Advances in molecular and cellular research over the past decade have provided insights into the pathogenic mechanisms, yet histopathological diagnosis is notoriously marked by controversy and complexity [3].

Histopathological analysis is the gold standard for diagnosing congenital colonic neural disorders, but it faces significant challenges. Differentiating between IND-B, HD, and normal variations requires meticulous evaluation of biopsy specimens, which are often limited in size and quality. The subjective nature of interpreting histological findings, such as submucosal ganglion hyperplasia in IND or the absence of ganglion cells in HD, can lead to diagnostic errors [9]. Furthermore, the need for multiple biopsy samples to ensure accurate diagnosis adds procedural complexity and increases the burden on patients and clinicians. Despite improvements in histological and immunohistochemical techniques, the lack of standardized diagnostic criteria continues to hinder clinical practice [3]. Diagnostic criteria, established with the Frankfurt Consensus in 1990 include among other methods enzyme histochemistry for acetylcholine esterase and lactate dehydrogenase, both of which limited to only frozen sections and therefore have serious limitations. Consequently, many attempts have been made to introduce new and more superior diagnostic criteria, well summarized by Terra et al. [10].

Therefore, the purpose of this study is to examine possible disturbances in the expression of some less extensively examined neuronal markers, namely the phosphatase and tensin homolog deleted on chromosome 10 (PTEN), calretinin, and the neuronal isoform of nitric oxide synthase (NOS1).

Materials and Methods

Biopsies from eight patients that underwent colo-rectal resection surgery were used for this study. Every patient gave written informed consent declaring that medical data acquired during the diagnostics and treatment period can be used for medical research purposes. The written informed consent document was submitted to the Ethics committee of Medical University Sofia and the Ethics committee of Medical University Sofia approved the study - under issued permission 23/25.11.2024, 5522/05.12.2024.

The patients' age ranged between 46 and 77 years old. They were hospitalized with persisting episodes of severe constipation and/or clinical signs of functional intestinal obstruction that were refractory to different types of clinical treatment. Different imaging and clinical studies showed no sign of tumor or other anatomical/physical factor for colon obstruction. Imaging and endoscopic studies disclosed only a segment of the right or left colon with variable length affected by lack of peristalsis and loss of normal colon haustrations. Resection surgical interventions were performed to

treat the colon obstruction, and full thickness colorectal biopsies were collected for histopathological analysis. The specimens were processed for paraffin embedding and subsequent slicing on a microtome at a thickness of 6 μm .

After acquisition of informed consent, an additional amount of slices was sectioned for the needs of this study. Thereafter, standardized avidin-biotin-peroxidase protocol was performed following the manufacturer's instructions. Applied antisera are presented in **Table 1**. The slides were scanned by means of Olympus VS120-S6-102 slide scanner and photomicrographs were captured via the Olympus VS-ASW Image Acquisition software. Finally, images were processed with Adobe Photoshop CC software.

Table 1. Antisera used in the immunohistochemical reactions

Antisera	Manufacturer	Catalogue Number	Host/Type	Dilution
PTEN	Elabscience®	E-AB-70070	Rabbit/Polyclonal	1:200
Calretinin	Elabscience®	PA6569, Clone No. YN00166m	Mouse/Monoclonal	1:200
NOS1	Elabscience®	E-AB-70065	Rabbit/Polyclonal	1:300

Results

In all cases of the control group, the enteric nervous system did not show any signs of alteration. The ganglia were readily recognizable in both plexuses. Neuronal count ranged between 3 and 5 per sectioned submucosal ganglion, and between 5 and 11 in the myenteric plexus.

PTEN expression was positive in all neural elements of the submucosal and myenteric nerve plexuses in all cases of the control group (**Fig. 1A, B**). Neuronal PTEN expression was strong with a particular nuclear highlight. Adjacent intra- and interganglionic fibers and glial cells showed medium but still significant expression, thus providing the ganglia with clear outlines and overall immunopositivity.

In the experimental group, we observed a marked reduction of PTEN expression in the submucosal nerve plexus in 75% of the cases (**Fig. 1C**) and in the myenteric nerve plexus in 62.5% of the cases (**Fig. 1D**). Such changes provided the ganglia with a more reticular outlook and rougher contours.

Immunohistochemical findings for calretinin in both plexuses of the control group were abundant. Neurons were clearly delineated and showed a significant staining reaction (**Fig. 2A**). Prominent reaction was also observed in fiber bundles through the *muscularis externa*, the submucosa, the *muscularis mucosae*, and the mucosa.

In all cases of the experimental group, findings were markedly scarce. The submucosal ganglia were noticeably fewer in number and therefore more difficult to locate. In the ones that were registered, the neuronal count did not differ significantly from the ones in the control group. The neuronal staining intensity was lower and the adjacent fiber bundles were in most cases indistinguishable (**Fig. 2B**). On several

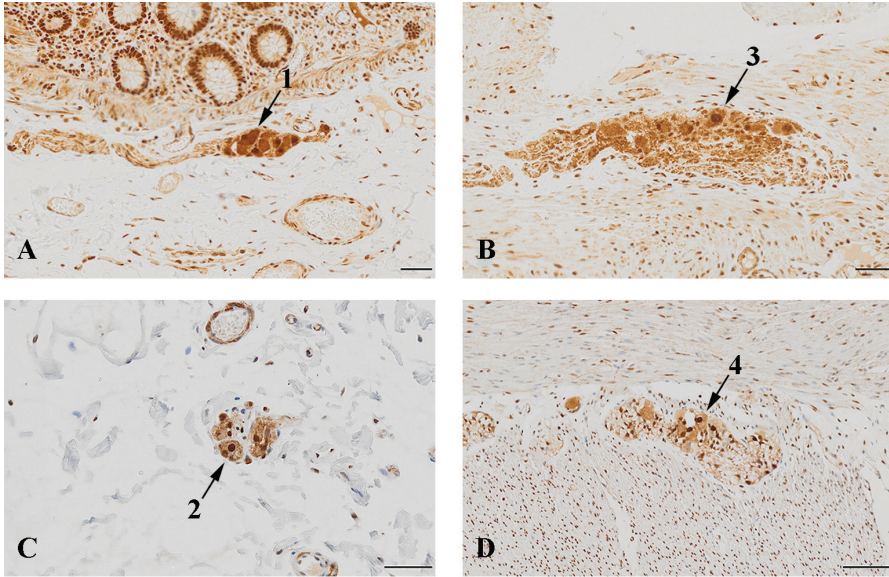


Fig. 1. Expression of PTEN in the submucosal plexus (A) and the myenteric plexus (B) of the control group, and submucosal plexus (C) and myenteric plexus (D) in the experimental group. Reactivity in the submucosal neurons (arrow 1) and in the myenteric neurons (arrow 2) in the controls appeared to be markedly higher compared to their counterparts in the experimental group (arrows 3 and 4 respectively). Scale bars: A, B, C – 50 μ m, D – 100 μ m.

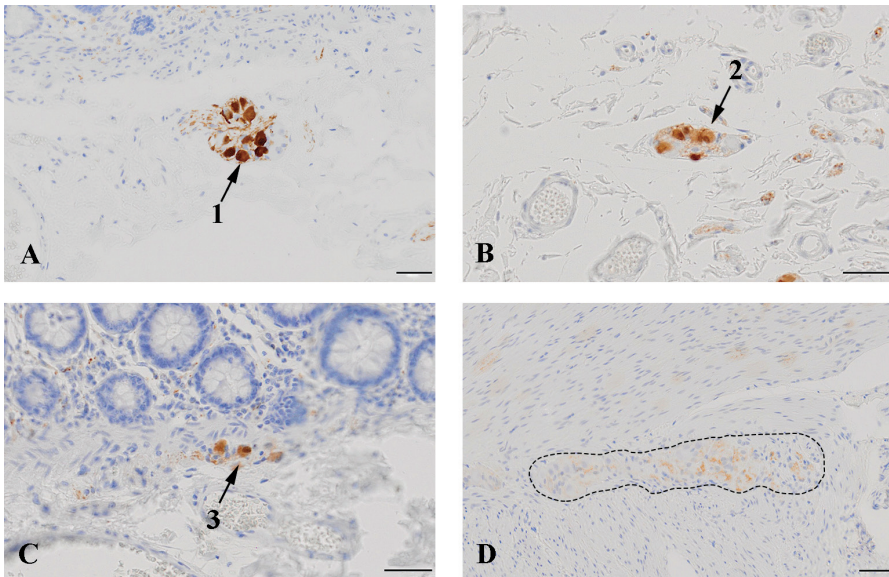


Fig. 2. Immunohistochemistry for calretinin in control group (A) and experimental group (B-D). Expression in the submucosal neurons in the control group (A, arrow 1) is notably higher than that of the experimental group (B, arrow 2). Note the presence of possible ectopic neurons in the *muscularis mucosae* in the experimental group (C, arrow 3). In the myenteric plexus of the experimental group, expression is practically non-existent (D); dashed line delineates the myenteric ganglion. Scale bars: 50 μ m.

occasions, positive neurons were seemingly registered in the *muscularis mucosae* (Fig. 2C). In the myenteric was even less: neuronal immunoreactivity was poor, and in many cases did not allow even basic differentiation of cell types (Fig. 2D).

NOS1 immunohistochemical findings were similar in all cases of the control and experimental groups. Submucosal ganglia were populated by several neurons, 1-2 of which showing poor to medium staining, and the rest were practically immunonegative (Fig. 3A, C). In the myenteric plexus of both cohorts, the reaction intensity of individual neurons was markedly stronger compared to the submucosal neurons, the rest showing poor or negative reaction (Fig. 3B, D). Only in few isolated myenteric ganglia we registered by visual inspection notably more intense reaction compared to the control group (Fig. 3D). Additionally, distinct bundles of positive beaded fibers were regularly observed in the ganglia.

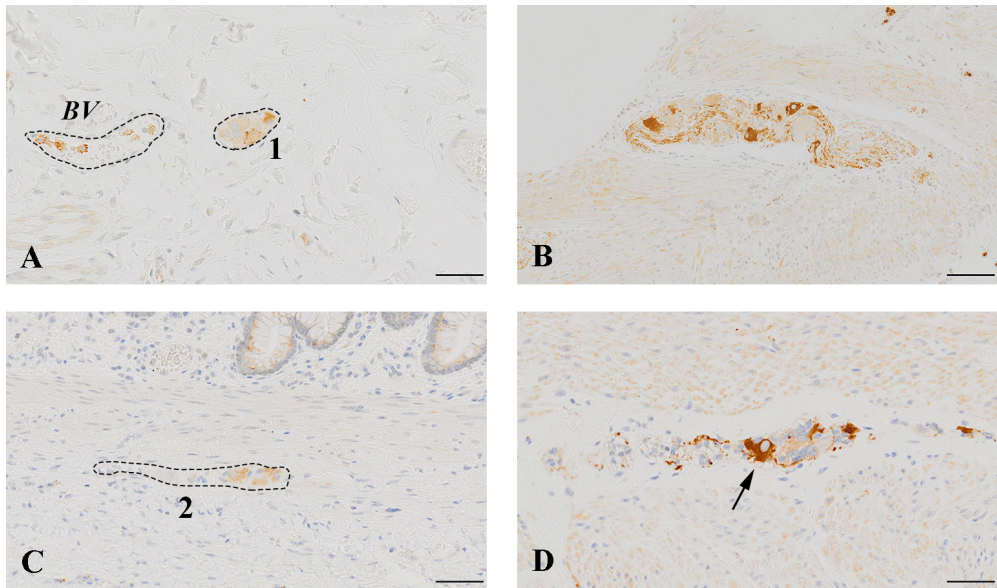


Fig. 3. NOS1-immunohistochemistry in the submucosal plexus (A) and the myenteric plexus (B) of the control group, and submucosal plexus (C) and myenteric plexus (D) in the experimental group. There were no measurable morphological differences between the submucosal ganglia in the controls (A, 1) and in the experimental group (C, 2). Note that blood vessels also contain immunoreactive cells (BV). Although in general the myenteric ganglia also did not show differences in the two cohorts, the arrow indicates a myenteric neuron in the experimental group that notably showed higher density, which was a rare finding. Scale bars: A, C, D – 50 μ m, B – 100 μ m.

Discussion

In this study, we examined the expression of three histopathological markers. One of them, in the face of calretinin, has been used as a major diagnostic tool for intestinal congenital pathologies for decades [8]. Therefore, any findings registered by immunostaining can be quite revealing regarding any underlying condition. Another marker, NOS1, is widely used for scientific purposes but is rarely a major choice when

it comes to diagnostics of that particular branch of pathology. Most likely, that is due to its selectivity in terms of neuronal expression, being expressed only in inhibitory neurons [6]. Still, being a well-known neuronal marker it is important for it to be fully elucidated in light of the variable intestinal conditions. PTEN-immunoreactivity is one that has most definitely not received enough scientific attention. Therefore, this article presents a minor but foundational contribution to future research.

The patients that underwent the resection interventions presented with symptoms traditionally attributed to HD, defined histopathologically as aganglionosis in a variable intestinal extent, but mostly restricted to the rectum [2]. Traditionally, HD presents itself during the newborn period by delayed passage of meconium. However, there have been clinical cases of both children and adults that present with signs of functional intestinal obstruction but do not meet the criteria for HD [12]. These cases were commonly regarded as variants of HD [5]. Such include IND-B, IASA, hypoganglionosis and others, of which with highest occurrence is IND-B [5]. HD was readily excluded from the possible causes of the functional obstruction of the cohort of this study due to notable presence of ganglionic cells. It is therefore no surprise that IND-B was established as working diagnosis in these cases.

IND-B has been a subject of significant scientific controversy during the last three decades and remains an undefined histopathological phenotype of uncertain clinical importance. Moreover, it is well accepted that the morphological findings may very well represent deviations from normality [3]. The morphological diagnostic criteria for IND-B have been repeatedly modified over the years, making comparisons between studies difficult and thus increasing the doubts and controversies [4]. It is not a purpose of this study to discuss diagnostic accuracy. However, it is important to note that while IND-B has been described in adults, the typical age period for receiving such diagnosis remains early childhood. Moreover, the ganglionic hyperplasia that classically defines IND-B [9] was not observed in the current specimens.

We observed a clear contrast in immunohistochemical patterns between the control and experimental groups, particularly regarding PTEN and calretinin expression. Interestingly, despite these notable differences, the NOS1 staining patterns appeared relatively similar in both cohorts. Together, these findings suggest that the conditions mimicking HD may involve selective disruptions in the molecular and structural integrity of the enteric nervous system, rather than a generalized neuronal deficit.

A striking observation was the notable PTEN expression differences we observed. In both plexuses of the control group, it was significant, which aligns with the established role of PTEN in regulating neuronal cell growth and survival [11]. In contrast, the reduced PTEN expression in most of the experimental samples proposes a link between compromised PTEN pathways and the pathogenesis of the variants of HD. This downregulation could potentially cause abnormalities in neuronal development and maintenance, consistent with prior work that has investigated the critical function of PTEN in neural crest-derived tissues [10].

Additionally, calretinin immunohistochemistry revealed a robust staining in the control specimens - unsurprising, given calretinin's reputation as a reliable marker for neuronal identification [8]. In the experimental group, we observed markedly reduced calretinin staining intensity. Since the neuronal counts in the submucosal plexus of the experimental samples did not differ greatly from controls, the reduced staining may indicate a potential loss of functional connectivity due to alteration in intracellular

calcium-buffering mechanisms, which play a key role in neuronal signaling [13]. Additionally, this possibly indicates that these conditions may involve subtle deficits in protein expression rather than outright neuronal loss.

The isolated neurons registered in the *muscularis mucosae* were a peculiar finding as this is a reported morphological sign for IND-B [9]. However, it should be noted that while those could represent ectopic neurons, it is also fully possible for them to be an optical illusion of submucosal ganglionic cells residing intimately on the inner aspect of the *muscularis mucosae*.

By contrast, NOS1 distribution and density patterns showed minimal differences between the two groups. In both cohorts, only a few neurons within the submucosal plexus stained positively for NOS1, while the myenteric plexus displayed a more robust reaction, with distinct beaded fibers consistently observed. This suggests that the nitric oxide-mediated pathways, at least based on NOS1 expression, could be relatively preserved in IND-B, hinting that not all neuronal subpopulations are equally vulnerable to the pathological processes.

Conclusions

Overall, this study demonstrates a complex interplay of molecular and structural alterations in the rectal neuronal structures of patients that underwent resection surgery, characterized by substantial reductions in PTEN and calretinin expression, yet largely preserved NOS1 reactivity. Understanding these specific changes holds significant relevance, as it may help refine diagnostic criteria for IND-B and related conditions and guide future research focused on targeted therapies. It is our belief that further investigations should explore the downstream pathways affected by PTEN and NOS1 dysregulation.

Acknowledgements. This study was fully funded by grant № D-177/03.08.2023 from Medical University – Sofia. It was performed under the permission of the heads of the *Dept. of Anatomy, Histology and Embryology*, Medical University of Sofia, *Dept. of General and Clinical Pathology*, Medical University of Sofia, *Dept. of General and Operative Surgery*, Medical University of Sofia, *Clinic of General and Liver Pancreatic Surgery*, University Hospital Alexandrovska Sofia. The authors want to express their special gratitude to all personnel of the above-mentioned departments.

References

1. **Doodnath, R., P. Puri.** Internal anal sphincter achalasia. – *Semin. Pediatr. Surg.*, **18**(4), 2009, 246-248.
2. **Hwang, S., R. P. Kapur.** Advances and pitfalls in the diagnosis of Hirschsprung disease. – *Surg. Pathol. Clin.*, **13**(4), 2020, 567-579.
3. **Kapur, R. P., M. Reyes-Mugica.** Intestinal neuronal dysplasia type B: An updated review of a problematic diagnosis. – *Arch. Pathol. Lab. Med.*, **143**(2), 2019, 235-243.
4. **Meier-Ruge, W. A., K. Ammann, E. Bruder, A. M. Holschneider, A. F. Schärli, P. P. Schmittenbecher, F. Stoss.** Updated results on intestinal neuronal dysplasia (IND B). – *Eur. J. Pediatr. Surg.*, **14**(6), 2004, 384-391.

5. **Puri, P., J. H. Gosemann.** Variants of Hirschsprung disease. – *Semin. Pediatr. Surg.*, **21**(4), 2012, 310-318.
6. **Sanders, K. M., S. M. Ward.** Nitric oxide and its role as a non-adrenergic, non-cholinergic inhibitory neurotransmitter in the gastrointestinal tract. – *Br. J. Pharmacol.*, **176**(2), 2019, 212-227.
7. **Serafini, S., M. M. Santos, A. C. A. Tannuri, C. Di Loreto, J. O. Gonçalves, U. Tannuri.** A new systematization of histological analysis for the diagnosis of Hirschsprung's disease. – *Clinics (Sao Paulo)*., **78**, 2023, 100198.
8. **Singh, S. K., U. K. Gupta, R. Aggarwal, R. A. Rahman, N. K. Gupta, V. Verma.** Diagnostic role of calretinin in suspicious cases of Hirschsprung's disease. – *Cureus*, **13**(2), 2021, 13373.
9. **Terra, S. A., P. L de Arruda Lourenção, M. G Silva, H. A Miot, M. A. M. Rodrigues.** A critical appraisal of the morphological criteria for diagnosing intestinal neuronal dysplasia type B. – *Mod. Pathol.*, **30**(7), 2017, 978-985.
10. **Terra, S. A., A. C. Gonçalves, P. L. T. A. Lourenção, M. A. M. Rodrigues.** Challenges in the diagnosis of intestinal neuronal dysplasia type B: A look beyond the number of ganglion cells. – *World J. Gastroenterol.*, **27**(44), 2021, 7649-7660.
11. **Terra, S. A., P. L. T. de Arruda Lourenção, M. A. M. Rodrigues.** PTEN Immunohistochemistry. – *Arch. Pathol. Lab. Med.*, **147**(5), 2022, 577-583.
12. **Vougas, V., K. Vardas, C. Christou, G. Papadimitriou, E. Florou, C. Magkou, D. Karamanolis, D. Manganas, S. Drakopoulos.** Intestinal neuronal dysplasia type B in adults: a controversial entity. – *Case Rep. Gastroenterol.*, **8**(1), 2014, 7-12.
13. **Zemheri, E., P. Engin Zerk, C. Ulukaya Durakbasa.** Calretinin immunohistochemical staining in Hirschsprung's disease: An institutional experience. – *North Clin. Istanbul.*, **8**(6), 2021, 601-606.

Histomorphological Evaluation of Medio-Lateral Asymmetry in the Adult Murine Cerebellar Cortex

Radoslav Spasov^{1}, Dimo Stoyanov¹, Ivan Ivanov², Anton Tonchev¹*

¹ *Department of Anatomy and Cell Biology, Medical University – Varna, Varna, Bulgaria*

² *Student in Medical University – Varna, Varna, Bulgaria*

* Corresponding author e-mail: radoslav.spasov@mu-varna.bg

The cells comprising the mammalian cerebellar cortex exhibit significant variability. Individual neurons demonstrate differences regarding key parameters depending on their location within the Cerebellum's cortical layer. We present evidence of histomorphological heterogeneity between the medial and lateral domains of the murine cerebellar cortex. Our findings show that the cerebellar cortex of normal adult mice has a surface area 42% smaller in the hemispheres compared to the Vermis and is unevenly distributed across the folia. In the Vermis, 4/10 folia constitute 55% of the total cortical surface, while in the hemispheres, 3/6 folia account for about 62%. The granule and molecular layers had lower surface area but increased thickness in the hemispheres, while the Purkinje cell layer was 46% shorter in the hemispheres compared to the Vermis. These findings advocate for caution when interpreting histomorphological changes in disease models based on the mouse cerebellum.

Key words: cerebellar cortex, molecular layer, thickness, granule layer, Purkinje cell layer

Introduction

The cerebellum is morphologically a highly complex brain region. The external morphology of the cerebellum is characterized by a plethora of sulci that mark highly branching foliations. The cerebellum is divided into one central part - vermis and two lateral parts on each side of the vermis - hemispheres. Larger fissures divide it into 3 lobes and smaller into 10 lobules, each of which contains gray and white matter [16, 18, 13]. Similar to the telencephalon, the cerebellar gray matter forms the outer aspect of the cortex, while the white matter is located deeper to the gray matter [1, 3, 5, 11, 19, 21, 22, 25]. In normal mice the Vermis contains ten folia usually denoted by numbers one to ten, while the hemispheres have six folia usually denoted by their names: Simple lobule (**LS**), crus 1 of ansiform lobule (**crus1**), crus 2 of ansiform lobule

(**crus2**), paramedian lobe (**PML**) and cupola of pyramis (**COP**), flocculonodular lobe (**FL**) [12, 15, 24]. The cortex gray matter is built by cells arranged in 3 layers: the molecular (ML), purkinje cell (PCL) and granular cell layer (GL). The classical view of the adult cerebellum states that it has a rather monotonously repetitive histological structure, but several pieces of evidence suggest that there are regional morphological differences at cellular level [7]. For example, PCs in the hemispheres have larger bodies than PCs in the Vermis [7, 17]. Granule and Golgi cells also show differences in size and packing densities between Vermis and lateral hemispheres [7, 10]. The packing density of granule cells and Purkinje cells is usually higher in the folial crowns as compared to fissures [7, 20]. Similar differences between vermis and hemispheres for the granule cells are reported across species. In this study we aim to explore if the histomorphological properties of the cerebellar cortex are constant throughout the cerebellum or there are some regional differences (between the vermis and the hemispheres). Here we show in the normal adult mouse cerebellum that not only the cell-to-cell morphological parameters exhibit regional heterogeneity but even the basic histomorphological features, such as layer thickness and surface area, are variable. These data stress that care should be taken when applying morphometric criteria to characterize cerebellar defects in mutant mouse models.

Material and Methods

Animals and tissue handling

Cerebellar tissues from normal adult mice were used from experiments following approval of the ethics committee of the state of Lower Saxony, Germany – Niedersächsische Landesamt für Verbraucherschutz und Lebensmittelsicherheit LAVES)/Oldenburg, resolution № 33.9-42502-04-11/0622 of 07.12.2011. Animals were sacrificed at P21, perfused with ice-cold 4% paraformaldehyde; the cerebellum was dissected and immersed in paraformaldehyde at 4°C. Prior to sectioning tissues were cryoprotected with PBS/Sucrose (15% and 30%), and embedded in OCT. The sections were cut at 16 µm.

Immunofluorescence

Sections were washed from the OCT in PBS, followed by antigen retrieval for 5 min at 95°C in citrate buffer. Blocking was performed with PBS/BSA/Triton for 1 hour at room temperature, primary antibodies were diluted in PBS/BSA/Triton and incubated overnight at 4°C. Secondary antibodies were incubated for 2 hours at room temperature, and DAPI was added last. Washing steps were done as needed. The following antibodies were used: to label PC, we used Calbindin manufactured by Santa Cruz with catalog number sc365360, used concentration 1:100 and Parvalbumin manufactured by Sigma Aldrich with catalog number p3088, used concentration 1:300. For secondary body we used Rabbit Thermo Fisher Scientific with catalog number A-11008, used concentration 1:300

Image acquisition

Images were acquired on a standard Leica confocal microscope with DFC 350 FX R2 camera and N PLAN 2.5x0.07 DRY objective.

Image analysis

We've done the surface measurement in Fiji (ImageJ) software using tiff files of micrographs stained with DAPI. We took the section levels for the medial micrographs at the level of the vermis, while the ones for the hemispheres were taken at the level of nucleus dentatus. We used the brush tool of Fiji for selection of the cortex/ML/GL, and subsequent creation of ROIs (regions of interest). The data was saved in the program's ROI manager as zip files. The tiff files which were calibrated (μm per pixel in accordance with the metadata of the original file). Results are presented as mm^2 . To measure the thickness of ML and GL we used ROIs and generated masks from these 2 layers. Then we used the function in Fiji - Analyze -> Local Thickness -> Local Thickness "(Masked, calibrated, silent)" option. The program provided heat maps of the thickness. We further added to them calibration and scale bars. For the length of the PCL we used micrographs from staining using anti-Calbindin and anti-Parvalbumin antibodies. We used the "segmented line" of Fiji to generate the ROIs. Then we connected each of the Purkinje cells with a line which passes through the middle of each Purkinje cell and on top of the tightly packed granular cell layer without crossing the border between the layers. This is how we formed a line which we called the "Purkinje cell layer length", and measured its length.

Results

Variability of the surface area of different folia in the cerebellar Vermis and hemispheres

We started our analysis by manually segmenting the cerebellar cortex and measuring its total surface cross-sectional area (sagittal levels). As expected, we found that the total area of sagittal sections was significantly smaller at lateral (hemispherical) levels as compared to medial (vermal) levels: $4.414 \text{ mm}^2 \pm 0.252$ (lateral), $7.568 \text{ mm}^2 \pm 0.342$ (medial) (**Fig.1 E**, $p < 0.001$). This was a decrease in the surface by approx 42%. The cortical surface area showed unequal distribution across the different folia. In the Vermis, different folia surfaces ranged from 6.6% to 19.5% of the total surface area. In the hemispheres, the range was greater: from 7.3% to 28% of the total surface area (**Fig.1 C, D**). The largest folia (IV, V, VI, IX) (4 out of 10) in the Vermis comprised $55\% \pm 0.16\%$ of the total cortical surface, while the largest folia (lobus simplex, Crus 1 of ansiform lobule and cupula of pyramid lobule) (3 out of 6) in the hemispheres composed ($62\% \pm 0.15\%$) of the total surface. The data of folia measurements are reported in **Table 1, 2** ($p < 0.001$).

Table 1. Distribution of folial surface across the cerebellum (vermis)

Folio #	I-II	III	IV-V	VI	VII	VIII	IX	X
Proportion of total Surface at this level	10.34% +/- 0.33%	10.09% +/- 0.23%	19.48% +/- 1.63%	16.78% +/- 1.15%	7.59% +/- 0.66%	10.13% +/- 0.50%	19.15% +/- 0.18%	6.43% +/- 0.27%

Table 2. Distribution of folial surface across the cerebellum (hemispheres)

Folial name	LS	Crus1	Crus 2	PML	COP	FLN
Proportion of total Surface at this level	19.29%	27.69%	09.25%	11.91%	24.27%	07.39%
	+/-	+/-	+/-	+/-	+/-	+/-
	0.39%	2.23%	0.49%	1.45%	0.66%	0.19%

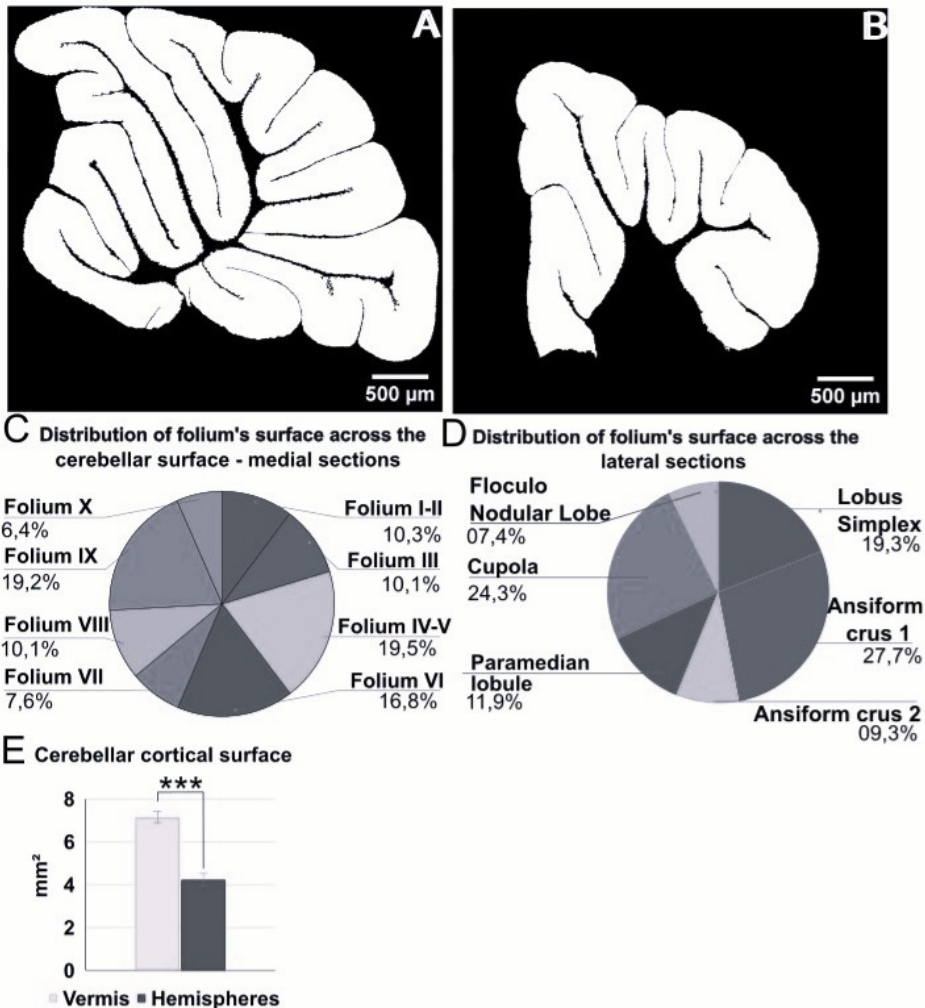


Fig. 1. Surface area of the cerebellar cortex and proportions of the area of individual folia out of the total surface. (A) and (B): digital masks; (E): diagram that represents the cerebellar cortical surface, ***p<0.001; (C) and (D): pie charts showing the representation of the surface of individual cerebellar folium from the total surface area in vermis and hemispheres, ***p<0.001.

Variability of surface area of ML and GL in the Vermis and hemispheres

We investigated the surface area of individual layers in medial and lateral anatomical levels of the adult cerebellum. To this aim, we studied the areas of ML and GL across the entire section of the cerebellar foliation. We performed the measurements following a manual segmentation of the ML and GL (Fig. 2, 3). We estimated the total surface of the ML at $3.791 \text{ mm}^2 \pm 0.139$ in the vermis and $2.274 \text{ mm}^2 \pm 0.107$ in the hemispheres (Fig. 2C, $p < 0.001$). We estimated the total surface of the GL at $3.374 \text{ mm}^2 \pm 0.132$ in the vermis vs $1.968 \text{ mm}^2 \pm 0.183$ in the hemispheres (Fig. 3C, $p < 0.001$). The proportion of the reduction of the total surface of ML and GL in the hemispheres as compared to the Vermis was similar, approx. 40%.

We next measured the thickness of the ML and GL. Unlike the areal measurements, the estimations of the thickness demonstrated that both layers were thicker in the hemispheres as compared to the Vermis. The average ML thickness in the Vermis was $125.555 \mu\text{m} \pm 3.289$, while in the hemispheres it was $149.629 \mu\text{m} \pm 3.412$ (Fig. 2D, $p < 0.001$). The average GL thickness in the Vermis was $121.863 \mu\text{m} \pm 4.102$, while in the hemispheres it was $140.606 \mu\text{m} \pm 7.782$ (Fig. 3D, $p < 0.01$). Thus, the ML was thicker by approx 20% in the hemispheres while the GL thickness increased by approx. 15%.

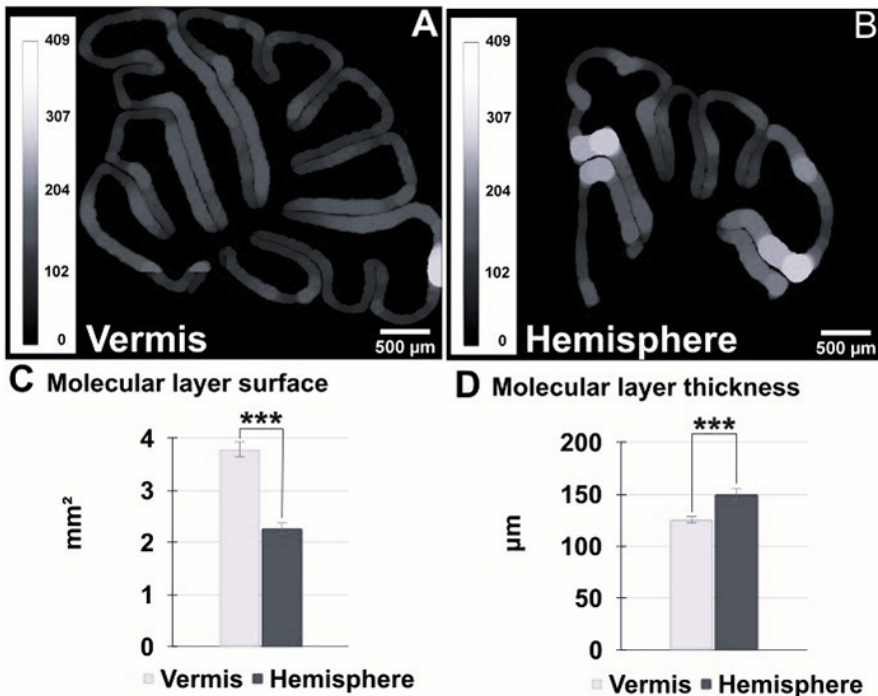


Fig. 2. Surface area and local thickness of the cerebellar molecular layer. (A) and (B): heat maps that represent the surface area and the local thickness of the molecular layer; (C) and (D): diagrams of surface and local thickness of the cerebellar molecular layer in the vermis and hemispheres, $*** p < 0.001$.

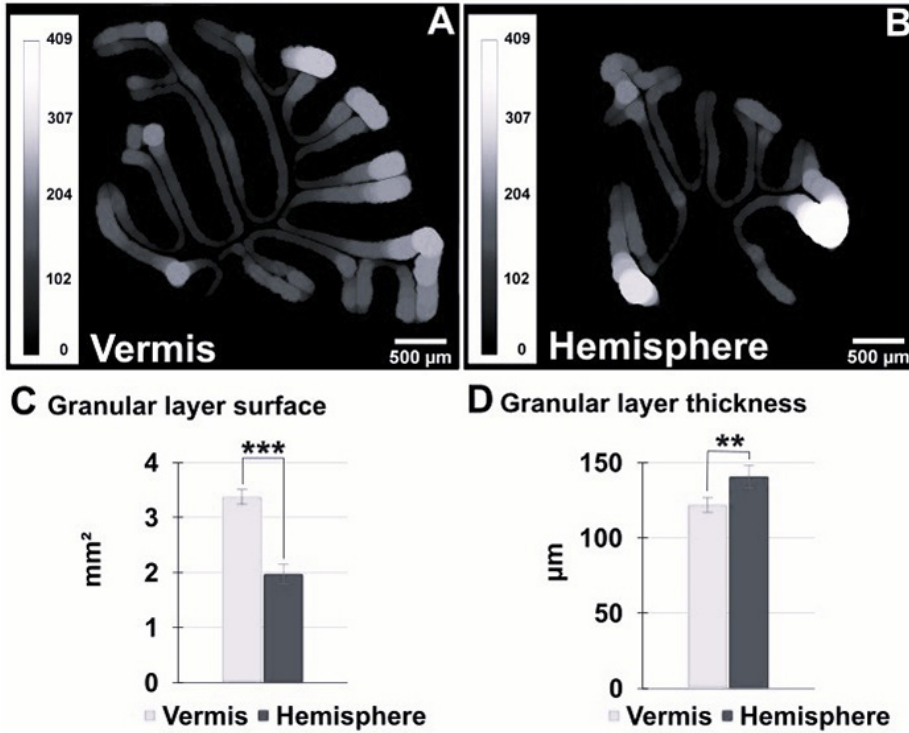


Fig. 3. Surface area and local thickness of the cerebellar granular layer. (A) and (B): heat maps that represent the surface area and the local thickness of the granular layer; (C) and (D): diagrams of the surface and local thickness of the cerebellar granular layer in vermis and hemispheres, *** $p < 0.001$, ** $p < 0.01$.

We also measured the length of the PCL (Fig. 4). In the vermis was 30.399 mm \pm 4.102 vs 16.048 μm^2 \pm 0.939 in the hemispheres (Fig. 4C, $p < 0.001$). Again, here we observed a decrease in the total length by nearly half – 46% in the hemispheres compared to the vermis.

Discussion

This is the first study showing the regional differences (between Vermis and hemispheres) in the surface area and the thickness of the cortex and its components, as well as the length of the Purkinje cell layer. The first main goal of our study was to compare the cerebellar cortical surface in the Vermis and hemispheres. Recent data show differences in the packing densities and cell size for different cell subpopulations (PC, Golgi neurons, granule cells) in the Vermis versus hemispheres. Here we aimed to explore whether this applies to its general morphometric description. First, we found that the total area of the cortex is more evenly spread in between the folia of the vermis compared to the hemispheres. More precisely the range between the smallest

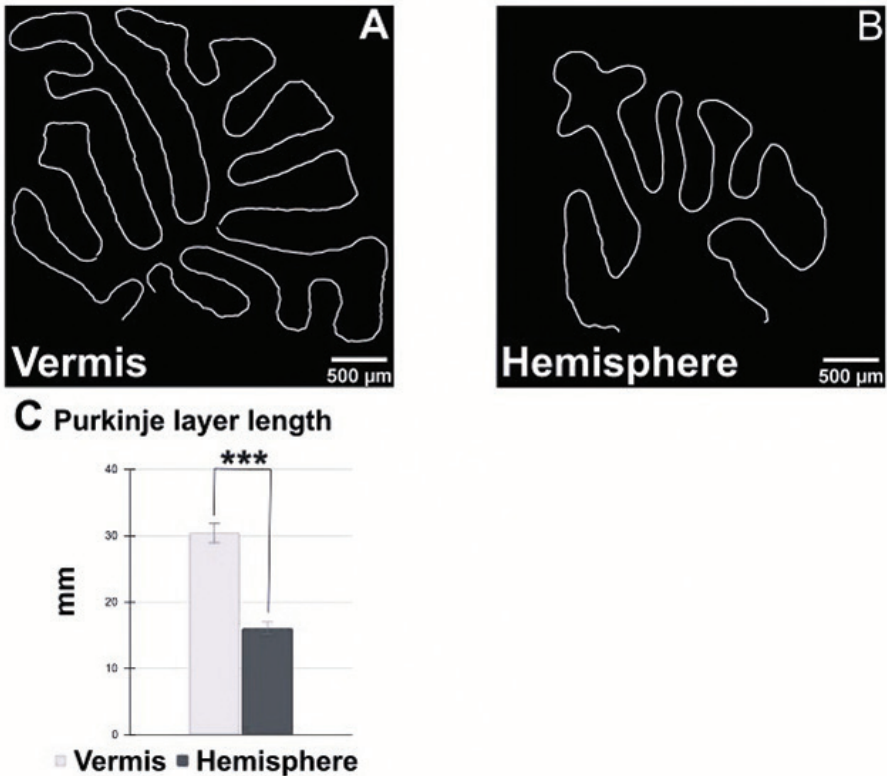


Fig. 4. Length of Purkinje cell layer. (A) and (B): lines that represent the Purkinje cell layer length; (C): diagram of the length in the Purkinje cell layer in Vermis and hemispheres, *** $p < 0.001$.

and biggest folium, as a percent of the total area, was 12.8% for the vermis versus 20.3% for the hemispheres. Our measurements in the Purkinje cell layer length show a severe decrease. That is indicative of the total cortical length and foliation complexity. Interestingly the cerebellar cortex is thicker overall in the hemispheres. This increase in thickness is due to thickening of both the ML and GL, thus the ML/GL thickness ratio is preserved. Our observations confirm previous studies [4, 7] describing that folium crowns have thinner cortices compared to the grooves. This is accompanied by a more densely packed PC and granule cells in the crown regions [2,4, 7]. The general thickening of the cortex in the hemispheres as compared to the Vermis might indicate of the existence of regional differences in cell density and ultrastructural morphology.

Conclusions

Changes in the cerebellar cytoarchitecture occur in various conditions [6, 8, 9, 14, 23]. In one of them – the autistic spectrum disorder (ASD) may reflect a disruption in neuronal networks during development [26, 27]. Our results suggest that the following

morphometric criteria might be used when evaluating morphological changes in different models: (i) the PCL length and cortical surface; (ii) the precise anatomical level (i.e. measurements should be performed at both medial and lateral levels); (iii) quantification of individual layers (i.e. measuring surface and thickness of the GL and ML); (iv) the proportion of each folium out of the total area at any given anatomical level. We hope our results might be helpful in providing a more comprehensive and structured workflow for morphological assessment of the adult cerebellum.

Acknowledgement: This work was funded by the “Science” Fund of the Medical University – Varna, project #20029.

References

1. **Amaral, D. G., M. P. Witter.** The three-dimensional organization of the hippocampal formation: A review of anatomical data. – *Neuroscience*, **31**, 1989, 571–591.
2. **Armstrong, D. M., R. F. Schild.** A quantitative study of the purkinje cells in the cerebellum of the albino rat. – *J. Comparative Neurology*, **139**, 1970, 449-456.
3. **Au, W. W., H. B. Treloar, C. A. Greer.** Sublaminar organization of the mouse olfactory bulb nerve layer. – *J. Comparative Neurology*, **446**, 2002, 68-80.
4. **Braitenberg, V., R. P. Atwood.** Morphological observations on the cerebellar cortex. – *J. Comparative Neurology*, **109**, 1958, 1-33.
5. **Briscoe, S. D., C. W. Ragsdale.** Evolution of the chordate telencephalon. – *Current Biology*, **29**, 2019, R647–R662.
6. **Campbell, D. B., J. B. North, E.J. Hess.** Tottering mouse motor dysfunction is abolished on the Purkinje cell degeneration (pcd) mutant background. – *Experimental Neurology*, **160**, 1999, 268-278.
7. **Cerminara, N. L., E. J. Lang, R. V. Sillitoe, R. Apps.** Redefining the cerebellar cortex as an assembly of non-uniform Purkinje cell microcircuits. – *Nat. Rev. Neurosci.*, **16**, 2015, 79-93.
8. **Danielian, P. S., A. P. McMahon.** Engrailed-1 as a target of the Wnt-1 signalling pathway in vertebrate midbrain development. – *Nature*, **383**, 1996, 332-334.
9. **Engelkamp, D., P. Rashbass, A. Seawright, V. V. Heyningen.** Role of Pax6 in development of the cerebellar system. – *Development*, **126**, 1999, 3585-3596.
10. **Geurts, F. J., J.-P. Timmermans, R. Shigemoto, E. De Schutter.** Morphological and neurochemical differentiation of large granular layer interneurons in the adult rat cerebellum. – *Neuroscience*, **104**, 2001, 499-512.
11. **Guillemot, F.** Cellular and molecular control of neurogenesis in the mammalian telencephalon. - *Current Opinion in Cell Biology*, **17**, 2005, 639-647.
12. **Heuer, K., N. Traut, A. A. De Sousa, S. L. Valk, J. Clavel, R. Toro.** Diversity and evolution of cerebellar folding in mammals. – *eLife*, **12**, 2023, e85907.
13. **Hull, C., W. G. Regehr.** The Cerebellar cortex. – *Annu. Rev. Neurosci.*, **45**, 2022, 151-175.
14. **Isaacs, K. R., L. C. Abbott.** Cerebellar volume decreases in the tottering mouse are specific to the molecular layer. - *Brain Research Bulletin*, **36**, 1995, 309-314.
15. **Kozareva, V., C. Martin, T. Osorno, S. Rudolph, C. Guo et al.** A transcriptomic atlas of mouse cerebellar cortex comprehensively defines cell types. – *Nature*, **598**, 2021, 214-219.

16. **Lara-Aparicio, S. Y., A. J. Laureani-Fierro, C. Morgado-Valle, L. Beltran-Parrazal, F. Rojas-Duran et al.** Latest research on the anatomy and physiology of the cerebellum. – *Neurology Perspectives*, **2**, 2022, 34-46.
17. **Lange, W.** Regional differences in the distribution of golgi cells in the cerebellar cortex of man and some other mammals. – *Cell Tissue Res*, **153**, 1974.
18. **Marzban, H., M. R. Del Bigio, J. Alizadeh, S. Ghavami, R. M. Zachariah, M. Rastegar.** Cellular commitment in the developing cerebellum. – *Front. Cell Neurosci.*, **8**, 2015.
19. **Meek, J.** Functional anatomy of the tectum mesencephali of the goldfish. An explorative analysis of the functional implications of the laminar structural organization of the tectum. – *Brain Research Reviews*, **6**, 1983, 247-297.
20. **Muller, U., H. Heinsen.** Regional differences in the ultrastructure of Purkinje cells of the rat. – *Cell Tissue Res*, **235**, 1984.
21. **Nagayama, S., R. Homma, F. Imamura.** Neuronal organization of olfactory bulb circuits. – *Front. Neural Circuits*, **8**, 2014.
22. **Nevin, L. M., E. Robles, H. Baier, E. K. Scott.** Focusing on optic tectum circuitry through the lens of genetics. – *BMC Biol.*, **8**, 2010, 126.
23. **Rossmann, I. T., E. DiCicco-Bloom.** Engrailed2 and cerebellar development in the pathogenesis of autism spectrum disorders. In: *Autism. Current theories and evidence.* (Ed. A. W. Zimmerman), Humana Press/Springer Nature, 2008, 3-40.
24. **Ullmann, J. F. P., M. D. Keller, C. Watson, A. L. Janke, N. D. Kurniawan et al.** Segmentation of the C57BL/6J mouse cerebellum in magnetic resonance images. – *NeuroImage* **62**, 2012, 1408-1414.
25. **Witter, M. P., F. G. Wouterlood, P. A. Naber, T. Van Haeften.** Anatomical organization of the parahippocampal-hippocampal network. – *Annals of the New York Academy of Sciences*, **911**, 2000, 1–24.
26. **Zhelezov, M.** Microglia as potential regulators of empathy and prosocial behavior – A hypothesis. – *Biomedical Reviews*, **27**, 2017, 69.
27. **Zhelezov, M.** Microglial adipobiology: a new concept for understanding the adipose tissue-brain crosstalk in health and disease. – *Adipobiology*, **10**, 2019, 25.

Aging of the Myenteric Plexus in the Rat Colorectal Region

Nikolay Genov^{1*}, Nikolay Dimitrov¹, Dimitrinka Atanasova^{1,2}

¹ *Department of Anatomy, Faculty of Medicine, Trakia University, Stara Zagora, Bulgaria*

² *Institute of Neurobiology, Bulgarian Academy of Sciences, Sofia, Bulgaria*

*Corresponding author e-mail: nikolay.genov@trakia-uni.bg

In senile organisms various changes occur at the level of the gastrointestinal tract. Not that many studies have been focused on the changes that develop in the connective tissue capsule positioned around the ganglia of the myenteric plexus. The aim of this study is to demonstrate the changes of the connective tissue around the ganglia of the Auerbach plexus. We have studied the colon of Wistar rats and have divided the animals into four groups: 3-months, 18-months, 28- and 48-months. Our study has demonstrated a 65% increase of the area of collagen fibers around the myenteric plexus in the 18- and 48-months old rats in comparison with the 3-months. The Orcein staining for elastic fibers has shown a 40% increase of their area around the myenteric ganglia of the proximal colon of the 18-months animals compared with the 3-months.

Key words: myenteric plexus, rat, colon, colorectal region, connective tissue, collagen fibers, elastic fibers

Introduction

The enteric nervous system (ENS) is a complex network of neurons that plays a major role into gastrointestinal motility, secretion, nutrient uptake [3, 6]. The biggest portion of the cells of the ENS is making the so-called myenteric plexus [10]. In the literature there are various sources that are presenting the existence of a collagen capsule surrounding the ganglia of the myenteric plexus [8]. A lot of studies are pointing at the existence of connective tissue molecules surrounding the ganglia of the Auerbach plexus [2, 6]. In senile organisms a general increase of the amount of that tissue is noticed [8].

The aim of the present study was to determine the overall change of the area of connective tissue elements, collagen and elastic fibers, around the ganglia of the myenteric plexus at the level of the rat large intestine in the different age groups.

Material and Methods

The scientific experiments were conducted on 20 Wistar rats divided into four groups: 3-, 18-, 28- and 48 months old. Their average weight was 180-450 g. The 3-months-old rats were delivered from the vivarium of the Faculty of Medicine at Trakia University – Stara Zagora. The others were obtained from project 13/17 of Trakia University – Stara Zagora, №174.

The animals were housed under an artificial 12-h light/dark cycle and at a temperature of 22 °C. Water and food pellets were supplied *ad libitum*. The experiments in this study were approved by the Research Ethics Committee at the Medical Faculty of Trakia University and the Commission for Ethical Treatment of Animals at the Bulgarian Food Safety Agency. All the experiments were carried out in full agreement with the Directive 2010/63/EU on the protection of animals used for scientific purposes.

All rats were anesthetized with 87 mg ketamine/kg of body weight and 13 mg xylazine/kg after simultaneous intraperitoneal injection and transcardially perfused first with cold 0.05 M phosphate buffered saline (PBS) and after that cold 4% paraformaldehyde (PFA) in 0.1 M phosphate buffer (PB), pH 7.36. The large intestine of the examined animals was dissected and divided into *caecum* (CAE), *proximal colon* (PC), *distal colon* (DC) and *rectum* (REC). The tissue samples were then immersed into the same fixative overnight at 4 °C. After that we followed the standard procedure for embedding the tissue in paraffin. The paraffin blocks were cut into 6 µm sections and were mounted onto chrome-gelatinized glass slides. For the purpose of the experiment we have stained the slides with the following standard histological stains: Azan, van Gieson and Orcein.

The microphotographs have been made with research microscope Leica DM1000 equipped with a digital camera Leica DFC 290. The images were processed with Adobe Photoshop 24.1.0 to achieve better contrast of the stained slides.

The free graphic analyzing software ImageJ (*National Institutes of Health, Bethesda, MD, USA*) was used to perform the morphometric analysis of the connective tissue capsule. In order to make the measurements, each of the microphotographs has been converted into an 8-bit image by the plug-in *Colour Deconvolution2*. That helped us to measure the percentage of the stained collagen and elastic fibers as part of the whole area of the ganglia of the myenteric plexus.

Statistical analysis was performed by GraphPad Prism® 8 software (San Diego, CA, USA). The comparison of the results has been conducted with Kruskal-Wallis Analysis as well as Ordinary one-way ANOVA followed by the multiple comparisons Dunn tests or Sidak's multiple comparisons test for the ordinary one-way ANOVA. Statistically significant differences were considered if p-values were <0.05.

Results

The connective tissue around the ganglia of the Auerbach plexus was presented with Azan, Van Gieson and Orcein staining. The usage of Azan classical histological stain presented the collagen fibers as a green blue network. After measuring the percentage of the collagen fibers as part of the whole area of the ganglia, the Kruskal-Wallis test showed no statistically significant difference between the examine groups: 3m Mdn = 20.98, 18m Mdn = 27.20, 28m Mdn = 23.42; H(2) = 3.157, p = 0.2063.

The acidic fucsin of the Veigert-van Gieson stain colored the collagen fibers in red. The Kruskal-Wallis test showed statistical significant difference between the percentage of the collagen fibers compared to the area of the ganglia in between the different groups of the examined animals: PC 3m (Mdn = 3.55), PC 18m (Mdn = 9.993), PC 48m Mdn = 10.23, DC 3m Mdn = 7.275, DC 18m Mdn = 31.86, DC 48m Mdn = 13.65, REC 3m Mdn = 4.5, REC 18m Mdn = 18.02, REC 48m Mdn = 28.31; $H(8) = 48.99$, $p < 0.0001$. Dunn's multiple comparison test showed that the significant change occurs in between DC 3m and DC 18m ($p < 0.005$), REC 3m and REC 18m ($p < 0.05$), REC 3m and REC 48m ($p < 0.001$).

Orcein stained the elastic fibers around the ganglia of the myenteric plexus in dark brown color. There were statically more elastic fibers in the aged groups: PC 3M Mdn = 8.106, PC 18M Mdn = 13.81, DC 3M Mdn = 5.425, DC 18M Mdn = 7.550, REC 3M Mdn = 13.32, REC 18M Mdn = 8.832; $H(5) = 15.22$.

Frequency distribution showed that the percentage of the collagen fibers around the myenteric plexus ganglia in 18m and 48m PC of Wistar rats has increased with 65% compared with the 3 months of age. At the level of the distal colon the percentage of the collagen capsule compared to the whole area of the ganglia has increased with 75% in comparison with the control. At the level of the rectum collagen capsule has increased with 71% for the first 15 months of the animals' life.

Orcein stained showed an increase of almost 40% of the elastic fibers around the ganglions of the Auerbach plexus of the 18 months rats compared with the 3 months old. This has been identified at the level of the proximal colon.

Discussion

In this study we attempt to present the existence of a structure around the ganglia of the myenteric plexus and to show its change with age. In some literature references the ganglia of the Auerbach's plexus are shown as structures without a capsule but rather directly positioned between the muscle layers of the intestines having a thin layer of fibroblast-like cells [11]. In others they are proving the existence of a capsule made of collagen and elastic fibers that are even piercing in between the perikaryons of the neurons of the myenteric plexus [8, 13]. The collagen structures around the ganglia of the Auerbach's plexus form a basement membrane (BM) [4], a key component of which is collagen type IV [7]. Collagen is one of the most abundant glycoproteins in the human body and is also a key component of the extracellular matrix (ECM) [12]. The usage of Azan and van Gieson stain helped us identify a well-defined collagen structure around the ganglia of the myenteric plexus at all of the levels of the large intestine. Some researchers are pointing to van Gieson as an exemplary method for representing the accumulation of collagen type I [9]. Recent studies show the existence of 28 different subtypes of collagen, some being fibril-forming (I, II, III) and others being network-forming, such as collagen type IV [14]. The increased number of stained structures around Auerbach's plexus by van Gieson in the aged animals could be related to the fibrotic shift of the collagen in the BM of the myenteric plexus.

In literature we have found that with age the amount of collagen and elastic tissue around the myenteric plexus increases [8] and other sources have pointed out that the total deposition of collagen in the aging intestines increases with about 16% [1].

Our study has proven the existence of a collagen capsule around the neurons of the myenteric plexus and has given a detailed characteristic of it at the different levels of the large intestine. We have identified the change of the collagen and elastic fibers with age but in contrast with literature the increase was significantly bigger and statistically significant on almost all the levels of *intestinum crassum*. That increase of the connective tissue deposition around the ganglia of the myenteric plexus could be in direct connection with the decreased motility of the intestines which has been presented as one of the main changes that occur at the level of the aging colon [12].

The method we used to conduct our morphometric analysis could be criticized but we are looking forward to use electron microscopy as well as confocal microscopy to define the changes that occur at molecular level as well as to study the specific proteins that increase or decrease at the aging myenteric plexus.

Conclusions

This is one of the few studies of that focuses on the connective tissue capsule positioned around the myenteric plexus. We have identified a significant change in the collagen and elastic fibers around the ganglia of the aging animals. Further studies are needed to determine the specific type of collagen that accumulates around the plexus. More work is required to evaluate the clinical significance of the observed change.

Acknowledgements. This research was funded by the Bulgarian Ministry of Education and Science under the National Program “Young Scientists and Postdoctoral Students – 2” program and the National Recovery and Resilience Plan (Project BG-RRP-2.004-0006-C02), as well as the Faculty of Medicine, Trakia University – Stara Zagora (Grant No. 8/2023).

References

1. **Baidoo, N., E. Crawley, C. H. Knowles, G. J. Sanger, A. Belai.** Total collagen content and distribution is increased in human colon during advancing age. – *PLoS One*, **17**(6), 2022, e0269689.
2. **Bannerman, P. G., R. Mirsky, K. R. Jessen, R. Timpl, V. C. Duance.** Light microscopic immunolocalization of laminin, type IV collagen, nidogen, heparan sulphate proteoglycan and fibronectin in the enteric nervous system of rat and guinea pig. – *Journal of Neurocytology*, **15**(6), 2986, 733–743.
3. **Brehmer, A.** Classification of human enteric neurons. – *Histochem. Cell Biol.*, **156**(2), 2021, 95-108.
4. **Dora, D., S. Ferenczi, R. Stavely, V. E., Toth, Z. V. Varga et al.** Evidence of a myenteric plexus barrier and its macrophage-dependent degradation during murine colitis: Implications in enteric neuroinflammation. – *Cellular and Molecular Gastroenterology and Hepatology*, **12**(5), 2021, 1617–1641.
5. **Filpa, V., M. Bistoletti, I. Caon, E. Moro, A. Grimaldi et al.** Changes in hyaluronan deposition in the rat myenteric plexus after experimentally-induced colitis. – *Scientific Reports*, **7**(1), 2017, 17644.
6. **Furness J. B.** The enteric nervous system and neurogastroenterology. – *Nat. Rev. Gastroenterol. Hepatol.* **9**(5), 2012, 286-294.
7. **Gatseva, A., Y. Y. Sin, G. Brezzo, T. Van Agtmael.** Basement membrane collagens and disease mechanisms. – *Assays in Biochemistry*, **63**(3), 2019, 297-312.

8. **Gomes, O. A., R. R. de Souza, E. A. Liberti.** A preliminary investigation of the effects of aging on the nerve cell number in the myenteric ganglia of the human colon. – *Gerontology*, **43**(4), 1997, 210-217.
9. **Guo, S. B., Z. J. Duan, Q. M. Wang, Q. Zhou, Q. Li, X. Y. Sun.** Endogenous carbon monoxide hepatic cystathionine- γ -lyase in rats with liver cirrhosis. – *Experimental and Therapeutic Medicine*, **10**(6), 2015, 2039-2046.
10. **Itsev, D.** Pre- and postnatal development of the enteric nervous system and endocrine cells in the human gut. *PhD Thesis*, 1990. [in Bulgarian]
11. **Komuro, T., P. Baluk, G. Burnstock.** An ultrastructural study of neurons and non-neuronal cells in the myenteric plexus of the rabbit colon. – *Neuroscience*, **7**(7), 1982, 1797–1806.
12. **Madsen, J. L.** Effects of gender, age, and body mass index on gastrointestinal transit times. – *Digestive Diseases and Sciences*, **37**(10), 1992, 1548-1553.
13. **Rodrigues de Souza, R., C. A. Ferraz de Carvalho, I. Watanabe.** Identification of collagen, elastic, elaunin and oxytalan fibres in ganglia of the myenteric plexus of the human oesophagus. – *Anatomy and Embryology*, **179**(1), 1988, 97-102.
14. **Tvaroška, I.** Glycosylation modulates the structure and functions of collagen: A review. – *Molecules* (Basel, Switzerland), **29**(7), 2024, 1417.

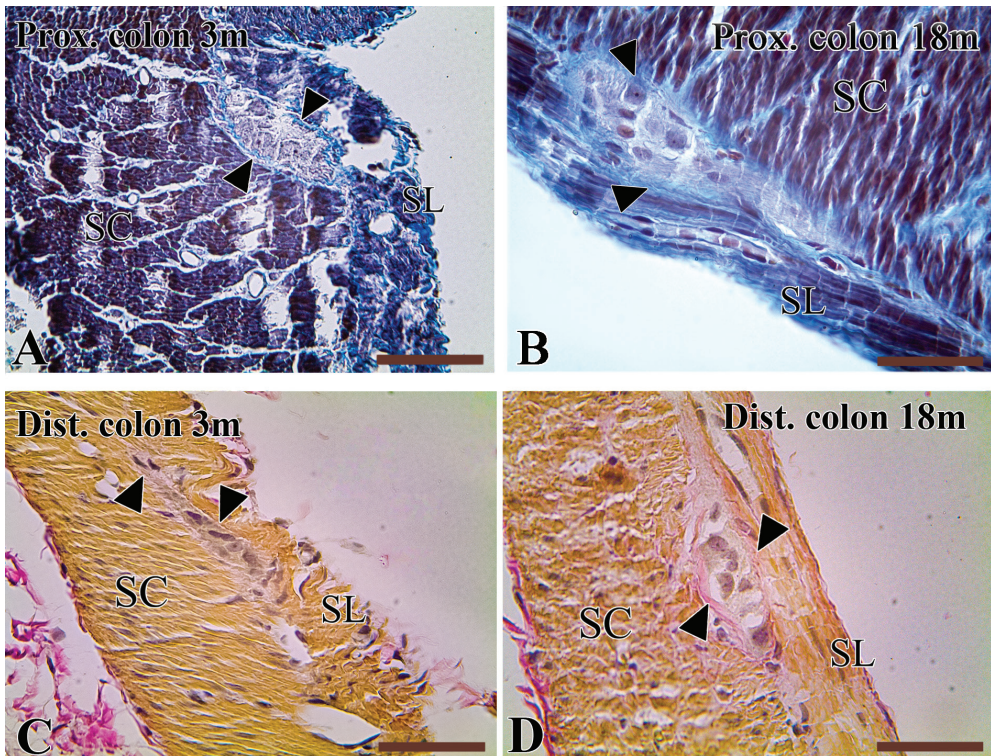


Figure 1. Azan (A-B) and van Gieson (C-D) staining of sagittal cut of proximal colon (A-B) and distal colon (C-D) of a 3 month (A, C) and 18 month (B, D) Wistar rat. Arrowheads indicate the collagen fibers that are encapsulating the ganglia of the myenteric plexus. SC-stratum longitudinale, SC- stratum circularare. Scale bars: 50 μ m.

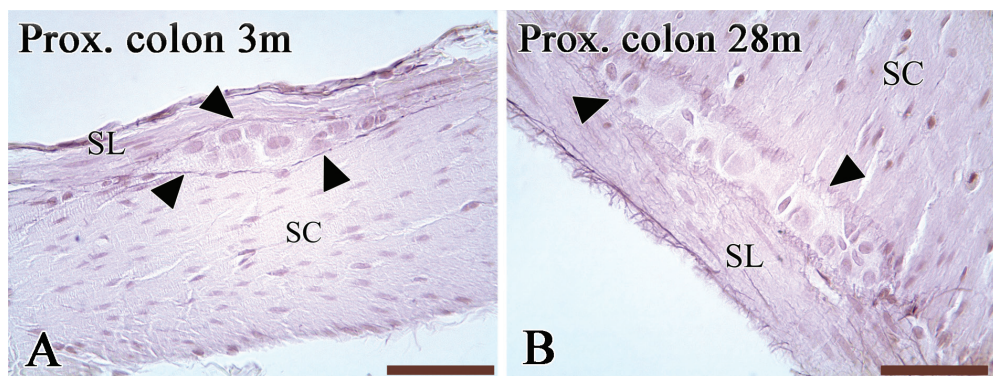


Figure 2. Orcein staining (A-B) of sagittal cut of proximal colon of a 3 month (A) and 28 month (B) Wistar rat. Arrowheads indicate the elastic fibers that are positioned around the ganglia of the Myenteric plexus. SC-*stratum longitudinale*, SC-*stratum circularare*. Scale bars: 50 μ m.

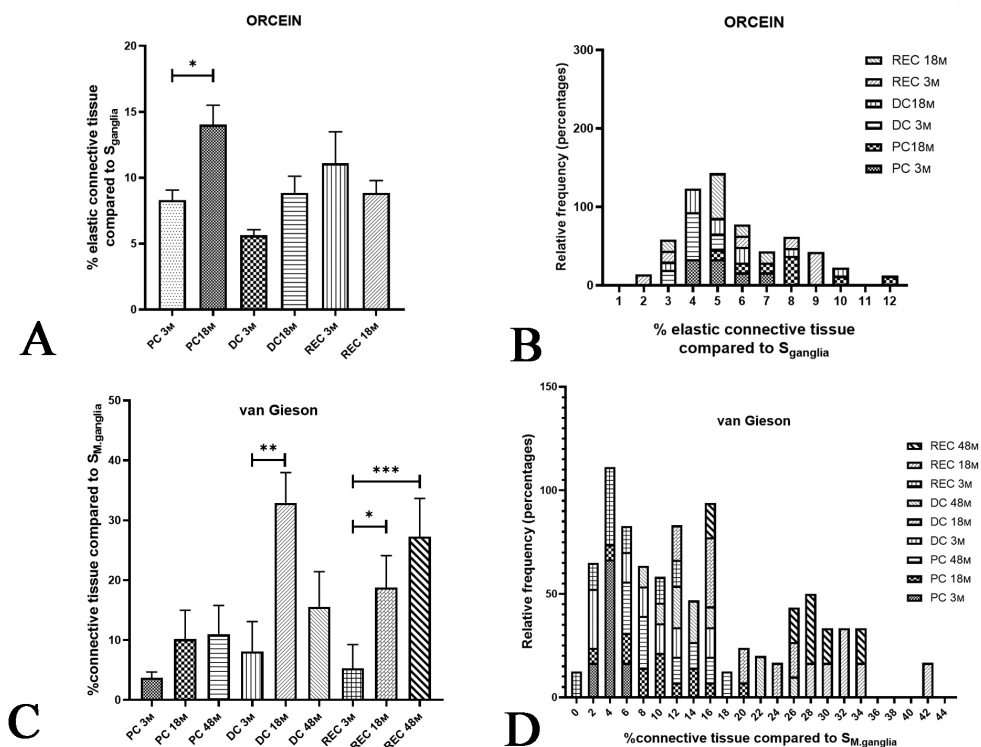


Figure 3. Histograms showing statistical comparison of the percentage of the area of the elastic fibers stained with Orcein (A) and collagen fibers stained with van Gieson (B) surrounding the ganglia and the whole area of the ganglia from the rat myenteric plexus. The line represents S.E.M. The data is compared using the Sidak's multiple comparisons test and Kruskal-Wallis test, where $p^* < 0.05$, $p^{**} < 0.01$, $p^{***} < 0.001$. Histograms showing the relative frequency in percent of a distribution of values for the percentage area of elastic fibers (B) and collagen fibers (D).

Alterations in the expression of TfR1, DMT-1 and Hepcidin in immature mice liver after chronic exposure to cobalt chloride

Anastasija Ilovska, Yordanka Gluhcheva*

Institute of Experimental Morphology, Pathology and Anthropology with Museum, Bulgarian Academy of Science, Sofia, Bulgaria

*Corresponding author e-mail: ilovskaanastasija@yahoo.com

Cobalt (Co) is an essential trace element and its cellular uptake follows a similar pattern to that of iron (Fe). Our aim was to study the effects of perinatal cobalt chloride (CoCl₂) exposure on iron homeostasis through changes in the expression of iron regulatory proteins - transferrin receptor 1 (TfR1), divalent metal transporter 1 (DMT-1) and hepcidin (Hepc) in the liver of 30-day old mice. Pregnant mice and their progeny were treated with daily doses of 75 mg/kg b.w. (low dose) or 125 mg/kg b. w. (high dose) CoCl₂ until postnatal day 30. The results show that prenatal and early postnatal exposure to CoCl₂ exerts a toxic effect on the liver, reducing the organ weight index and altering the expression profile of the proteins involved in iron metabolism regulation. Weaker expression of TfR1 and DMT-1 was observed in the samples of mice exposed to the low dose CoCl₂.

Key words: cobalt chloride, iron-regulatory proteins, liver, in vivo model, toxicity

Introduction

Cobalt (Co) is an essential trace element for human and animals, but high doses can negatively affect human health. The average daily intake of Co ranges from 5 to 45 µg, with food sources such as leafy vegetables, meat, fish, dairy products, and drinking water being the main contributors of cobalt in the general population's diet. Organic Co plays a key role as a metal component in vitamin B12 (cyanocobalamin), while inorganic cobalt compounds are considered toxic to both the environment and humans when present to excessive levels [4]. Studies on long-term exposure of laboratory animals to Co ions show that they accumulate in organs such as kidney, liver, spleen, heart, stomach, intestines, muscle, brain and testis [6]. The concentration of Co is also elevated in blood, serum and urine [14]. If cobalt concentration exceeds normal levels in the body, its ions compete with iron (Fe) for

binding to macromolecules, disrupting the activity of iron-regulatory proteins and altering various biochemical pathways [5].

The existing data suggest that Co is taken up by cells through transferrin receptors interaction, with an uptake pattern similar to that of iron. The serum iron transport protein- transferrin (Tf) can carry not only two Fe^{3+} , but also other metal ions, such as cobalt. Diferic Tf is bound to membrane TfR1 and then internalized by clathrin-dependent endocytosis. Iron, following its reduction to Fe^{2+} by STEAP3, is then exported to the cytosol via divalent metal transporter 1 (DMT-1), and TfR1 is recycled back to the cell surface [18]. Iron is either used in metabolic processes, such as the synthesis of hemoproteins and Fe-S clusters, transferred to the labile iron pool, or exported from the cell by ferroportin (FPN) [2]. Iron metabolism is regulated through the hepcidin/ ferroportin axis at the systemic level, with hepcidin acting as a negative regulator of iron flow.

There are limited data on the *in vivo* effects of Co exposure on tissue-specific expression of proteins involved in iron metabolism (TfR1, DMT1, Hpc) and their complex interactions, along with the associated health risks. The aim of the present study is to investigate the alterations in Fe- regulatory proteins (TfR1, DMT-1, hepcidin) expression in the liver of immature (30-day-old) mice after chronic exposure to cobalt chloride.

Materials and Methods

I. Experimental design

Experimental animals were purchased from the Experimental and breeding base for laboratory animals (EBBLA) – Slivnitsa, Bulgaria. After one-week acclimatization female ICR (Institute of Cancer Research) mice were mated to male ICR mice. Once pregnancy was confirmed, the female ICR mice were placed in individual standard polypropylene cages and treated 2-3 days before delivery with cobalt chloride ($\text{CoCl}_2 \times 6\text{H}_2\text{O}$) at a daily dose of 75 mg/kg b.w. (low dose) or 125 mg/kg b.w. (high dose) until the offspring reach 30 days of age. CoCl_2 was dissolved in tap water to ensure that mice obtained the required daily dose. The mothers were provided with 15 ml per day and the 25-day-old mice received 3 ml of the solution. Mice were kept in the institute's animal facility at a temperature of 23 ± 2 °C, with a 12:12h light- dark cycle. The weight changes of the experimental mice were monitored weekly to adjust the dosage accordingly. Additionally, the daily consumption of the test solution or tap water was monitored. On postnatal day 25 the pups were housed in individual cages to ensure equal access to the solution. The treatment continued until postnatal day 30. Age-matched animals obtaining regular tap water, served as controls. The newborn pups were sacrificed on day 30, and their livers were excised and prepared for future analysis. No significant differences were observed in the indicators between male and female experimental animals, which is why both sexes are included in the present study.

The experimental design was carried out in accordance with to the ARRIVE (Animal Research: Reporting of In Vivo Experiments) guidelines and EU Directive 2010/63/EU for animal experiments. The study was approved by the Bulgarian Agency for Food Safety, Approval number 282 from 24.09.2020.

II. Morphological studies

Liver's tissue samples were fixed in Bouin solution for 24 hours, dehydrated in an ascending alcohol series up to 100%, cleared with xylene, impregnated in molten paraffin and then embedded in fresh molten paraffin. The tissues were cut to 5 μm thick sections, which were later used for immunohistochemical studies.

II.a. Liver index

Livers of controls and Co-treated mice were excised, weighed and liver index was calculated as a ratio of liver weight to body weight.

II.b Immunohistochemistry for TfR1, hepcidin and DMT-1

All incubations were conducted at room temperature, unless stated otherwise. Initially, the 5 μm sections of control and Co-treated animals were deparaffinated and rehydrated, then heated in 0.01M citrate buffer (pH 6.0) for antigen retrieval. In the case of DMT1, a 0.05M glycine buffer (pH 3.5 and 0.01% EDTA) was used. Endogenous peroxidase activity was blocked with 3% H_2O_2 dissolved in methanol, followed by four 5-minute washes in TBS. To block nonspecific background staining, the sections were incubated for 5 minutes with Super Block. After the 5-minute washing steps were repeated, a blocking kit containing avidin and biotin (Vector Laboratories, Inc., CA, USA) was added to block endogenous biotin. Primary rabbit polyclonal anti-TfR1 antibody, anti-hepcidin antibody and anti-DMT1 antibody were added (for TfR1- 1:100, for hepcidin- 1:400, for DMT1- 1:100; Wuhan Elabscience Biotechnology Co. Ltd., China) and the samples were incubated overnight at 4°C. After four 5-minute washes in TBS, sections were incubated with a biotinylated secondary antibody. After four additional 5-minute washes in TBS, sections were incubated with anti-rabbit UltraTek HRP for 10 min (UltraTek HRP Anti-Mouse Staining System, ScyTek Laboratories, USA). Sections were washed four times in TBS, and the immunohistochemical reaction was visualized with 3,3'-diaminobenzidine (liquid DAB; DAKO Corp.). The reaction was stopped with water and then the sections were counterstained with hematoxylin and mounted in Entellan. The sections were observed under a Leica DM 5000B light microscope (Leica Microsystems, USA).

Negative controls were represented by samples incubated without the primary antibody.

III. Statistical analysis

The results are presented as mean values \pm Standard Deviation (SD). The significance of the differences between the experimental groups was assessed using one-way ANOVA with Bonferroni post-hoc test at a significance level of $p < 0.05$.

Results and Discussion

Previous studies show that cobalt is transferred from food into the mother's milk [10], which means that the newborn pups were exposed to Co during their nursing period. The body weight of Co-exposed animals was affected by chronic treatment with CoCl_2 , indicating potential changes in liver weight index as well.

Prenatal and early postnatal exposure to CoCl_2 resulted in a decreased liver index, with the reduction being significant ($p \leq 0.001$) in the mice exposed to the higher dose of CoCl_2 (125 mg/kg b.w.) (**Fig. 1**). Hepatocytes are crucial targets in both acute and chronic toxicity. Subsequently, the liver index is an important indicator in toxicological studies. It reflects the impact of various hepatotoxins, and its decrease is usually associated with a reduction in functional activity and/or hepatocellular damage [1]. The significant reduction in the liver index after chronic CoCl_2 intake demonstrates its toxic effects in 30-day-old immature mice. A lower liver index has also been observed when the experimental animals were treated with other metals, such as cadmium and lead [20]. The liver is responsible for synthesis of key factors in iron metabolism; therefore, changes in liver index will lead to alterations in Fe content. Our previous data revealed significantly increased iron levels in the liver tissue following exposure to CoCl_2 [9].

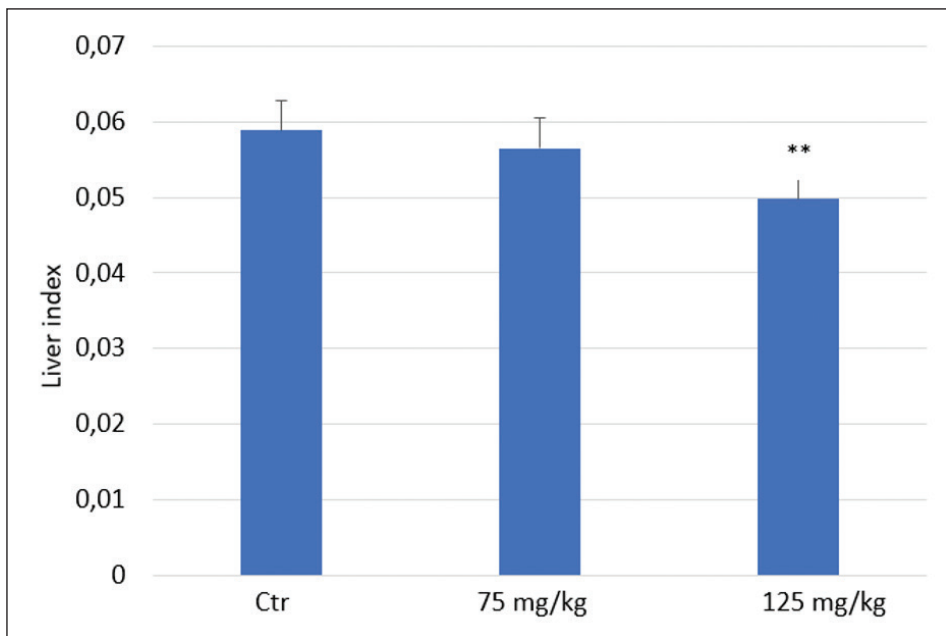


Fig. 1. Changes in liver index (liver weight to body weight ratio) of day 30 control and Co-exposed mice. ** $p < 0.01$

Changes in the expression of the Fe-regulatory proteins TfR1, hepcidin and DMT-1 were observed by immunohistochemistry of liver sections from both control and Co- treated mice. TfR1 is ubiquitously expressed and post-transcriptionally regulated by iron status via the iron regulatory protein system, leading to an increase in TfR1 under low iron conditions and a decrease TfR1 under high iron conditions [3]. We found that TfR1 expression in cobalt-treated 30-day-old mice is primarily detected in Kupffer cells, whereas TfR1 expression in control samples is periportal. When treated with high dose of CoCl_2 (125 mg/kg b.w.), receptor expression is not only found in Kupffer cells, but is also periportal (**Fig. 2**) indicating altered pattern of TfR1 distribution in the

liver tissue. Expression of TfR1 is known to be upregulated by hypoxia and CoCl_2 is the most commonly used hypoxia-mimicking agent in experimental studies [11]. Our novel data for altered pattern of TfR1 protein expression could be due to cobalt-induced hypoxia rather than iron concentration. The previous scientific data showed that iron accumulation gradient decreased towards the central part of the lobule (periportal). In cases of iron overload, this gradient is even more pronounced [7]. Our data for pronounced expression of TfR1 in Co-exposed mice with a high daily dose of CoCl_2 could explain increased iron concentrations in the liver of treated mice. On the other hand, it has been proven that transferrin receptors also bind cobalt, as the mechanism of interaction and accumulation in cells is similar to that of iron [15].

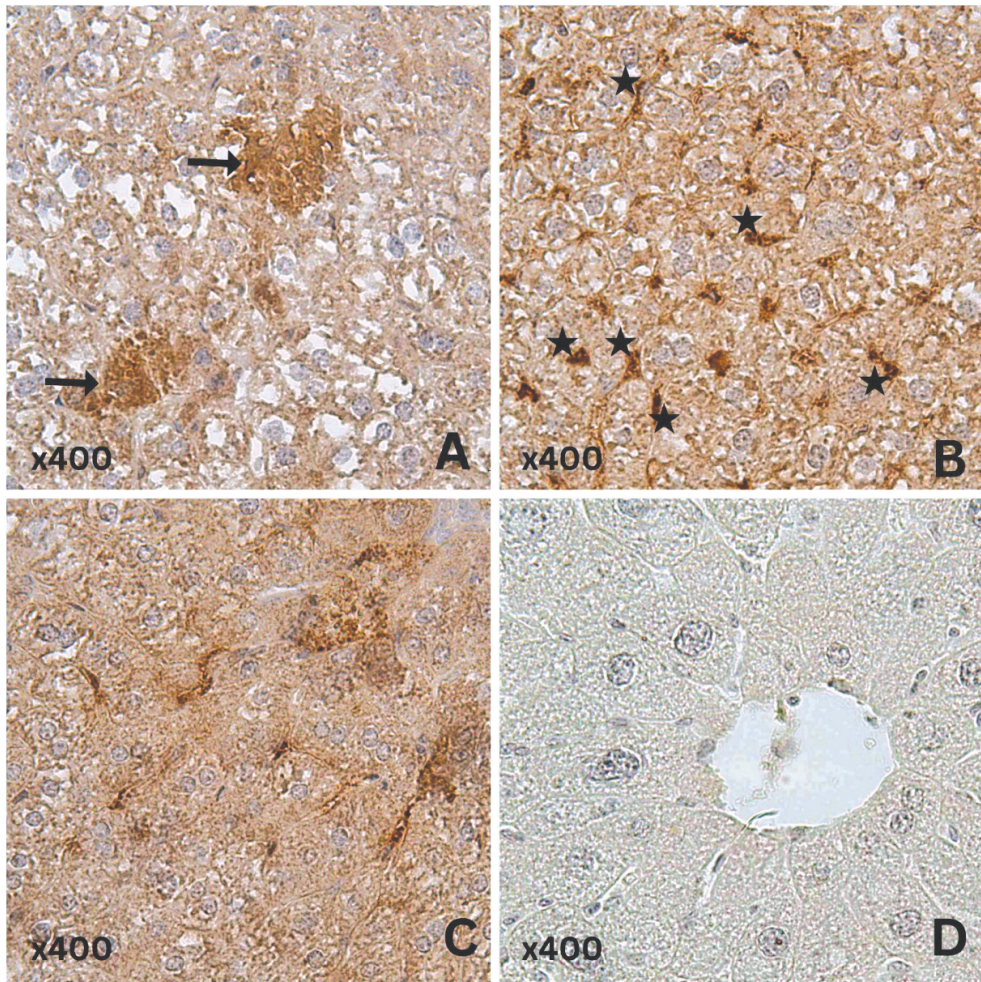


Fig. 2. Immunohistochemical expression of TfR1 in immature mouse liver: Control (A), 75 mg/kg CoCl_2 (B), 125 mg/kg CoCl_2 (C), negative control (D). TfR1 immunoreactivity in the periportal (arrows) and Kupffer cells (stars). $\times 400$

Our new findings showed that Hepcidin is weakly visualized in the cytoplasm of hepatocytes in the liver of controls and is slightly increased in the CoCl_2 treated experimental groups (**Fig.3**). Hepcidin has a key role to systemic iron regulation, which means that any changes in its expression are of critical importance. Studies show that hepcidin is highly expressed in the liver and has also been detected in various other tissues, including the heart, adipose tissue, alveolar and splenic macrophages, the retina, and different regions of the brain [13]. Hepcidin expression is regulated by body iron levels and rises when iron concentration is high. According to the scientific literature, cobalt-induced hypoxia suppresses hepcidin expression. On the other hand, it has been established that activation of Kupffer cells inhibits hepcidin expression [17]. Furthermore, the weaker hepcidin expression after CoCl_2 exposure might stimulate erythropoiesis, which is known to reduce hepcidin concentration [12].

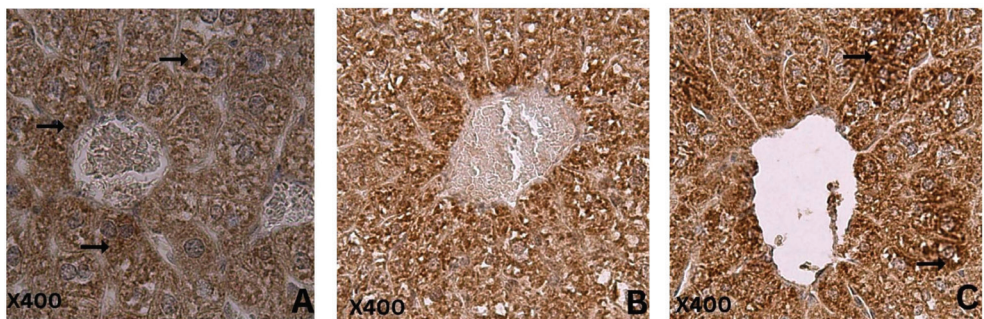


Fig. 3. Immunohistochemical expression of hepcidin in immature mouse liver: Control (A), 75 mg/kg CoCl_2 (B), 125 mg/kg CoCl_2 (C). Hepcidin immunoreactivity in the hepatocytes (arrows). $\times 400$

Expression of DMT-1 was observed in hepatocytes located near the central vein of the hepatic lobule, as well as in the endothelial cells of blood vessels. Notably, weaker protein expression of the protein was seen in liver sections from mice treated with a low dose of CoCl_2 (**Fig. 4**), whereas treatment with high dose did not produce any changes in intensity of immunostaining. According to the literature, DMT-1 is expressed in liver hepatocytes and participates in the regulation of iron metabolism by importing iron bound to transferrin or non-transferrin-bound iron [19]. To date, the role of DMT-1 in hepatocytes *in vivo* concerning iron metabolism remains unclear and our data provide new knowledge to DMT-1 regulation in the liver. It is known that weak expression of DMT1 is associated with increased oxidative phosphorylation and glycolysis, which serves as an early signal for tumor recurrence in patients who have undergone surgery for hepatocellular carcinoma [8]. In addition to iron, DMT-1 also binds and transports other divalent metal ions, such as cobalt, which could explain altered expression in CoCl_2 -treated animals.

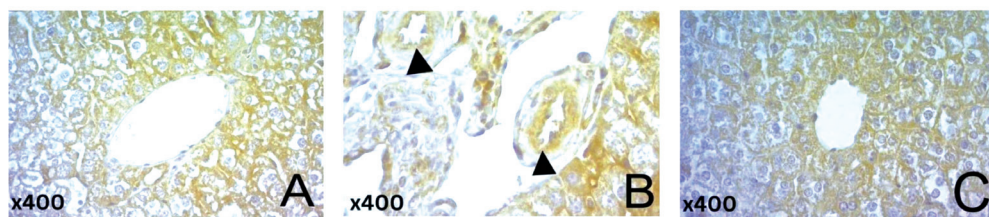


Fig. 4. Immunohistochemical expression of DMT1 in immature mouse liver: Control (A), Blood vessel of the control (B), 75 mg/kg CoCl₂ (C). DMT1 immunoreactivity in the endothelial cells (arrowheads). ×400

Conclusion

Although cobalt is an essential trace element, it can cause serious damage when present in high concentration and with long-term exposure. In our study, prenatal and early postnatal exposure to CoCl₂ exerts a toxic effect on the liver, reducing the liver index and altering the activity of proteins involved in iron metabolism regulation. Chronic intake leads to significant iron accumulation in the liver, resulting from altered pattern of TfR1 protein expression and slightly suppressed expression of hepcidin. Our novel data on altered expression of iron regulatory proteins (TfR1, hepcidin and DMT-1) under chronic CoCl₂ exposure suggested that cobalt regulates their expression via diverse mechanisms. Enhanced erythropoiesis significantly reduces hepatic hepcidin production in both mice and humans, promoting the increased transfer of dietary iron and stored iron into the bloodstream for the synthesis of heme and hemoglobin by developing erythrocytes in the bone marrow [16]. Our study indicates that erythropoiesis plays a key role in regulating iron metabolism by inhibiting hepcidin production.

Acknowledgements. This work was supported by Grant No. DNTS/Russia 02/1/14.06.2018 from the Bulgarian National Science Fund.

References

1. **Cattley, R., J. Cullen.** Liver and Gall Bladder. - In: *Haschek and Rousseaux's Handbook of Toxicologic Pathology*, **3**, 2013, 1509–1566.
2. **Drakesmith, H., E. Nemeth, T. Ganz.** Ironing out Ferroportin. - *Cell Metab.*, **22**, 2015, 777-787.
3. **Fisher, A. L., C.Y. Wang, Y. Xu, K. Joachim, X. Xiao, S. Philips, G. A. Moschette, V. M. Alfaro- Magallanes, J. L. Babitt.** Functional role of endothelial transferrin receptor 1 in iron sensing and homeostasis. - *Am. J. Hematol.*, **97**, 2022, 1548-1559.
4. **Genchi, G., G. Lauria, A. Catalano, A. Carocci, M. S. Sinicropi.** Prevalence of Cobalt in the Environment and Its Role in Biological Processes. - *Biology (Basel)*, **12**, 2023, 1335.
5. **Gleason, J. E., D. J. Corrigan, J. E. Cox, A. R. Reddi, L. A. McGinnis, V. C. Culotta.** Analysis of hypoxia and hypoxia-like states through metabolite profiling. - *PLoS One*, **6**, 2011, 24741.
6. **Gluhcheva, Y. G., V. N. Atanasov, J. M. Ivanova, E. H. Pavlova.** Chronic exposure to cobalt compounds — an *in vivo* study. - *Cent. Eur. J. Biol.*, **9**, 2014, 973–981.

7. **Graham, R. M., A. C. Chua, C. E. Herbison, J. K. Olynyk, D. Trinder.** Liver iron transport. – *World J. Gastroenterol.*, **13**, 2007, 4725–4736.
8. **Hoki, T., E. Katsuta, L. Yan, K. Takabe, F. Ito.** Low DMT1 Expression Associates With Increased Oxidative Phosphorylation and Early Recurrence in Hepatocellular Carcinoma. – *J. Surg. Res.*, **234**, 2019, 343-352.
9. **Ilovska, A.** The effect of chronic treatment with cobalt chloride on iron metabolism in the liver of immature mice. *BSc thesis*, Sofia University “St. Kliment Ohridski“, 2024, p.54.
10. **Kincaid, R. L., M. T. Socha.** Effect of Cobalt Supplementation During Late Gestation and Early Lactation on Milk and Serum Measures1. – *J. Dairy Sci.*, **90**, 2007, 1880–1886.
11. **Muñoz-Sánchez, J., M. E. Cháñez-Cárdenas.** The use of cobalt chloride as a chemical hypoxia model. - *J. Appl. Toxicol.*, **39** (4), 2019, 556–570.
12. **Nemeth, E., T. Ganz.** Hcpidin and Iron in Health and Disease. – *Annu. Rev. Med.*, **74**, 2023, 261-277.
13. **Rishi, G., V. N. Subramaniam.** The liver in regulation of iron homeostasis. – *Am. J. Physiol. Gastrointest. Liver Physiol.*, **313**, 2017, 157-165.
14. **Simonsen, L. O., A. M. Brown, H. Harbak, B. I. Kristensen, P. Bennekou.** Cobalt uptake and binding in human red blood cells. - *Blood Cells Mol. Dis.*, **46**, 2011, 266-276.
15. **Smith, T.** Human serum transferrin cobalt complex: Stability and cellular uptake of cobalt. – *Bioorg. Med. Chem.*, **13**, 2005, 4576–4579.
16. **Srole, D. N., T. Ganz.** Erythroferrone structure, function, and physiology: Iron homeostasis and beyond. – *J. Cell Physiol.*, **236**, 2021, 4888–4901.
17. **Theurl, M., I. Theurl, K. Hochegger, P. Obrist, N. Subramaniam, N. Rooijen, K. Schuemann, G. Weiss.** Kupffer cells modulate iron homeostasis in mice via regulation of hepcidin expression. – *J. Mol. Med. (Berl)*, **86**, 2008, 825-835.
18. **Vogt, A. S., T. Arsiwala, M. Mohsen, M. Vogel, V. Manolova, M. F. Bachmann.** On Iron Metabolism and Its Regulation. – *Int. J. Mol. Sci.*, **22**, 2021, 4591.
19. **Wang, C. Y., M. Knutson.** Hepatocyte divalent metal-ion transporter-1 is dispensable for hepatic iron accumulation and non-transferrin-bound iron uptake in mice. – *Hepatology*, **58**, 2013, 788-798.
20. **Zou, H., J. Sun, B. Wu, Y. Yuan, J. Gu, J. Bian, Z. Liu, Z. Liu.** Effects of Cadmium and/ or Lead on Autophagy and Liver Injury in Rats. – *Biol. Trace Elem. Res.*, **198**, 2020, 206-215.

Pathogenesis and Diagnostic Complexities of Granuloma Faciale

Mary Gantcheva^{1, 2 *}, Valentina Broshtilova³

¹ Institute of Experimental Morphology, Pathology and Anthropology with Museum, Bulgarian Academy of Science, Sofia, Bulgaria

² Acibadem City Clinic Mladost, Sofia, Bulgaria

³ Department of Internal Diseases, Pharmacology and Clinical Pharmacology, Pediatrics, Epidemiology, Infectious diseases and Skin diseases, Faculty of Medicine, Sofia University “St. Kliment Ohridski”, Sofia, Bulgaria

*Corresponding author e-mail: mary_gant@yahoo.com

We present a case with granuloma faciale – a rare and idiopathic disorder characterized by the formation of asymptomatic red-brown plaque, most commonly on the face. Correct diagnosis of the disease requires a histopathological examination. Despite of the name, there are no granulomas but rather an eosinophil and neutrophil predominant infiltrate and a leucocytoclastic vasculitis with a typical grenz zone. Etiology is unknown and usually there is a therapeutic resistance, which determines a chronic-recurrent course with a psycho-emotional tension from the patient.

Key words: Granuloma faciale, Grenz zone, tissue eosinophilia, histology

Introduction

Granuloma faciale (GF) is a rare, chronic inflammatory dermatosis that belongs to the group of idiopathic eosinophilic dermatoses. These conditions, which include several rare dermatological syndromes of unclear etiology, are characterized by tissue eosinophilia as a central pathogenetic feature. GF presents with a distinctive clinical appearance, characteristic histopathological findings, and a chronic-recurrent course, often with partial therapeutic resistance.

Granuloma faciale is generally benign, without systemic involvement, and its etiopathogenesis remains unclear. The disease most commonly affects middle-aged white men. Skin lesions typically appear as erythema-infiltrative plaques with a raised border and a slightly sunken, livid center. The disease may start with solitary papules or nodules that grow peripherally and may coalesce. The lesions can reach several

centimeters in diameter, with smooth surfaces, no ulceration, a slight accentuation of the follicular ostia, and peripheral telangiectasias. In some cases, the skin may develop a “peau d’orange” appearance.

The lesions are often asymptomatic and primarily localized to the face, particularly the perinasal, zygomatic, preauricular, or forehead areas [6]. However, extrafacial involvement of the scalp, trunk, and limbs can occur [9]. There is no known association with underlying diseases, and laboratory tests usually show only mild peripheral eosinophilia.

A biopsy is essential for diagnosing granuloma faciale. A key feature is the preservation of the subepidermal papillary dermis, known as the Grenz zone. Histopathologically, the upper dermis shows a dense mixed inflammatory infiltrate consisting of neutrophils, eosinophils, and lymphocytes, while skin adnexa remain unaffected. Leukocytoclastic vasculitis with typical nuclear debris may also be seen. Chronic lesions often show a histiocytic infiltrate with pronounced fibrosis and capillary proliferation [4].

GF is a chronic inflammatory dermatosis that does not involve systemic organs. The cutaneous lesions tend to persist for long periods, rarely resolving spontaneously. The disease’s therapeutic resistance and unclear pathogenesis contribute to its chronic, persistent course, making treatment difficult and leading to patient dissatisfaction.

Case report

We present a case of a 45-year-old white male who developed an erythema-infiltrative plaque with a yellowish tint on his forehead four years ago. The lesion did not cause subjective symptoms and persisted despite treatment with potent topical corticosteroids. In the last few months, the patient developed a circumscribed erythematous livid



lesion with follicular accentuation on the apex of the nose (**Fig. 1**). A dermatologist recommended a biopsy to exclude basal cell carcinoma, and the lesion was initially diagnosed as primary T-cell cutaneous lymphoma due to pronounced infiltration by CD4-positive cells. The patient was referred to a hematology clinic for further staging.

At the clinic, a second dermatological consultation suggested granuloma faciale. Dermoscopy showed linear, arborizing vessels, dilated follicular openings, and brown dots, further supporting the diagnosis.

A new biopsy revealed the characteristic Grenz zone, a pronounced mixed inflammatory infiltrate in the upper dermis with many neutrophils, eosinophils, and lymphocytes, along

Fig. 1. Well-demarcated erythematous plaque with glossy appearance, localized to the dorsum of the nose.

with single histiocytes and a more pronounced fibrous reaction in the lower dermis (**Fig. 2**). These findings were consistent with the clinical diagnosis of GF.

The patient underwent topical calcineurin inhibitors therapy (0.1% tacrolimus ointment). After one month of follow-up, a slight flattening and mild reduction in the lesion's diameter was observed.

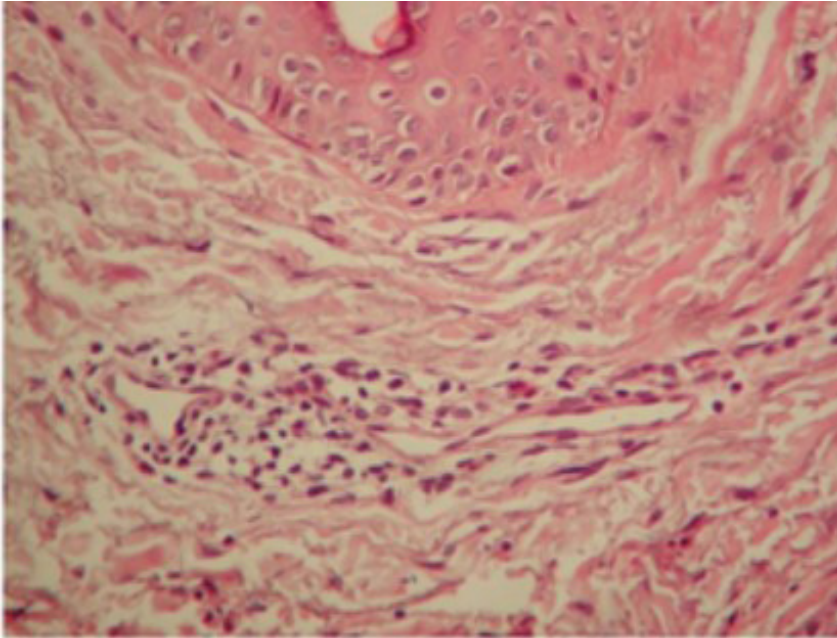


Fig. 2. Eosinophilic granuloma – follicular hyperkeratosis, uniform acanthosis, Grenz zone, mild to moderate perivascular infiltrate of lymphocytes, neutrophils and single eosinophils in the fibrous papillary dermis. (Hematoxylin-Eosin, $\times 400$).

Discussion

Granuloma faciale is a rare, chronic inflammatory dermatosis with a benign course, no systemic involvement, and an unclear etiopathogenesis. First described in the 1950s [7], GF is characterized by erythematous livid plaques, primarily affecting the face, with a persistent course and pronounced therapeutic resistance. The exact pathogenesis remains unclear, but several theories have been proposed.

One hypothesis speculates that chronic actinic damage plays a significant role in its development, as cutaneous efflorescences are commonly found on photoexposed areas and may flare up following photoexposure [10]. Other researchers suggest that granuloma faciale could be a localized reaction to the deposition of circulating immune complexes, resembling a form of limited small vessel vasculitis [5]. Studies have also shown that tissue eosinophilic infiltration in GF correlates directly with the migration of CD4-positive lymphocytes that produce interleukin-5 (IL-5) in the affected tissues. As a result, GF is suspected to be a dermatological prodrome of monoclonal expansion of a specific lymphocyte subset, which induces eosinophilic chemotaxis

and the proliferation of tissue macrophages, leading to a subsequent local, persistent fibrous reaction [8]. Some researchers argue that a gamma-interferon-mediated process directly activates the complement system, causing tissue destruction and resulting in chronic fibrous changes mediated by tissue macrophages [1].

The correct diagnosis of GF can be established through its distinctive clinical features and characteristic histopathological findings. Biopsy analysis is essential to rule out key differential diagnoses, including erythema elevatum diutinum, chronic discoid lupus erythematosus, sarcoidosis, lymphoid infiltration, primary cutaneous lymphomas, basal cell carcinoma, and skin infections such as lupus vulgaris [13].

The treatment of GF remains challenging, as there are no universally effective therapeutic options. A variety of treatments have been attempted, including dapsone, clofazimine, antimalarials, isoniazid, topical corticosteroids, intralesional injections with gold salts and depo-corticoids, dermabrasion, laser ablation, surgical excision, local PUVA therapy, and calcium-neurin inhibitors [3,11]. However, the clinical responses to these treatments are highly variable, and no single therapy has proven to be consistently effective.

Recently, topical JAK inhibitors such as tofacitinib and ruxolitinib have emerged as promising treatments for GF. Given that inflammatory mediators associated with the development of this disorder – specifically interleukin-5 and interferon-gamma – signal through the JAK pathway, these inhibitors may offer a targeted approach to managing GF [2, 12]. However, further randomized controlled studies are needed to confirm their efficacy, safety, and optimal dosing for this condition.

Conclusion

Granuloma faciale is a rare chronic inflammatory dermatosis with an unclear etiopathogenesis, characterized by persistent violaceous plaques primarily on the face. Its diagnosis is challenging due to clinical similarity to other dermatological conditions, but the characteristic histopathological findings, including the preservation of the Grenz zone and a mixed inflammatory infiltrate, are key to confirming the condition. While the exact cause remains uncertain, various theories suggest that chronic actinic damage, immune complex deposition, or T-cell-mediated immune responses may play important roles in its development.

Treatment of GF remains difficult and often unsatisfactory, with variable responses to therapies such as topical corticosteroids, dapsone, and calcineurin inhibitors. Despite this, newer treatments, such as topical JAK inhibitors like ruxolitinib, show promise, targeting inflammatory pathways involved in the condition. However, further randomized controlled trials are necessary to establish their long-term efficacy, safety, and optimal use in managing granuloma faciale.

This case highlights the diagnostic complexities and treatment challenges associated with GF. As a condition that is both clinically and histopathologically distinctive, it requires careful attention from healthcare providers. Continued research and clinical trials will be crucial to improving our understanding of the disease and optimizing therapeutic strategies.

References

1. **Barnadas, M., R. Curell, A. Alomar.** Direct immunofluorescence in granuloma faciale: a case report and review of literature. – *J. Cutan Pathol.*, **20**, 2006, 442-446.
2. **Chen, A., C. S. Harview, Rand, J. Harms.** Refractory granuloma faciale successfully treated with adjunct topical JAK inhibitor. – *JAAD Case Rep.*, **33**, 2023, 91-94.
3. **Erceg, A., E. de Jong, P. van de Kerkhof, M. Seyger.** The efficacy of pulsed dye laser treatment for inflammatory skin diseases: a systematic review. – *J. Am. Acad. Dermatol.*, **69**, 2013, 609-615.
4. **Le Boit P.** Granuloma faciale: a diagnosis deserving of dignity. – *Am. J. Dermatopathol.*, **24**, 2002, 440-443.
5. **Marcoval, J., A. Moreno, J. Peyr.** Granuloma faciale: a clinicopathological study of 11 cases. – *J. Am. Acad. Dermatol.*, **51**, 2004, 269-273.
6. **Ortonne, N., J. Wechsler, M. Bagot, E. Grosshans, B. Cribier.** Granuloma faciale: a clinicopathological study of 66 patients. – *J. Am. Acad. Dermatol.*, **53**, 2005, 1002-1009.
7. **Pinkus, H.** Facial granuloma. – *Dermatologica*, **105**, 1952, 85-99.
8. **Selvaag, E., B. Roald.** Immunohistochemical findings in granuloma faciale. The role of eosinophilic granulocytes. – *J. Eur. Acad. Dermatol. Venereol.*, **14**, 2000, 517-518.
9. **Surana, T., G. Arghyaprasun, B. Saugato, N. Falguni, C. Gobinda, H. Chinmay.** Granuloma faciale: exclusively extrafacial. – *Indian J. Dermatol.*, **58**, 2013, 245.
10. **Thiyanaratnam, J., S. Doherty, B. Krishnan, S. Hsu.** Granuloma faciale: case report and review. – *Dermatol. Inline J.*, **15**, 2009, 3.
11. **Tojo, G., T. Fujimura, Y. Kambayashi, K. Kikuchi, S. Aiba.** Successful treatment of granuloma faciale with topical tacrolimus: a case report and immunohistochemical study. – *Case Rep. Dermatol.*, **4**, 2012, 158-162.
12. **Wong, A., S. Stahly, J. Kieffer, C. Dunn, R. Nathoo.** Topical ruxolitinib for the treatment of granuloma faciale. – *JAAD Case Rep.*, **36**, 2023, 73-74.
13. **Ziemer, M., K. Schwede, J. Simon, U. Paasch.** Atypical erythema elevatum diutinum or extrafacial granuloma faciale? – *Dtsch Dermatol Ges.*, **11**, 2013, 178-180.

Review Articles

Palatogenesis and Palatoschisis. A Review on the Cellular and Molecular Mechanisms of Development

Marcello Guarino

Department of Anatomical Pathology, Hospital of Viterbate, Italy

*Corresponding author e-mail: marcello.guarino@gmail.com

The formation of the palate is a highly complex developmental process beginning with the growth of facial primordia and the subsequent fusion of the nasal and maxillary prominences, thus giving rise to the primary palate and upper lip. Development of the secondary palate occurs through the union of bilateral palatal shelves arising from the maxillary prominences that fuse with each other on the midline, thus leading to a continuous palate that definitively separates the oral and nasal cavities. If the intricate process underlying craniofacial morphogenesis is disrupted, an orofacial cleft may occur. The cellular and molecular bases of palate shelf fusion have not yet been clearly elucidated. Therefore, this review focuses mainly on the recent advances in knowledge about secondary palatogenesis, with special attention to the cellular and molecular mechanisms involved in the fusion of the apposing shelves as well as their failure to properly take place, thus generating clefting.

Key words: palatogenesis, cleft lip and cleft palate, medial edge epithelia (MEE), medial epithelial seam (MES), epithelial-mesenchymal transition, apoptosis, cell migration

Introduction

Cleft palate is a congenital deformity characterised by a defect in the roof of the oral cavity, resulting from abnormal embryonal development. Cleft lip and cleft palate are among the most common birth defects, affecting approximately 1 in 700 live-born babies [13, 16, 38, 48, 56]. The palate acts as a mechanical barrier separating the mouth from the nasal cavities, allowing breathing and simultaneous food intake. Structurally, it consists of a bony hard part anteriorly and a muscular soft part posteriorly, the latter functioning as a valve that closes the nasal airway, thus permitting swallowing and directing airflow during speaking [44]. Patients with cleft lip or cleft palate require significant care from birth to adulthood engaging many medical disciplines, including nursing, maxillofacial and plastic surgery, otolaryngology, orthodontics, speech therapy,

audiology, psychological and genetic counselling, and therefore they impose a substantial economic burden [56, 73, 78]. There is a wide variability in incidence of cleft lip or cleft palate in relation to geographic origin, ethnicity and socioeconomic status [15, 49, 71, 74]. In general, Asian or Latin American populations have the highest frequencies, Caucasian populations intermediate, and African populations the lowest, thus suggesting that the contribution of individual susceptibility genes can vary noticeably across different populations [13, 16]. However, the aetiology is heterogeneous, complex and multifactorial, involving both genetic and environmental factors, as well the interactions between them. Indeed, a further degree of complexity is provided by the interplay of both gene-gene and gene-environment interactions, contributing differently to the two main types of cleft in the clinical setting, non-syndromic and syndromic orofacial clefts [13, 70, 72, 76]. Clefts are usually classified as either cleft lip with or without palate involvement, or cleft that involves the palate alone [51]. Approximately 70% of cases of cleft lip with or without cleft palate, and 50% of cleft palate alone occur as isolated entities, with no other apparent associated abnormalities, and are therefore commonly termed isolated, non-syndromic clefts; the remaining cases are part of complex syndromes that, in addition to clefting, also include further anomalies [47, 51]. There is a 2:1 male to female ratio for cleft lip with or without cleft palate, and approximately a 1:2 male to female ratio for cleft palate alone [13, 16, 56]. Furthermore, syndromic clefting can be as a feature of chromosomal syndromes, inherited disorders affecting a single gene, or syndromes induced by teratogens, such as alcohol, tobacco smoke and drugs [11]. Approximately 500 syndromes associated with cleft lip or palate caused by a genetic defect have been identified [41]; the most common are Pierre Robin sequence, Van der Waude syndrome, DiGeorge/Velocardial syndrome, Stickler syndrome, Loeys-Dietz syndrome, Apert syndrome, Crouzon syndrome, and Treacher Collins syndrome [11, 77].

Cleft lip with or without cleft palate and cleft palate alone have historically been considered separate entities owing to their different developmental origins, and different epidemiology, genetics and family patterns [16, 47]. However, there is definitely a certain degree of overlap between all of these deformities. Since the formation of the upper lip/primary palate precedes the fusion of the secondary palate, disruption in the development of the upper lip/primary palate may compromise the correct contact between the secondary palatal structures and, therefore, cleft lip and cleft palate have a high co-morbidity [16, 30]. An integration of epidemiological, candidate gene and genome-wide essays as well as studies on animal models, has recently greatly deepened our understanding of the causes of both syndromic and non-syndromic clefts. However, due to the broad genetic heterogeneity, departure from the Mendelian inheritance models and the need for very large data sets, there has been less progress in our knowledge on the genetic contribution to the aetiology of non-syndromic clefts [13]. Mouse models have been commonly used in research on orofacial clefts due to the possibility of multiple genetic modifications and the high similarity between mouse and human facial morphogenesis [26]. Genetic manipulations in mice coupled with detailed morphological and molecular analyses of mutant mouse models has revealed that facial development is regulated by an extensive network of signalling molecules and transcription factors with abundant crosstalk between the distinct pathways, some of which are under post-transcriptional control [5, 21, 42, 43, 44, 64, 69, 75].

The following discussion will cover the cellular and molecular mechanisms of palatogenesis and the developmental alterations underlying cleft lip and cleft palate. Although cleft lip with or without cleft palate is the most common type of orofacial cleft, the cellular and molecular bases of upper lip/primary palate development have not been studied as thoroughly as those of secondary palate, possibly due to more limited usable models to study upper lip development [30]. Accordingly, this review covers in more detail secondary palatogenesis and clefting, with less discussion on the mechanisms underpinning lip/primary palate morphogenesis and clefting.

Facial Development

Face morphogenesis requires coordination of a series of complex events, including cell proliferation, migration, differentiation, and death [2, 16, 41, 64]. In humans, palate development starts around the 4th week of gestation with the growth, fusion and rearrangement of five primordia consisting of a core of mesenchymal cells originating mainly from the proliferation and migration of cranial neural crest cells, covered by an epithelium of ectodermal origin. At the rostral boundary of the primitive mouth (stomodeum) there is an unpaired median frontonasal prominence, while two paired maxillary prominences flank the primitive mouth and two paired mandibular prominences lie below (**Fig. 1**). As facial primordia grow by proliferation of their mesenchyme, the surface ectoderm bi-stratifies and undergo a critical differentiation to form a thin outer layer of flattened and tightly connected periderm cells characterised by a non-adhesive apical surface, thus allowing only highly controlled adhesion [2, 41]. Indeed, formation of the upper lip and secondary palate requires spatiotemporally regulated inter-epithelial adhesions and subsequent dissolution of the newly-formed intervening epithelial seams between the maxillary and medial/lateral nasal processes, and between the palatal shelves, respectively [41]. Initially, the facial prominences of the right and left sides are widely separated from each other, but they progressively move towards the midline [16]. Thickening around the nasal placodes divides the frontonasal prominence into paired medial and lateral nasal processes at the 5th week. Then, at the 6th week the continuous growth of the maxillary prominences medially pushes the medial nasal processes towards the midline that eventually coalesce around the 7th week and, meanwhile, the freely projecting bases of the medial nasal prominences fuse with the adjacent maxillary and lateral nasal prominences. The fused medial nasal processes form the inter-maxillary segment from which the philtrum of the upper lip, the primary palate, the upper central region of the jaw and the middle part of the nose are formed. Formation of the upper lip takes place through a fusion process that includes epithelial adherence between nasal and maxillary prominences, formation of a seam, and then its dissolution by apoptosis and/or epithelial-mesenchymal transition (EMT) [2, 16, 32]. A Pbx-dependent regulatory network seems to control this fusion mediated by the Pbx/Wnt/p63/Irf6 pathway promoting apoptosis [17], cross-talking with the Pbx/Snail/Smad/E-cadherin pathway leading to EMT [46]. The dual effect of the transcription factor Pbx is not surprising, as many lines of evidence indicate that apoptosis and EMT can be alternative, complementary or sequential processes that secure normal tissue morphogenesis [46] (also *vide infra*, in the discussion on the secondary palatogenesis). Failure in the fusion between the maxillary and medial/lateral nasal processes results in

cleft lip that can extend into the nostril and/or primary palate [2, 16, 26, 32, 67]. Extension to the nostril indicates that the defective fusion also involved the lateral nasal process [32]. The primary palate includes a small triangular area of hard palate anterior to the incisive foramen and the central maxillary alveolar arch with the four incisor teeth, and its development is completed together with lip closure by the end of the 6th week [41]. The lateral nasal processes form the nasal alae, while the maxillary prominences contribute to the lateral parts of the upper lip and, by merging with the mandibular prominences below, contribute to form the cheeks. The mandibular prominences also fuse at the midline to form the lower lip and jaw [16].

Secondary palatogenesis occurs from the 6th to the 12th week of development [2, 16, 26, 41]. It begins with the outgrowth of bilateral intra-oral projections known

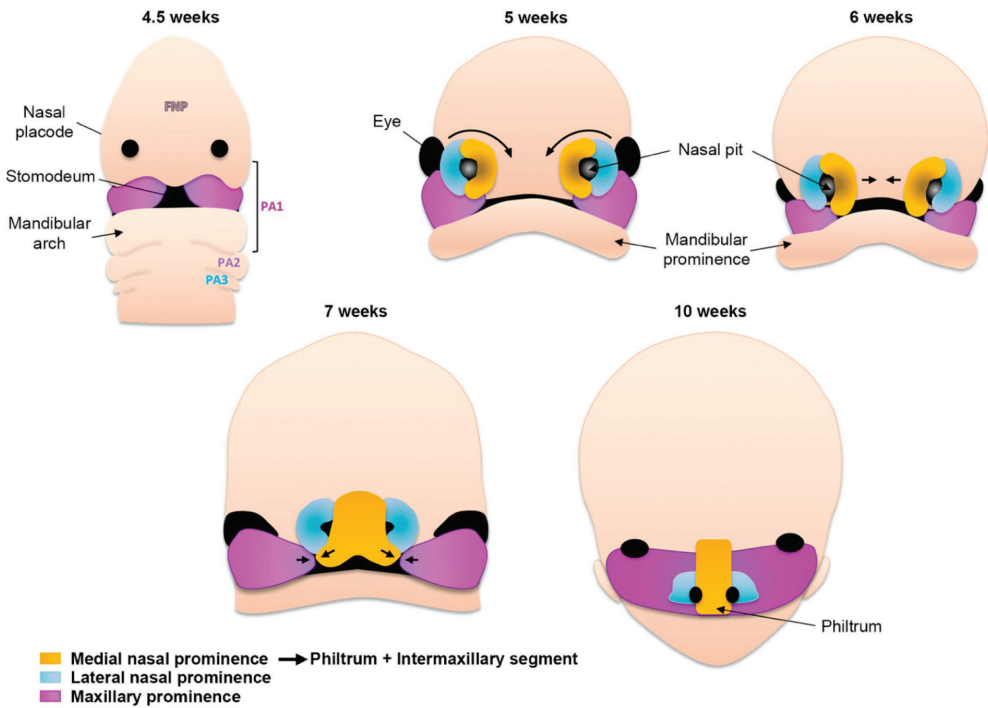


Fig. 1. Schematic drawing depicting human facial morphogenesis. At 4.5 weeks the facial primordia include the frontonasal prominence (FNP, *beige*) with nasal placodes placed rostrally to the stomodeum, the paired maxillary prominences (*dark pink*) flanking the stomodeum, and the mandibular prominences (*beige*) placed caudally; derivatives of the first pharyngeal arch (PA1) are indicated. At 5 weeks thickening of the frontonasal prominence around the nasal placodes results in medial (*yellow*) and lateral (*blue*) nasal prominences. Medial nasal prominences converge (6 weeks) and coalesce on the midline (7 weeks), thus giving rise to the intermaxillary segment and, therefore, to the middle of the nose and the philtrum of the lip (10 weeks), while the remaining upper lip arises from the maxillary prominences. The lateral nasal prominences form the nasal alae. From Antiguas, Paul and Dunnwald (ref. 2), reprinted by kind courtesy.

as palatal shelves arising from the oral side of the maxillary prominences (**Fig. 2A**). At first, they grow vertically downward along the sides of the tongue (**Fig. 2B**) but, at around the 7th week, as the mandible grows and lengthens and the tongue descends into the oral cavity creating space above it, they elevate above the dorsum of the tongue (**Fig. 2C**). Mouth opening, tongue protrusion and hiccup movements, and their associated pressure changes, probably facilitate palate shelf elevation [16]. In general, female human embryos elevate their palate shelves about 1 week later than males; this might possibly explain the higher female incidence of cleft palate alone, due to prolonged risk of developmental errors, or to greater exposure to teratogenic agents [16]. After elevation, the palatal shelves further grow horizontally towards the midline, and fi-

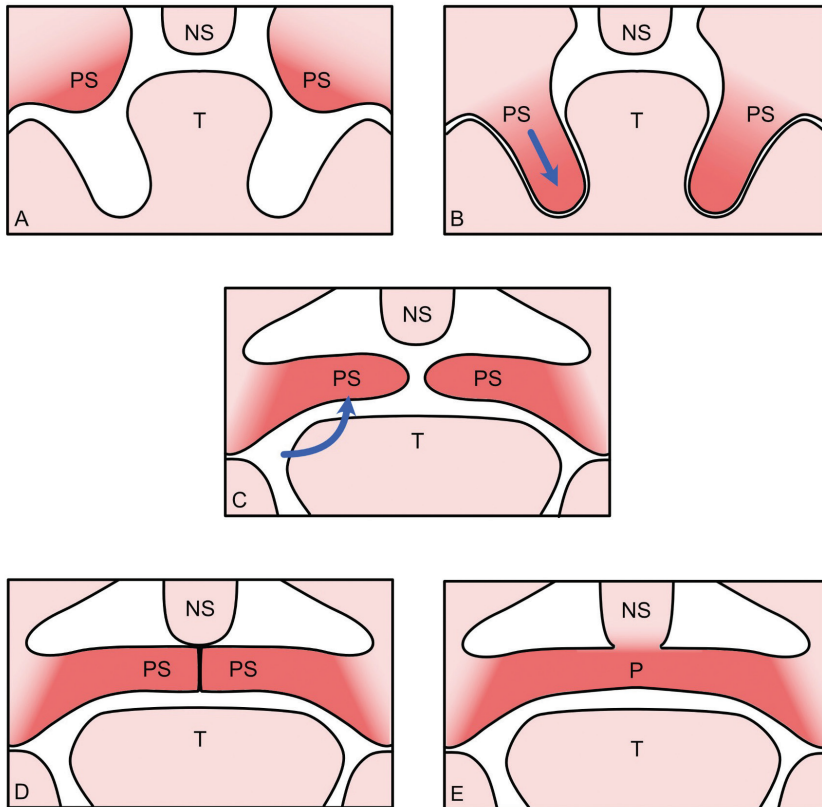


Fig. 2. Highly schematic drawing depicting the stages of secondary palate development. (A) At 6 weeks, palatal buds appear on the intra-oral sides of the maxillary processes, and initiate their growth downwards. (B) The palatal shelves grow down along the sides of the tongue that in this stage is placed high in the oral cavity, filling it almost entirely. (C) At 7 weeks, the tongue drops and flattens, thus allowing the palatal shelves to elevate above the dorsum of the tongue until they reach a horizontal position, and grow further towards each other. (D) At 8 weeks, the shelves adhere to each other through their medial edge epithelia (MEE) at their tips, which then merge to form the medial epithelial seam (MES). (E) At 12 weeks, dissolution of the MES leads to mesenchymal confluence and complete fusion of the shelves to form a continuous palate, which also fuses with the overlying nasal septum. PS, palatal shelves; T, tongue; NS, nasal septum; P, palate.

nally contact each other at the 8th week. The epithelia at the tips of the palatal shelves, called medial edge epithelia (MEE), adhere each other and merge to form a midline epithelial seam (MES) (**Fig. 2D**). Initial adhesion between the opposing shelves occurs in the middle of the palate shelves and proceeds anteriorly and posteriorly, similar to a “zipper” closing in both directions, ending at the incisive foramen anteriorly and the uvula posteriorly [2]. Between the 9th and the 12th weeks of gestation the epithelium of the MES disintegrates, thus leading to confluence of the mesenchymal stroma and palate continuity [2, 15, 16, 50] (**Fig. 2E**). Moreover, the united palate fuses anteriorly with nasal septum and the primary palate. The completion of the fusion process therefore leads to the definitive division of the oronasal space into separate oral and nasal cavities. Clefts of the palate can arise due to failure at any of the steps of palatogenesis, including palatal shelf growth, elevation, or fusion [2, 11, 16, 21, 26, 44, 64]. The primitively bi-layered epithelium covering the palatal shelves has different fates. Indeed, the mucosal lining of the oral side of the palate will differentiate into stratified squamous epithelium, while the epithelium of the nasal side will differentiate into respiratory-type pseudo-stratified, ciliated epithelium. The palatal mesenchyme will differentiate anteriorly into bone to form the hard palate, and posteriorly into muscle - thanks to myogenic cells derived from the mesoderm - to form the soft palate.

Molecular Regulation of Palatal Shelf Growth and Patterning

Growth of the palate shelves requires epithelial-mesenchymal interactions regulated by an intricate network of signalling pathways and transcription factors with extensive crosstalk between them, the disruption of which can be instrumental in the developmental pathogenesis of clefting. A wealth of genes have been implicated in the palatal growth of both animal models and humans, and it has been found that also a single gene mutation can lead to cleft. Although there are a plenty of molecules with a known role in palate development, the underlying principles of molecular signalling in palate morphogenesis can basically be attributable to the Shh, FGF, BMP, Wnt and - as we will see specifically later - TGF β signalling pathways [19, 21, 42, 43, 44, 57, 64].

The central player in the organisation and regulation of palatal shelf growth is definitely Sonic hedgehog homolog (Shh) signalling that cross-talks with Fibroblast growth factor (FGF) and Bone morphogenetic proteins (BMPs) (**Fig. 3**). Shh is already expressed in the early oral epithelium prior to palate shelf outgrowth [42, 59]. Abrogation of Smoothed (Smo), i.e. the transducer of Shh signalling, results in defective shelf growth and cleft palate, thus highlighting a critical role of Shh signalling for palate development. The mesenchymal expression of the transcription factors Foxf1/2 and Osr2 is activated by Shh, which also regulates the expression of the cell cycle activators Cyclin D1/2 in the palatal mesenchyme, thus sustaining its proliferation and growth [40]. The epithelial expression of Shh is largely dependent on the mesenchymally expressed FGFs, with FGF10 inducing, whereas FGF7 repressing Shh expression in the palate epithelium. Shh positively regulates FGF10 expression through the Osr2 transcription factor in the mesenchyme and, therefore, FGF10 and Shh act in a positive feedback loop to maintain each other's expression [42]. Moreover, a further Shh/Foxf/FGF18/Shh feedback loop has been identified in which the transcription factors Foxf1/2 downstream of Shh control Shh expression

in the epithelium [65]. In addition, maintenance of Shh expression also requires the mesenchymal transcription factors Msx1 in the anterior palate, and Pax9 in the posterior palate. Indeed, Msx1 is restricted to the anterior part of the developing palate and regulates anterior palate mesenchyme proliferation through activation of BMP4 which, in turn, signals to the epithelium to maintain Shh expression. While BMP4 expression in the anterior palate is dependent on Msx1, and each stimulates the expression of the other, BMP4 expression in the posterior palate is dependent on Pax9. BMP4 is fundamental to maintain Shh expression which, in turn, also induces BMP2 expression in the mesenchyme that promotes palatal growth. Pax9 is also upstream of Osr2 and FGF10. Therefore, Pax9 controls the Osr2/FGF10/FGFr2b/Shh, Msx1/BMP4/Shh and the BMP4/Shh pathways, with both Pax9 and Shh signalling converging on Osr2 transcription factor (Fig. 3). In summary, Pax9 regulates two major

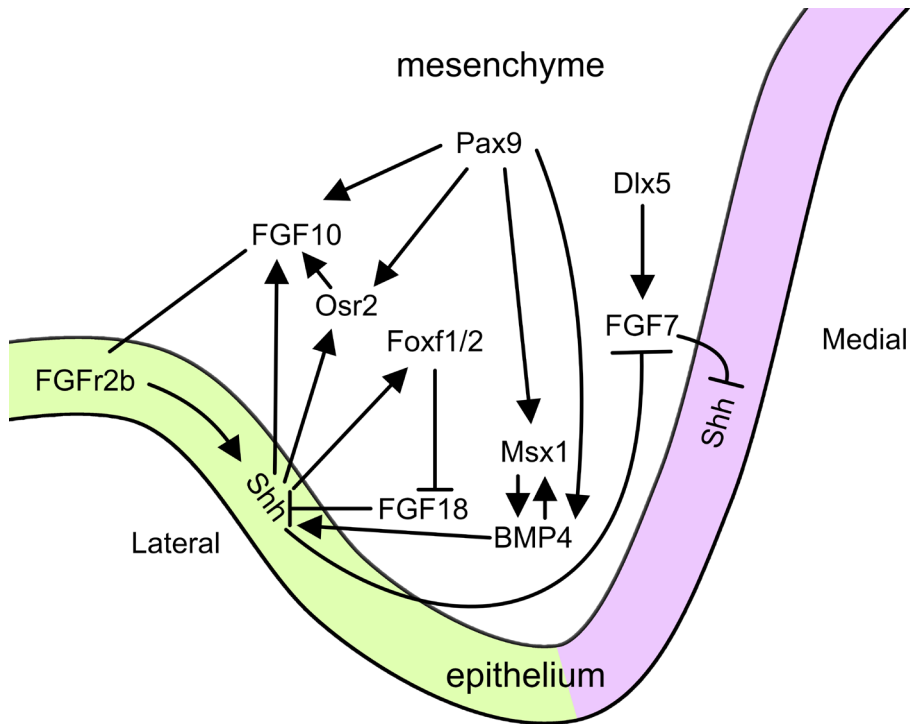


Fig. 3. Molecular control of palatal shelf development. Highly simplified diagram of signalling interactions in a developing palate shelf with the medial side on the right. Shh is expressed in the epithelium and acts in a feedback loop with the FGF10 expressed in the mesenchyme to self-maintain their expression, thus ensuring palatal growth. Another feedback loop between Msx1 and BMP4 also helps to maintain Shh expression in the anterior palate. Pax9 regulates these feedback loops and, furthermore, acts upstream of BMP4 to sustain Shh expression in the epithelium of the posterior palate. Another feedback loop involving the mesenchymal transcription factors Foxf1/2 also regulates Shh signalling. Expression of FGF7 in the mesenchyme is maintained by the transcription factor Dlx5, and both are restricted to the medial side of the palate where FGF7 and Shh repress the expression of each other. Arrows represent induction, blunt arrows indicate inhibition.

feedback loops that control growth and patterning in the developing palate, one involving FGF, the other involving BMP4, both aimed at maintaining Shh expression in the epithelium and, therefore, the consequent effect of stimulating palate shelf growth [43]. In addition to Msx1 and Pax9, other transcription factors including Shox2, Barx1, Mn1 and Tbx22 are differentially expressed along the anteroposterior axis, with Shox2 being restricted to the anterior palate, and Barx1, Mn1 and Tbx22 expressed in the posterior palate mesenchyme, where Mn1 acts upstream of Tbx22 to regulate posterior palatal growth [42]. Wnt5a is another signal affecting palate shelf growth with higher levels in the anterior region and a graded anteroposterior expression. Wnt5a appears to be a requirement for palatal mesenchymal cell proliferation and migration, mediated through non-canonical Wnt pathway and, indeed, its deficiency in mice causes cleft palate resulting from impaired palate shelf growth [27].

Lip and Palate Development and Clefting

Cleft lip with or without cleft palate and cleft palate alone (Fig. 4) result from defective embryonic morphogenesis between the 6th and 12th week of human gestation [38]. Cleft lip may arise from disturbances in cell proliferation, survival and migration of the neural crest-derived cells to facial primordial buds resulting in impaired growth, or in defective fusion between the nasal and maxillary processes [7, 42]. Cleft palate

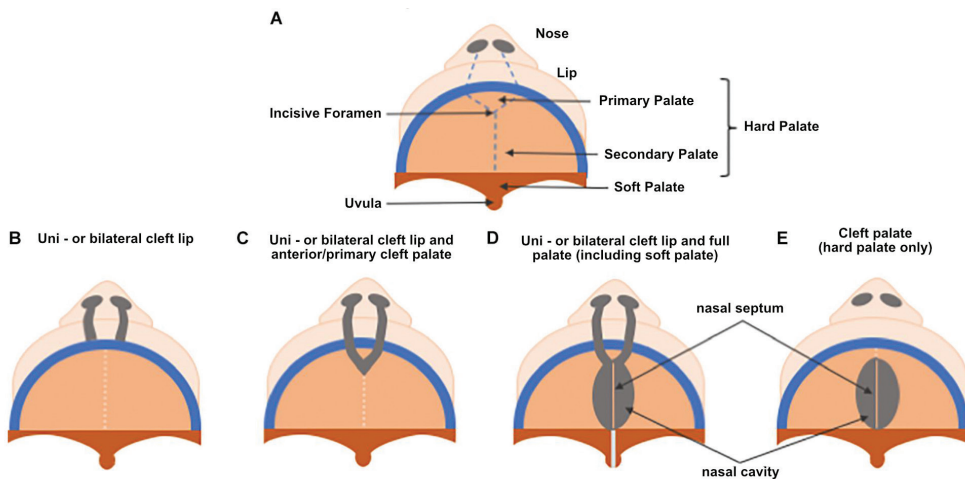


Fig. 4. Schematic representation of some clinical forms of cleft lip and/or palate in humans. There are various classification systems for cleft lip and cleft palate. For example, cleft lip can be classified as unilateral or bilateral; incomplete or complete; in the latter, the cleft involves the entire thickness of the upper lip and, in addition, the alveolar ridge and primary palate are often involved. Cleft palate can be unilateral or bilateral, and incomplete or complete (refs. 11, 64). In the diagram shown here, the defects are depicted as bilateral, with different degrees of involvement. (A) Normal anatomy of lip and palate. (B,C) Bilateral cleft lip, without (B), and with involvement of the primary palate (C). (D) Bilateral cleft lip with cleft of both the primary and secondary palate, comprising the soft palate. (E) Cleft palate involving only the secondary hard palate. Kindly reprinted from Paiva, Maas, dos Santos, Granjeiro, Letra (ref. 56).

may result from disorders at any stage of secondary palatogenesis, i.e. from impaired palatal shelf growth; delayed or failed shelf elevation; failure of shelf fusion or lack of degeneration of the MES; failure of mesenchymal consolidation and/or differentiation; or post-fusion rupture [16, 42, 50].

As we have seen, the upper lip arises from morphogenesis of the frontonasal prominence and fusion with the maxillary processes, whereas at a different time the secondary palatal shelves grow inside the primitive mouth from the maxillary processes. In some cases cleft palate may result entirely by a localised failure in the palate developmental program, but this does not happen in other cases. Fusion between the secondary palatal shelves occurs much later in embryogenesis than upper lip closure, and it is known that failure of lip formation can secondarily affect palatal shelf contact and cause cleft palate [32]. According to Ferguson, cleft secondary palate as a consequence of the cleft lip would occur in most cases because the tongue tip would become trapped above the cleft pre-maxilla, thus maintaining its high early position in the oral cavity, thus hindering palate shelf elevation and resulting in cleft secondary palate [16]. Furthermore, since palate development occurs concurrently with growth and expansion of the whole craniofacial complex, abnormalities of structures more or less in the vicinity of the palatal shelves can hinder the process that leads to contact between the opposing shelves, thus resulting in secondary cleft palate [5, 7, 42]. Therefore, in some cases of cleft palate the defect is not intrinsic to the palatal shelves, but results from different and unrelated morphological anomalies in surrounding or remote anatomical structures [14, 16], usually as a part of a syndrome comprising other malformations. It is known that initially the two palatal shelves grow downward, lateral to the tongue; at this point, the tongue is narrow and tall, almost completely filling the oral cavity; only during the 7th week the two palatal shelves dramatically change their positions and elevate to a horizontal position above the dorsum of the tongue [45] (**Fig. 2B, C**). Abnormal persistence of the upwardly displaced tongue will therefore result in a physical obstruction to palatal shelf elevation and, therefore, to cleft palate [5]. One of the better known examples of cleft palate as a secondary consequence of other craniofacial malformations is the Pierre Robin sequence, in which the lower jaw is either small (micrognathia) or set back from the upper jaw (retrognathia), resulting in failure of tongue descent, and thus causing a physical obstacle to palatal shelf elevation by the displaced tongue [5].

Below, we discuss the single phases of normal palatogenesis in relation with examples of cleft palate, mostly deriving from animal model studies.

Palatal shelf formation

Failure of palatal shelf formation is a rare, severe defect resulting from abnormal molecular networks operating between the palatal bud epithelium and mesenchyme, and involving Shh, BMP and FGF, occurring during early steps of palatogenesis. Shh is a key early signal that drives palatal shelf outgrowth through signalling from the epithelium to the underlying mesenchyme to promote palatal growth. As we have seen Shh, FGF and BMP functions in feedback loops that promote cell proliferation and, therefore, growth of the palatal shelves [5, 58, 59]. As one might expect, FGFR2b mutation affects the initial development of the palatal shelves and results in complete cleft palate [58]. On the other hand, Shh signalling is required for the activation of several important transcription factors in the mesenchyme, including Msx1, Foxf1/2 and Osr2

[65]. In animal studies, targeted mutation of *Msx1*, *Osr2* or *Shox2* generates cleft palate caused by altered mesenchymal proliferation [21]. Both *Osr2*^{-/-} and *Pax9*^{-/-} mouse embryos exhibit cleft palate and significant reduction in FGF10 expression in the developing palatal mesenchyme [68].

Palatal shelf elevation

Around the 7th week of gestation the palatal shelves rapidly elevate into a horizontal position above the tongue, thus suggesting that they have an intrinsic capability to elevate. There remains controversy concerning the mechanisms responsible for palatal shelf elevation. It has been proposed that the intrinsic shelf elevation force might be produced either by the generation of turgor pressure following hydration of the extracellular matrix or, alternatively, by proliferation, migration or contraction of the palatal shelf mesenchymal cells [50]. Many evidences indicate that the shelf elevation force is related to the presence of hyaluronan in the mesenchymal extracellular matrix. Hyaluronan is a glycosaminoglycan capable of binding a large amount of water, and therefore it could generate osmotic pressure [50]. The role of mesenchymal cell proliferation/migration in the palatal shelf elevation is more controversial, particularly considering the rapidity with which shelf elevation occurs. However, the production of an elevating force could be related to changes in cytoplasmic microfilament apparatus of the mesenchymal cells. Indeed, palatal shelf mesenchymal cells before elevation appear elongated and polarised, the cells nearest the basement membrane being perpendicularly aligned to the it. After shelf elevation, these cells became more rounded, possibly indicative of cell contraction, and this could be the means of generating the shelf elevation force, also indicating that actin-based contractility could be involved [50]. Since the elevation of the palate shelves is a rapid event, compared to alternative processes such as differential cell growth/migration, the actin-driven contraction model fits better than others. *Osr2* regulates palatal mesenchymal cell proliferation and palatal shelf elevation [68], and it has been reported the occurrence of delayed palate shelf elevation in *Osr2*^{-/-} (38), as well as in *PDGFC*^{-/-} (12) mutant mice.

Failure of elevation due to abnormal adhesion and the role of periderm. A specific cause of failure of palate shelf elevation is the adhesion/fusion of the growing palatal shelves with the tongue or mandible. Under normal conditions, palatal shelves do not fuse with other oral structures, and this function is ensured by the presence of the non-sticky periderm layer [2]. Any factor that interferes with the differentiation and maintenance of the periderm can cause premature, abnormal adhesions. Peridermal cells differentiate from the basal layer through finely tuned molecular signalling. Basal cells express the transcription factor p63 that maintains the proliferative potential of the basal layer [60], but also activates Jag2/Notch signalling through FGFR2b, and induces *Irf6* expression [42]. In supra-basal cells p63 becomes down-regulated, as Notch signalling represses p63 and, on the other hand, *Irf6* promotes proteasome-mediated p63 protein degradation, thus determining the periderm specification. Therefore, in these cells *Irf6* becomes strongly expressed, whereas p63 is down-regulated, as *Irf6* converges with Jag2/Notch signalling to drive periderm differentiation through feedback down-regulation of p63. In this way, periderm differentiation of supra-basal cells is induced and maintained by *Irf6* and Jag2/Notch signalling acting synergistically [41]. It follows that a malfunction of these pathways no longer ensures protection from unwanted adhesions, and therefore inappropriate fusion of other structures with the

palate shelves can prevent their elevation and cause cleft palate [7]. For example, in mice that do not express FGF10 - which is upstream of FGFR2b - the palatal shelf epithelium fuses with the tongue and the epithelium covering the mandible, thus preventing palatal shelf elevation. In these mice there is a severe reduction in the expression of Jag2 that disrupts the Jag2/Notch signalling and, therefore, periderm differentiation [10]. In humans, a gene that has been associated with inappropriate adhesions is Tbx22 and, indeed, mutations of this gene have been reported in families with X-linked cleft palate and ankyloglossia [10].

We will return to the question of the periderm when we discuss the formation and breakdown of the MES.

Contact and adhesion between the palatal shelves

Once elevated into a horizontal position, the palate shelves further grow until they contact each other at the midline (**Fig. 2C, D**). Failure of palatal shelves to meet after elevation is the most common type of cleft palate defect documented in animal studies [7]. In addition to its function in regulating the fate of the MEE/MES (*vide infra*), TGF β 3 is also critical for proper proliferation of the cranial neural crest-derived palatal mesenchyme in the palatal buds [7], thus underscoring the crucial role of TGF β 3 signalling in controlling the entire process of palatogenesis [21]. Mice lacking TGF β 2 in the palate shelf mesenchyme develop a cleft palate due to reduced horizontal extension of the shelves [28]. Similarly, embryos lacking PDGFC activity show delayed elevation and hypoplastic palatal shelves that are unable to meet [12]. After their elevation and further growth, the palatal shelves must quickly acquire the competence to adhere and fuse. These are crucial steps taking place through a sequence of events, including contact, adhesion and merging of the two opposing MEEs, thus creating the single MES [21] (**Fig. 2D**). Competence for palatal shelf adhesion is precisely regulated. As we saw, before contact the MEE epithelium of the palatal shelves is composed of two layers: (a) the inner, basal layer of cuboidal cells sitting on a basement membrane; and (b) the outer layer of flattened peridermal cells. These two epithelial layers have different fates during palatal fusion. The basal epithelial layers of each MEE are destined to adhere to each other and to fuse, thus forming the MES which becomes stabilised by cell-cell junction systems formed between the adhered cells [14, 26]. While there is a general agreement that the cells of the basal layer will form the MES, the role of peridermal cells is not so clear. The presence of a continuous periderm layer on the MEE acts as a non-sticking barrier and, therefore, removal of the periderm appears to be a prerequisite for the merging of the two MEEs and palatal fusion [2]. It was initially thought that the periderm detached from the tips of the palatal shelves before they came into contact, so that initial contact between the shelves would be achieved *via* exposed MEE basal cells [18, 20]. Indeed, classical morphological studies seemed to indicate that, just prior to adhesion between the apposing shelves, the nuclei of the periderm cells became pyknotic, the cells detached and died by apoptosis [18,20]. However, other investigators have demonstrated that the initial contact between palatal shelves and some degree of weak adhesion instead takes place between the periderm cells of the apposing shelves, mediated *via* chondroitin sulphate proteoglycan expressed on the filopodia produced by the periderm to increase the surface area available for interconnection [26]. Therefore, whereas some peridermal cells may indeed shed away and die by apoptosis prior to contact between palatal shelves [14, 54], most of them persist in

the MEEs and migrate out downward and upward along the oro-nasal axis, where they will participate in the formation of the epithelial triangles observed in the MES [14, 9, 26, 60]. Many studies have revealed an essential involvement of TGF β 3 signalling in this process as well as in all subsequent phases of fusion [5, 42]. TGF β 3 expression is specifically expressed in MEE cells, including the periderm layer, already prior to palatal shelf adhesion [10, 43]. Notably, in TGF β 3^{-/-} mice filopodia are absent, chondroitin sulphate proteoglycan is not expressed, the periderm cells fail to migrate away, and a cleft palate occurs [26, 62]. Indeed, according to Taya, O’Kane and Ferguson [62], the production of TGF β 3-induced filopodia might be considered as diagnostic of increased cell motogenic/migratory activity of the MEE. Such increased activity would also be important for the rapid interdigitation of opposing palatal MEE cells following contact, to secure a firm fusion [62]. On the other hand, enhanced motogenic and migratory activity would also have a role in the subsequent disruption of the MES, through MEE cell migration towards the oral and nasal surfaces. Thus, according to these studies, TGF β 3 could intervene in all phases of palate fusion by stimulating inter-palatal MEE cell adhesion and by enhancing cell migration both during MES formation and during its disruption [62]. Therefore, it should be highlighted that the periderm probably has an instrumental role in MES formation in response to TGF β 3, as in absence of TGF β 3 peridermal cells fail to migrate out of the MES [41, 62]. Thus, current data does not support the hypothesis that periderm undergoes complete sloughing/apoptosis prior to palate shelf adhesion [18,20], but rather are consistent with the periderm playing an active role in maintaining epithelial integrity and stability through palate fusion [41].

As we have seen, proper periderm differentiation and maintenance are key in palatogenesis by preventing abnormal adhesion of palatal shelves to other oral structure. Mice lacking Jag2, FGF10, Irf6, or Grhl3 gene function exhibit aberrant adhesion or fusion of palatal shelves to mandible and/or tongue and, therefore, develop a cleft palate [44]. Indeed, molecular networks including FGF10/FGFr2b/Jag2/Notch and p63/Irf6 signalling, as well as Grhl3 transcription factor, are essential in driving differentiation of the periderm [5, 43, 44] (**Fig. 5A**). Irf6 is a direct target of p63, and p63 has been shown to positively regulate FGFr2b and Jag2 expression [42]. Animals with malfunctioning Jag2, Fgf10, Irf6, and Grhl3 genes have abnormal intra-oral adhesions and a cleft palate phenotype [5]. The central player in this molecular network is Irf6, whose loss of function in humans has been associated with clefting in Van der Woude syndrome, as well as in cases of non-syndromic clefting [38]. P63 is expressed in basal cells of the MEEs and becomes down-regulated in supra-basal cells when periderm differentiation is achieved [42]. As we have already mentioned, during ongoing epithelial stratification, the transcription factor p63 activates FGFr2b/Jag2/Notch signalling and the expression of Irf6, which in turn down-regulate p63 in the supra-basal cell layer, thus inducing p21-mediated cell cycle exit and allowing periderm differentiation [42, 44]. Therefore, both Jag2/Notch and Irf6 signalling seem to be activated by and negatively feedback to p63 to direct periderm differentiation/maintenance [42]. On the other hand, it has been seen that the expression of Irf6 is also crucial for MES dissolution. Indeed, once formed, the MES must be eliminated to obtain mesenchymal confluence and palate continuity. Biological systems often use similar mechanisms to achieve different outcomes and, indeed, as we shall see in the following paragraph, the same Irf6/p63/p21 pathway used for periderm differentiation is reutilised to facilitate MES dissolution [41, 42, 44].

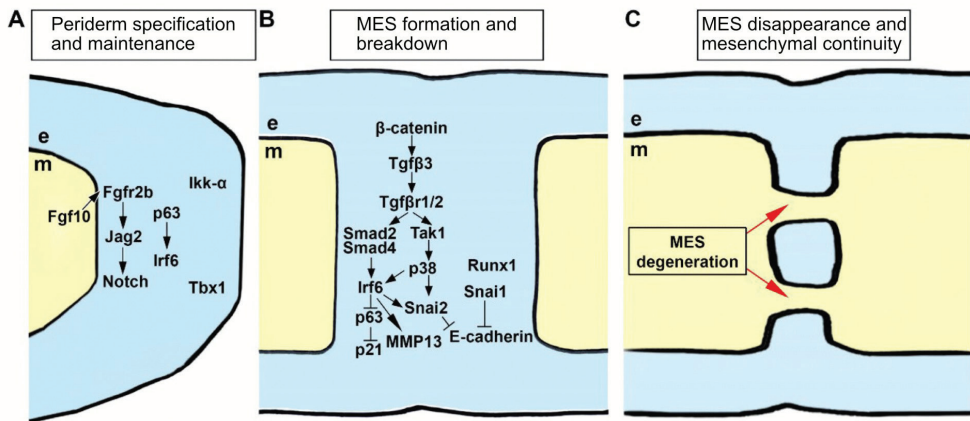


Fig. 5. Highly schematic representation of the molecular and morphological stages of palatal shelf fusion: from periderm differentiation and maintenance in the MEE (A), through the union of separate MEEs into the single MES and its initial breakdown (B), to MES disappearance and generation of a continuous palate (C). (A) Molecular control of epithelial/periderm differentiation in the MEE cells prior to palatal shelf contact. The MEE is formed by basal cells and a thin layer of periderm resulting from stratification of basal cells. Active FGF10/FGFr2b/Jag2/Notch and p63/Irf6 signalling together to Ikka and Tbx1 promote the differentiation and maintenance of the periderm, thus ensuring that inappropriate adhesions of the MEE do not occur. (B) The apposing palatal shelves have come into contact and, in order for them to adhere to each other and form the MES the periderm must migrate away. However, once formed also the MES must be eliminated. TGFβ3 signalling - probably under the control of Wnt/β-catenin - plays a fundamental role in these processes through both Smad-dependent and -independent pathways that activate Irf6/p63/p21 signalling, thus leading to cell-cycle arrest that favours apoptosis as well as MMP activation that mediates basement membrane disruption and extracellular matrix remodelling. TGFβ3 and Irf6 also activate Snail to loosen E-cadherin-based cell-cell adhesions, thus favouring motility/EMT of MEE cells. Runx1 is expressed in the MEE and is required for anterior palate fusion [5]. (C) The MES breaks up into epithelial islands, and becomes substituted by infilling mesenchymal tissue, until its complete disappearance, thus ensuring palate continuity. See the text for further explanation. Kindly reprinted from Won, Kim, Won, Shin (modified, from ref. 64).

Formation and breakdown of the MES

Fusion of the secondary palate requires juxtaposition of the MEE cells that cover the tips of the palatal shelves, and thereby the transformation of the separate MEEs into a single MES (Fig. 6). While adhesion between the opposing MEEs is taking place, some peridermal cells may become trapped between the adhered basal cells, where they may continue to migrate towards the oral and nasal epithelia or die by apoptosis [14]. However, once formed, the MES appears to be composed primarily of juxtaposed basal MEE cells. Morphologically, it consists of a seam comprised of two or three layers of epithelial cells, surrounded on both sides by an intact basement membrane. The constituent cells appear to interdigitate and form new cell-cell adhesion systems that stabilise the forming seam [15]. Nevertheless, the newly formed MES must be removed to allow mesenchymal continuity throughout the fused palate. The breakdown

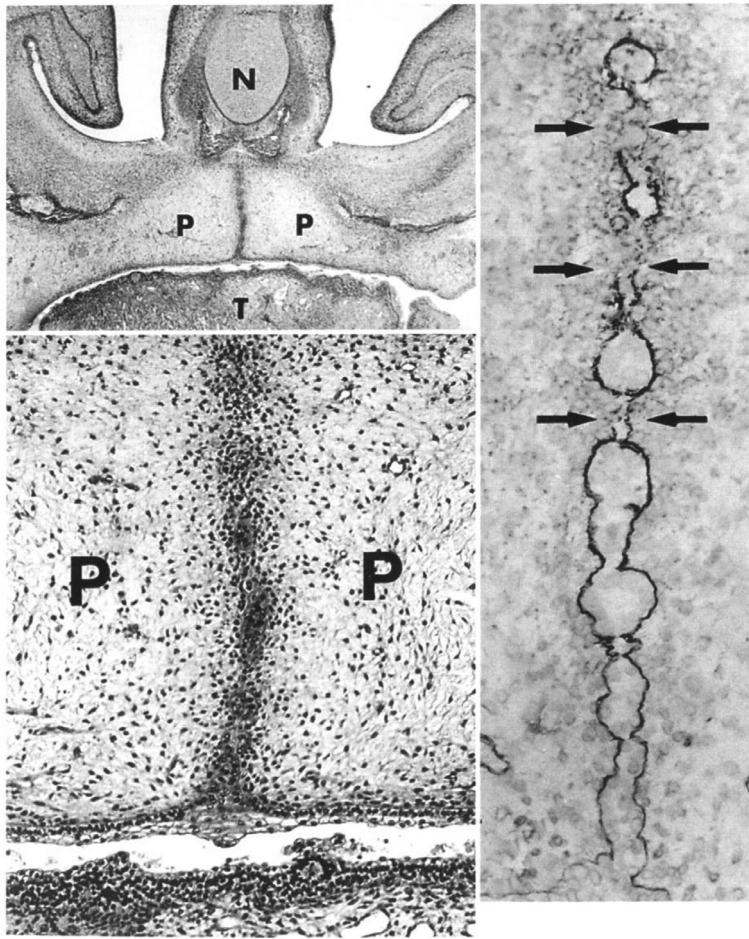


Fig. 6. Fusing palate of a 9-week-old human foetus. (A, upper left; B, below left) Haematoxylin and eosin-stained coronal section from the anterior palate region, showing well established fusion between the palate shelves with the intervening MES exhibiting noticeable breakdown (magnified in B). (C, right) An adjacent section from the same sample stained with antibodies to collagen type IV shows the MES surrounded by a basement membrane exhibiting evident areas of disruption (arrows). Correspondingly, the MES shows fragmentation/disintegration and formation of epithelial islands. Basement membrane disruption, which is a consistent finding during MES breakdown, is indicative of tissue rearrangement, but does not specifically address any of the hypothesised mechanisms for MES dissolution. As a matter of fact, basement membrane degradation may be compatible with epithelial-mesenchymal transition (EMT), apoptosis, or even migration of MES cells. Indeed, while basement membrane degradation is necessary to allow the translocation of transitioning cells from the epithelial compartment to mesenchyme during EMT (refs. 18, 25), basement membrane degradation can also occur as a consequence of apoptosis, the so-called “cataptosis” (ref. 9). Finally, extracellular matrix-degrading metalloproteinases have been suggested to play a role in the initiation of MES breakage that occurs during collective epithelial migration, another proposed mechanism for palate fusion (ref. 62). P, palate shelves; N, nasal septum; T, tongue. From Guarino et al. (ref. 25), reprinted with permission of Elsevier.

of the MES is morphologically characterised by thinning of the epithelium thickness, basement membrane disruption, breaking up of the seam into epithelial islands, mesenchymal penetration between them and, eventually, the complete disappearance of every trace of the intervening epithelium [15, 18, 20, 34, 45] (**Fig. 5C**, **Fig. 6B, C**). Kim and coworkers [37] proposed an interesting model of MES formation/dissolution. They demonstrated the creation of a transient multilayered MES in which palatal fusion proceeds through concurrent convergence, cell intercalation and displacement, apoptosis and extrusion of the MES epithelium along the the oro-nasal axis and, ultimately, MES breakage into epithelial islands [37, 41] (**Fig. 7**).

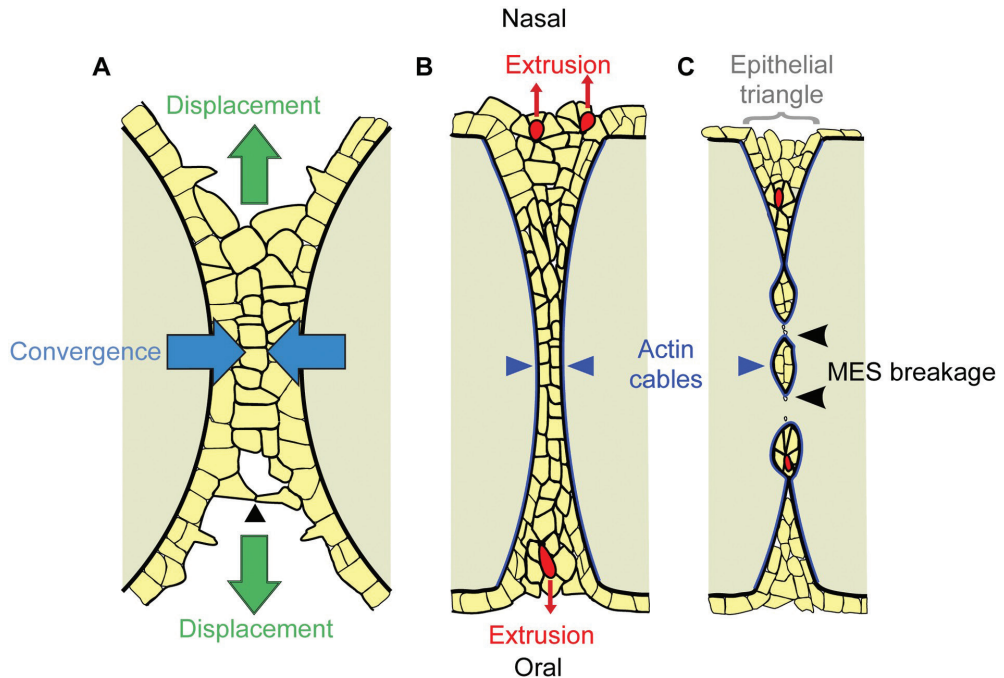


Fig. 7. Convergence and extrusion model by Kim and colleagues (ref. 37), proposed to explain the formation and breakdown of the (MES). (A) Formation of the MES is initiated by cellular protrusions which transiently create epithelial bridges (arrowhead), to establish contact between the shelves and give rise to a multilayered MES epithelium that then converges towards the midline, in conjunction with cell intercalation and oral and nasal cell displacement of MEE cells. (B) The formation of actin cables and multicellular rosettes is associated with extrusion of cells on the oral and nasal surfaces of the palate. (C) Contraction of the actin cables leads to breakage of the seam into islands, and further oro-nasal cell extrusion contributes to the formation of epithelial triangles. Kindly reprinted from Kim, Lewis, Singh, Ma, Adelstein, Bush (ref. 37).

The signals responsible for MES degradation are not yet fully understood, but there is evidence that TGF β 3 signalling still plays a prominent role. Indeed, TGF β 3 could promote MES degeneration by inducing cell cycle arrest and apoptosis, reducing epithelial cell adhesion, and favouring cell migration and extracellular matrix remodelling [26]. After binding to its membrane receptors, TGF β 3 activates Smad2/

Smad4 and the p38 MAPK pathways which, through the Irf6/p63 signalling, regulate p21 expression in the MES cells [5] (**Fig. 5B**). Indeed, quite similar to its function in periderm differentiation, Irf6 expression would cause down-regulation of p63 and an increase in p21 expression in the MES cells, which contributes to their cell cycle exit, thus favouring apoptosis and, therefore, degeneration of the midline seam [42]. In addition, TGF β 3 signalling also favours Snail-mediated disruption of epithelial adhesion and MMP-dependent breakdown of extracellular matrix. Actually, some of the events downstream of TGF β 3 are crucial to both the formation and dissolution of the MES (**Fig. 7**). Parallel activation of Snail family transcription factors downstream of TGF β 3 could, on one hand facilitate periderm sloughing and migration by loosening MEE basal cell/periderm cell adhesion through down-regulation of E-cadherin [44], and on the other hand it could contribute to promoting MEE cell apoptosis [5, 52]. Furthermore, Snail-driven E-cadherin-dependent loosening of cell-cell adhesion could be functional to the facilitation of cell intercalation, displacement or migration occurring either during the formation or the breakdown of the MES. Therefore, it is possible that Snail-mediated down-regulation of E-cadherin could, on the one hand favour the migration and apoptosis of the periderm in the approaching MEEs as well as basal cell displacement/intercalation to form the MES and, on the other hand, it could promote the disintegration of the MES itself after its formation by facilitating MES basal cell migration [44, 52]. Moreover, TGF β 3-dependent E-cadherin down-regulation could also underlie MES breakdown into small epithelial islands, a consistent step in MES dissolution [55] (**Fig. 6B, C, Fig. 7C**). E-cadherin is required for palate shelf fusion, but it is down-regulated by TGF β 3, thus indicating a complex role of this adhesion molecule in the fusion process. Mutations of CDH1/E-cadherin, which deletes the extracellular cadherin repeat domains needed for cell-cell adhesion, have been associated with cleft lip/palate in families with hereditary diffuse gastric cancer [67]. Furthermore, TGF β 3 is implicated in the remodelling of the extracellular matrix through the regulation of matrix metalloproteinase (MMP) function, including MMP13 [67]. Indeed, TGF β 3-induced MMP activation is responsible for the basement membrane disruption observed during dissolution of the MES, as well as for the reorganisation of the interstitial matrix necessary to achieve confluence of the palatal stroma after the disappearance of the MES, thus forming a united secondary palate [14].

The mechanism of palatal closure should ensure the strength of palatal fusion, such as the resistance to the muscular forces of the tongue and cheeks [6]. This would initially be provided by the establishment of firm epithelial cell-cell adhesions and desmosomes during the formation of the MES [20], and later strengthened by progressive mesenchymal infilling during MES breakdown, thus permitting merging and continuity of the core stromal component of the palatal shelves and consolidation of the fusion [6].

The mechanism behind the disappearance of the MES

The cellular mechanisms and dynamics that lead to the disappearance of the MES have been the subject of discussion and debated among three main, non-exclusive hypotheses [2, 5, 14, 21]: (a) epithelial-mesenchymal transition (EMT) of the MES that could allow the intervening seam epithelium to migrate and become incorporated into the

mesenchyme of the palatal stroma; (b) death of the MES cells by apoptosis that would lead to MES disintegration; (c) migration of MES cells in the oro-nasal directions which would allow their incorporation into the epithelial lining of the oral and nasal cavities.

Below we will analyse these hypotheses individually, and also mention models of MES removal that combine two or more cellular mechanisms.

Epithelial-mesenchymal transition (EMT)

In his comprehensive paper published in 1988, Ferguson [15] carefully described the fusion of the secondary palate shelves and the morphological features of MES dissolution. He also noted that some MES cells migrated into the palatal stroma where they became indistinguishable from other mesenchymal cells, and interpreted these cells as a specific subpopulation of “basal stem cells able to migrate” [15]. In their study published the following year, Fitchett and Hay [18] reexamined the mechanism of MES dissolution, and demonstrated that MES cells elongated into the adjacent mesenchyme through basement membrane discontinuities, lost epithelial characteristics, and acquired characteristics quite similar to migrating fibroblasts. The authors definitively interpreted the finding as an example of epithelial-mesenchymal transition (EMT). The possibility of a role of TGF β 3 in EMT during palatal fusion has been extensively investigated [10, 29, 34]. TGF β 3 could be the main EMT inducer by signalling *via* both Smad-dependent and PI3K or p38 MAPK pathways, thus leading to activation of the key Snail family transcription factors necessary for down-regulating E-cadherin, and thereby EMT induction [29, 67]. On the other hand, MMP13 expression is strongly induced by TGF β 3, and it is possible that this metalloproteinase specifically expressed in the MEE/MES and in adjacent mesenchyme during palatal fusion, could initiate EMT by promoting basement membrane degradation, thus influencing cell-cell and/or cell-matrix interactions [4]. According to this model, the disruption of the basement membrane is a significant and early event, because it could be instructive to initiate EMT and, on the other hand, it would allow the passage of transitioning cells into the mesenchymal compartment. However, regardless of its significance, basement membrane degradation is indeed consistently observed during MES degradation (**Fig. 6C**). In brief, according to the EMT hypothesis the MES would undergo progressive disintegration through disruption of the basement membrane, loss of cell-cell junctions and the epithelium-specific molecules E-cadherin and cytokeratin, while gaining vimentin intermediate filaments. Then, transitional cells would migrate into the stroma and become indistinguishable from the mesenchymal cells [18, 25]. EMT is known to occur in embryogenesis [35], play a role in pathological conditions including fibrosis [34], cancer histogenesis and progression [24, 25], and can be easily reproduced under experimental conditions [23]. The EMT-based model became very popular, and the establishment of the concept of EMT as the prevailing mechanism of palate fusion led to a wealth of studies attributing roles to different molecules, including TGF β 3, Lef1, Smads, Rho, PI3K, MMPs, Twist and Snail as possible mediators of palatal EMT [29, 55, 67]. However, subsequent studies have produced inconclusive results regarding a significant role of EMT in MES dissolution, and there is the possibility that, if the above-mentioned molecules may indeed play a role in palatal fusion, it could not necessarily be related to EMT [21].

Apoptosis

The longest-standing model to explain the disappearance of the MES has been programmed apoptotic cell death and, even today, many evidences support a major role for apoptosis in MES removal [5, 8, 9]. Overall, many findings fit well with the apoptotic death model [64]. For example, cell proliferation is rarely observed in the MES, and many MES cells are TUNEL- and active caspase 3-positive during palatal fusion, indicative of ongoing apoptosis [14, 64]. Moreover, TGF β 3 signalling seems to play an important role in favouring MES apoptosis, and it is known that lack of TGF β 3 in mice embryos allows palatal shelves to adhere at the midline, but not to fuse due to the persistence of the MES [34]. Periderm migration out the MEE/MES is known to be important to trigger basal MEE cell death [9], and TGF β 3 signalling is known to play a significant role in both periderm migration and cell cycle arrest of the MEE cells [64]. *Irf6* is a fundamental factor responsible for induction and maintenance of periderm differentiation in the MEE, and it is a direct target of p63 [22] and, in fact, p63 and *Irf6* function in a regulatory feedback loop to control both epithelial proliferation and periderm differentiation [22]. In the MES, *Irf6* is up-regulated through both TGF β 3/Smads and TGF β 3/p38 MAPK pathways, and leads to down-regulation of p63 and, therefore, increased p21 expression [64]. This mechanism is believed to favour cell cycle exit and, together with activation of Snail, to promote apoptosis and subsequent degeneration of the MES [5, 64]. Maintenance of oral periderm integrity also depends on Jag2-Notch signalling, and TGF β 3 is crucial for the down-regulation of Jag2, likely a another key mechanism by which TGF β 3 disrupts periderm function, thus facilitating MEE basal cell adhesion and fusion [64]. In conclusion, TGF β 3 signalling would allow periderm migration out of the MES, thus causing on one hand complete palatal fusion, on the other hand it would reduce the proliferative potential of MES basal cells, thereby favouring MES cell loss through apoptosis (**Fig. 5**). According to Cuervo and Covarrubias, the MES essentially degenerates by programmed cell death triggered by the adhesion between the apposing shelf epithelia [9]. Prior to the fusion, periderm cells cover the MEEs and act as a barrier for direct contact between the opposing MEE basal cells, which actually is a requirement for MEE cell death activation. Thus, periderm should shed away or migrate out of the MEE/MES to allow contact between the apposing basal cells, and thereby activate their apoptosis. These authors also found that activation of cell death promoted the degradation of the basement membrane underlying the dying MES cells, a process that they call “cataptosis”, and suggested that dying cells would directly activate MMPs, including MMP13, eventually responsible for the basement membrane degradation [9].

Cell migration

Migration of cells of the MES along the midline towards the oral or nasal surface epithelia is another mechanism that has been proposed to explain the disappearance of the MES [6]. According Carette and Ferguson [6], MES cells would migrate nasally and orally out of the seam where they are recruited into, and constitute the epithelial triangles on both the oral and nasal aspects of the fusing palate. Subsequently, these transitory migrating cells would become incorporated into the oral and nasal epithelia on the surfaces of the palate [6]. However, other studies seem to indicate that the majority of cells that migrate along the midline towards the oral and nasal surfaces are peridermal cells, rather than basal MEE cells. Indeed, Cuervo and Covarrubias

[9] demonstrated that epithelial triangles at oral and nasal ends of the MES do not appear to result from basal MEE cell migration, but rather from periderm cell migration, and that the migration of periderm cells out from the MEE is necessary to initiate and complete normal shelf fusion [9]. According to the authors, TGF β 3 could play a role in promoting the migration of peridermal cells along the oro-nasal axis which then accumulate at the bottom and top of the MES to form the epithelial triangles, possibly important for sealing the ends of the MES [9]. A recent paper demonstrated the importance of actomyosin dynamics in palate fusion whereby the MES is removed through actomyosin-dependent collective cell migration of epithelial trails and islands of basal cells in order to allow mesenchymal confluence, independently of the occurrence of programmed cell death, since blocking apoptosis did not prevent MES removal [63]. Indeed, by novel static- and live-imaging, these authors detected a unique form of collective epithelial migration, whereby the MES would be removed through streaming migration of collections of epithelial cells to reach the oral and nasal epithelial surfaces. This mechanism of MES elimination depended exclusively on the contractility of actomyosin filament system generating a peristaltic-type propulsive force, and not by apoptosis, as genetic suppression of the intrinsic apoptotic regulators BAX and BAK did not prevent successful MES disappearance [63].

Combined model hypotheses

For three decades there has been a heated debate as to whether MES cells became mesenchymal through EMT, died by apoptosis, or migrated into the oral or nasal surface epithelia. However, it is also possible that more than one of these mechanisms, or even all of them, are physiologically used to remove the MES.

Using an organ culture system, Jin and Ding [31] observed the migration of MES epithelial cells towards the nasal side – but not towards the oral side – of the fusing shelves, and simultaneously demonstrated the presence at some distance from the mid-line of β -galactosidase-labelled cells in the mesenchymal stroma of the palate shelves, indicative of their epithelial origin and, therefore, of the occurrence of a mechanism of palate fusion based on both migration and EMT.

Ahmed and colleagues [1] proposed a mechanism of MES disintegration whereby MES cells would sequentially undergo cell cycle arrest, EMT-mediated cell migration and apoptosis in response to TGF β 3. These data suggest that TGF β 3 induced different phenotypic changes at different times functional to palatal MES dissolution: cell cycle arrest, repression of E-cadherin-based cell–cell adhesion and migration and, finally, apoptosis of post-EMT migrated cells. Indeed, before undergoing apoptosis, MES cells showed gradual phenotypical alteration, changing from cohesive epithelial to fully migratory fibroblastoid, indicative of EMT.

Studies by Benson et al. [3] are consistent with a model of MES degradation where seam epithelial cells would undergo EMT and/or death by apoptosis, thus leading to confluence of the palatal stroma. In addition to TGF β 3, a further signal for initiating palatal fusion and EMT could be provided by members of the Ephrin family [3]. Indeed, TGF β 3 and Ephrin signalling could cooperate in seam dissolution: both would induce a migratory phenotype in cultured MEE cells [3] and, in addition, TGF β 3 could also promote apoptosis [1, 54].

Ke and colleagues [36] investigated the role of Irf6 in the molecular mechanisms underlying palate fusion using palatal shelf organ culture. The authors found that

TGF β 3 up-regulated Irf6 which, in turn, increased Snail, thus promoting EMT. On the other hand, Irf6 could also lead to apoptosis *via* the p63/p21 signalling cascade. These results indicate the TGF β 3/Irf6 pathway can lead to different results, EMT or apoptosis, and that both mechanisms could contribute to MES dissolution during normal palatal fusion.

According to Nakajima and colleagues [53], multiple mechanisms would contribute to removing the MES to form a single, continuous palate. Coincident with the strong expression of TGF β 3 in the MES, both EMT and apoptotic changes could be observed among the cells at the midline, and, in addition, cells of the MES could also migrate collectively as clustered aggregates into the oral and nasal epithelial layers. Basically, the MES would undergo collective cell migration, EMT, and eventually apoptosis, which might be a form of post-EMT apoptosis (“lethal” EMT). Therefore, some of the MEE-derived mesenchymal cells would be lost by apoptosis, but the remaining ones, characterised by sustained high expression of TGF β 3 and TGF β receptors, would be adopted into the palatal stroma. Meanwhile, crowding force due to epithelial migration would cause cell extrusion at the epithelial triangles, releasing MEE cells to the oral and nasal surfaces of the palate. Due to these multiple biological events, the number of cells of the MES is decreased, thus causing discontinuities in the seam and formation of epithelial islands, until complete disappearance [53].

Logan and coworkers [45] proposed a new model that incorporates features of partial EMT along with collective cell migration. In such a model, TGF β and Ephrin signalling would induce a partial EMT in a subpopulation of MES cells, but nevertheless the cells would appear to move together as a cohesive sheet. Indeed, these EMT-transformed cells would serve as leader cells of a movable cell collection. This scenario would also fit with the breaking of the epithelial seam into islands before its complete dissolution. Each island could be a population of relatively epithelial-like cells attached to more fibroblast-like leader cells. The resulting motile collective units would migrate following leader cells that provide the moving force.

Recently, hypotheses have been proposed based on the formation and dissolution of the MES by cell convergence and extrusion. These studies reveal an essential role for actomyosin contractility-driven convergence and cell intercalation in the formation of the MES, and subsequent cell displacement and extrusion during MES breakdown. These models mechanistically connect most of the cellular behaviours previously observed palatal fusion, including early extension of filopodial protrusions by periderm cells, cell shape changes, cell displacement and cell migration in the oro-nasal directions during MES formation and breakdown, apoptotic cell death and actomyosin-driven MES convergence [42] (**Fig. 7**). Indeed, Kim and coworkers [37] examined cell behaviour during palatal fusion using a combination of genetic lineage labelling, tissue-specific gene inactivation, and live imaging. The authors reveal an essential role for actomyosin contractility, cell intercalation and displacement, apoptosis and MES cell extrusion at the oro-nasal surfaces. Whereas an argument against apoptosis as the major mechanism for MES dissolution argued that massive cell death of the MES cells would weaken the fusion site and potentially lead to separation of the palatal shelves [61], by using live imaging Kim et al. [37] demonstrated a process of MES cell extrusion, during which converging MES cells form rosettes, and the cells in the centre of these rosettes are squeezed out by multicellular actin cables. Therefore, apoptosis in the MES does not involve the simultaneous death of all cells that could weaken the

fusion site, but rather it would occur through the extrusion of the apoptotic cell by its neighbouring cells that remain viable. The forces for the convergence and extrusion events would be provided by actomyosin contractility requiring Rho kinase- and myosin light chain kinase-mediated activation of non-muscle myosin [37, 42](Fig. 7).

In conclusion, according to the most recent views, MES disappearance could require actomyosin contractility as well as by TGFβ3/Irf6-regulated cell cycle arrest/apoptosis and MMP13-mediated extracellular matrix breakdown [42]. On the other hand, some other molecules, in particular the transcription factors Runx1 [53] and Snail [52], could be required for MES formation/breakdown during palatal fusion. Snail family transcription factors have been implicated in EMT by directly repressing cell-cell adhesion components, therefore it is possible that Snail, downstream or in cooperation with TGFβ3/Irf6 signalling, works by loosening adhesion between either periderm and MEE basal cells to form the MES, or between basal MEE cells in the formed MES, thus contributing to its ultimate dissolution [42, 64](Fig. 5B), perhaps even through the induction of actual EMT [35] (Fig. 8).

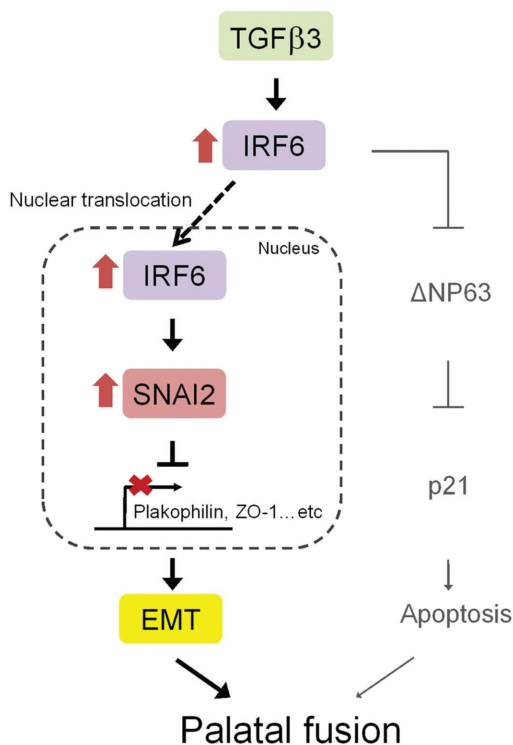


Fig. 8. Diagram depicting TGFβ3/Irf6 signalling pathway leading to EMT or, alternatively, apoptosis during palatal fusion. TGFβ3 up-regulates the expression of Irf6 and enhances its nuclear translocation, which then would increase the expression of Snail transcription factors which, in turn, could induce EMT of the MES cells. In addition, Irf6 down-regulates p63, which will result in induction of p21 expression, thus favouring MES cell apoptosis. Both of these events could occur in the process of palatal fusion, and contribute to MES disintegration. Kindly reprinted from Ke, Xiao, Chen, Lo, Wong (ref. 36).

Conclusions

Orofacial defects including cleft lip and cleft palate are among the most common congenital birth anomalies, and are caused by failure of the facial/palatal processes to grow or fuse properly during the first trimester of gestation. The cellular and molecu-

lar mechanisms governing normal palatogenesis and their failure in orofacial clefting have not definitively been elucidated. On the other hand, the care of patients with cleft lip and cleft palate continues to be a cause for concern, and therefore, prevention of these deformities remains the ultimate objective of research. Thus, advances on the mechanisms underlying orofacial clefting as well as their relationships with genetic and environmental factors are the key to preventing these disfiguring birth defects. Moreover, further study of the events involved in palatogenesis could not only improve our understanding of the developmental pathogenesis of these deformities, but could also provide clinical and prognostic information. For example, knowing the molecular defect underlying the cleft in a given patient can provide information in the healing of the palate after surgical repair and therefore the risks for post-operative complications, as it is known that approximately 10% of patients develop wound complications following surgical repair of cleft palate. The observation that patients with Van der Woude syndrome, which in most cases is caused by *Irf6* mutation, had worse surgical outcome based on surgical wound healing complications, compared with patients with non-syndromic cleft [33], suggests the importance of a detailed knowledge of the etiological mechanism underlying orofacial clefting. Currently, numerous genes and molecular pathways involved in normal palatogenesis and pathological clefting have been identified. As an increasingly number of molecular studies are rapidly improving our knowledge on the signalling networks underlying palate development, their integration with notions on genetic-environmental factors and tissue morphogenetic events leading to clefting could translate into the creation of new strategies for the prevention, treatment and prognosis of these defects.

Acknowledgements. The author would like to thank Fabio Nangeroni for his useful suggestions and technical support.

References

1. **Ahmed, S., C. C. Liu, A. Nawshad.** Mechanisms of palatal epithelial seam disintegration by transforming growth factor (TGF) β 3. – *Developmental Biology*, **309**, 2007, 193-207.
2. **Antiguas, A., B. J. Paul, M. Dunnwald.** To stick or not to stick: adhesions in orofacial clefts. – *Biology*, **11**, 2022, 153.
3. **Benson, M. D., M. J. Serrano.** Ephrin regulation of palate development. – *Frontiers in Physiology*, **3**, 2012, 376.
4. **Blavier, L., A. Lazaryev, J. Groffen, N. Heisterkamp, Y. A. DeClerck, V. Kaartinen.** TGF- β 3-induced palatogenesis requires matrix metalloproteinases. – *Molecular Biology of the Cell*, **12**, 2001, 1457-1466.
5. **Bush, J. O., R. Jiang.** Palatogenesis: morphogenetic and molecular mechanisms of secondary palate development. – *Development*, **139**, 2012, 231-243.
6. **Carette, M. J., M. W. Ferguson.** The fate of medial edge epithelial cells during palatal fusion in vitro: an analysis by Dil labelling and confocal microscopy. – *Development*, **114**, 1992, 379-388.
7. **Chai, Y., R. E. Maxson Jr.** Recent advances in craniofacial morphogenesis. – *Developmental Dynamics*, **235**, 2006, 2353-2375.

8. **Cuervo, R., C. Valencia, R. A. Chandraratna, L. Covarrubias.** Programmed cell death is required for palate shelf fusion and is regulated by retinoic acid. – *Developmental Biology*, **245**, 2002, 145-156.
9. **Cuervo, R., L. Covarrubias.** Death is the major fate of medial edge epithelial cells and the cause of basal lamina degradation during palatogenesis. – *Development*, **131**, 2004, 15–24.
10. **D’Souza, R. N., L. B Ruest, R. J. Hinton, K. K. Svoboda.** Development of the craniofacial complex. In: *Bone and development. Topics in bone biology* (Eds. Bronner, F., Farach-Carson, M., Roach, H.), London. Springer, 2010, 153-181.
11. **Deshpande, A. S., S. L. Goudy.** Cellular and molecular mechanisms of cleft palate development. – *Laryngoscope Investigative Otolaryngology*, **4**, 2019, 160-164.
12. **Ding, H., X. Wu, H. Boström, I. Kim, N. Wong, B. Tsoi, A. Nagy.** A specific requirement for PDGF-C in palate formation and PDGFR- α signaling. – *Nature Genetics*, **36**, 2004, 1111-1116.
13. **Dixon, M. J., M. L. Marazita, T. H. Beaty, J. C. Murray.** Cleft lip and palate: understanding genetic and environmental influences. – *Nature Reviews Genetics*, **12**, 2011, 167-178.
14. **Dudas, M., W. Y. Li, J. Kim, A. Yang, V. Kaartinen.** Palatal fusion – Where do the midline cells go?: A review on cleft palate, a major human birth defect. – *Acta Histochemica*, **109**, 2007, 1-14.
15. **Ferguson, M. W.** Palate development. – *Development*, **103** (Supplement), 1988, 41-60.
16. **Ferguson, M. W.** The orofacial region. In: *Textbook of fetal and perinatal pathology* (Eds. J.S. Wigglesworth, D.B Singer), Boston, Blackwell Scientific Publications, 1991, 843-880.
17. **Ferretti, E., B. Li, R. Zewdu, V. Wells, J. M. Hebert, C., Karner, L. Selleri.** A conserved Pbx-Wnt-p63-Irf6 regulatory module controls face morphogenesis by promoting epithelial apoptosis. – *Developmental Cell*, **21**, 2011, 627-641.
18. **Fitchett, J. E., E. D. Hay.** Medial edge epithelium transforms to mesenchyme after embryonic palatal shelves fuse. – *Developmental Biology*, **131**, 1989, 455-474.
19. **Greene, R. M., M. M. Pisano.** Palate morphogenesis: current understanding and future directions. – *Birth Defects Research Part C: Embryo Today: Reviews*, **90**, 2010, 133-154.
20. **Griffith, C. M., E. D. Hay.** Epithelial-mesenchymal transformation during palatal fusion: carboxyfluorescein traces cells at light and electron microscopic levels. – *Development*, **116**, 1992, 1087-1099.
21. **Gritli-Linde, A.** Molecular control of secondary palate development. – *Developmental Biology*, **301**, 2007, 309-326.
22. **Gritli-Linde, A.** p63 and IRF6: brothers in arms against cleft palate. – *Journal of Clinical Investigation*, **120**, 2010, 1386-1389.
23. **Guarino, M., F. Giordano.** Experimental induction of epithelial-mesenchymal interconversions. – *Experimental and Toxicologic Pathology*, **47**, 1995, 325-334.
24. **Guarino, M., F. Giordano, F. Pallotti, G. Polizzotti, P. Tricomi, E. Cristofori.** Malignant mixed müllerian tumor of the uterus. Features favoring its origin from a common cell clone and an epithelial-to-mesenchymal transformation mechanism of histogenesis. – *Tumori Journal*, **84**, 1998, 391-397.
25. **Guarino, M., P. Micheli, F. Pallotti, F. Giordano.** Pathological relevance of epithelial and mesenchymal phenotype plasticity. – *Pathology-Research and Practice*, **195**, 1999, 379-389.

26. **Hammond, N. L., M. J. Dixon.** Revisiting the embryogenesis of lip and palate development. – *Oral Diseases*, **28**, 2022, 1306-1326.
27. **He, F., W. Xiong, X. Yu, R. Espinoza-Lewis, C. Liu, S. Gu, Y. Chen.** Wnt5a regulates directional cell migration and cell proliferation via Ror2-mediated noncanonical pathway in mammalian palate development. – *Development*, **135**, 2008, 3871-3879.
28. **Ito, Y., J. Y. Yeo, A. Chytil, J. Han, P. Bringas Jr, A. Nakajima, Y. Chai.** Conditional inactivation of Tgfb2 in cranial neural crest causes cleft palate and calvaria defects. – *Development*, **130**, 2003, 5269–5280.
29. **Jalali, A., X. Zhu, C. Liu, A. Nawshad.** Induction of palate epithelial mesenchymal transition by transforming growth factor β 3 signaling. – *Development, Growth & Differentiation*, **54**, 2012, 633-648.
30. **Ji, Y., M. A. Garland, B. Sun, S. Zhang, K. Reynolds, M. McMahon, C. J. Zhou.** Cellular and developmental basis of orofacial clefts. – *Birth Defects Research*, **112**, 2020, 1558-1587.
31. **Jin J. Z. J. Ding.** Analysis of cell migration, transdifferentiation and apoptosis during mouse secondary palate fusion. – *Development* **133**, 2006, 3341-3347.
32. **Jiang, R., J. O. Bush, A. C. Lidral.** Development of the upper lip: morphogenetic and molecular mechanisms. – *Developmental Dynamics*, **235**, 2006, 1152-1166.
33. **Jones, J. L., J. W. Canady, J. T. Brookes, G. L. Wehby, J. L’Heureux, B. C. Schutte, M. Dunnwald.** Wound complications after cleft repair in children with Van der Woude syndrome. – *Journal of Craniofacial Surgery*, **21**, 2010, 1350-1353.
34. **Kaartinen, V., X. M. Cui, N. Heisterkamp, J. Groffen, C. F. Shuler.** Transforming growth factor- β 3 regulates transdifferentiation of medial edge epithelium during palatal fusion and associated degradation of the basement membrane. – *Developmental Dynamics*, **209**, 1997, 255-260.
35. **Kalluri, R.** EMT: when epithelial cells decide to become mesenchymal-like cells. – *Journal of Clinical Investigation*, **119**, 2009, 1417-1419.
36. **Ke, C. Y., W. L. Xiao, C. M. Chen, L. J. Lo, F. H. Wong.** IRF6 is the mediator of TGF β 3 during regulation of the epithelial mesenchymal transition and palatal fusion. – *Scientific Reports*, **5**, 2015, 12791.
37. **Kim, S., A. E. Lewis, V. Singh, X. Ma, R. Adelstein, J. O. Bush.** Convergence and extrusion are required for normal fusion of the mammalian secondary palate. – *PLoS Biology*, **13**, 2015, e1002122.
38. **Kousa, Y. A., B. C. Schutte.** Toward an orofacial gene regulatory network. – *Developmental Dynamics*, **245**, 2016, 220-232.
39. **Lan, Y., C. E. Ovitt, E. S. Cho, K. M. Maltby, Q. Wang, R. Jiang.** Odd-skipped related 2 (Osr2) encodes a key intrinsic regulator of secondary palate growth and morphogenesis. – *Development* **131**, 2004, 3207-3216.
40. **Lan, Y., R. Jiang.** Sonic hedgehog signaling regulates reciprocal epithelial-mesenchymal interactions controlling palatal outgrowth. – *Development*, **136**, 2009, 1387–1396.
41. **Lan, Y., R. Jiang.** Mouse models in palate development and orofacial cleft research: Understanding the crucial role and regulation of epithelial integrity in facial and palate morphogenesis. – *Current Topics in Developmental Biology*, **148**, 2022, 13-50.
42. **Lan, Y., J. Xu, R. Jiang.** Cellular and molecular mechanisms of palatogenesis. – *Current Topics in Developmental Biology*, **115**, 2015, 59-84.
43. **Lane, J., V. Kaartinen.** Signaling networks in palate development. – *Systems Biology and Medicine*, **6**, 2014, 271-278.

44. **Li, C., Y. Lan, R. Jiang.** Molecular and cellular mechanisms of palate development. – *Journal of Dental Research*, **96**, 2017, 1184-1191.
45. **Logan, S. M., L. B. Ruest, M. D. Benson, K. K. Svoboda.** Extracellular matrix in secondary palate development. – *Anatomical Record*, **303**, 2020, 1543-1556.
46. **Losa, M., M. Risolino, B. Li J. Hart, L. Quintana, I. Grishina, L. Selleri.** Face morphogenesis is promoted by Pbx-dependent EMT via regulation of Snail1 during frontonasal prominence fusion. – *Development*, **145**, 2018, dev157628.
47. **Marazita, M. L.** The evolution of human genetic studies of cleft lip and cleft palate. – *Annual Review of Genomics and Human Genetics*, **13**, 2012, 263-283.
48. **Meng, L., Z. Bian, R. Torensma, J. W. Von den Hoff.** Biological mechanisms in palatogenesis and cleft palate. – *Journal of Dental Research*, **88**, 2009, 22-33.
49. **Mossey, P. A., J. Little, R. G. Munger, M. J. Dixon, W. C. Shaw.** Cleft lip and palate. – *Lancet*, **374**, 2009, 1773-1785.
50. **Moxham, B. J.** The development of the palate—a brief review. – *European Journal of Anatomy*, **7**, 2003, 53-74.
51. **Murray, J. C.** Gene/environment causes of cleft lip and/or palate. – *Clinical Genetics*, **61**, 2002, 248-256.
52. **Murray, S. A., K. F. Oram, T. Gridley.** Multiple functions of Snail family genes during palate development in mice. – *Development*, **134**, 2007, 1789-1797.
53. **Nakajima, A., F. C. Shuler, A. O. Gulka, J. I. Hanai.** TGF- β signaling and the epithelial-mesenchymal transition during palatal fusion. – *International Journal of Molecular Sciences*, **19**, 2018, 3638.
54. **Nawshad, A.** Palatal seam disintegration: to die or not to die? that is no longer the question. – *Developmental Dynamics*, **237**, 2008, 2643-2656.
55. **Nawshad, A., D. Medici, C. C. Liu, E. D. Hay.** TGF β 3 inhibits E-cadherin gene expression in palate medial-edge epithelial cells through a Smad2-Smad4-LEF1 transcription complex. – *Journal of Cell Science*, **120**, 2007, 1646-1653.
56. **Paiva, K. B. S., C. S. Maas, P. M. D. Santos, J. M. Granjeiro, A. Letra.** Extracellular matrix composition and remodeling: Current perspectives on secondary palate formation, cleft lip/palate, and palatal reconstruction. – *Frontiers in Cell and Developmental Biology*, **7**, 2019, 340.
57. **Reynolds, K., P. Kumari, L. Sepulveda Rincon, R. Gu, Y. Ji, S. Kumar, C. J. Zhou.** Wnt signaling in orofacial clefts: crosstalk, pathogenesis and models. – *Disease Models & Mechanisms*, **12**, 2019, dmm037051.
58. **Rice, R., B. Spencer-Dene, E. C. Connor, A. Gritli-Linde, A. P. McMahon, C. Dickson, D. P. Rice.** Disruption of Fgf10/Fgfr2b-coordinated epithelial-mesenchymal interactions causes cleft palate. – *Journal of Clinical Investigation*, **113**, 2004, 1692-1700.
59. **Rice, R., E. Connor, D. P. Rice.** Expression patterns of Hedgehog signalling pathway members during mouse palate development. – *Gene Expression Patterns*, **6**, 2006, 206-212.
60. **Richardson, R., K. Mitchell, N. L. Hammond, M. R. Mollo, E. N. Kouwenhoven, N. D. Wyatt, J. Dixon.** p63 exerts spatio-temporal control of palatal epithelial cell fate to prevent cleft palate. – *PLoS Genetics*, **13**, 2017, e1006828.
61. **Sun, D., S. Baur, E. D. Hay.** Epithelial–mesenchymal transformation is the mechanism for fusion of the craniofacial primordia involved in morphogenesis of the chicken lip. – *Developmental Biology*, **228**, 2000, 337-349.
62. **Taya, Y., S. O’Kane, M. W. Ferguson.** Pathogenesis of cleft palate in TGF- β 3 knockout mice. – *Development*, **126**, 1999, 3869-3879.

63. **Teng, T., C. S. Teng, V. Kaartinen, J. O. Bush.** A unique form of collective epithelial migration is crucial for tissue fusion in the secondary palate and can overcome loss of epithelial apoptosis. – *Development*, **149**, 2022, dev200181.
64. **Won, H. J., J. W. Kim, H. S. Won, J. O. Shin.** Gene regulatory networks and signaling pathways in palatogenesis and cleft palate: a comprehensive review. – *Cells*, **12**, 2023, 1954.
65. **Xu, J., H. Liu, Y. Lan, B. J. Aronow, V. V. Kalinichenko, R. Jiang.** A Shh-Foxf-Fgf18-Shh molecular circuit regulating palate development. – *PLoS Genetics*, **12**, 2016, e1005769.
66. **Yu, W., L. B. Ruest, K. K. Svoboda.** Regulation of epithelial-mesenchymal transition in palatal fusion. – *Experimental Biology and Medicine*, **234**, 2009, 483-491.
67. **Yu, W., M. Serrano, S. San Miguel, L. B. Ruest, K. K. Svoboda.** Cleft lip and palate genetics and application in early embryological development. – *Indian Journal of Plastic Surgery*, **42**, 2009, S35-S50.
68. **Zhou, J., Y. Gao, Y. Lan, S. Jia, R. Jiang.** Pax9 regulates a molecular network involving Bmp4, Fgf10, Shh signaling and the Osr2 transcription factor to control palate morphogenesis. – *Development*, **140**, 2013, 4709-4718.
69. **Zhou, J., M. Zhang, M. Tan, Y. Ji, S. Shu, Y. Liang.** MiRNA-470-5p suppresses epithelial-mesenchymal transition of embryonic palatal shelf epithelial cells by targeting Fgfr1 during palatogenesis. – *Experimental Biology and Medicine*, **248**, 2023, 1124-1133.
70. **Zhou, R., M. Wang, W. Li, S. Wang, Z. Zhou, J. Li, T. H. Beaty.** Gene-Gene Interactions among SPRY s for Nonsyndromic Cleft Lip/Palate. – *Journal of Dental Research*, **98**, 2019, 180-185.
71. **Zhou, X., Y. Jiang, J. Fang, H. Wang, D. Xie, H. Kuang, J. He.** Incidence of cleft lip and palate, and epidemiology of perinatal deaths related to cleft lip and palate in Hunan Province, China, 2016–2020. – *Scientific Reports*, **13**, 2023, 10304.
72. **Zhou, Y., V. Sinnathamby, Y. Yu, L. Sikora, C. Y. Johnson, P. Mossey, J. Little.** Folate intake, markers of folate status and oral clefts: An updated set of systematic reviews and meta-analyses. – *Birth Defects Research*, **112**, 2020, 1699-1719.
73. **Zhu, K. J., K. T. Kuo, M. J. Heron, B. Hassan, M. N. Njoroge, A. Galaria, R. J. Redett III.** Risk factors for obstructive sleep apnea in patients with cleft palate. – *Annals of Plastic Surgery*, **94**, 2025, S311-S314.
74. **Zhu, Y., H. Miao, Q. Zeng, B. Li, D. Wang, X. Yu, F. Liu.** Prevalence of cleft lip and/or cleft palate in Guangdong province, China, 2015–2018: a spatio-temporal descriptive analysis. – *BMJ open*, **11**, 2021, e046430.
75. **Zhu, S., H. Song, L. Zhong, S. Huo, Y. Fang, W. Zhao, X. J. Zhu.** Essential role of Msx1 in regulating anterior-posterior patterning of the secondary palate in mice. – *Journal of Genetics and Genomics*, **49**, 2022, 63-73.
76. **Zhu, Y., Y. Zhang, Y. Jiang, H. Cai, J. Liang, H. Li, J. Hou.** Retinoic acid upregulates METTL14 expression and the m6A modification level to inhibit the proliferation of embryonic palate mesenchymal cells in cleft palate mice. – *International Journal of Molecular sciences*, **25**, 2024, 4538.
77. **Zhuang, D. Y., S. N. Sun, Z. J. Hu, M. Xie, Y. X. Zhang, L. L. Yan, H. B. Li.** Two novel pathogenic variants in the TCOF1 found in two Chinese cases of Treacher Collins syndrome. – *Molecular Genetics & Genomic Medicine*, **12**, 2024, e2405.
78. **Zong, Y., X. Cheng, W. Xia, Z. Xie, Y. Yang, B. Shi, H. Huang.** The correlation between OSA-related quality of life and two mental statuses in adolescent Chinese patients with cleft palate: a comprehensive study. – *Frontiers in Pediatrics*, **10**, 2022, 985375.

Keep Your Head Attached: The Sperm Connecting Piece

Maya Markova

*Department of Biology, Medical Faculty, Medical University of Sofia, 2 Zdrave Street, BG-1431
Sofia, Bulgaria*

* Corresponding author e-mail: mayamarkov@gmail.com

The sperm neck, or connecting piece, connects the head to the more distal tail regions. It is composed of two centrioles (proximal and distal) and specific pericentriolar cytoskeletal structures surrounding them: basal plate attached to the nucleus, capitulum, and striated (or segmented) columns continuing into the outer dense fibers. Together, these structures form the head-tail coupling apparatus of the spermatozoon. In mammals, the distal centriole undergoes a profound structural modification which allows efficient transmission of the tail movements to the head. Mutations in genes encoding neck cytoskeletal proteins lead to separation of the head from the tail, acephalic spermatozoa, and infertility.

Key words: spermatozoa, sperm neck, cytoskeleton, ultrastructure, infertility

Introduction

The sperm cell consists of two main regions with very different structure and functions: the head, which carries the genetic material (nucleus) and the lytic compartment (acrosome), and the tail, which contains the motility apparatus (axoneme) and the power generator (mitochondria). The most proximal part of the tail, often considered a third region, is the neck, which encloses the centrioles. Because it anchors the rest of the tail and attaches it to the head, the neck is also termed connecting piece, especially when referring to its elaborate cytoskeletal structures collectively called head-tail (or head-to-tail) coupling apparatus [18]. The present review describes these structures in relation to their functions, with emphasis on recent data and concepts.

The centrioles

During spermiogenesis, one of the centrioles, called proximal, orients itself orthogonally to the future cell axis and binds to the nucleus (**Fig. 1A, 2A**). The other centriole, called distal, is oriented along the cell axis and becomes the basal body of

the tail as the axoneme is built over it [17]. Since oocyte centrosomes disassemble at an early stage of oogenesis, the sperm cell must bring into the zygote not only its haploid set of chromosomes but also a functional centrosome as a contribution to the future organism.

In the ancestral (or primitive) spermatozoon found in animals with external fertilization, both sperm centrioles have the canonical cylindrical structure. However, in mammals and some other animals, one of the centrioles becomes structurally atypical during spermatogenesis [1]. In mammals, this is the distal centriole serving as basal body. For a long time, it was considered degenerated, and the proximal centriole was regarded as the sole ancestor of the centrioles of the embryo. However, recent data indicate that the distal centriole undergoes modification rather than degeneration during mammalian spermiogenesis: it acquires a specialized fan-like structure based on doublets rather than triplets (**Fig. 1A**), which includes assembly of specific new

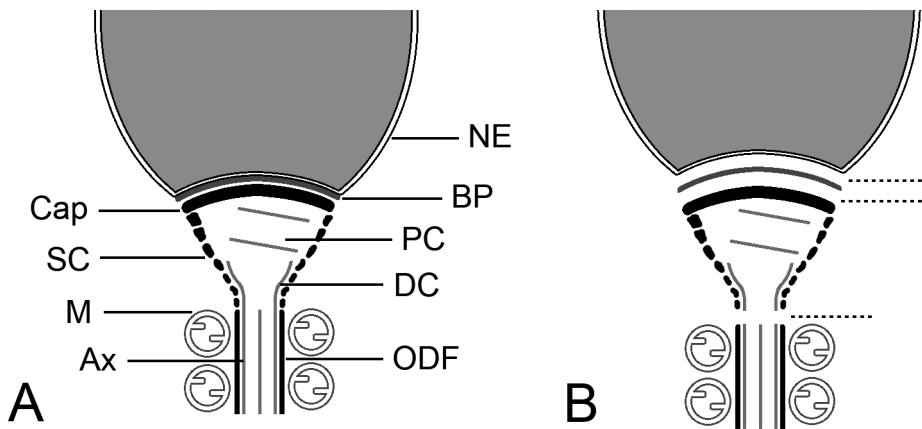


Fig. 1. A. Schematic drawing of the connecting piece of a non-rodent mammalian spermatozoon in longitudinal section. The cell membrane is omitted. NE, nuclear envelope; BP, basal plate; Cap, capitulum; PC, proximal centriole; DC, distal centriole; SC, striated columns; M, mitochondria; Ax, axoneme; ODF, outer dense fibers. B. The three possible positions of the head – tail separation in acephalic spermatozoa (dashed lines).

elements [2]. Moreover, it is sufficiently preserved to induce formation of a daughter centriole in the zygote [3, 5]. A notable exception are the murid rodents: in their spermiogenesis, both centrioles degenerate (**Fig. 2B**), and embryonic centrioles are formed de novo at blastocyst stage [9].

In the primitive spermatozoon, the canonical centrioles attach the tail to the head and anchor the axonemal microtubules, so that the dynein-induced sliding of microtubule doublets relative to one another is converted to flexing. Centriolar modifications that deviate from this ancestral structure are best studied in mammals and insects. While the modifications in the two groups are quite different, and the groups themselves are only distantly related, a common feature is that they both have internal fertilization. This led to the supposition that the structural changes affecting sperm centrioles are adaptations to the high biomechanical requirements of internal fertilization, which includes

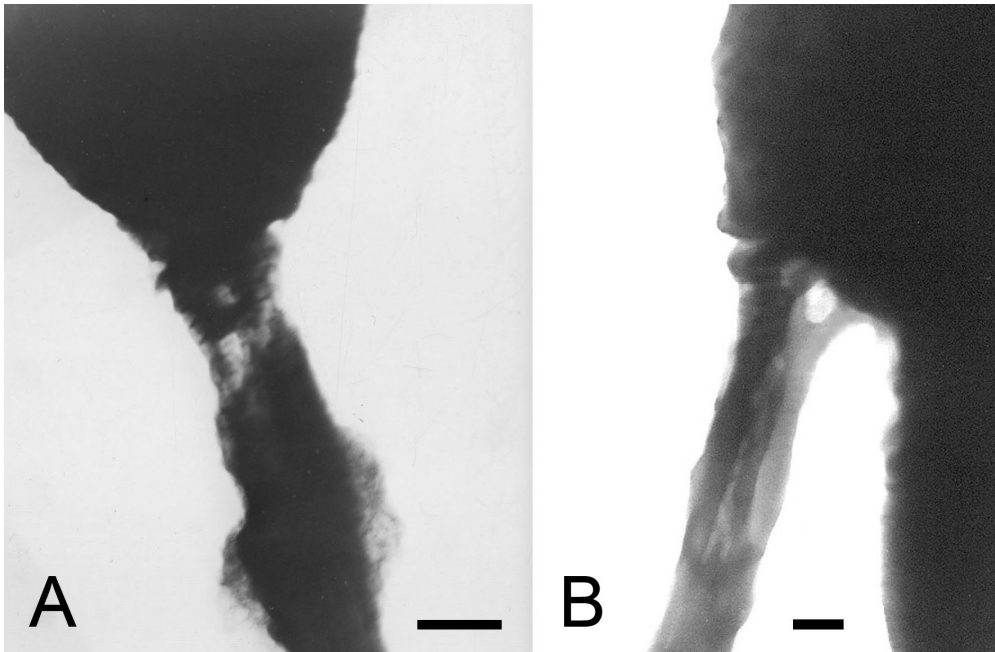


Fig. 2. Mammalian sperm necks observed as whole-mounts after nonionic detergent and high salt extraction. A. Human spermatozoon, with transverse view of the proximal centriole. Bar = 500 nm. B. Mouse spermatozoon, showing an empty vault where the proximal centriole has resided. Bar = 200 nm. From [13].

navigating a complex path in the female genital tract through its viscous secretions. This hypothesis was tested by comparing the structure of fish sperm centrosomes with regard to their fertilization mode, and it was found that 20.6% of internal fertilizers had evolved atypical sperm centrioles versus only 0.8% of external fertilizers [19]. A recently proposed theory postulates that the atypical structure of mammalian distal centriole makes it dynamic, so that beating of the tail generates a coordinated kinking movement of the head which contributes to progressive motility [10].

Pericentriolar cytoskeletal structures

While centrioles can be regarded as organizers of the sperm connecting piece, they are not the only supporting structures located there. In mammals, sperm centrioles are surrounded by an elaborate complex of cytoskeletal elements with specific structure and composition (**Fig. 1A**). It develops from dense material that accumulates around the centrioles during spermatogenesis and can be regarded as atypical pericentriolar material [10]. The most distal part of the nucleus ends with a shallow concave pit called implantation fossa which marks the beginning of the neck. The nuclear envelope in this region is narrowed, devoid of pores and with periodic thickenings between the two closely positioned nuclear membranes [4]. On the outer nuclear membrane covering the implantation fossa, an electron-dense layer called basal plate is overlaid.

A broad convex sheet named capitulum fits into the concave surface of the basal plate and binds to it through thin fibers. The other (distal) side of the capitulum is connected to the proximal centriole [17].

A characteristic complex of nine assymmetric elongated supports surrounds the centrioles. Because of their cross-banded appearance under the electron microscope, they are called striated or segmented columns. Anteriorly, they fuse with the capitulum – in fact, have been described by some observers to form the capitulum by sharp bending. Posteriorly, the striated columns continue into nine thick tail filaments surrounding the axoneme and called outer dense fibers. Despite the intimate connection between the two structures in the mature spermatozoon, during spermatogenesis the outer dense fibers form much later than the striated columns and apparently independently, and fuse with them at a still later stage [17]. The segmentation of the columns is most pronounced at their proximal ends and decreases distally to the point of their fusion with the outer dense fibers [14].

Although the striated columns and their continuations – the outer dense fibers, lack motor activity, they are important for the progressive motility of the spermatozoa. The mechanical forces generated by the motor protein dynein in the axoneme are transferred from the microtubule doublets to the outer dense fibers, and from them to the striated columns [11]. This mechanism utilizing the mechanically resistant periaxonemal and pericentriolar cytoskeletal elements is better suited for mammalian spermatozoa than the ancestral arrangement relying only on the interaction between two relatively fragile structures, the axoneme and the basal body. However, the striated columns should not be regarded as solid anchors. They are in fact flexible, and adjust their positions in response to the flagellar beating. Together with the centrioles, they form a dynamic basal complex that, in addition to connection, provides movement transmission between the tail and the head [10].

Composition and molecular defects of sperm neck pericentriolar cytoskeleton

Despite the unique role of sperm centrioles and the atypical structure of one of them, they remain tubulin-based complexes like their counterparts in other tissues, though detailed studies of their composition will certainly reveal specific components absent in centrioles of somatic cells. The pericentriolar cytoskeletal structures are much more intriguing in this respect, because they lack known analogs in other cells and the analysis of their composition meets considerable methodological difficulties.

As in many other cases, the composition of the connecting piece and the roles of individual components have been elucidated by rare genetic disorders and experiments with knockout animals. Among the most severe sperm abnormalities are the so-called acephalic or decapitated spermatozoa, in which the absence or defect of a key neck protein leads to separation of the head from the tail and presence of headless tails and occasional tailless heads in the ejaculate [4]. The separation can occur at three different levels: between the nuclear envelope and the basal plate, between the basal plate and the capitulum (most common), and between the neck and the middle piece (**Fig. 1B**) [17].

A testis-specific protein named SPATA6 (spermatogenesis-associated protein 6) is an important component of the striated columns and the capitulum; in knockout mice, these structures fail to develop, leading to decapitation [20]. Two other proteins important for the head-to-tail attachment have been identified by the high proportion

of mutations in their genes found in patients with acephalic spermatozoa: SUN5 and PMFBP1 (polyamine modulated factor 1 binding protein 1). SUN5 is a nuclear envelope protein, and mutations in it lead to absence of implantation fossa [25]. Mutations affecting PMFBP1 cause separation between the basal plate and the nuclear envelope, a defect observed also in knockout mice. Normally, the three proteins interact, with PMFBP1 sandwiched between SUN5 and SPATA6 [23]. The interaction is likely to involve other participants; another protein, named CENTLEIN, links SUN5 and PMFBP1, and knockouts for it produce acephalic spermatozoa. Knockouts for SUN5 have CENTLEIN localized on the decapitated tail, and knockouts for PMFBP1 on the detached head [21].

The connection established in spermiogenesis between the outer dense fibers and the striated columns poses the question whether they share protein components. Four major proteins have been identified in the outer dense fibers: Odf1, Odf2, Odf3 and Odf4, with the former two most prominent [22]. ODF1 (HspB10) is present in the basal plate, the capitulum, and the striated columns. Mouse knockouts for it have apparently normal spermiogenesis but their epididymal and ejaculate spermatozoa are decapitated, indicating inability of spermatozoa to withstand the mechanical forces associated with active movement [6]. The point of breakage has not yet been specified. ODF2 colocalizes and interacts with ODF1 and tubulin in sperm neck pericentriolar structures as well as the outer dense fibers. By alternative splicing, the same gene produces a universal centrosomal protein called cenexin. Homozygous knockout mouse embryos with deleted exon 9 die at preimplantation stage [16], apparently because of the lack of functional cenexin. While heterozygous knockout males in this study had normal spermatozoa and were fertile, another heterozygous knockout with deleted exons 6 and 7 displayed haploinsufficiency, with spermatozoa decapitated by separation of the neck from the middle piece [7]. A missense mutation of ODF2 was found in an infertile patient with abnormal sperm tails, but its deleterious effects were limited to the outer dense fibers [24]. There are no data about ODF3 mutations in the literature, and ODF4 homozygote knockouts are infertile due to bent sperm flagella but there is no decapitation [8].

More examples of proteins important for head-to-tail attachment are summarized in [17]. Several of them are designated by CCDC (coiled-coil domain-containing) and a number. CCDC proteins are overrepresented in spermatogenesis [15]; ODF2 and ODF3 also contain long coiled coils. This is not surprising, since the spermatozoon contains an elaborate system of specific cytoskeletal elements resembling the intermediate filaments which are based on long coiled-coil domains. When spermatozoa are subjected to a chemical dissection procedure which extracts all cytoplasmic components of somatic cells except intermediate filaments, the specific cytoskeletal structures of the sperm cells are preserved, including the striated columns and the capitulum [12]. Future studies will provide deeper knowledge about the fascinating structure of the sperm connecting piece which is instrumental for successful fertilization.

Acknowledgements: This work was supported by Grant No. D-137/14.06.2022 of the Medical University of Sofia.

References

1. **Avidor-Reiss, T.** Rapid evolution of sperm produces diverse centriole Structures that reveal the most rudimentary structure needed for function. – *Cells*, **7**, 2018, 67.
2. **Avidor-Reiss, T., A. Carr, E. L. Fishman.** The sperm centrioles. – *Mol. Cell. Endocrinol.*, **518**, 2020, 110987.
3. **Avidor-Reiss, T., R. Uzbekov.** Revisiting the mystery of centrioles at the beginning of mammalian embryogenesis. – *J. Assist. Reprod. Genet.*, **40**, 2023, 2539-2543.
4. **Chemes, H. E., E. T. Puigdomenech, C. Carizza, S. B. Olmedo, F. Zanchetti, R. Hermes.** Acephalic spermatozoa and abnormal development of the head-neck attachment: a human syndrome of genetic origin. – *Hum. Reprod.*, **14**, 1999, 1811-1818.
5. **Fishman, E. L., K. Jo, Q. P. H. Nguyen, D. Kong, R. Royfman, A. R. Cekic, S. Khanal, A. L. Miller, C. Simerly, G. Schatten, J. Loncarek, V. Mennella, T. Avidor-Reiss.** A novel atypical sperm centriole is functional during human fertilization. – *Nat. Commun.*, **9**, 2018, 2210.
6. **Hoyer-Fender, S.** Development of the Connecting Piece in ODF1-Deficient Mouse Spermatids. – *Int. J. Mol. Sci.*, **23**, 2022, 10280.
7. **Ito, C., H. Akutsu, R. Yao, K. Yoshida, K. Yamatoya, T. Mutoh, T. Makino, K. Aoyama, H. Ishikawa, K. Kunimoto, S. Tsukita, T. Noda, M. Kikkawa, K. Toshimori.** Odf2 haploinsufficiency causes a new type of decapitated and decaudated spermatozoa, Odf2-DDS, in mice. – *Sci. Rep.*, **9**, 2019, 14249.
8. **Ito, C., T. Makino, T. Mutoh, M. Kikkawa, K. Toshimori.** The association of ODF4 with AK1 and AK2 in mice is essential for fertility through its contribution to flagellar shape. – *Sci. Rep.*, **13**, 2023, 2969.
9. **Khanal, S., A. Jaiswal, R. Chowdanayaka, N. Puente, K. Turner, K. Y. Assefa, M. Nawras, E. D. Back, A. Royfman, J. P. Burkett, S. H. Cheong, H. S. Fisher, P. Sindhwani, J. Gray, N. B. Ramachandra, T. Avidor-Reiss.** The evolution of centriole degradation in mouse sperm. – *Nat. Communication*, **15**, 2024, 117.
10. **Khanal, S., M. R. Leung, A. Royfman, E. L. Fishman, B. Saltzman, H. Bloomfield-Gadêlha, T. Zeev-Ben-Mordehai, T. Avidor-Reiss.** A dynamic basal complex modulates mammalian sperm movement. – *Nat. Commun.*, **12**, 2021, 3808.
11. **Lindemann, C. B., K. A. Lesich.** Functional anatomy of the mammalian sperm flagellum. – *Cytoskeleton (Hoboken)*, **73**, 2016, 652-669.
12. **Markova, M. D.** Electron microscopic observations of human sperm whole-mounts after extraction for nuclear matrix and intermediate filaments (NM-IF). – *Int. J. Androl.*, **27**, 2004, 291-295.
13. **Markova, M. D.** Knowledge through destruction: Studies of sperm structure using chemical dissection. Sofia, Simelpress, 2024, 119 [in Bulgarian].
14. **Ounjai, P., K. D. Kim, P. V. Lishko, K. H. Downing.** Three-dimensional structure of the bovine sperm connecting piece revealed by electron cryotomography. – *Biol. Reprod.*, **87**, 2012, 73.
15. **Priyanka, P. P., S. Yenugu.** Coiled-coil domain-containing (CCDC) proteins: functional roles in general and male reproductive physiology. – *Reprod. Sci.*, **28**, 2021, 2725-2734.
16. **Salmon, N. A., R. A. Reijo Pera, E. Y. Xu.** A gene trap knockout of the abundant sperm tail protein, outer dense fiber 2, results in preimplantation lethality. – *Genesis*, **44**, 2006, 515-522.

17. **Tapia Contreras, C., S. Hoyer-Fender.** The Transformation of the centrosome into the basal body: similarities and dissimilarities between somatic and male germ cells and their relevance for male fertility. – *Cells*, **10**, 2021, 2266.
18. **Teves, M. E., E. R. S. Roldan.** Sperm bauplan and function and underlying processes of sperm formation and selection. – *Physiol. Rev.*, **102**, 2022, 7-60.
19. **Turner, K., N. Solanki, H. O. Salouha, T. Avidor-Reiss.** Atypical centriolar composition correlates with internal fertilization in fish. – *Cells*, **11**, 2022, 758.
20. **Yuan, S., C. J. Stratton, J. Bao, H. Zheng, B. P. Bhetwal, R. Yanagimachi, W. Yan.** Spata6 is required for normal assembly of the sperm connecting piece and tight head-tail conjunction. – *Proc. Natl. Acad. Sci. USA*, **112**, 2015, E430-E439.
21. **Zhang, Y., C. Liu, B. Wu, L. Li, W. Li, L. Yuan.** The missing linker between SUN5 and PMFBP1 in sperm head-tail coupling apparatus. – *Nat. Commun.*, **12**, 2021, 4926.
22. **Zhao, W., Z. Li, P. Ping, G. Wang, X. Yuan, F. Sun.** Outer dense fibers stabilize the axoneme to maintain sperm motility. – *J. Cell. Mol. Med.*, **22**, 2018, 1755-1768.
23. **Zhu, F., C. Liu, F. Wang, X. Yang, J. Zhang, H. Wu, Z. Zhang, X. He, Z. Zhang, P. Zhou, Z. Wei, Y. Shang, L. Wang, R. Zhang, Y. C. Ouyang, Q. Y. Sun, Y. Cao, W. Li.** Mutations in PMFBP1 cause acephalic spermatozoa syndrome. – *Am. J. Hum. Genet.*, **103**, 2018, 188-199.
24. **Zhu, Z. J., Y. Z. Wang, X. B. Wang, C. C. Yao, L. Y. Zhao, Z. B. Zhang, Y. Wu, W. Chen, Z. Li.** Novel mutation in ODF2 causes multiple morphological abnormalities of the sperm flagella in an infertile male. – *Asian J. Androl.*, **24**, 2022, 463-472.
25. **Zhu, F., F. Wang, X. Yang, J. Zhang, H. Wu, Z. Zhang, Z. Zhang, X. He, P. Zhou, Z. Wei, J. Gecz, Y. Cao.** Biallelic SUN5 mutations cause autosomal-recessive acephalic spermatozoa syndrome. – *Am. J. Hum. Genet.*, **99**, 2016, 942-949.

ANTHROPOLOGY AND ANATOMY 32 (2)

Original Articles

Do Foot Dimensions Influence Stature Estimation: A Study among the Bhumij Tribal Population of Northern Odisha, India

Sitikantha Panda¹, Priyanka Das¹, Monali Goswami^{1}*

¹*Department of Anthropology and Tribal Studies, MSCB University, Takatpur, Baripada-757003, Mayurbhanj, Odisha, India*

*Corresponding author e-mail: goswami_monali@rediffmail.com

In forensic science, medical examinations, or anthropological investigations, stature is considered as one of the critical characteristics for establishing personal identity. The present study is an attempt to estimate stature from different foot measurements among the Bhumij tribal population of Mayurbhanj, Northern Odisha. This study included 202 adult Bhumij tribal people (males-89; females-113) without foot abnormalities or injuries. All anthropometric measurements were recorded following the standard procedures. The findings reveal that no significant sex difference was found between the right and left foot among both the males and females. A linear and multiple regression equation was developed for the estimation of stature from various foot measurements. The multivariate regression formulas are used to calculate the stature from the foot dimensions in both sexes and give a better prediction of stature than the univariate type. Thus, stature could be estimated with reasonable accuracy from the different foot length measurements.

Key words: Forensic Science, Personal identification, Stature, Foot Dimension, Bhumij

Introduction

Forensic anthropology aims to focus on constructing a biological profile from mutilated remains and also utilizing techniques to estimate fundamental traits for identification [40]. Stature is crucial in medical-legal procedures, identifying individuals and aiding in forensic research, and development of profiles for unidentified victims or suspects [18]. Anthropometric data is crucial for international market product creation, enhancing comfort, safety, health, and well-being in footwear design. Humans develop change in size and form of their feet mostly due to the physical strain associated with walking on both feet [55]. A crucial area of forensic research is estimating stature of the deceased from fragmented and badly decomposed human remains, damaged or severed limbs or sections of limbs, or incomplete skeletal remains. In the event of a crime, accident, or natural disaster, these remains are essential for identifying the person. On the other hand, measurements of stature can be obtained from footprints, handprints, or shoes found at the scene of a crime. Anthropologists, medical experts, and anatomists using anthropometric techniques have estimated the size and length of bones from unknown body parts and skeletal remains for more than a century [26]. Recently due to the increase in the number of man-made and natural disasters, including bomb explosions, wars, terrorism, and airline crashes, as well as cyclones, tsunamis, earthquakes, and floods, this has become increasingly crucial. In these situations, the forensic pathologist frequently expresses an opinion on the deceased's identity. [22, 30, 40]. Personal identification is crucial in mass disaster investigations, as disintegrated body parts are common. Due to genetic diversity in Indian populations, correlations between body parts and stature vary across different geographical locations, necessitating separate studies for each group [44]. Footprint measurements are crucial in developing countries like Bangladesh, India, and Pakistan, as people walk barefoot for socioeconomic reasons. Footprints are found at crime locations, including theft and murder, and can be analyzed during stature estimation for criminal identification [41].

The study on different body segments has been used to illustrate and compare the variations across various ethnic groups and to explain their energy expenditure, lifestyle, and locomotor habits [7]. Stature is a highly significant growth and development indicator that is employed in clinical settings and is indispensable in nutrition and health studies. In addition to body weight, stature is a crucial factor in the computation of body composition, basal metabolic rate, body mass index, and basal energy expenditure [17]. Thus, stature has been estimated using body proportions and the measurements of various body segments, such as the vertebral column, the long bones of the limbs, and the bones of the hand and foot [45, 51]. Numerous studies have been done to determine stature using data from the hand, foot as well as from the trunk, limbs, long and short bones, and hand and foot prints [36, 47]. Several studies have also shown the correlation of stature with foot length [8, 13, 25, 26, 54]. A study conducted by Krishan et al. [31] concluded that foot length was more authentic variable than foot breadth variable. Studies also revealed that female foot measurements are comparatively smaller than those of males [21, 31, 39, 46, 50]. Evidence suggests that a shoe left at a crime site can estimate the victim's stature [12, 1]. In the absence of all evidence, body measurements and proportions can be used to solve crimes, such as using footprints, handprints, or footprints at crime sites [4, 14,15, 49].

While several research papers have been published on various Indian communities, there are surprisingly few studies on the tribal community of Eastern India. Therefore,

the purpose of the current study was to estimate stature from foot measurements among the adult Bhumij indigenous tribal community of Northern Odisha and to ascertain the association between stature and all foot dimensions.

Material and Methods

The present cross-sectional study was conducted among the Bhumij tribal population of the Khunta block of the Mayurbhanj district of Northern Odisha. Etymologically, the term ‘Bhumija’ means ‘one who is born out of the soil’. The study participants included 202 (Male-89, Female-113) Bhumij adult population aged above 18 years of age. The information about the age of the participants was taken from Aadhar card or voter card and was crosschecked with the participants. Only healthy participants free from any deformity of the foot were included in the study. The data were collected in May 2023.

Anthropometric measurements were collected using the standard technique and the relevant landmarks [33]. The data for the present study included stature, length of the foot from each toe (T1, T2, T3, T4, and T5 respectively), foot breadth at the ball and foot breadth at the heel. All the foot measurements were taken using the standard protocol [31]. The informed consent was obtained from all subjects. The study was approved by the competent authorities of the Institutional Ethical Committee, MSCB University and has been conducted according to the principles expressed in the Declaration of Helsinki.

Stature: The vertical distance between the floor and the point vertex, or the highest point on the head when held in the Frankfurt Horizontal plane, is known as the stature. Martins anthropometer was used to measure the participant’s stature to the closest 0.1 cm, while they had to stay upright and without any footwear or helmet. For recording foot measurements, the participant was made to stand so that both feet were slightly apart with equal pressure on both. The Martin’s sliding caliper was placed horizontally on the landmarks and the measurement was taken (**Fig. 1**). Different landmarks on the foot are described in **Table 1**. TEM (Technical error of measurement) was calculated for the anthropometric variables [56] and the majority of the values were under the permissible limit (0.08 – 0.61).

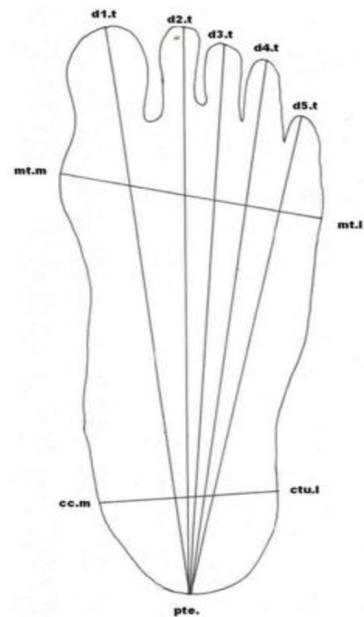


Fig. 1. Landmarks of different foot anthropometric measurements (Source- Krishna et al. 2001)

Table 1. Land marks of different foot measurements

SL. No.	Foot anthropometric measurements	Landmarks
1	Foot length	Distance from the pternion point to the frontal end of the longest toe of the feet
2	Foot breadth at ball	Distance between the anterior epiphyses of the first metatarsal and the fifth metatarsal.
3	Foot breadth at heel	Distance between the medial and lateral sides of the heel.
4	T1	Distance from pternion to the most anterior point of the first toe
5	T2	Distance from pternion to the most anterior point of the second toe
6	T3	Distance from pternion to the most anterior point of the third toe
7	T4	Distance from pternion to the most anterior point of the forth toe
8	T5	Distance from pternion to the most anterior point of the fifth toe

T1 – Foot length at first toe, T2 – Foot length at second toe, T3 – Foot length at third toe , T4 – Foot length at fourth toe , T5 – Foot length at fifth toe

Statistical Analysis

The foot anthropometric data and stature of the participants collected were analysed using Statistical Package for Social Science (SPSS, version 18) computer software. Foot measurements were compared for bilateral asymmetry and sexual dimorphism using paired and unpaired t-tests respectively. Subsequently no significant differences is observed between the measures of both the feet (right and left), therefore, further analysis is done from the mean values of both the feet. [23]. Pearson’s correlation coefficient was obtained to find correlation between stature and various foot measurements. A *p* value of <0.05 was considered to be statistically significant. Stature was estimated from the foot measurements by using linear and multiple regression analysis. The linear regression model for stature estimation is derived as S (stature) = $a + b x \pm SEE$, where, ‘a’ is constant, ‘b’ is the regression coefficient of the independent variable (individual foot measurement), ‘x’ is an individual foot measurement and SEE is Standard Error of Estimate. Multiple regression models were considered for reconstruction of stature from foot length (T1 to T5) and foot breadth measurements.

Results

Descriptive statistics for the foot measurements of left and right feet of both males and females are presented in **Table 2**. An independent t-test was performed but no significant difference ($p > 0.05$) was observed between the measures of the left foot and right foot.

Thus, bilateral asymmetry is absent and subsequent analyses were done with the mean values of both the feet (males and females).

Table 2. Mean and standard deviations of foot measurements stratified by sex

variable	Male		t	p-value	Female		t	p-value
	right (mean±sd)	left (mean±sd)			right (mean±sd)	left (mean±sd)		
Foot Length	23.90±1.15	23.93±1.15	0.137	0.892	22.01±1.01	22.05±1.15	0.263	0.793
Ball Breadth	9.43±0.69	9.47±0.68	0.422	0.673	8.48±0.54	8.57±0.55	1.223	0.223
Heel Breadth	5.97±0.42	5.89±0.46	-1.241	0.216	5.48±0.47	5.40±0.49	-1.254	0.211
T1	23.63±1.20	23.69±1.23	0.356	0.722	21.78±1.04	21.80±1.17	0.150	0.881
T2	23.41±1.21	23.42±1.17	0.050	0.960	21.46±1.09	21.40±1.12	-0.401	0.689
T3	22.48±1.15	22.50±1.16	-0.149	0.822	20.57±1.12	20.56±1.10	-0.083	0.934
T4	21.49±1.13	21.46±1.09	-0.209	0.835	19.53±1.09	19.51±1.06	-0.197	0.844
T5	20.13±1.02	20.05±1.10	0.480	0.632	18.26±1.01	18.23±0.94	-0.237	0.813

Table 3. Sexual differences in different foot measurements

Variables	male (mean±sd)	female (mean±sd)	t	p-value
Stature	159.44±5.85	148.47±7.26	11.89	.000*
Weight	52.71±9.54	45.03±7.40	6.25	.032*
Foot Length	23.91±1.13	22.02±1.06	12.04	.000*
Ball Breadth	9.45±0.65	8.52±0.51	11	.000*
Heel Breadth	5.93±0.38	5.44±0.40	8.84	.000*
T1	23.66±1.19	21.79±1.07	11.52	.000*
T2	23.42±1.16	21.43±1.08	12.35	.000*
T3	22.49±1.11	20.56±1.08	12.35	.000*
T4	21.47±1.06	19.52±1.03	13.09	.000*
T5	20.09±1.02	18.24±0.92	13.25	.000*

* Highly significant

All foot measurements except stature showed statistically significant difference ($p < 0.05$) between the male and female participants (**Table 3**). **Table 4** shows the results of the correlation between stature and all foot measurements. In males, statistically significant positive correlation ($p < 0.05$) was observed between all foot measures and stature. Similar results were also observed among the female participants except ball breadth and heel breadth. It is also evident that foot length and toe length 5 (T5) of males can give better prediction of stature when compared with foot length and toe length 5 (T5) of females. The correlation of stature with foot length for males is 0.642, which shows strong correlation but the correlation of stature with ball breadth and heel breadth are 0.351 and 0.438, which shows a moderate correlation. Among females, correlation of stature with foot length is 0.434 which shows moderate correlation but correlation of stature with ball breadth and heel breadth are 0.193 and 0.063, which shows low correlation.

Table 4. Pearson Correlation (r) between stature and different foot dimensions

variables	male		female	
	r	p-value	r	p-value
Foot Length	0.642***	.000 Ψ	0.434**	.000 Ψ
Ball Breadth	0.351**	.001 Ψ	0.123*	.193
Heel Breadth	0.438**	.000 Ψ	0.175*	.063
T1	0.625***	.000 Ψ	0.408**	.000 Ψ
T2	0.640***	.000 Ψ	0.404**	.000 Ψ
T3	0.610***	.000 Ψ	0.368**	.000 Ψ
T4	0.629***	.000 Ψ	0.334**	.000 Ψ
T5	0.678***	.000 Ψ	0.332**	.000 Ψ

Ψ – Highly significant

***Strong degree Correlation- Coefficient value lies between ± 0.50 and ± 1

**Moderate degree Correlation: Coefficient value lies between ± 0.30 and ± 0.49

*Low degree Correlation: Coefficient value lies below ± 0.29

The simple linear regression equations for the estimation of stature from all explanatory variables are presented in **Table 5**. All the foot measurements did not show any significant differences between the left and right feet; hence the mean of right and left feet together was used to derive linear regression models from individual foot measurements. The determination coefficient (R^2) and standard error of estimate (SEE) are also shown in the table. All the correlation coefficients were found to be statistically significant ($p < 0.05$) except ball breadth and heel breadth in female. Thus, stature is positively and significantly related to various foot measurements. However, measurements of the length of the foot have greater correlation values than those of the breadth (**Figs. 2, 3, 4**).

These regression models can be used for stature estimation from the different foot measurements. The present study showed that foot length measurements are more accurate indicators of stature than foot breadth measurements. Among the foot length measurements,

T5 gives the most accurate estimation of stature by linear regression analyses. It was observed that the SEE (0.759) value is minimal and the predictive accuracy (R^2) is maximum (0.4602) for T5 but the accuracy of all other measurements in stature estimation were comparable among the foot length measurements. Similarly, among females, of all the foot length measurements, T5 gives the most accurate estimation of stature by linear regression analyses. It was observed that the SEE value is minimal and the predictive accuracy (R^2) is maximum for T5 but the accuracy of all other measurements in stature estimation were comparable among the foot length measurements.

Table 5. Linear regression equation for reconstruction of stature from different foot measurements

Variable	male					female				
	Equation	SEE	r	R^2	Sig.	Equation	SEE	R	R^2	Sig.
Foot Length	$y=4.094+.124(FL)$.873	.642	.412	.000*	$y=12.567+.064(FL)$.966	.434	.188	.000*
Ball Breadth	$y=3.228+.039(BB)$.613	.351	.123	.001*	$y=7.230+.009(BB)$.512	.123	.015	.193
Heel Breadth	$y=1.364+.029(HB)$.346	.438	.192	.000*	$y=3.974+.010(HB)$.404	.175	.031	.063
T1	$y=3.250+.128(T1)$.941	.625	.390	.000*	$y=12.800+.061(T1)$.988	.408	.167	.000*
T2	$y=3.090+.128(T2)$.901	.640	.409	.000*	$y=12.463+.060(T2)$	1.000	.404	.163	.000*
T3	$y=4.022+.116(T3)$.886	.610	.372	.000*	$y=12.443+.055(T3)$	1.01	.368	.135	.000*
T4	$y=3.162+.115(T4)$.834	.629	.396	.000*	$y=12.470+.048(T4)$.977	.334	.112	.000*
T5	$y=1.108+.119(T5)$.759	.678	.460	.000*	$y=11.949+.042(T5)$.879	.332	.110	.000*

* Highly significant

The multiple linear regression equations are derived for stature estimation from different foot length (Foot length, T1, T2, T3, T4, T5) and foot breadth (Ball breadth and Heel breadth) measurements. The values of coefficient of determination of foot length and foot breadth measurements of both males and females are presented in **Table 6**.

Table 6. Multiple regression equations for estimation of stature by using different foot measurement

Measurements	Sex	Models	R ²	S.E.E.
Foot length, T1, T2, T3, T4, T5	Male	$73.04+3.27(FL)-1.57(T1)-0.10(T2)-1.32(T3)+0.44(T4)+3.26(T5)$	0.455	4.32
	Female	$83.55+4.22(FL)-1.83(T1)+0.14(T2)+0.98(T3)-0.42(T4)-0.17(T5)$	0.193	6.71
FBB, FBH	Male	$108.48+1.96(BB)+5.46(HB)$	0.233	5.18
	Female	$125.44+0.99(BB)+2.67(FB)$	0.035	7.20

FL – Foot length at first toe, T2 – Foot length at second toe, T3 – Foot length at third toe, T4 – Foot length at fourth toe, T5 – Foot length at fifth toe, FBB – Foot breadth at ball, FBH – Foot breadth at heel.

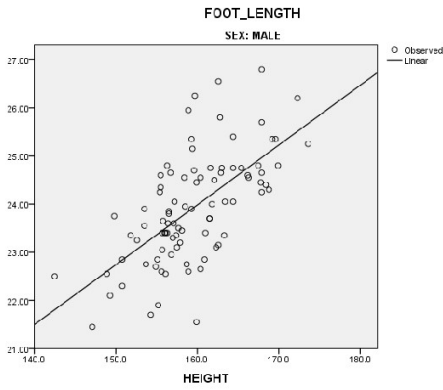


Fig. 2A

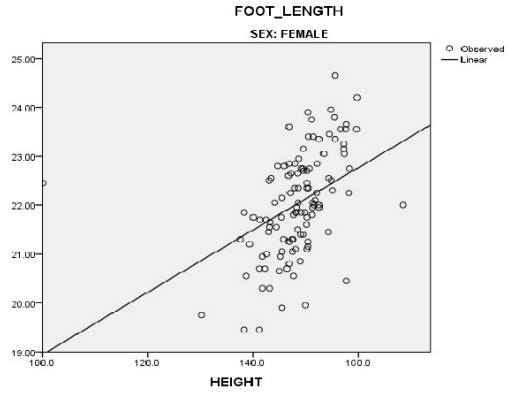


Fig. 2B

Fig. 2. Scatter diagram of stature and foot length for males and females

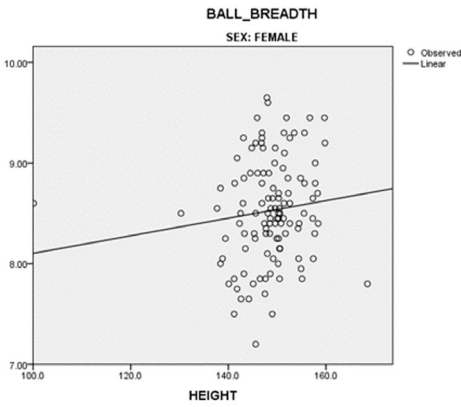


Fig. 3A

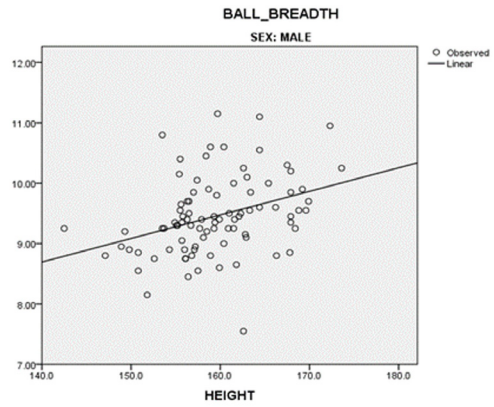


Fig. 3B

Fig. 3. Scatter diagram of stature and ball breadth for males and females

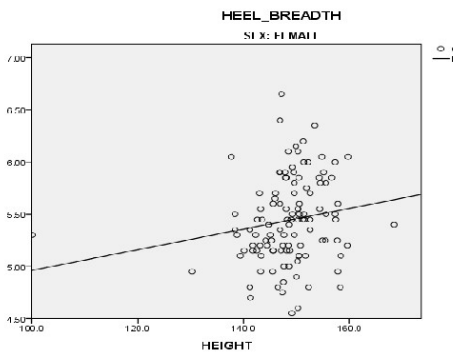


Fig. 4A

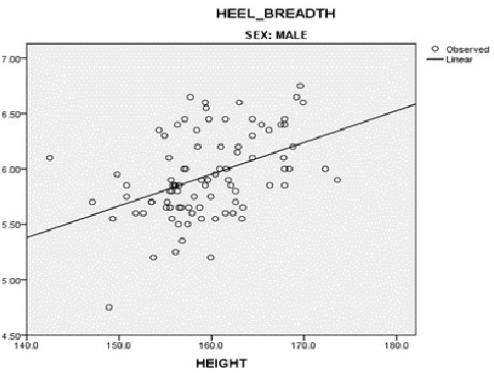


Fig. 4B

Fig. 4. Scatter diagram of stature and heel breadth for males and females

Table 7. Regression equation for estimation of stature among different populations of India

S. No.	Area and population	Age Groups	Sex	Regression equation	r	Year	Author
1	Karnataka	18-60	M	H = 69.346 + 3.66 FL	0.636	2013	Dayananda
2	Gujrat	18 and above	M	H=75.45+3.64 FL	0.65	2007	Pate1 M Shah
			F	H=75.41+3.43 FL	0.80		
3	Sri Lanka	18-32	M	H=79.042+3.590 FL	0.72	2008	I. Ilayperuma
			F	H=65.549+3.944 FL	0.71		
4	Haryana, India	18-42	F	H=65.194+4.068 LFL	0.719	2008	Jakhar
			M	H=80.671+3.648 LFL	0.725		
5	Pune, India	18-30	M	H=90.0+3.2 FL	0.645	2012	Sanli
			F	H=72.8+3.7 FL	0.702		
6	Delhi	18 and above	M	H = 98.32 + 3.05 FL	0.808	2011	Mukta Rani
7	Pakistan	18-30	M	H = 104.455 + 2.591 FL	0.581	2015	Maalik AR
8	North India	18-60	M	H = 90.27 + 2.93 FL	0.764	2008	Krishnan K
9	Gulbarga	18-25	M	H= 86.9 + 3.40 FL	0.82	2016	Karaddi <i>et al.</i>
10	Maharashtra	18 and above	M	H=72.8 + 3.7 FL	0.70	2011	Khanapurkar <i>et al.</i>
11	Gujarat	18 and above	M	H= 77.35 + 3.605 RFL	0.73	2015	Upadhyay MC <i>et al.</i>
12	India	18-50	M	H = 68.58 + 4.036 FL	0.72	2007	Agnihotri
13	West Bengal	18-50	M	H= 83.518 + 3.282 FL	0.62	2008	Sen and Ghosh
			F	H= 67.009 + 3.707 FL	0.69		
14	Aurangabad	18-25	M	H= 58.46+4.29 RFL	0.79	2016	Pandey and Kulkarni
			F	H=113.45+1.69 RFL	0.46		
15	Cuttack	18-25	M	H=-27.77 + 7.695 FL	0.224	2012	Mohanty <i>et al.</i>
			F	H=77.85 + 3.58 FL	0.259		
16	Mayurbhanj	18 and above	M	H=4.094+0.124 FL	0.642	2024	Present study
			F	H=12.567+0.064 FL	0.434		

The foot length measurements showed greater estimation accuracy than foot breadth measurements. It is further observed that the multiple regression models with higher values of coefficient of determination R^2 tend to estimate stature more accurately than the respective linear regression models for length and breadth measurements. In **Table 7**, comparison of the coefficient of correlation (r) from different studies has been presented.

Discussion

In biological anthropological studies along with medico-legal investigations, body stature evaluation is important [20]. In addition, anthropologists with forensic expertise assist in personal identification by determining a person's age, sex, and ethnicity. The relative completeness of the skeleton determines the gender from the unknown skeletal remains. Estimating an individual's stature is an essential initial step in identifying remains that have been severely damaged [16]. Foot length and stature have a biological connection and using foot length stature can be determined [11].

In the present study, utmost care was taken to ensure the precision of anthropometric measurements. The measurement errors have a substantial effect on the accuracy and reliability of the standards in forensic science which ultimately affect the forensic anthropology case work involving anthropometry [27]. Our study reveals no significant variation and errors associated with the technique in anthropometric measurements (**Table 2**). Therefore, a set of standards in the estimation of stature from foot and its parts produced by the present study are reliable.

India is a multi-racial, multi-ethnic and multicultural land of great diversity. The stature estimation is considered as important parameters in the identification of a person by measuring various long bones [33]. Patel et al., 2007 [42] estimated height from measurements of foot length in the Gujrat region.

The present study is unique in its sample selection. The study populations were selected from the Bhumij tribal population of Mayurbhanj district of Odisha. Tribals are known to be socially, environmentally, culturally and even genetically secluded communities. While literature abounds with forensic anthropological studies of estimating stature with hand and foot dimensions, very few studies have selected a homogenous group as study population [27, 30]. Due to strong influence of genetic and environmental factors on the height of the individual, homogeneity of the study population is vital in formulating the regression equations.

The present study shows that there is no bilateral asymmetry between the left and right feet of both males and females. Such finding was also observed in the study conducted by Kautilya et al. (2013) [28] among the urban population of Chennai. Hemy et al. (2013) [19] and Jimenez-Ormeno et al. (2013) [23] have also reported the same findings.

In the present study, males showed higher mean values in all the parameters studied than among females and the difference being highly statistically significant. This finding is in accordance with several studies where significant gender difference was observed [5, 10, 25]. Similarly, stature estimation studies by Giles and Vallandigham 1991 [14], and Krishan et al. 2012 [31], and have reported statistically significantly higher values for males. In the present study, all the foot measurements in both the males and females exhibited a statistically significant correlation with stature, which advocates their use for stature estimation. However, the extent of correlation is lower than other two reported

studies from North India [24]. The values of correlation co-efficient of males and females for estimation of stature from foot length was remarkable in the present study (0.64 in males and 0.43 in females). Foot length is more positively related than foot breadth.

There is paucity of workers who have considered foot length and foot breadth for stature estimation. The observations of the present study suggest that these parameters can be utilized to formulate equations to predict stature. Present study has established that though regression formula and multiplication factor, both are useful to determine stature from foot dimensions, regression formula measures stature more precisely than multiplication factor. Krishan et al. (2012) [31] also observed such finding for Rajput (India) population. The present study may be helpful in the estimation of stature where other possible means of identification are not useful.

Conclusion

It is found that there exists a significant sexual dimorphism in male and female population. Males have higher values than the females in dimensions of foot. This study discovered a strong positive association between foot length and stature. A linear and multiple regression equation was developed for the estimation of stature from various foot measurements. The multivariate regression formulas used to calculate the stature from the foot dimensions in both the sexes and give a better prediction of stature than the univariate type. Thus, it was observed that both linear and multiple regression equation are equally sensitive for prediction of stature. The strength of the correlation tends to be enhanced when more than one associative factor was introduced in the derivation of regression equations. Thus, it can be concluded that stature could be estimated with reasonable accuracy from the different foot length measurements.

The data obtained in the present study can be used to obtain certain population specific anthropometric indices amongst the tribal population. The data and subsequently the results obtained in the present study, to the best of the knowledge of the author, is the first ever documented anthropological work on the Bhumij tribe.

Acknowledgements: The authors would like to acknowledge all participants who voluntarily contributed to the success of this study.

Reference

1. **Abdel-Malek, A. K., A. M. Ahmed, S. A. E. A. El Sharkawi, N. A. E. M. Abd El.** Prediction of stature from hand measurements. – *Forensic Sci. Int.*, **46(3)**, 1990, 181-187.
2. **Abledu, J. K., G. K. Abledu, E. B. Offei, E. M. Antwi.** Determination of sex from footprint dimensions in a Ghanaian population. – *PloS one*, **10(10)**, 2015, e0139891.
3. **Arif Rasheed, M., A. Nasreen, A. Riasat, F. Ra'ana, Khalid.** A study on estimation of stature from foot length. – *Professional med j-q*, **22(5)** 2015, 632-639.
4. **Ashizawa, K., C. Kumakura, A. Kusumoto, S. Narasaki.** Relative foot size and shape to general body size in Javanese, Filipinas and Japanese with special reference to habitual footwear types. – *Ann. Hum. Biol.*, **2 (2)**, 1997, 117-129.
5. **Babu, R. S., V. Deepika, B. R. Potturi.** Estimation of stature from foot length. – *Indian J. Pharm. Sc.*, **3(3)**, 2013, 266-270.

6. **Behera, H., S. K. Patra**, Revitalizing tribal linguistic heritage: Preserving the Bhumij and Mundari languages in Mayurbhanj. – *IJCRT*, **11**(7), 2021, 57-69.
7. **M., Chiba, K. Terazawa**. Estimation of stature from somatometry of skull. – *Forensic Sci. Int.*, **97**(2-3), 1998, 87-92.
8. **Chikhalkar, B. G., A. A. Mangaonkar, S. D. Nanandkar, R. G. Peddawad**. Estimation of stature from measurements of long bones, hand and foot dimensions. – *J. Indian Acad. Forensic Med.*, **32**(4), 2010, 329-33.
9. **Cordeiro, C., J. I. Munoz-Barus, S. Wasterlain, E. Cunha, D. N. Vieira**. Predicting adult stature from metatarsal length in a Portuguese population. – *Forensic Sci. Int.*, **193**(1-3), 2009, 131-e1.
10. **Danborn, B., A. Elukpo**. Sexual dimorphism in hand and foot length, indices, stature-ratio and relationship to stature in Nigerians. – *Int. J. Forensic Sci.*, **3**(1), 2008, 379-383.
11. **Devi, T. P., P. Kumar, K. P. Pratim, L. P. Chandravanshi, M. Chauhan**. Estimation of Stature from foot length in male indigenous population of Assam Region. – *The Foot*, **49**, 2021, 101840.
12. **Feldesman, M. R., J. K Lundy**. Stature estimates for some African Plio-Pleistocene fossil hominids. – *J. Hum. Evol.*, **17**(6), 1988, 583-596.
13. **Geetha, G. N., S. A. Athavale**. Estimation of stature from hand and foot measurements in a rare tribe of Kerala state in India. – *JCDR*, **9**(10), 2015, HC01.
14. **Giles, E., P. H. Vallandigham**. Stature estimation from foot and shoeprint length. – *J. Forensic sci.*, **36**(4), 1991, 1134-1151.
15. **Gordon, C. C., J. E. Buikstra**. Linear models for the prediction of stature from foot and boot dimensions. – *J. Forensic Sci.*, **37**(3), 1992, 771-782.
16. **Grivas, T. B., C. Mihos, A. Arapaki, E. Vasiliadis**. Correlation of foot length with stature and weight in school age children. – *J. Forensic Leg. Med.*, **15**(2), 2008, 89-95.
17. **Harkema, S. J., S. L. Hurley, U. K. Patel, P. S. Requejo, B. H. Dobkin V. R. Edgerton**. Human lumbosacral spinal cord interprets loading during stepping. – *J. Neurophysiol.*, **77**(2), 1997, 797-811.
18. **Hemy, N., A. Flavel, N. I. Ishak, D. Franklin**. Estimation of stature using anthropometry of feet and footprints in a Western Australian population. – *J. Forensic Leg. Med.*, **20**(5), 2013, 435-441.
19. **Hemy, N., A. Flavel, N. I. Ishak, D. Franklin**. Sex estimation using anthropometry of feet and footprints in a Western Australian population. – *Forensic Sci. Int.*, **231**(1-3), 2013, 402-e1.
20. **Ilayperuma, I., B. G. Nanayakkara, K. N. Palahepitiya**. A model for reconstruction of personal stature based on the measurements of foot length. – *GMJ*, **13**(1), 2008, 6-9.
21. **Ismaila, S. O**. Anthropometric data of hand, foot and ear of university students in Nigeria. – *LJS*, **15**(8), 2009, 15-20.
22. **Jagadish Rao, P. P., J. Sowmya, K. Yoganarasimha, R. G. Menezes, T. Kanchan, R. Aswinidutt**. Estimation of stature from cranial sutures in a South Indian male population. – *Int. J. Leg. Med.*, **123**, 2009, 271-276.
23. **Jiménez-Ormeño, E., X. Aguado, L. Delgado-Abellán, L. Mecerreyes, L. M. Alegre**. Foot morphology in normal-weight, overweight, and obese schoolchildren. – *Eur. J. Pediatr.*, **172**, 2013, 645-652.
14. **Kamal, R., P. K. Yadav**. Estimation of stature from different anthropometric measurements in Kori population of North India. – *Egypt J. Forensic Sci.*, **6**(4), 2016, 468-477.

16. **Jawaduddin, K. M., S. Ahmad.** Stature prediction from anthropometric feet dimensions: A Study of Relationship. – *IEBM*, 7(2), 2018, 159.
17. **Kanchan, T., K. Krishan, S. ShyamSundar, K. R. Aparna, S. Jaiswal.** Analysis of footprint and its parts for stature estimation in Indian population. – *The Foot*, 22(3), 2012, 175-180.
18. **Kanchan, T., R. G. Menezes, R. Moudgil, R. Kaur, M. S. Kotian, R. K. Garg.** Stature estimation from foot dimensions. – *Forensic Sci. Int.*, 179(2-3), 2008, 241-e1.
19. **Kautilya, D. V., P. Bodkha, P. Poothanathan.** Determination of stature and sex from anthropometry of the foot among south Indians. – *IJRLS*, 3(2), 2013, 22-26.
20. **Khanapurkar, S., A. Radke.** Estimation of stature from the measurement of foot length, hand length and head length in Maharashtra region. – *Indian J. Basic Appl. Med. Res.*, 1(2), 2012, 77-85.
21. **Krishan, K.** Estimation of stature from footprint and foot outline dimensions in Gujjars of North India. - *Forensic Sci Int.*, 175(2-3), 2008, 93-101.
22. **Krishan, K., T. Kanchan, N. Passi, J. A. DiMaggio.** Stature estimation from the lengths of the growing foot - A study on North Indian adolescents. – *The Foot*, 22(4), 2012, 287-293.
23. **Kumar, S., R. Garg, K. Mogra, R. Choudhary.** Prediction of stature by the measurement of head length in population of Rajasthan. – *J. Evol. Med. Dent. Sci.*, 2(14), 2013, 1334-1339.
24. **Lohman ,T. G., A. F. Roche, R. Martorell.** *Anthropometric standardization reference manual.* Human Kinetics Books, Illinois. 1988.
25. **Moorthy, T. N., A. M. B. Mostapa, R. Boominathan, N. Raman.** Stature estimation from footprint measurements in Indian Tamils by regression analysis. – *Egypt J. Forensic Sci.*, 4(1), 2014, 7-16.
26. **Muthusami, P., R. Ananthkrishnan, P. Santosh.** Need for a nomogram of renal sizes in the Indian population—findings from a single center sonographic study. – *Indian J. Med. Res.*, 139(5), 2014, 686-693.
27. **Nagesh, K. R., G. P. Kumar.** Estimation of stature from vertebral column length in South Indians. – *Leg. Med.*, 8(5), 2006, 269-272.
28. **Narde, A. L., A. P. Dongre.** Body stature estimation based on foot length and foot breadth. – *JIAFM*, 35(3), 2013, 245-248.
29. **Ogbanga, N., A. Nelson, S. Gino, D. J. Wescott, H. L. Mickleburgh, T. P. Gocha, N. Procopio.** The impact of freezing on the post-mortem human microbiome. - *Front. Ecol. Evol.*, 11, 2023,1151001.
30. **Oommen, M. A., K. Shanker.** Elevational species richness patterns emerge from multiple local mechanisms in Himalayan woody plants. – *Ecol.*, 86(11), 2005, 3039-3047.
31. **Ozaslan, A., B. Karadayi, M. O. Kolusayin, A. Kaya, H. Afsin.** Predictive role of hand and foot dimensions in stature estimation. – *Rom. J. Leg. Med.*, 20(1), 2012, 41-46.
32. **Palla, S., A. Shivajirao.** Anthropometric examination of footprints in South Indian population for sex estimation. – *Forensic Sci. Int.: Reports*, 9, 2024,100354.
33. **Patel, S. M., G. V. Shah, S. V. Patel.** Estimation of stature from measurements of foot length in Gujarat region. – *J. Anat. Soc. India*, 56(1), 2007, 25-27.
34. **Potdar, A. B., P. Rathod, P. A. Potdar, M. M. Desai.** A study of estimation of stature from forearm length. – *IJFMT*, 13(2), 2019, 219-221.
35. **Rang P., A. K. Goswami, S. K. Dey, A. Baske.** Estimation of stature with hand and foot dimensions – A study amongst adult population of North Bengal. – *Int. J. Acad. Med. Pharm.*, 5(5), 2023, 619-624.

36. **Radoinova, D., K. Tenekedjiev, Y. Yordanov.** Stature estimation from long bone lengths in Bulgarians. – *Homo*, **52**(3), 2002, 221-232.
37. **Rani, M., A. K. Tyagi, V. K. Ranga, Y. Ran, A. Murari.** Stature estimates from foot dimensions. – *Indian J.*, **11**(1), 2011, 26-30.
38. **Rastogi, P., K. R. Nagesh, & K. Yoganarasimha.** Estimation of stature from hand dimensions of north and south Indians. – *Leg. Med.*, **10**(4),2008, 185-189.
39. **Reel, S., S. Rouse, W. V. Obe, P. Doherty.** Estimation of stature from static and dynamic footprints. – *Forensic Sci. Int.*, **219**(1-3), 2012, 283-e1.
40. **Saxena, S. K.** A study of correlations and estimation of stature from hand length, hand breadth and sole length. – *Anthropol. Anz.*, **42**(4) 271-276, 1984.
41. **Singla, R., M. Bedi, M. Biswas.** Sex estimation from foot anthropometry in Haryanvi Jats and North Indian Mixed Population. – *Indian J.*, **12**(1),2012, 13-16.
42. **Smith, S..** Stature estimation of 3–10-year-old children from long bone lengths. – *J. Forensic Sci.*, **52**(3),2007, 538-546.
43. **Srivastava, A., V. K. Yadav.** Reconstruction of stature using hand and foot dimensions among Indian population. – *J. Eng. Sci. Emg. Tech.*, **6**, 2014, 400-404.
44. **Suntnoore, D., S. Karaddi, P. Babladi, A. Mugadlimath, S. S Garampalli, B. S. Patil.** To study determination of stature by foot length in females. – *IJ CRR*, **5**(16), 2013, 15.
45. **Tharmar, N., K. Mohamed, M. H. B. Yaacob, J. P. Thomas.** Estimation of stature based on foot length of Malays in Malaysia. – *AJFS*, **43**(1), 2011, 13-26.
46. **Witana, C. P., J. Feng, R. S. Goonetilleke.** Dimensional differences for evaluating the quality of footwear fit. – *Ergon*, **47**(12), 2004, 1301-1317.
47. **Ulijaszek, S. J., J. A. Lourie.** Intra- and inter-observer error in anthropometric measurement. In: *Anthropometry: The individual and the population*, Cambridge, Cambridge University Press, 30-55, 1994.

Morphofunctional Anthropometric Asymmetry in Adolescent Tennis Players

Albena Dimitrova^{1,2*}

¹ Department of Anthropology and Anatomy, Institute of Experimental Morphology, Pathology and Anthropology with Museum, Bulgarian Academy of Sciences, Sofia, Bulgaria;

² Department of Anatomy and Biomechanics, National Sports Academy "Vassil Levski", Sofia, Bulgaria

*Corresponding author e-mail: albena_84@abv.bg

The study aims to assess youth tennis players' anthropometric characteristics and determine the level and direction of the morphofunctional asymmetry. In total, 239 tennis players aged 8-17 years were assessed. Anthropometric measurements were done bilaterally, using Martin-Saller' method. A hand grip test was performed to define static arm strength. Statistical analysis was made by SPSS 16.00. The units of asymmetry were calculated using Nacheva's equation. Tennis players from both sexes had higher values of forearm muscle mass than the upper arm's muscle mass. There were significant sexual differences, according to hand grip strength, with priority for boys. A moderate level of bilateral differences was reported in the forearm area and muscle-fat ratios. The hand grip strength, which has a high level of asymmetry, also showed large bilateral differences due to the higher loading of the forearm muscles. Tennis training in youth athletes leads to anthropometric asymmetry in the dominant upper limb.

Key words: tennis players; morphofunctional characteristics; asymmetry; adolescents

Introduction

Systematic physical load, mainly on the dominant part of the body, is a prerequisite for asymmetric changes in the bilateral body segments. These adaptive mechanisms of the body aim to preserve the athlete's physical abilities, but on the other hand can be a precondition for injuries and disproportions in the bones, as well as for deformities [9, 10]. Anthropometric asymmetry in sports depends on the type of physical activity and the level of sports discipline [2, 8]. Asymmetric changes are observed in the upper limbs (racquet sports, volleyball, basketball, handball, golf, etc.), mainly in the dimensions of the circumference of the arm and forearm [12] and the size of the epicondylar diameter of the humerus [15].

Different studies associated inter-limb asymmetry greater than 10-15% with increased incidences of injury. Some researchers declared that the asymmetry is more pronounced in the upper extremities than in the lower extremities, with right-sided prevalence [17, 25, 28]. Bilateral differences in morphological parameters (mainly in arm circumference, forearm, epicondylar diameter of the humerus) were observed in athletes practicing different sports, such as tennis, canoeing, golf, baseball and boxing [4, 8, 13, 14]. Tsolakis et al. established the relationship between the presence of asymmetry in the upper and lower limbs and the age of the athlete. The authors concluded that the higher percentage of asymmetry in the upper limbs is manifested at the age of 10-13 years, while in the lower limbs at 14-17 years [27].

Competitive tennis is a combination of shots with different types of ball spin. This is associated with multiple movements in the elbow and shoulder joints. The elbow joint allows flexion from 180 to 40 degrees, where one muscle extensor of the arm counteracts several muscle flexors. In the execution of the reverse blow (backhand), initial blow and overhead blow and those in the air, the optimal execution depends on the speed of extension of the arm in the elbow joint. This type of sport is associated with performing a series of uneven movements and high physical exertion (hitting the ball when serving sometimes exceeds 200 km/h), for a long time (between 60 and 300 min).

A significant number of studies worldwide prove that in tennis, the bilateral differences of the upper extremities and the uneven physical load inevitably lead to an asymmetric accumulation of muscle mass and an unbalance in muscle tones and the consequent disproportions in the skeletal structure [1, 7, 22, 23, 29].

The study aims to assess youth tennis players' anthropometric characteristics and to determine the level and direction of the asymmetry.

Material and Methods

A total of 239 tennis players (152 boys and 87 girls) age 8-17 years were assessed. All tennis players (TP) have training experience in tennis for two years and at least ten hours weekly. All athletes took part in regional, national or international championships. Participants were divided into three experimental groups according to age classification in sports practice (group I: 8-10 years old; group II: 11-13 years old; group III: 14-17 years old). The anthropometric measurements were taken using the classical method of Martin-Saller (1957). Body mass index (BMI) is calculated by a well-known formula using the mean height and weight values. Thirty-three anthropometric features were bilaterally measured because of the asymmetry analysis. Body composition components were determined by means of multi-frequency bioelectrical impedance measurements, which were taken with the use of an InBody (model: 170) analyzer, with eight electrodes. For accurate analysis, the following requirements had to be met: the measurements of each athlete were made at least two hours after a meal and at least 12 hours before training.

A hand grip test (European Test of Physical Fitness - EUROFIT) defines static arm strength. The right hand grip strength (RHGS, kg) and left hand grip strength (LHGS, kg) are measured using a standard calibrated handgrip dynamometer at a standing position with the shoulder adducted and neutrally rotated and elbow in full

extension. The statistical analysis was done using the software package SPSS 16.00 for Windows (IBM, USA). Paired T-test ($p \leq 0.05$, $p \leq 0.01$, $p \leq 0.001$) was applied to assess the bilateral differences of the anthropometric traits. The age- and sex-related differences were defined by the use of One-Way ANOVA, as well as Post hoc procedures for multiple comparisons (Tukey, HSD-test) and independent T-test, respectively ($p \leq 0.05$, $p \leq 0.01$, $p \leq 0.001$). The asymmetry coefficients (units of asymmetry, UA) of the assessed anthropometric features are calculated by Nacheva's equation (1986), modified by us. Percentile method was applied to determine the normative values to the units of asymmetry in adolescent tennis players (**Table 1**) and the profile of the morphofunctional anthropometric asymmetry was established. The TP and their parents completed informed consent and voluntarily participated in the study. The study protocol was reviewed and approved by the Ethical Committee of the Institute of Experimental Morphology, Pathology and Anthropology with Museum-Bulgarian Academy of Sciences (Protocol № 3/11.04.2018) and was conducted in agreement with the principles stated in the Declaration of Helsinki for human studies [30].

Table 1. Normative values to the level of asymmetry (units of asymmetry, UA) in adolescent tennis players.

	min	max
Relative symmetry	0.00 UA	0.49 UA
Weak asymmetry	0.50 UA	1.49 UA
Moderate asymmetry	1.50 UA	3.49 UA
High asymmetry	3.50 UA	7.49 UA
Very high asymmetry	7.50 > UA	

Results and Discussion

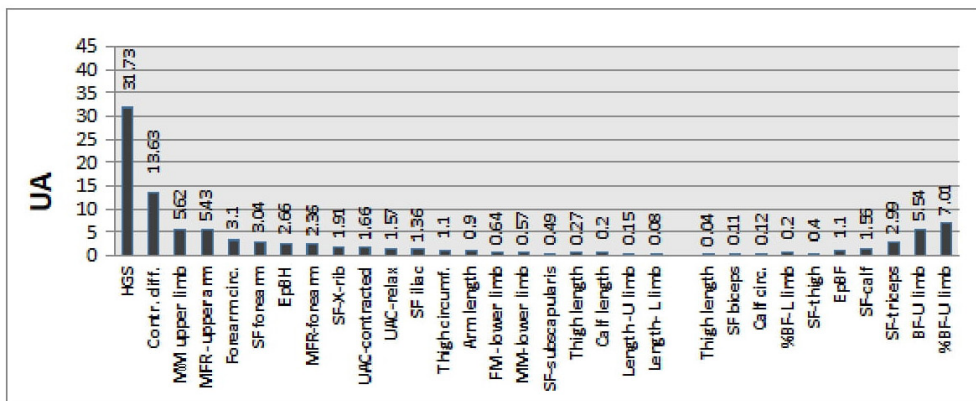
Contemporary findings emphasize the complexity of asymmetries and their relationships with physical and sports performance and highlighting the need for further research [3, 11, 16, 26]. The current study presents the bilateral differences in morphological variables of adolescent tennis players.

Optimal linear growth of the body shows age- and sex-specific dependence [19, 20, 21]. The results obtained in the current study confirmed those of the other scientific researches on physical development of youth and adolescents shown in increasing the sizes of anthropometric features highlighted in 8-10 years old girls and 14-17 years old boys [18, 20].

The linear growth of the body increases significantly throughout the assessed age period from 140.10 cm to 174.02 cm in boys and from 144.23 cm to 168.25 cm in girls, at the ages 8-17. Well expressed sexual differences were observed in the first and third age groups, with priority for boys ($p < 0.05$). Body weight is 32.70 kg in boys and 37.38 kg in girls from the first age group ($p < 0.05$) and reached 60.64 kg (in males) and 60.91 kg (females) in the third age group. The mean values of BMI also differ significantly

between sexes. At the age period 8-10 years the average values for BMI in male TP are 16.62 kg/m² and girls TP in this age group are distinguished by a significantly higher BMI (17.90 kg/m²) (p≤0.01). In the period 11-13 years the BMI in both sexes reaches almost the same values (19.15 kg/m² - boys, 19.72 kg/m² - girls). The largest sex-related differences are found in the period 14-17 years, when the BMI reaches values of 20.08 kg/m² in boys and 21.66 kg/m² in girls (p≤0.001).

Figures 1 to 6 present data for the profile of morphofunctional asymmetry of the 8-17-year-old TP. The active physical load of certain muscle groups of the dominant upper extremity in tennis players leads to a decrease in body fat mass (BF), with better-developed muscle mass (MM). Moderate bilateral differences were reported in the forearm area (forearm circumference, forearm skin fold) and muscle-fat ratios of the arm and forearm. The established high degree of asymmetry in hand grip strength is indirect evidence of the large bilateral differences in this part of the upper limbs. With increasing age, the asymmetry in the studied anthropometric signs decreases and these changes are more pronounced in males. Contrary to our results Chapelle et al. assessing youth TP according to their maturity offset, sex and training volume displayed a significantly higher lean mass asymmetry in males with the increase of the age. The authors also found an increment of bone mineral density asymmetry in relation with maturity status [5].



HGS-hand grip strength; **Contr. diff.**-contractile difference; **MM upper limb**- muscle mass upper limb; **MM-lower limb**- muscle mass lower limb; **BF-U limb**-body fat upper limb; **%BF-U limb** - percent body fat of the upper limb; **FM-lower limb**- fat mass lower limb; **%BF-L limb**- percent body fat of the lower limb;**MFR-upper arm**- muscle-fat ratio upper arm; **MFR-forearm**- muscle-fat ratio of the forearm; **UAC-contracted** - upper arm circumference-contracted; **UAC-relax**-upper arm circumference- relax; **EpBH**- epicondylar diameter of humerus; **EpBF**- epicondylar diameter of the femur; **Forearm circ.** -forearm circumference; **Thigh circumf.**- thigh circumference; **Calf circ.**- calf circumference; **Length- U Limb**- length upper limb; **Length- L limb** -length lower limb; **SF-thigh**- thigh skinfold; **SF-calf**- calf skin fold; **SF-triceps**- triceps skinfold; **SF-X-rib**- X-rib skinfold; **SF biceps**- biceps skinfold; **SF-subscapularis** - scinfold subscapularis; **SF forearm**- forearm skinfold; **SF iliac**- iliac skinfold

Fig. 1. Profile of morphofunctional anthropometric asymmetry in 8-10 years old male tennis players

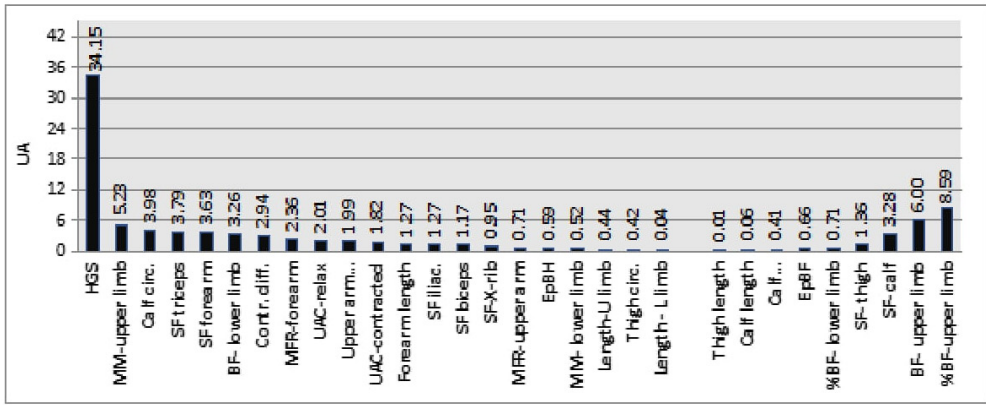


Fig. 2. Profile of morphofunctional anthropometric asymmetry in 11-13 years old male tennis players

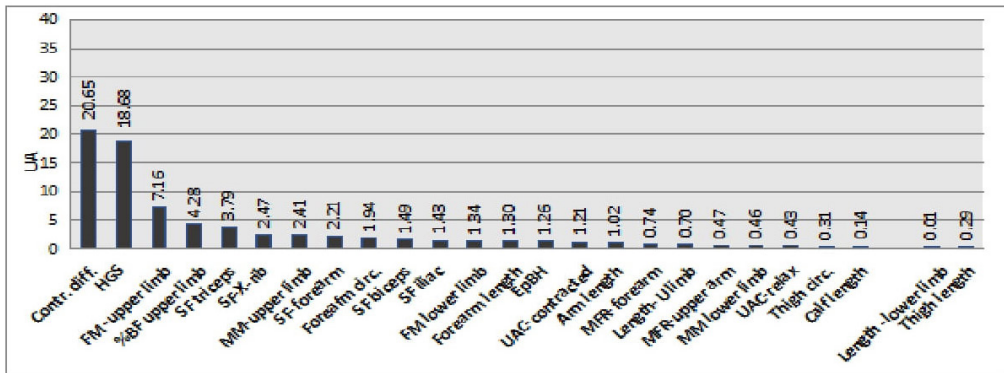


Fig. 3. Profile of morphofunctional anthropometric asymmetry in 14-17 years old male tennis players

Relative symmetry or slight asymmetry was found in the majority of the assessed limbs lengths and widths. The bilateral differences in most of the examined anthropometric signs are with a predominant right-sided asymmetry of the upper limb and left-sided in the lower limb. Sanchez-Muñoz et al. found certain asymmetric manifestations in the dimensions of the epicondylar diameters of the femur and humerus in females in favor of the dominant limb [23].

In male tennis players, all limb circumferences have right-sided asymmetry, except leg circumference (which is left-sided); in girls, all circumferences of the upper limb are right-sided, while in the lower limb all circumferences show left-sided asymmetry. A moderate manifestation of body asymmetry ($UA \geq 1.50$) was observed in most of the upper limb circumferences. Schluga and Filho et al. reported larger sizes in the dominant part of the body, with significant differences observed in forearm circumference (4.76%) and hip circumference (2.32%) [24].

The assessment of bilateral differences in BF assessed by the thickness of seven skin folds (SF) in both sexes showed the greatest asymmetry in four of them - triceps SF, biceps SF, forearm SF and calf SF. The asymmetry of the upper limb is characterized by the skin fold of the triceps (most strongly manifested at the age of 14-17 years) and forearm skin fold (biggest bilateral differences in 11-13-year-old boys and 14-17-year-old girls) while in the lower limb the biggest differences are reported in the calf skin fold in the age 11-13 years (boys) and 14-17 years (girls).

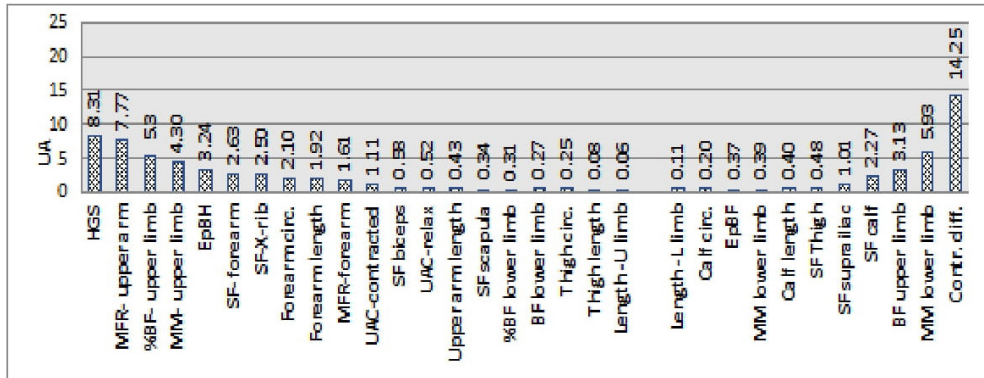


Fig. 4. Profile of morphofunctional anthropometric asymmetry in 8-10 years old female tennis players

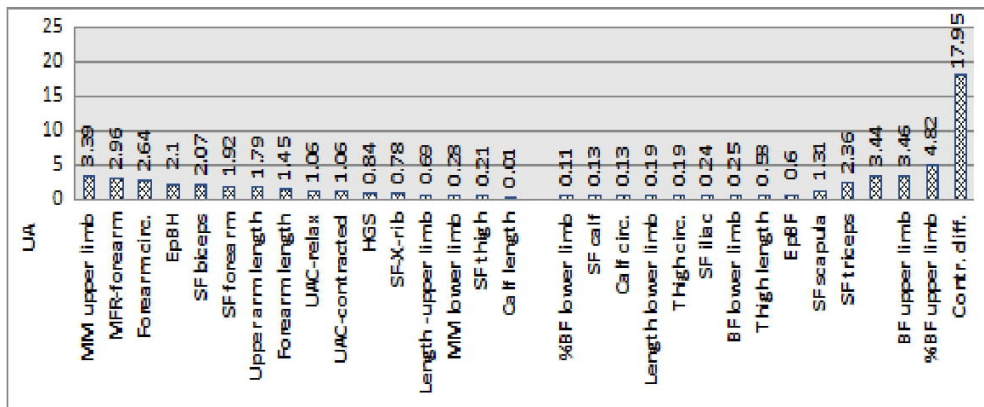


Fig. 5. Profile of morphofunctional anthropometric asymmetry in 11-13 years old female tennis players

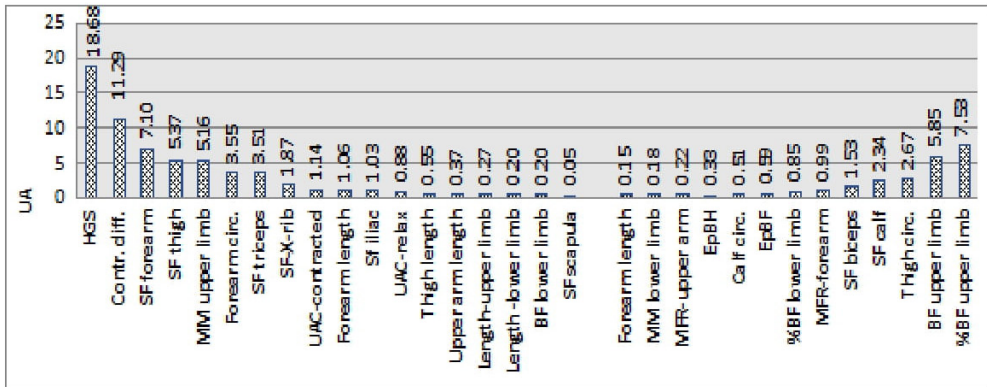


Fig. 6. Profile of morphofunctional anthropometric asymmetry in 14-17 years old female tennis players

Conclusions

In conclusion, we found that tennis is a sport that may cause asymmetric distribution of fat mass and lean mass, especially in the upper limbs.

The methodology applied by us provides objective information about the interrelationship in the system “type of sports activity – morphofunctional characteristics – health status”.

References

1. **Abrahão, A., M. Ricardo, D. Mello.** Anthropometric differences between the hemispheric body right and left of adult and children tennis instructors to beginners in the sport and incidence of postural deviations. – *Fitness & Performance Journal*, **7**(4), 2008, 264-270 [in Portuguese].
2. **Auerbach, B. M., C. B. Ruff.** Limb bone bilateral asymmetry: variability and commonality among modern humans. – *J. Hum. Evol.*, **50**, 2006, 203-218.
3. **Bell, D. R., J. L. Sanfilippo, N. Binkley, B. C. Heiderscheit.** Lean mass asymmetry influences force and power asymmetry during jumping in collegiate athletes. – *Journal of Strength and Conditioning Research*, **28**, 2014, 884–891.
4. **Calbet, J. A. L., C. Dorado, P. Diaz-Herrera, L. P. Rodríguez-Rodríguez.** High femoral bone mineral content and density in male football (soccer) players. – *Med. Sci. Sports Exerc.*, **33**(1), 2001, 1682-1687.
5. **Chapelle, L., E. D’Hondt, N. Rommers, P. Clarys.** Development of upper-extremity morphological asymmetries in male and female elite youth tennis players: A longitudinal study. – *Pediatric Exercise Science*, **36**(2), 2023, 91-97.
6. **Ceroni, D., X. E. Martin, C. Delhumeau, N. J. Farpour-Lambert.** Bilateral and gender differences during single-legged vertical jump performance in healthy teenagers. – *Journal of Strength and Conditioning Research*, **26**, 2012, 452–457.

7. **Del-Fresno, D., G. Vicente-Rodriguez, J. M. González-Ravé, L. A. Moreno, P. Rey-López.** Body composition and fitness in elite Spanish children tennis players. – *J. Hum. Sport Exerc.*, **5**(2), 2010, 250-264.
8. **Dorado, C., J. Sanches -Moysi, G. Vicente, J. A. Serrano, L. R. Rodríguez, J. A. L. Calbet.** Bone mass, bone mineral density and muscle mass in professional golfers. – *J. Sports Sci.*, **20**, 2002, 591-597.
9. **Ducher, G., D. Courteix, S. Meme, C. Magni, J. F. Viala, C. L. Benhamou.** Bone geometry in response to long-term tennis playing and its relationship with muscle volume: a quantitative magnetic resonance imaging study in tennis players. – *Bone*, **37**(4), 2005, 457-466.
10. **Hides, J., W. Stanton, M. Freke, S. Wilson, S. McMahon, C. Richardson.** MRI study of the size, symmetry and function of the trunk muscles among elite cricketers with and without low back pain. – *British Journal of Sports Medicine*, **42**, 2008, 809–813.
11. **Jordan, M. J., P. Aagaard, W. Herzog.** Lower limb asymmetry in mechanical muscle function: A comparison between ski racers with and without ACL reconstruction. – *Scandinavian Journal of Medicine in Science and Sports*, **25**(3), 2015, 301-309.
12. **Kannus, P., H. Haapasalo, M. Sankelo, H. Sievanen, M. Pasanen, A. Heinonen, P. Oja, I. Vuori.** Effect of starting age of physical activity on bone mass in the dominant arm of tennis and squash players. – *Ann. of Internal Med.*, **123**, 1995, 27-31.
13. **Komi, P. V.** *Strength and power in sport.* – *The Encyclopaedia of sports medicine, volume III*, Wiley-Blackwell, 1996, 284-288.
14. **Krawczyk, B., M. Skład, B. Majle.** Lateral asymmetry in upper and lower limb measurements in selected groups of male athletes. – *Biol. Sport*, **15** (1), 199833-199838.
15. **Leone, M., G. Lariviere.** Anthropometric and biomotor characteristics of elite adolescent male athletes competing in four different sports. – *Science & Sports*, **13** (1), 1998, 26-33.
16. **Liu, T., J. L. Jensen.** Age-related differences in bilateral asymmetry in cycling performance. – *Research Quarterly for Exercise and Sport*, **83**, 2012, 114–119.
17. **Malina, R.M., C. Bouchard, O. Bar-Or.** *Growth, maturation and physical activity*, 2nd edition, Human Kinetics, 2004.
18. **Mitova, Z.** Anthropological characteristics of physical development, body composition and body protection in 9-15 year old children and adolescents from Sofia. – *PhD Thesis*, 2009, Sofia. [in Bulgarian].
19. **Nikolova G., D. Dantchev.** Age changes in the basic anthropometric characteristics of the average Bulgarian females. – *Series on Biomechanics*, **37**(1), 2023, 5-12.
20. **Nacheva, A., Y. Zhecheva, I. Yankova, Z. Filcheva.** Physical development of children and adolescents in Bulgaria, at the border between the XXth and XXIst centuries. – “Prof. M. Drinov” Academic Publishing House, Sofia, 2012. [In Bulgarian].
21. **Nikolova G., D. Dantchev.** Gender dependence of the geometric and mass-inertial characteristics via a 3D biomechanical model of the human body. – *Series on Biomechanics*, **36**(1), 2022, 113-119.
22. **Rogowski, I., G. Ducher, O. Brosseau, C. Hautier.** Asymmetry in volume between dominant and nondominant upper limbs in young tennis players. – *Pediatric Exercise Science*, **20**, 2008, 263–272.
23. **Sánchez-Muñoz, C., D. Sanz, M. Zabala.** Anthropometric characteristics, body composition and somatotype of elite junior tennis players. – *Br. J. Sports Med.*, **41**, 2007, 793-799.

24. **Schluga-Filho, J. L., M. R. Ribas., L. O. Nogueira, J. C. Andrade, P. Fernandes, J. C. Bassan.** Motor and morphological profile of tennis players from 11 to 15 years old. – *Rev. Andal. Med.*, **9**(3), 2016, 114–118.
25. **Tomkinson, G. R., L. A. Léger, T. S. Olds, G. Cazor.** Secular trends in the performance of children and adolescents (1980–2000): an analysis of 55 studies of the 20 m shuttle run test in 11 countries. – *Sports Med.*, **33**(4), 2003, 285–300.
26. **Trivers, R., B. Fink, M. Russell, K. McCarty, B. James, B. G. Palestis.** Lower body symmetry and running performance in elite Jamaican trackand field athletes. – *PLOS One*, **9**, 2014, 1–8.
27. **Tsolakis, C. H., C. H. Katsikas.** Long term effects of a combined physical conditioning and fencing training adoprogram on neuromuscular performance in elite fencers. – *Int. J. Fitness*, **2**(1), 2006, 35-42.
28. **Ulijaszek, S. J., C. G. N. Mascie-Taylor.** *Anthropometry: the individual and the population*, New York, Cambridge University Press, 2005.
29. **Vergauwen, L., A. J. Spaepen, J. Lefevre, P. Hespel.** Evaluation of stroke performance in tennis. – *Med. Sci. Sports Exerc.*, **30**(8), 1998, 1281-1288.
30. **World Medical Association.** Declaration of Helsinki – Ethical Principles for Medical Research Involving Human Subjects. – *WMAJ*, **54**(4), 2008, 122-125.

Morphometric Analysis of Burn-Induced Gastric Mucosal Injury and Effect of Melatonin

Minka Hristova^{1,}, Nadezhda Stefanova², Maria Tzaneva², Antoniya Hachmeriyan¹, Ganka Bekyarova¹*

¹ Department of Physiology and Pathophysiology, Medical University of Varna, Varna 9002, Bulgaria

² Department of General and Clinical Pathology, Forensic Medicine and Deontology, Faculty of Medicine, Medical University of Varna, Varna 9002, Bulgaria

* Corresponding author e-mail: hristova.minka@abv.bg

Curling's ulcers are acute gastric mucosal injuries and are among the complications that affect the gastrointestinal system after severe thermal trauma. Melatonin, a multifunctional molecule, exerts various gastroprotective effects. We examined and presented a semiquantitative evaluation of the effect of melatonin on burn-induced acute gastric mucosal lesions. Melatonin (10 mg per kg body mass) was administered immediately and 12 hours after skin injury in a rat burn model. The therapeutic potential of melatonin was examined using macroscopic and microscopic morphometric analysis. The erosion index (EI) and percentage of protection (PP) were calculated. The depth of erosion, epithelial necrosis, hemorrhage, and inflammation were also evaluated. Melatonin successfully decreased the scores of all detected macroscopic and microscopic alterations and had therapeutic effects in 69,32% of cases with burn-induced gastric mucosal injury. In conclusion, the administration of melatonin can effectively improve gastric mucosal injury after a burn.

Key words: melatonin, burns, gastric mucosa, erosion

Introduction

Severe thermal injury continues to be a serious health problem [31]. Burns involving more than 30% of the total body surface area (TBSA) are accompanied by multiple complications affecting almost all organs and systems and cause burn shock [31, 28].

Systemic response manifestations and the development of complications further worsen the condition of patients with severe burns. Therefore, these critically ill patients require intensive care, a multidisciplinary approach, and prevention of possible complications that could affect different organs and systems [36, 29].

The gastrointestinal tract (GIT) is among the systems that are affected after burn trauma. The injuries affect all of its parts – stomach, small and large intestines [8]. Gastrointestinal (GI) complications are often observed in patients with more than 20% TBSA burns [32]. Burns increase the risk of damage to the mucous membranes and the formation of ulcers, known as Curling's ulcers [10].

Curling's ulcers are acute gastric mucosal lesions and are one of the most common visceral complications early after severe burns. This lesion has been recognized as a potentially life-threatening event in critically ill patients [40]. In the past, the incidence of Curling's ulcers was higher [24], but in recent decades it has been drastically decreased, due to improved therapeutic approach and prophylaxis [10]. Nevertheless, a retrospective study updated the data and found mucosal postburn injuries and determined that the frequency of gastric ulcer is greater compared to the frequency of duodenal and both ulcer types [10].

Stress-induced damage to the gastric and duodenal mucosa can be observed after physical trauma, shock, hemorrhage, and sepsis [16]. For this reason, stress gastritis is defined as end-organ failure of the stomach in critical illness [16].

Despite successful prophylaxis of Curling's ulcers, the presence of severe burns or other severe clinical conditions poses an increased risk of developing gastric complications. In some cases, critically ill patients do not respond to medication treatment and this condition requires surgical intervention to control bleeding [16].

Melatonin (n-acetyl-5-methoxytryptamine), indoleamine derived from tryptophan, is a hormone secreted primarily by the pineal gland in the brain. Clinical and experimental research have shown a plethora of therapeutic effects of melatonin as an antioxidant, anti-inflammatory, and antiapoptotic agent [9], which determine its organoprotective properties. Additionally, melatonin is a promising adjunctive drug in critical situations such as hemorrhagic shock [37], sepsis [15], and surgery [13]. Melatonin has manifested strong protective effects on various organs following burn injuries [1, 2]. Experimental studies have shown that melatonin has gastroprotective activity against gastric mucosal injury induced by ethanol [6], non-steroidal anti-inflammatory drugs [27] and stress conditions [4, 11].

The aim of this study is to present a semiquantitative evaluation of the gastroprotective effect of melatonin in burn-induced gastric mucosal injury in an experimental rat model. For this purpose, a macroscopic and microscopic morphometric analysis of the changes in the gastric mucosa was carried out.

Material and Methods

Animals

The experimental procedures were approved by the Home Office for Care and Use of Laboratory Animals and were performed with careful consideration of the ethics of animal experimentation according to the International Guiding Principles for Animal Research approved in Bulgaria (No. 90000088/2008) and Directive 2010/63/EU on the protection of animals used for scientific purposes.

Experimental design

We used age-matched male Wistar rats weighing between 220 and 250 g. Animals were housed at 20 °C and offered standard rat chow and water *ad libitum*. They were kept in dark/light cycles (DL = 12:12 h) in individual wire-bottomed cages. The lights were turned off at 8:00 p.m. and turned on at 8:00 a.m. to achieve a physiological photoperiod. Rats fasted for 12 hours and were allowed free access to water before injury.

Thermal injury and melatonin treatment

Twenty-four animals were randomly divided into three groups (n = 8 in each group) as follows: the control, i.e., the non-burned (C), the vehicle-treated burned group (B), and the melatonin-treated burned group (B + M). After light ether inhalation, general anesthesia was performed using thiopental (30 mg/kg i.p.). In order to accomplish a third-degree burn over 30% of the total body surface area (TBSA), hot boiling water (90°C) was applied to the back of the animals for a period of 10 s. For those rats that were subjected to burn injury, 4 mL of physiological saline was applied intraperitoneally (i.p.) for immediate resuscitation following burn injury.

Melatonin (N-acetyl-5-methoxytryptamine, Merck, Darmstadt, Germany) at a dose of 10 mg/kg body weight (b.w.) dissolved in vehicle (2% ethyl alcohol diluted in physiological saline to constitute 5 mL/kg i.p.) was administered. Melatonin and vehicle were applied immediately i.p. after burns in the morning between 8:00 and 9:00 a.m. and 12 hours after thermal skin injury. All animals were given buprenorphine (0.3 mg/kg i.p. b.w.) twice daily for post-burn pain control. No animals died during the observed period.

The animals were re-anesthetized with thiopental and sacrificed 24 hours after the burn trauma. Stomachs were immediately removed and incision was made along the greater curvature and irrigated with saline solution (0.9% NaCl). Two blinded observers assessed macroscopic and microscopic changes.

Macroscopic assessment of gastric mucosal injury

The severity of erosions is scored with a hand lens using the following arbitrary scoring system modified by the method described by Srivastava et al. (1991) [35]: Shedding of epithelium = 10; Petechial and frank hemorrhages = 20; One or two erosions = 30; More than two erosions = 40; Perforation = 50.

The mean erosion score for each animal was calculated and expressed as the erosion index (EI) [39]. Evaluation and an erosion index in groups are calculated: $EI = EN + ES + EP \times 10^{-1}$. Where: EN = Average of number of erosions per animal; ES = Average of severity score; EP = Percentage of animals with erosions.

The percentage of erosion protection (PP) was determined as follows [39]: % Protection = $((C - T)/C) \times 100$. Where: C = Mean erosion index in the negative control group (the vehicle-treated burned group); T = Mean erosion index in the treated group (the melatonin-treated burned group).

Histopathological analysis

Stomach tissue specimens were fixed in 10% buffered formalin (pH 7.2), dehydrated in an ascending series of ethyl alcohol (70%-100%), and cleared in methyl benzoate. After that, they were embedded in paraffin wax. Tissue sections of 5 µm were stained with hematoxylin and eosin (H&E) and examined using a light microscope

(Olympus BH-2, Tokyo, Japan). The presence of hemorrhages, epithelial necrosis, and inflammatory cells infiltration were evaluated using the following scale: 0 – no; 1 – low; 2 – moderate; 3 – high. The presence and depth of erosions were assessed using the following scale: 0- none; 1- up to 1/3 of the total thickness of the mucosa; 2 – up to 2/3 of the total thickness of the mucosa; 3 - more than 2/3 of the total thickness of the mucosa is involved [34].

Statistical analysis

GraphPad Prism (version 9.0, GraphPad Software, San Diego, CA, USA) was used to conduct all statistical analyses. Numerical data were expressed as mean values and standard error of means. A one-way ANOVA test followed by Dunnett's post-hoc test was applied to evaluate the significant differences between the mean values of studied groups. The results were considered significant for a p-value less than 0.05.

Results

Macroscopic assessment

The gastric mucosa in the control group is pale pink and has preserved mucosal relief (**Fig. 1 A**). In the burned group (B), there is pronounced hyperemia of the gastric mucosa with erosions, located mainly on the surface of the mucosal folds. The bottom of the erosions is brownish in color (**Fig. 1 B1, B2**). In the melatonin-treated group, there are fewer erosions and only in separate areas, the mucosa is hyperemic (**Fig. 1 C**). Evaluation of the macroscopic changes of the gastric mucosa are given in **Fig. 1** and **Table 1**.

Microscopic assessment

The gastric mucosa of the animals from the control group had a preserved histological structure. Our results showed the presence of erosions in the gastric mucosa in all animals in the burn group. Morphometric analysis showed a prominent depth of the erosions, accompanied by epithelial necrosis. With a possible maximum score of 3.0, the average mean values were 2.75 ± 0.164 and 2.25 ± 0.25 , respectively. Hemorrhagic changes were observed in three of the animals in the experimental group (37.5%), with a mean score of 0.375 ± 0.183 . Thermal injury caused a prominent inflammatory reaction with a morphometric score of 1.625 ± 0.183 .

Melatonin administration lowered all morphometric scores. The mean scores of the depth of erosions and epithelial necrosis were reduced by 54,55% ($p < 0.0001$ compared to the burn group) and 66.67% ($p < 0.0001$ compared to the burn group), respectively. Melatonin has a prominent effect on hemorrhagic changes, which were completely abolished in the treated group ($p = 0.0374$ compared to the burned group). Although not significantly, melatonin reduced the inflammatory infiltrate in the gastric mucosa compared to that observed in the burn group (1.25 ± 0.164). These results indicate the beneficial effect of the treatment on the maintenance of the integrity of the tissue structure. Microscopic alterations in gastric mucosa are summarily presented in **Fig. 2** and **Table 2**.

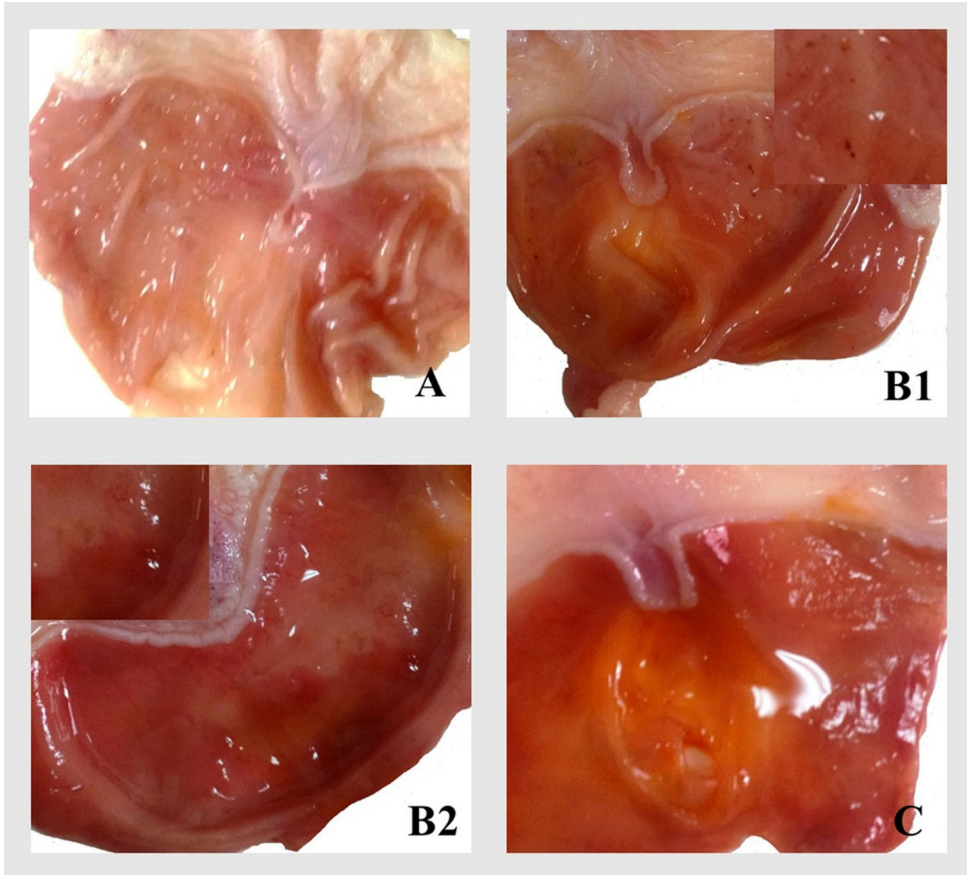


Fig. 1. Macroscopic changes in the gastric mucosa and the effect of melatonin in burn injury. Controls (A); burned rats (B1, B2); burned rats, treated with melatonin (C). Representative data.

Table 1. Melatonin effect on the macroscopic changes of the gastric mucosa after severe thermal trauma. Results are expressed as the mean \pm SEM; **** $p < 0.0001$ vs. control group; * $p < 0.05$ vs. control group; *** $p < 0.005$ vs. burned, non-treated group. Controls (C); burned rats (B); burned melatonin-treated rats (B + M).

<i>Group</i>	ES	EN	EI	PP/ [%]
C	0.0	0.0	0.0	
B	45 \pm 3,273****	5,125 \pm 1,172****	50,13 \pm 3,652****	
B + M	15 \pm 7,319***	0,375 \pm 0,375***	15,38 \pm 7,651***	69,32

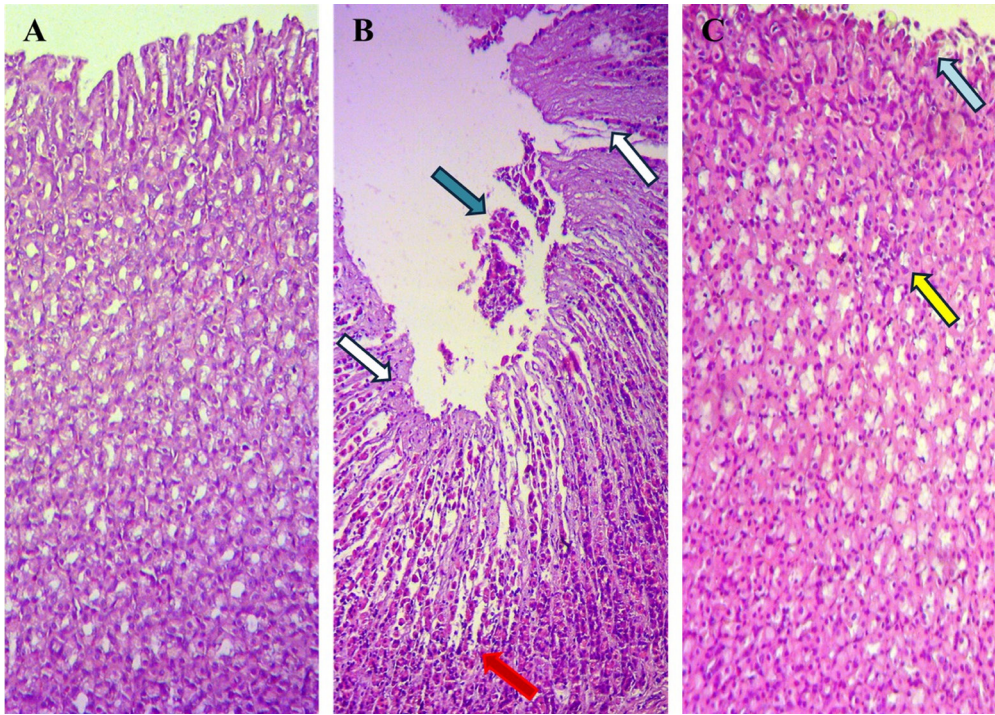


Fig. 2. Histopathological changes in the gastric mucosa and the effect of melatonin in burn injury. (A) Control group – the architecture of the gastric mucosa is preserved. (B) Burn group – erosion of the gastric mucosa with cellular debris (blue arrow), area of necrosis (white arrow), and underlying degenerative changes of the epithelial cells (red arrow). (C) Group with burn and melatonin treatment – normal preserved architecture of the gastric mucosa with desquamation of the covering epithelium (light blue arrow) and inflammatory infiltrate (yellow arrow) in the lamina propria of the mucosa. Representative images. Hematoxylin and eosin staining, magnification, 200x.

Table 2. Melatonin effect on scores of histopathological parameters in gastric mucosa after severe thermal trauma. Results are expressed as the mean \pm SEM; **** $p < 0.0001$ vs. control group; * $p < 0.05$ vs. control group; †††† $p < 0.0001$ vs. control group; † $p < 0.05$ vs. control group; **** $p < 0.0001$ vs. burned, non-treated group; * $p < 0.05$ vs. burned, non-treated group. Controls (C); burned rats (B); burned melatonin-treated rats (B + M).

Group	Depth of erosion	Epithelial necrosis	Hemorrhage	Inflammatory infiltrate
C	0.0	0.0	0.0	0.0
B	2.75 \pm 0.164****	2.25 \pm 0.25****	0.375 \pm 0.183*	1.625 \pm 0.183****
B + M	1.25 \pm 0.164††††****	0.75 \pm 0.164†****	0.0*	1.25 \pm 0.164††††

Discussion

Acute postburn gastric mucosal injuries vary in degree of damage and can clinically manifest differently- from erosive gastritis, as asymptomatic lesions and occult GI bleeding to aggressive clinically significant GI bleeding, anemia, and death [29]. Every clinical manifestation is a sign of disrupted tissue homeostasis with limited survival strategies and a prevalence of processes that cause cell death [17].

This experimental rat model was used to monitor macroscopic and morphological changes in the gastric mucosa and the effect of intraperitoneally administered melatonin. Full-thickness skin injury results in damage to the stomach after 24 hours. Direct examination revealed changes in the mucosa in all animals exposed to burn, which proves the high risk of organ involvement in this type of trauma. The calculations based on the number of visible erosions, average values of the erosion severity, and the percentage of animals with erosions determined a high erosion index in the burn group. Light microscopic examination of the tissue samples showed that the depth of erosions, epithelial necrosis, hemorrhages, and inflammatory infiltrate were high in the burn group and corresponded to the results of the macroscopic examination.

Multiple factors are involved in the pathogenesis of stress ulcers, which contribute to the high mortality rate in critically ill burn patients [21]. Severe burn causes systemic stress and initiates a cascade of events, that compromises the blood perfusion to the gastrointestinal mucosa [29]. As a result, tissue hypoperfusion and hypoxia occur and lead to disrupted energy metabolism [40]. The production of gastroprotective factors (prostaglandins, bicarbonate, mucus) decreases, and this results in the development of multiple superficial erosions of the gastric mucosa due to loss of the integrity of the mucosal barrier [29]. Microcirculatory disorders are a trigger factor for cellular destructive processes such as oxidative stress and apoptosis [5, 18, 19, 21].

In our study, melatonin significantly reduced gastric mucosal injury. Macroscopic analysis showed a markedly reduced number and severity of erosions in the gastric mucosa, which leads to a reduction in the erosion index compared to the burn group. We also found a similar beneficial effect of melatonin on microscopic tissue changes. We observed a reduction of inflammatory cells infiltration and a significant limitation of the depth of erosions and the manifestations of epithelial necrosis and hemorrhages in animals treated with melatonin compared to those without treatment.

The change in macroscopic and microscopic scores can be explained by the properties of melatonin as a multifunctional molecule with a prominent pleiotropic biological action [12, 23]. Melatonin elevates the antioxidant capacity and increases the expression of antioxidant enzymes Cu/Zn superoxide dismutase [20] and heme oxygenase-1 [18] and suppresses lipid peroxidation in gastric mucosa postburn injury [5, 19]. Moreover, melatonin effectively ameliorates burn-induced gastric mucosal injury and modulate apoptosis through the expression of Bcl-2 family proteins [19].

The beneficial effects of melatonin on the gastric mucosa are not limited to the antioxidant and antiapoptotic action of the indole. Exogenously administered melatonin and its precursor L-tryptophan, are mucoprotectors that contribute to ulcer healing and enhance the microcirculation at the ulcer margins [7].

It is known that physical stress is the immediate response of the patient after a major thermal injury [30, 22]. Melatonin administration suppresses catecholamine synthesis [25] and significantly attenuates the adrenocortical secretory response to acute

and chronic stress [26]. In light of these facts, it may be considered that melatonin, by influencing acute stress, may have a beneficial effect on the organism, including the gastrointestinal system.

According to modern guidelines, proton pump inhibitors (PPIs) and histamine-2 receptor antagonists are used for Curling's ulcer prophylaxis [29]. The duration of stress ulcer prophylaxis is different [33]. PPIs are known to have adverse effects in short-term use, and especially in long-term use [38, 33]. In this regard, the low toxicity of melatonin [14] defines it as a molecule with promising therapeutic potential. In addition, co-treatment of rats with melatonin and ranitidine or omeprazole protects against stress ulceration in doses at which either of these alone could not protect the stomach [3].

Despite good management, Curling's ulcers remain a cause of considerable morbidity and mortality [29]. Therefore, response to treatment, prevention of ulcer recurrence, or ongoing gastrointestinal complications are essentially important for clinical practice [29].

Conclusions

The present study reveals a significant manifestation of the pathological changes in the gastric mucosa during burn. Melatonin successfully reduces both macroscopic and microscopic alterations. Melatonin provides a high level of protection and limits processes in the mucosal layer of the stomach wall. In this way, it can prevent the development of gastric ulcers and more serious postburn complications requiring surgical intervention.

These findings may inspire future research on the use of melatonin, alongside standard pharmacological agents, to prevent Curling's ulcers, acute gastric injuries from various causes, and other gastrointestinal diseases where oxidative stress, apoptosis, and inflammation play a key role in their pathogenesis.

References

1. **Al-Ghoul, W. M., S. Abu-Shaqra, B. G. Park, N Fazal.** Melatonin plays a protective role in postburn rodent gut pathophysiology. - *Int. J. Biol. Sci.*, **6** (3), 2010, 282-293.
2. **Bai, X., T. He, J. Gao, Y. Liu, J. Liu, S. Han, Y. Li, J. Shi, J. Han, K. Tao, S. Xie, H. Wang, & D. Hu.** Melatonin prevents acute kidney injury in severely burned rats via the activation of SIRT1. - *Sci. Rep.*, **6**, 2016, 32199.
3. **Bandyopadhyay, D., A. Bandyopadhyay, P. K. Das, R. J. Reiter.** Melatonin protects against gastric ulceration and increases the efficacy of ranitidine and omeprazole in reducing gastric damage. - *J. Pineal Res.*, **33**(1), 2002, 1-7.
4. **Bandyopadhyay, D., K. Biswas, U. Bandyopadhyay, R. J. Reiter, R. K. Banerjee.** Melatonin protects against stress-induced gastric lesions by scavenging the hydroxyl radical. - *J. Pineal Res.*, **29**(3), 2000, 143-151.
5. **Bekyarova, G., B. Galunska, D. Ivanova, T. Yankova.** Effect of melatonin on burn-induced gastric mucosal injury in rats. - *Burns*, **35**(6), 2009, 863-868.

6. **Bilici, D., H. Süleyman, Z. N. Banoğlu, A. Kiziltunç, B. Avci, A. Ciftçioğlu, S. Bilici.** Melatonin prevents ethanol-induced gastric mucosal damage possibly due to its antioxidant effect. – *Dig. Dis. Sci.*, **47**(4), 2002, 856–861.
7. **Brzozowska, I., P. C. Konturek, T. Brzozowski, S. J. Konturek, S. Kwieciën, R. Pajdo, D. Drozdowicz, M., Ptak A. Pawlik, E. G. Hahn.** Role of prostaglandins, nitric oxide, sensory nerves and gastrin in acceleration of ulcer healing by melatonin and its precursor, L-tryptophan. – *J. Pineal Res.* **32**(3), 2002, 149-162.
8. **Çakir, B., B. C. Yeğen.** Systemic responses to burn injury. – *Turk. J. Med. Sci.*, **34**(4), 2004, 215-226.
9. **Chitimus, D. M., M. R. Popescu, S. E. Voiculescu, A. M. Panaitescu, B. Pavel, L. Zagrean, A. M. Zagrean.** Melatonin's impact on antioxidative and anti-inflammatory reprogramming in homeostasis and disease. – *Biomolecules*, **10**(9), 2020, 1211.
10. **Choi, Y. H., J. H. Lee, J. J. Shin, Y. S. Cho.** A revised risk analysis of stress ulcers in burn patients receiving ulcer prophylaxis. – *Clin. Exp. Emerg. Med.*, **2**(4), 2015, 250-255.
11. **Choudhary, P., T. Roy, A. Chatterjee, V. K. Mishra, S. Pant, S. Swarnakar.** Melatonin rescues swim stress induced gastric ulceration by inhibiting matrix metalloproteinase-3 via down-regulation of inflammatory signaling cascade. - *Life Sci.*, **297**, 2022, 120426.
12. **Dubocovich, M. L., M. A. Rivera-Bermudez, M. J. Gerdin, M. I. Masana.** Molecular pharmacology, regulation and function of mammalian melatonin receptors. – *Front. Biosci.*, **8**, 2003, d1093-108.
13. **Eghbal, M. A., A. Eftekhari, E. Ahmadian, Y. Azarmi, A. Parvizpur.** A Review of biological and pharmacological actions of melatonin: oxidant and prooxidant properties. – *J. Pharma Reports*, **1**, 2016, 106.
14. **Escames, G., D. Acuña-Castroviejo, L. C. López, D. X. Tan, M. D. Maldonado, M. Sánchez-Hidalgo, J. León, R. J. Reiter.** Pharmacological utility of melatonin in the treatment of septic shock: experimental and clinical evidence. – *J. Pharm Pharmacol.*, **58**(9), 2006, 1153-1165.
15. **Galley, H. F., L. Allen, P. J. Colin, S. P. Galt, N. R. Webster.** Dose assessment of melatonin in sepsis (DAMSEL2) study: Pharmacokinetics of two doses of oral melatonin in patients with sepsis. – *J. Pineal Res.* **73**(4), 2022, e12830.
16. **Goede, M. R., D. I. Soybel, W. Chen.** Management of stress ulcers. 2024. Available at <https://www.uptodate.com/contents/management-of-stress-ulcers/print>
17. **Gudipaty, S. A., C. M. Conner, J. Rosenblatt, D. J. Montell.** Unconventional ways to live and die: cell death and survival in development, homeostasis, and disease. – *Ann. Rev. Cell. Dev. Biol.*, **34**, 2018, 311-332.
18. **Hristova, M., G. Bekyarova, M. Tzaneva.** Heme oxygenase-1 upregulated by melatonin: potential protection against burn-induced oxidative gastric mucosal injury. - *Journal of IMAB–Annual Proceeding Scientific*, **21**(2), 2015, 779-783.
19. **Hristova, M., M. Tzaneva, G. Bekyarova, D. Chivchibashi, N. Stefanova, Y. Kiselova-Kaneva.** Molecular mechanisms of melatonin protection from gastric mucosal apoptotic injury in experimental burns. – *Molecules*, **23**(4), 2018, 749.
20. **Hristova, M., O. Tasinov, M. Tzaneva, D. Chivchibashi, Y. Kiselova-Kaneva, G. Bekyarova.** Effect of melatonin on the gastric antioxidant defence in experimental burn trauma. – *Vet. Med.-Czech*, **67**, 2022, 379–386.
21. **Işeri, S. O., I. E. Gedik, C. Erzik, B. Uslu, S. Arbak, N. Gedik, B. C. Yeğen.** Oxytocin ameliorates skin damage and oxidant gastric injury in rats with thermal trauma. – *Burns*, **34**(3), 2008, 361-369.

22. **Jeschke, M. G., D. L. Chinkes, C. C. Finnerty, G. Kulp, O. E. Suman, W. B. Norbury, L. K. Branski, G. G. Gauglitz, R. P. Mlcak, D. N. Herndon.** Pathophysiologic response to severe burn injury. – *Ann. Surg.*, **248**(3), 2008, 387-401.
23. **Jockers, R., P. Maurice, J. A. Boutin, P. Delagrangé.** Melatonin receptors, heterodimerization, signal transduction and binding sites: what's new? – *Br. J. Pharmacol.*, **154**(6), 2008, 1182-1195.
24. **Kirksey, T. D., J. A. Moncrief, B. A. Jr. Pruitt, J. A. Jr. O'Neill.** Gastrointestinal complications in burns. – *Am. J. Surg.*, **116**(5), 1968, 627-633.
25. **Komatsubara, M., T. Hara, T. Hosoya, K. Toma, N. Tsukamoto-Yamauchi, N. Iwata, K. Inagaki, J. Wada, F. Otsuka.** Melatonin regulates catecholamine biosynthesis by modulating bone morphogenetic protein and glucocorticoid actions. – *J. Steroid Biochem. Mol. Biol.*, **165**(Pt B), 2017, 182-189.
26. **Konakchieva, R., Y. Mitev, O. F. Almeida, V. K. Patchev.** Chronic melatonin treatment and the hypothalamo-pituitary-adrenal axis in the rat: attenuation of the secretory response to stress and effects on hypothalamic neuropeptide content and release. – *Biol. Cell.*, **89**(9), 1997, 587-596.
27. **Majumder, R., M. Datta, A. Banerjee, D. Bandyopadhyay, A. Chattopadhyay.** Melatonin protects against ketorolac induced gastric mucosal toxic injuries through molecular mechanism associated with the modulation of Arylakylamine N-Acetyltransferase (AANAT) activity. – *Chem. Biol. Interact.*, **382**, 2023, 110611.
28. **Nielson, C. B., N. C. Duethman, J. M. Howard, M. Moncure, J. G. Wood.** Burns: pathophysiology of systemic complications and current management. – *J. Burn Care Res.*, **38**(1), 2017, e469-e481.
29. **Nishat, N., M. E. Rodriguez-Rodrigue, C. Pamugo, V. V. Y. Montalvo, M. Nwosu, D. A. Vargas, M. G. Olave, S. E. A. Pereira, S. E. M. Ruiz, M. I. G. Coral.** Emergency Management of Curling Ulcers: Exploring strategies for timely diagnosis and intervention in critical care settings. - *Open Access Journal of Surgery*, **15**(2), 2024.
30. **Norbury, W. B., D. N. Herndon, L. K. Branski, D. L. Chinkes, M. G. Jeschke.** Urinary cortisol and catecholamine excretion after burn injury in children. – *J. Clin. Endocrinol. Metab.*, **93**(4), 2008, 1270-1275.
31. **Radzikowska-Büchner, E., I. Łopuszyńska, W. Fliieger, M. Tobiasz, R. Maciejewski, J. Fliieger.** An overview of recent developments in the management of burn injuries. – *Int. J. Mol. Sci.*, **24**(22), 2023, 16357.
32. **Rapaka, S., P. K. Datta, S. Sharma.** Delineating gastrointestinal dysfunction variants in severe burn injury cases: a retrospective case series with literature review. – *Southwest J. Pulm. Crit. Care Sleep*, **28**(3), 2024, 40-48.
33. **Siddiqui, A. H., U. Farooq, F. Siddiqui.** Curling ulcer. [Updated 2023 Apr 16]. In: StatPearls [Internet]. Treasure Island (FL): StatPearls Publishing; 2025 Jan-. Available at <https://www.ncbi.nlm.nih.gov/books/NBK482347/>
34. **Simões, S., R. Lopes, M. C. D. Campos, M. J. Marruz, M. E. M. da Cruz, L. Corvo.** Animal models of acute gastric mucosal injury: Macroscopic and microscopic evaluation. – *Animal Model Exp. Med.*, **52**(2), 2019, 121-126.
35. **Srivastava, S. K., C. Nath, M. B. Gupta, S. Vrat, J. N. Sinha, K. N. Dhawan, G. P. Gupta.** Protection against gastric ulcer by verapamil. – *Pharmacol. Res.*, **23**(1), 1991, 81-86.

36. **Stanton, E.W., A. Manasyan, C. M. Thompson, G. P. Patel, A .M. Lacey, T. E. Travis, S. Q. Vrouwe, C. C. Sheckter, J. Gillenwater.** Venous thromboembolism incidence, risk factors, and prophylaxis in burn patients: a national trauma database study. – *J. Burn Care Res.*, 2024, irae171.
37. **Yang, F. L., Y. M. Subeq, C. J. Lee, R. P. Lee, T. C. Peng, B. G. Hsu.** Melatonin ameliorates hemorrhagic shock-induced organ damage in rats. – *J. Surg. Res.*, **167**(2), 2011, e315-321.
38. **Yibirin, M., D. De Oliveira, R. Valera, A. E. Plitt, S. Lutgen.** Adverse effects associated with proton pump inhibitor use. - *Cureus*, **13**(1), 2021, e12759.
39. **Yismaw, Y. E., M. Abdelwuhab, D. B. Ambikar, A. E. Yismaw, D. Derebe, W. Melkam.** Phytochemical and antiulcer activity screening of seed extract of *Cordia africana* lam (Boraginaceae) in pyloric ligated rats. – *Clin. Pharmacol.*, **12**, 2020, 67-73.
40. **Zhu, L., Z. C. Yang, A. Li, D. C. Cheng.** Reduced gastric acid production in burn shock period and its significance in the prevention and treatment of acute gastric mucosal lesions. – *World J. Gastroenterol.*, **6**(1), 2000, 84-88.

A Case of Sarcoidosis in a Forensic Setting – What Has Been Found as Case of Death

Natasha Davceva^{1}, Blagica Krsteska², Gorica Popova³*

¹ *Institute of Forensic medicine and criminalistics, Faculty of medicine Ss Cyril and Methodius University in Skopje, North Macedonia; Faculty of medical sciences, Goce Delcev University, Stip North Macedonia; Faculty of medicine University of Maribor, Republic of Slovenia;*

² *Institute of pathology, Faculty of medicine Ss Cyril and Methodius University in Skopje, North Macedonia;*

³ *University Clinic for Respiratory Diseases in Children “Kozle”-Skopje. Faculty of medical sciences, Goce Delcev University, Stip, North Macedonia*

* Corresponding author e-mail: drdavcevamk@yahoo.com

Sarcoidosis is a multisystem inflammatory disease of unknown etiology with a particular clinical and pathological picture. Pathologically can be confirmed with the finding of non-caseating (non-necrotizing) granulomas containing epithelioid cells and large multinucleated giant cells. Sarcoidosis is associated with an increased risk of premature death; it is twice as high as the general population. The common cause of death includes: cardiac failure due to cardiac sarcoidosis, lung disease associated with pulmonary hypertension, infection etc. In this case presentation we show finding of another and not so common cause of cardiac death in a patient with sarcoidosis i.e. bacterial myocarditis represented by clusters of bacterial colonies throughout the myocardial tissue.

Key words: sarcoidosis, cardiac sarcoidosis, bacterial myocarditis

Introduction

Sarcoidosis is a multisystem inflammatory disease of unknown etiology. Mainly it is considered as autoimmune disease, where T-cells play a central role with the excessive cellular immune reaction. Microbial, environmental and genetic factors have been proposed so far as possible agents. Pathologically is manifested with non-caseating (non-necrotizing) granulomas containing epithelioid cells and large multinucleated giant cells. They are predominantly found in lungs and lymph nodes, but the disease is also visible to skin (erythema nodosum), eyes (conjunctivitis and uveitis), spleen (splenomegaly), liver, kidneys, bone marrow and especially involves the metabolism

of calcium, nervous and musculoskeletal system [8]. Löfgren syndrome, characterized by fever, bilateral hilar lymphadenopathy and acute onset of erythema nodosum and migratory polyarthritis is also characteristic of sarcoidosis [6].

The sarcoidosis is generally considered as non-fatal disease with very diverse incidence, from 1-5 per 100,000 in East Asia countries to 14-16 per 100,000 in Scandinavian countries and Canada. In Southern Europe, estimates are lower than in the North. The average age at diagnosis is around 50 years. Several studies, but not all, show a bimodal distribution of age primarily related to sex. Even though many studies report a female to male ratio of 1:1, more males than females are diagnosed at 20–45 years old, whereas incidence peaks in females later (at 50–65 years old) [1].

As possible risk factors are considered: genetic predisposition, infection, occupation, environmental factors [1].

In 5 to 10% of cases sarcoidosis is asymptomatic and can be found only by autopsy [3].

Although described more than 100 years ago (by Boeck, the Norwegian dermatologist), the knowledge about the involvement of myocardium i.e. the cardiac sarcoidosis is more recent [2].

Cardiac sarcoidosis occurs in at least 25% of patients with sarcoidosis in the USA, and accounts for as many as 13–25% of deaths from sarcoidosis [1]. In Japan, sarcoid heart disease is more common and responsible for as many as 85% of deaths from sarcoidosis [1]. The characteristics and the comprehensiveness of the clinical picture in cardiac sarcoidosis depend on the location and extent of the glaucomatous inflammation and the subsequent fibrosis in the myocardium and especially depend on the involvement of the conduction system [7].

According to some authors, sarcoidosis should be suspected in any patient, younger than expected, presenting with complete heart block or heart failure [5], which is of great forensic medicine importance.

Hence, in a forensic setting, the importance of sarcoidosis, and particularly of cardiac sarcoidosis, comes from its occurrence as a possible cause of sudden death in relatively young persons, 30 to 50 years old.

In this case presentation we show finding of another and not so common cause of cardiac death in a patient with sarcoidosis i.e. bacterial myocarditis represented by clusters of bacterial colonies throughout the myocardial tissue.

Presentation of the case

By the order of the public prosecutor, a body of the 42 years old man, the foreign citizen with temporary residence in our country, has been admitted to the Institute of forensic medicine for forensic autopsy, because of sudden unexpected death and unknown cause of death.

He was found unresponsive in his apartment and was urgently transmitted to hospital, where he died after several hours of intensive care and cardio pulmonary resuscitation. He died under the clinical picture of cardiogenic shock. Uncertain data have been received that he suffered of sarcoidosis during alive.

Autopsy finding

Macroscopic feature of organs

On autopsy we found a body of a 42 years old male, with asthenic osteomuscular constitution.

During the external examination dominated a feature of dehydration, asthenia, livid colorization of the skin, especially on head and neck, but also livid to pink colorization of the skin of the entire body. Also, apparent conjunctivitis and uveitis has been found.

During the examination of the internal organs, there dominated the finding of granulomatous lymphadenitis. The hilar lymph node enlargement has been found, with a diameter of until 3 cm. The lymph nodes have been well demarcated, with lack of central necrosis and on their cut surface they appeared to be grayish to yellowish (**Fig. 1A**).



Fig. 1A

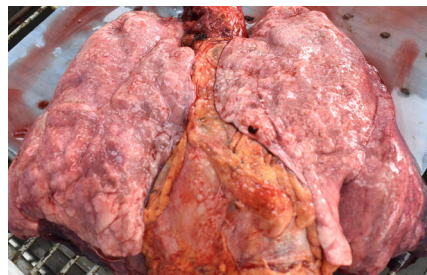


Fig.1B

Fig. 1. A. Granulomatous lymphadenitis characteristic for sarcoidosis; **B.** Gross appearance of the lungs.

The surface of the lungs was uneven and somewhat cloudy. In some places there were found fibrous whitish changes, due to which in some places there are irregularities on the surface of the lungs (**Fig. 1B**).

Regarding to the extrapulmonary disease, it has been found hepatomegaly of 2040 grams and splenomegaly of 470 grams.

The brain has been swollen with a reddish colorization of the meninges due to the obvious hyperemia.

The macroscopic appearance of the heart has been non-specific. The heart enlargement has been found and pericardial adhesions and thickening of the endocardium. Macroscopically, no specific feature has been found on myocardium.



Specific feature has been found on kidneys. Tiny whitish granuloma-like formations with the diameter of 0,1 to 0,2 cm have been found disseminated throughout the kidney tissue. (**Fig. 2**).

Fig. 2. Tiny whitish granuloma-like formations in the kidney tissue.

The stomach contained around 200 ml of dark brown contents with a coffee ground appearance and around 50 ml of dark red coagulated blood have been found in the duodenal bulb, but only small amount of blood streaking the intestinal contents has been found in the intestinal lumen. Erosions of the gastral and duodenal mucosa have been obvious.

Microscopical findings

Sarcoidosis has been presented with non-caseating epithelioid granulomas with tightly packed epithelioid cells, Langhans giant cells and lymphocytes, mostly seen in pleura and connective tissue septa (**Fig. 3A, B**).

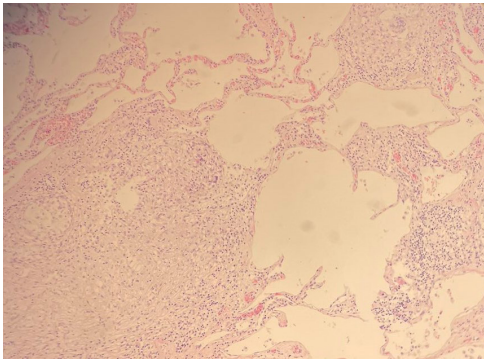


Fig. 3A

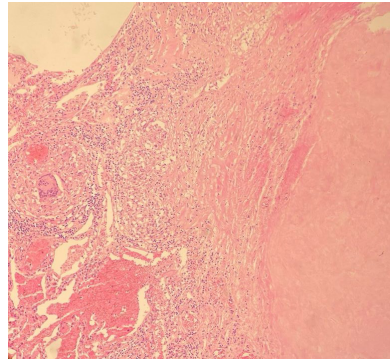


Fig. 3B

Fig. 3. Non-caseating granulomas in lung. Hematoxylin-Eosin Staining. A. \times 100; B. \times 400

There have been found large confluent epithelioid granulomas in hilar lymph nodes with broad areas of hyalinization. The granulomas are composed of epithelioid histiocytes with intermingled mature lymphocytes. The histiocytes show oval nuclei and abundant eosinophilic cytoplasm. Occasional giant cells are seen (**Fig. 4 A, B**). The Ziehl-Neelsen stain was found to be negative.

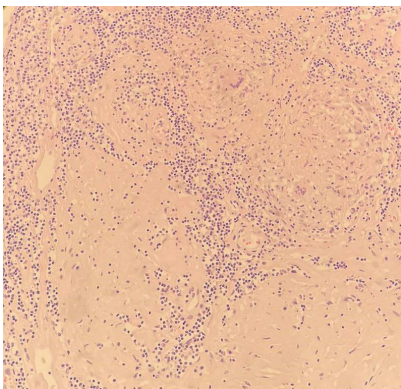


Fig. 4A

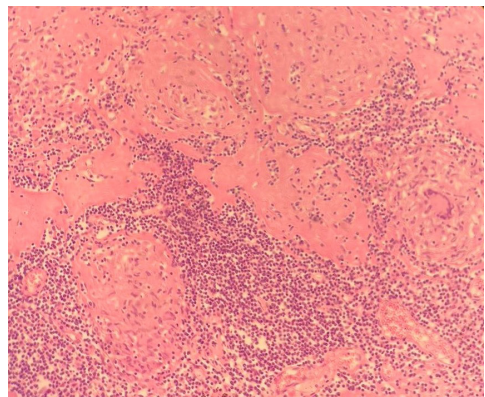


Fig. 4B

Fig. 4. Sarcoid granulomas in mediastinal lymph nodes. Hematoxylin-Eosin Staining. A. \times 100; B. \times 400

Multifocal areas of bacterial colonies were found in the myocardium and both kidneys with abscess formation (Fig. 5 and Fig. 6).

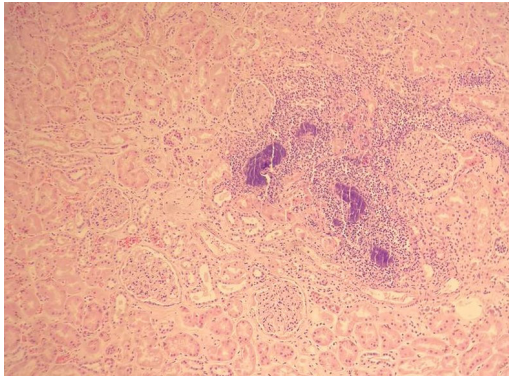


Fig. 5A

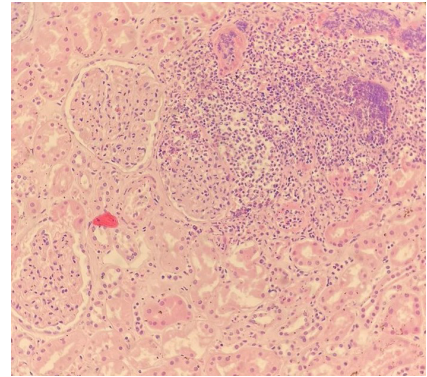


Fig. 5B

Fig. 5. Acute pyelonephritis. Colony of bacteria with abscess formation. Hematoxylin-Eosin Staining. A.×100; B.×400

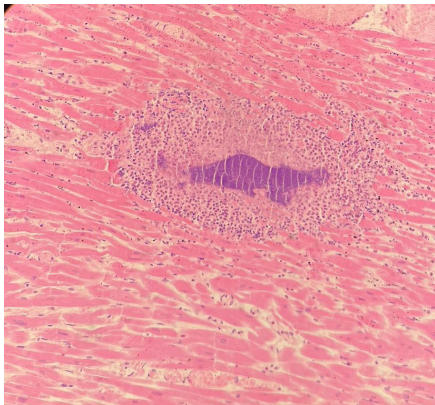


Fig. 6A

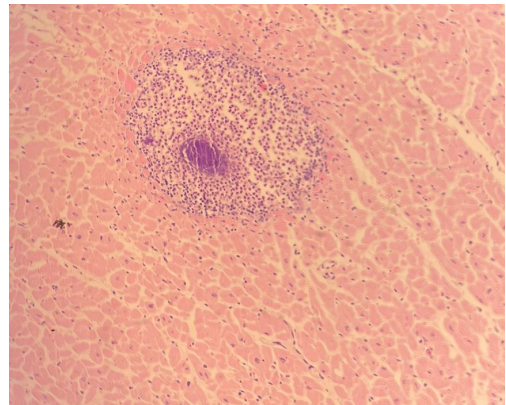


Fig. 6B

Fig. 6. Acute bacterial myocarditis. Colony of bacteria with abscess formation. Hematoxylin-Eosin Staining. A.×100; B.×400

Toxicology results

Ante-mortem toxicology analyses performed in the hospital had been qualitative and had shown the presence of cannabis and cocaine. During hospitalization of several hours, the deceased has been treated with atropine and corticosteroids. Exactly the atropine and corticosteroids have been found on post-mortem toxicology with no traces of psychoactive substances.

Post-mortem biochemistry investigation pointed on the high value of enzymes characteristic for myocardial necrosis: Troponin I>50000,0; Creatine kinase (CK) of 80148,34 and Creatine kinase MB (CK-MB) of 4359,19.

Discussion and concluding the cause of death

The ante-mortem information about sarcoidosis in the analyzed autopsy case, has been unofficial and the diagnosis of sarcoidosis had to be carried out.

As by the literature, clinically and pathologically Sarcoidosis is described as a multisystem inflammatory disease characterized by the formation of noncaseating granulomas in affected organs, most of it in lungs and thoracic lymph nodes which are engaged in more than 90% of all cases [4]. However, virtually every organ can be involved: the eyes (keratitis and uveitis), skin (erythema nodosum) and liver are affected in 15%–30% of cases. Sarcoidosis of the nervous system and heart is less common (2%–10%). Sarcoidosis mimics several diseases, making the diagnosis challenging. Of note, 10%–15% of patients are asymptomatic, and diagnosis is incidental, for example, following a chest radiograph. Lofgren syndrome (acute onset of fever, erythema nodosum, ankle arthritis, and bilateral hilar adenopathy) is characteristic finding for sarcoidosis.

There have been also described certain radiological criteria for the diagnosis of sarcoidosis.: bilateral and symmetrical lymphadenopathy localized in the hila and mediastinum, ground-glass opacities and consolidations, and interlobular septal thickening. Fibrotic progression is marked by loss of lung volume, honeycombing with traction bronchiectasis, bullae, and coarse septal bands [3].

According to the previously noted, the complete clinical and pathological picture of sarcoidosis has been found in our autopsy case (lymphadenopathy, lung changes, keratitis and uveitis etc). But, the exact cause of death had to be carried out.

Regarding to the cause of death in sarcoidosis patients, reference data show that sarcoidosis is associated with an increased risk of premature death, by some references it is twice as high as the general population. Respiratory failure due to extensive pulmonary disease is a common cause of death up to 60% of deaths. Nonfatal cardiac sarcoidosis and ischemic heart disease leading to heart failure is present 20% of deaths in sarcoidosis. Risk of infection is also high in sarcoidosis, especially because of the immunosuppressant treatment in some patients [1]. Opportunistic infections are rarely seen in these patients but can cause serious complications. Sarcoidosis-associated pulmonary hypertension diagnosed in up to 3%–20% of patients with sarcoidosis is also associated with high morbidity and mortality [1].

Speaking about the case, after the exclusion of the toxicology finding, most of the autopsy findings were obviously pointing to a cardiac death i.e. the cyanosis, dark red blood in the body, congestion and also the clinical data obtained ante-mortem.

Where the heart failure is involved in a patient with diagnosed sarcoidosis, the diagnosis of cardiac sarcoidosis has to be considered as a possible cause of death. The diagnosis of cardiac sarcoidosis is clinical and pathological. For the clinical diagnosis three or more of four major criteria are involved: high-grade atrioventricular block or fatal ventricular arrhythmia; basal thinning of the ventricular septum or abnormal ventricular wall anatomy and LV contractile dysfunction. Clinical diagnosis is confirmed when the criterion of positive myocardial uptake of ^{67}Ga citrate scintigraphy or ^{18}F -FDG PET. Histological diagnosis is confirmed when endomyocardial biopsy demonstrates non-caseating epithelioid cell granulomas [7].

In the case analyzed here, dysfunctional elements for the clinical diagnosis of cardiac sarcoidosis obviously couldn't have been perceived on autopsy and the

hospitalization time has been too short for detailed investigation. Also, the presence of non-caseating epithelioid cell granulomas in the myocardium tissue has not been confirmed by histology. Instead, clear proof of bacterial myocarditis has been perceived histologically by clusters of bacterial colonies with abscess formation. Very similar finding has been seen in kidneys where abscess formations could have been perceived even macroscopically on a cut surface. Therefore, bacterial myocarditis has been established as a diagnosis.

In conclusion, this interesting case shows that sarcoidosis is very complex disease, even it is generally considered as non-fatal. However, it has been shown previously that sarcoidosis patients are twice as much prone to death comparing them to the general population. The specific cause of death in those cases can be found among lung disease, cardiac sarcoidosis but also the infection, especially when the corticosteroid therapy is involved. In our analyzed case death has been attributed to cardiac failure due to histologically proved bacterial myocarditis.

References

1. **Arkema, E. V., Y .C. Cozier.** Sarcoidosis epidemiology: recent estimates of incidence, prevalence and risk factors. – *Curr. Opin. Pulm. Med.*, **26**(5), 2020, 527–534.
2. **Doughan, A.R., B. R. Williams.** Cardiac sarcoidosis. *General cardiology.* – *Heart*, **92**, 2006, 282–288.
3. **Nikolova, S.** Distinctive manifestations of pulmonary sarcoidosis on high resolution computed tomography. *KNOWLEDGE – International Journal*, **57**(4), 2023, 451-456.
4. **Rossides M., P. Darlington, S. Kullberg, E. V. Arkema.** Sarcoidosis: Epidemiology and clinical insights. – *Journal of Internal Medicine*, **293**, 2023, 668–680.
5. **Smedema, J. P., G. Snoep, M. P. G. Kroonenburgh, R. J. Geuns, W.R. M. Dassen, A. P. Gorgels, H. J. G. M. Crijns.** Cardiac involvement in patients with pulmonary sarcoidosis assessed at two university medical centers in the Netherlands. – *Chest*, **128**(1), 2005, 30-35.
6. **Tana, C.** Sarcoidosis: An old but always challenging disease. – *Diagnostics*, **11**(4), 2021a, 696.
7. **Tana, C., C. Mantini, I. Donatiello, L. Mucci, M. Tana, F. Ricci, F. Cipollone, M. A. Giamberardino.** Clinical features and diagnosis of cardiac sarcoidosis. – *J. Clin. Med.*, **10**(9), 2021b, 1941.
8. **Tana, C., M. Drentb, H. Nunese, V. Kouranosf, F. Cinettog, N. T. Jessurund, P. Spagnoloi.** Comorbidities of sarcoidosis. – *Annals of Medicine*, **54**(1), 2022, 1014–1035.

Preliminary Anthropological Data of Inhumated Bone Remains from Late Medieval (Ottoman period) Necropolis from Object No. 7, along the Route of Road I-1 (E79), „Vidin-Ruzhintsi-Montana“, Near the Village of Turnyane, Vidin Region, Bulgaria

Nadezhda Atanassova^{1,}, Elena Vasileva²*

¹ *Dept. Anthropology and Anatomy, Institute of Experimental Morphology, Pathology and Anthropology with Museum, Bulgarian Academy of Sciences, Sofia, Bulgaria*

² *Dept. of Medieval Archaeology, National Archaeological Institute with Museum, Bulgarian Academy of Sciences, Sofia, Bulgaria*

*Corresponding author e-mail: naditimeva@gmail.com

The aim of this article is to represent the preliminary results of anthropological characteristics and paleopathological analysis of bone remains discovered during the rescue archaeological excavations of the Christian necropolis from Ottoman period (15th – 17th centuries) near the village of Turnyane, Vidin Region, Northwestern Bulgaria. Standard anthropological methods of investigation were applied. Up to the present moment, bone remains from 17 individuals have been analyzed, covering grave structures from different sectors of the necropolis and individuals ranging from infancy to the end of the mature age group. The age-at-death identification of investigated buried show that the ratio of subadults to adults is 2.4:1 (71%:29%). In the sex-identified individuals, the male/female distribution is equal (4/5). The paleopathological analysis reveals a large number of pathological changes in the dental-jaw system, the cranial, and postcranial skeletons, which is typical for the populations inhabited Bulgarian lands during the Ottoman period.

Key words: Late Medieval (Ottoman period) settlement, Christian necropolis, paleoanthropology, paleopathology

Introduction

In 2020 – 2021 the settlement was recorded and surveyed in connection with the construction of the I-1 road (E-79) and is located about 300 m east of the village Turnyane, Vidin region. Most structures were excavated from the Late Middle Ages - buried

and above-ground dwellings, ovens, hearths, pits, graves. The archaeological material in all these dwellings consists of numerous ceramic fragments, including fragments of imported ceramics (majolica), animal bones, metal objects of daily life, coins and isolated bone finds, all dating from the 15th to 17th centuries. Three necropolises were also recorded and investigated - from the Early Bronze Age (EBA), the Middle Bronze Age (MBA) and the Middle Ages. The necropolis from the RBE is represented by 16 cremation graves without urns. The necropolis from the SBE is represented by 26 urns with cremation. The mediaeval necropolis is represented by 141 graves with inhumation (**Fig. 1**). The mediaeval necropolis was recorded almost entirely in the north-eastern part of the site, with the exception of two graves which lay outside the boundaries of the necropolis. All the 141 graves were inhumations. The necropolis is Christian

in character and the graves are aligned in a west-east direction. The grave pits, as far as they were recorded, have a rectangular or trapezoidal shape. The buried individuals lay on their backs with the lower limbs extended and the upper limbs in various positions (**Figs. 2, 3**). During the study of the necropolis, an almost correct layout of the grave pits was noticed, which was oriented from south to north.

In a few of the graves, finds were found. These are personal belongings of the buried - jewelry and parts of clothing. This fact completely overlaps with the information we know from other similar necropolises, namely that graves from this period rarely have a rich inventory.

The results of the radiocarbon analysis give a period from 1470/80 to 1637/39, which is consistent with the material found in the other structures examined and allows us to assign the necropolis to the settlement. The documentary analyses carried out at this stage have enabled us to



Fig. 1. The general plan of the excavated Christian necropolis (from the 15th to the 17th c.) near the village of Turnyane.



Fig. 2. Grave No 39. Skeleton *in situ*



Fig. 3. Grave No 41. Skeleton *in situ*

prove with certainty that the settlement was founded in the 15th century and is recorded in the Ottoman registers and maps of 1530 under the name Tiryani and is located in the kaza Vidin.

This paper includes preliminary results from anthropological characteristics and paleopathological analysis of bone remains discovered during the rescue archaeological excavations of the mentioned above Late Medieval necropolis (15th – 17th centuries) near the village of Turnyane, Vidin Region, Northwestern Bulgaria.

Material and Methods

The material in this paper includes inhumated human bone remains from 15 graves from different sectors of the excavated necropolis. In the grave structures, individuals have been identified ranging from infancy to the end of the mature age group. Standard anthropological methods were applied for the age and sex identification of the buried [2, 3, 4, 5, 7, 8, 9, 14, 19, 20, 21, 23, 24]. The reconstruction of the stature [12, 17] and evaluation of the body mass [13] of adults was carried out depending on the state of the preserved long limb bones. Height categorizations are according to Martin rubrics [7]. Pathological changes and congenital anomalies of the cranial and postcranial skeleton were identified using the methods of Aufderheide, Rodriguez-Martin [1]; Ortner, Putschar [10]; Ortner [11]. The age distribution of dental enamel hypoplasia was analyzed by correlating the horizontal defect line (Linear enamel hypoplasia - LEH) with the corresponding age, based on Zubov's charts [24] for the development of deciduous and permanent dentition.

Results

The results of the individual anthropological analysis are as follows:

➤ **Grave No 13**

Grave inventory: No

Condition of the skeletal material: Poor. Skull and postcranial skeleton – fragmented and incompletely preserved.

Age at death: Infans I (5-6 years) - The age was reconstructed based on dental status, while the estimation based on the preserved long bones indicated a younger age, in the range of 2.5 to 3 years.

Sex: Undetermined sex because of the young age of the individual.

Dentition: Deciduous, incomplete.

Morphological dental marks: Not observed.

Cranial pathology: Strongly expressed *cribra orbitalia* (CO) on the superior orbital roof of the right orbit, the left is fragmented.

Anatomical cranial variations: Not observed.

Dental-jaw pathology: Pitting enamel hypoplasia (PEH) on the lower second deciduous molars.

Postcranial pathology: Not observed.

➤ **Grave No 23**

Grave inventory: Bronze ring – hoop, on the phalanx of the right upper limb.

Condition of the skeletal material: Poor. Skull and postcranial skeleton – fragmented and incompletely preserved.

Age at death: Maturus (55-60 years) - The age was reconstructed based on the degree of synostosis of the cranial sutures and dental abrasion.

Sex: Most probably female - skeleton shows characteristics for both sexes with prevalence for female sex (pelvis – fragmented).

Stature: 149.90 cm (by Pearson [12]) – “under middle” stature

153.81 cm (149.79÷157.82) (by Trotter-Gleser [17]) – “middle” stature

Body weight assessment: 61.20 kg

Dentition: Permanent, incomplete.

Morphological dental marks: Not observed.

Cranial pathology: Not observed.

Anatomical cranial variations: Not observed.

Dental-jaw pathology: Extremely deteriorated dental status - caries and late carious complications, including ante mortem tooth loss.

Postcranial pathology: Strongly expressed degenerative-dystrophic changes (DJD) in all regions of the spine and weakly expressed in the right shoulder joint ; ankylosis of two thoracic vertebrae; lateral epicondylitis in the area of the left elbow joint (the right cannot be registered because of fragmentary of the distal end of right humerus).

➤ **Grave No 26**

Grave inventory: No

Condition of the skeletal material: Poor. Skull and postcranial skeleton – fragmented and incompletely preserved.

Age at death: Juvenis (14-15 years) - The age was reconstructed based on dental status and epiphyseal development.

Sex: Probably male – sex was reconstructed by some skull features.

Dentition: Permanent, incomplete.

Morphological dental marks: Tubercle of Carabelli (2nd degree) - Europoid odontological feature.

Cranial pathology: Recombinant form of *cribra orbitalia* (CO) on the superior orbital roof - bilaterally. Trace of healed trauma above the right orbit caused by hitting with a sharp tool.

Anatomical cranial variations: Not observed.

Dental-jaw pathology: Pitting enamel hypoplasia (PEH) on the lower second molars. Linear enamel hypoplasia (LEH) – two horizontal lines on the upper central incisors and premolars, which correspond to stress in the physical development of the individual at 1-2 years of age.

Postcranial pathology: Not observed.

➤ **Grave No 30**

Grave inventory: No

Condition of the skeletal material: Poor. Skull and postcranial skeleton – fragmented and incompletely preserved.

Age at death: Juvenis (15-16 years) - The age was reconstructed based on dental status and epiphyseal development.

Sex: Most probably male – sex was reconstructed by some pelvic and skull features, and measurements of the limb bones.

Dentition: Permanent, incomplete.

Morphological dental marks: Tubercle of Carabelli (4th degree) - Europoid odontological feature.

Cranial pathology: Porotic hyperostosis (PH) in the area of the auditory foramina – bilaterally. Trace of healed trauma on the middle part of the right parietal bone without traces of an infectious process.

Anatomical cranial variations: Not observed.

Dental-jaw pathology: A small amount of tartar on the lower central teeth. Pitting enamel hypoplasia (PEH) on the lower first and second molars. Linear enamel hypoplasia (LEH) – two horizontal lines on the lower canines and first premolars, which correspond to stress in the physical development of the individual at 2-3 years of age.

Postcranial pathology: Porotic hyperostosis (PH) on long bones, especially on the humerus bones. Spina bifida occulta (S4-S5).

Additional bone material: Human bone remains of two children in Infans I - approximately 3 and 5-6 years old at the time of death.

➤ **Grave No 39**

Grave inventory: Bronze button under the right rib in the upper part of the chest

Condition of the skeletal material: Skull – fragmented and incompletely preserved. Postcranial skeleton – well preserved.

Age at death: Infans II (12-13 years) - The age was reconstructed based on dental status.

Sex: Undetermined.

Dentition: Mixed, incomplete.

Morphological dental marks: Not observed.

Cranial pathology: Serpens endocrania symmetrica (SEM) on the endocranial surface of the occipital bone. Weakly expressed cribra orbitalia (CO) on the superior orbital roof – bilaterally.

Anatomical cranial variations: Not observed.

Dental-jaw pathology: Pitting enamel hypoplasia (PEH) on the lower left second milk molar, first and second permanent molars. Linear enamel hypoplasia (LEH) – three horizontal lines on the upper central incisors and canines, which correspond to stress in the physical development of the individual at 1-2-3 years of age.

Postcranial pathology: Porotic hyperostosis (PH) on long bones, especially on the humerus bones and sternal surface of both clavicles.

➤ **Grave No 41**

Grave inventory: Glass ball (bead without a hole).

Condition of the skeletal material: Skull and postcranial skeleton – fragmented and incompletely preserved.

Age at death: Maturus (45-49 years) - The age was reconstructed based on the symphyseal pubis surface.

Sex: Male – the sex was reconstructed by pelvic and skull characteristics, as well as by the measurements of limb bones.

Stature: 174.57 cm (by Pearson [12]) – “tall” stature

82.22 cm (178.21÷186.52) (by Trotter-Gleser [17]) – “very tall” stature

Body weight assessment: 81.33 kg

Dentition: Permanent, incomplete.

Cranial pathology: Not observed.

Anatomical cranial variations: Persistent metopic suture.

Postcranial pathology: Spina bifida occulta (S1-S2). Enthesopathies on the distal ends of both fibulae. Periosteal reactions on the medial surface of the diaphysis of the left tibia and on the posterior surface of the diaphysis of the left femur. Moderately expressed degenerative-dystrophic changes (DJD) in the area of both knee joints and of the right elbow joint; lateral epicondylitis – bilaterally, more pronounced on the right humerus.

➤ **Grave No 44**

Grave inventory: Two earrings, copper alloy; two hollow moon-shaped pendants preserved; one earring, copper alloy, multi-component; three buttons, copper alloy, spherical, with an eye for sewing - three preserved and one fragmented; 1 coin – bronze; four bronze buttons in the area of the cervical vertebrae; two bronze coins (one of which was pierced), a bead and a bronze amulet/medallion with a chain, in the area of the left femur.

Condition of the skeletal material: Poor. Skull and postcranial skeleton – fragmented and incompletely preserved.

Age at death: Juvenis (18-19 years) - The age was reconstructed based on dental status and epiphyseal development.

Sex: Female – sex of the individual was reconstructed by pelvic and skull characteristics, as well as by the measurements of limb bones.

Dentition: Permanent, incomplete.

Morphological dental marks: Not observed.

Cranial pathology: Not observed.

Anatomical cranial variations: Not observed.

Dental-jaw pathology: Caries on the lower preserved molars. The lower second molars are impacted or either lost ante mortem (X-ray is required). Rotation of the lower left canine.

Postcranial pathology: Strongly expressed periosteal reaction on the medial surface of the diaphysis of the left tibia.

➤ **Grave No 47**

Grave inventory: No

Condition of the skeletal material: Skull – fragmented and incompletely preserved; postcranial skeleton – well preserved but incompletely preserved.

Age at death: Infans I (2-3 years) - the age was reconstructed based on dental status and length of the preserved long bones.

Sex: Undetermined sex because of the young age of the individual.

Dentition: Deciduous, incomplete.

Morphological dental marks: Tubercle of Carabelli (third degree) – Europoid

odontological feature.

Cranial pathology: Serpens endocrania symmetrica (SEM) on the endocranial surface of the occipital bone. Porotic hyperostosis (PH) in the area of the auditory foramina and parietal bones (on the ectocranial surface) – bilaterally.

Anatomical cranial variations: Not observed.

Dental-jaw pathology: Pitting enamel hypoplasia (PEH) on the right second lower deciduous molars. Rotation of the lower right deciduous canine.

Postcranial pathology: Bone lesions on the bodies of the thoracic vertebrae. Porotic hyperostosis on both femurs and both fibulae.

➤ **Grave No 53**

Grave inventory: Bronze pins in the lower jaw area, bronze button in the skull area.

Condition of the skeletal material: Poor. Skull and postcranial skeleton – fragmented and incompletely preserved.

Age at death: Maturus (40-44 years) - The age was reconstructed based on the degree of synostosis of the cranial sutures, symphyseal pubis surface and dental abrasion.

Sex: Most probably female - skeleton shows characteristics for both sexes with prevalence for female sex (pelvis – fragmented).

Stature: 160.48cm (by Pearson [12]) – “tall” stature

166.11 cm (162.16÷170.06) (by Trotter-Gleser [17]) – “tall” stature

Body weight assessment: 62.30 kg

Dentition: Permanent, incomplete.

Morphological dental marks: Cannot be observed.

Cranial pathology: Not observed.

Anatomical cranial variations: Not observed.

Dental-jaw pathology: Extremely deteriorated dental status – caries and late carious complications, including ante mortem tooth loss.

Postcranial pathology: Spina bifida occulta (S4-S5). Moderate to strongly expressed degenerative-dystrophic changes (DJD) in the lumbar region of the spine. Lateral epicondylitis – bilaterally, more strongly expressed on the left humerus. In the examined individual, perforation of the fossa olecrani of both humerus was recorded.

➤ **Grave No 54**

Grave inventory: No

Condition of the skeletal material: Poor. Skull and postcranial skeleton – fragmented and incompletely preserved.

Age at death: Baby (6 months – 1 year) - the age was reconstructed based on dental status and length of the preserved long bones.

Sex: Undetermined sex because of the young age of the individual.

Dentition: Deciduous, incomplete.

Cranial pathology: Porotic hyperostosis (PH) on the endocranial surface of both parietal bones.

Anatomical cranial variations: Not observed.

Dental-jaw pathology: Not observed.

Postcranial pathology: Periosteal reaction on the diaphysis of both humerus bones.

➤ **Grave No 107**

Grave inventory: Bronze button from the shoulder area.

Condition of the skeletal material: Poor. Skull and postcranial skeleton – fragmented and incompletely preserved.

Age at death: Adultus (25-26 years) – The age was reconstructed based on the symphyseal pubis surface and degree of synostosis of the cranial sutures. The abrasion of the preserved teeth is weak - grade 2.

Sex: Female – sex of the individual was reconstructed by pelvic and skull characteristics, as well as by the measurements of limb bones.

Stature: 148.03 cm (by Pearson [12]) – “short” stature

150.92 cm (147.00÷154.85) (by Trotter-Gleser [17]) – “under middle” stature

Body weight assessment: 53.56 kg

Dentition: Permanent, incomplete.

Morphological dental marks: Not observed.

Cranial pathology: Partial premature synostosis of the coronal cranial suture without cranial deformity.

Anatomical cranial variations: Not observed.

The scopic analysis of the skull revealed features which are not characteristic of the Europoid phenotype: facial prognathism, the nasal aperture is wide and the nasal bridge is flat; a heart-shaped nasal aperture; rectangular orbits.

Dental-jaw pathology: Extremely deteriorated dental status - caries and late carious complications, including ante mortem tooth loss and jaw cysts.

Postcranial pathology: Myositis ossificans on the midshaft of the right humerus.

➤ **Grave No 127**

Grave inventory: No

Condition of the skeletal material: Poor. Skull and postcranial skeleton – fragmented and incompletely preserved.

Age at death: Maturus (40-44 years) – The age was reconstructed based on the symphyseal pubis surface, degree of synostosis of the cranial sutures, tooth abrasion and first rib surface.

Sex: Male – the sex was reconstructed by pelvic and skull characteristics, as well as by the measurements of limb bones.

Stature: 164.05 cm (by Pearson [12]) – “middle” stature

169.98 cm (165.81÷174.49) (by Trotter-Gleser [17]) – “above middle” stature

Body weight assessment: 72.70 kg

Dentition: Permanent, incomplete.

Cranial pathology: Not observed.

Anatomical cranial variations: Additional wormian bones in both halves of the lambdoid cranial suture.

Dental-jaw pathology: Extremely deteriorated dental status – caries and late carious complications, including ante mortem tooth loss and mandibular cyst. Large amount of tartar on the left upper and lower tooth rows. Pitting enamel hypoplasia (PEH) on the lower molars. Linear enamel hypoplasia (LEH) – three horizontal lines on the lower canines, which correspond to stress in the physical development of the individual at 1-2-3 years of age.

Postcranial pathology: Spina bifida occulta (S4-S5).

➤ **Grave No 129**

Grave inventory: No

Condition of the skeletal material: Poor. Skull and postcranial skeleton – strongly fragmented and incompletely preserved.

Age at death: Infans II (7-8 years) - The age was reconstructed based on dental status.

Sex: Undetermined.

Dentition: Mixed, incomplete.

Morphological dental marks: Not observed on the preserved teeth.

Cranial pathology: Porotic hyperostosis (PH) on the region of glabella and both porotic acusticus externus.

Anatomical cranial variations: Not observed.

Dental-jaw pathology: Caries on the lower first deciduous molars. Pitting enamel hypoplasia (PEH) on the both lower deciduous second molars.

Postcranial pathology: Not observed.

➤ **Grave No 135**

Grave inventory: Three multi-piece earrings, a string of beads and a coin, eight hairpins, on the front of the skull there is a partially preserved headband made of textile with bronze plates.

Condition of the skeletal material: Poor. Skull and postcranial skeleton – strongly fragmented and incompletely preserved.

Age at death: Infans II (7-8 years) - The age was reconstructed based on dental status. The age determined by the length of the long bones is in the range of 3 to 3.5 years, which indicates a delay in the individual's physical development.

Sex: Most probably female.

Dentition: Mixed, incomplete.

Morphological dental marks: Shovel-shaped upper central incisors - grade 1. This morphological dental trait is characteristic of the Mongoloid phenotype – it occurs in up to 70%, while in Europeid phenotype it does not exceed 15%.

Cranial pathology: *Serpens endocrania symmetrica* (SEM) on the endocranial surface of the occipital bone. Moderately to strongly expressed PH on the ectocranial surface of glabella, porotic acusticus externus (bilaterally) and posterior parts of parietal bones. Moderately (2nd degree) expressed *cribra orbitalia* (CO) on the superior orbital roof – bilaterally.

Anatomical cranial variations: Metopism. Additional wormian bones - three on the right lambdoid suture and one on the left side.

Dental-jaw pathology: Multiple caries on the deciduous teeth. Maxillar cyst in the area of the right deciduous molars. Pitting enamel hypoplasia (PEH) on the lower right first permanent molar. Linear enamel hypoplasia (LEH) on the upper central incisors – four horizontal lines, which correspond to stress in the physical development of the individual at 1-2 years of age.

Postcranial pathology: Porotic hyperostosis (PH) on the tibial bones.

➤ **Grave No 136**

Grave inventory: No

Condition of the skeletal material: Skull – fragmented and incompletely preserved. Postcranial skeleton - the long bones of the limbs are well preserved.

Age at death: Infans I (20-24 months) - The age was reconstructed based on dental status.

Sex: Undetermined sex because of the young age of the individual.

Dentition: Deciduous, incomplete.

Morphological dental marks: Not observed.

Cranial pathology: Weakly expressed *cribra orbitalia* (CO) on the superior orbital roof - bilaterally. *Serpens endocrania symmetrica* (SEM). Porotica hyperostosis on the endocranial surface of the left parietal bone, on the ectocranial surface of the skull base, maxillar, zygomatic bones and glabella.

Anatomical cranial variations: Not observed.

Dental-jaw pathology: Pitting enamel hypoplasia (PEH) on the lower second deciduous molars.

Postcranial pathology: Porotic hyperostosis (PH) on the posterior surface of femoral bones and anterior surface of humeral bones.

Discussion

The condition of the skeletons (including the cortical layer) is relatively good, which allows for a thorough anthropological and paleopathological analysis.

So far in the study, in terms of age, adolescent individuals up to 18/20 years old predominate, with a ratio of 2.4:1 (71%:29%). The individuals under 7 years of age (*Infans I*) predominate [Fig. 4]. In sex-identified individuals, the male/female distribution is equal (4/5).

The stature is reconstructed in two males and three females as it was mentioned above. A comparison was made between these values and the average stature for male and female skeletal series dated to the Ottoman period (15th-19th centuries), from the territory of Central Western and Southwestern Bulgaria [22], as well as with the

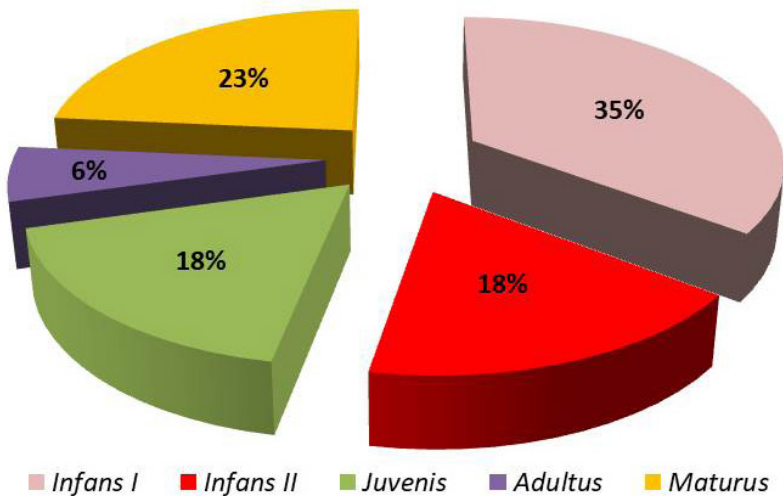


Fig. 4. Distribution of the investigated individuals by age-at-death

analyzed data in the statistical yearbooks for the height of all conscripts in the late 19th and early 20th centuries (1897-1920) [16]. The man from grave No. 41 of the Tarnyane series is with “tall” and “very tall” stature according to the Pearson [12] and Trotter-Gleser [17] formulas, and the differences with the male buried in grave No. 127, as well as with the average values for the synchronous skeletons, are statistically significant [Fig. 5], which is explained not only by genetic determination, but also by better living conditions for the individual from grave No. 41. The height of the male individual from grave No. 127 from Tarnyane is closest to the mean stature in Christian skeletal series from the Ottoman period [22]. The stature of the women interred in

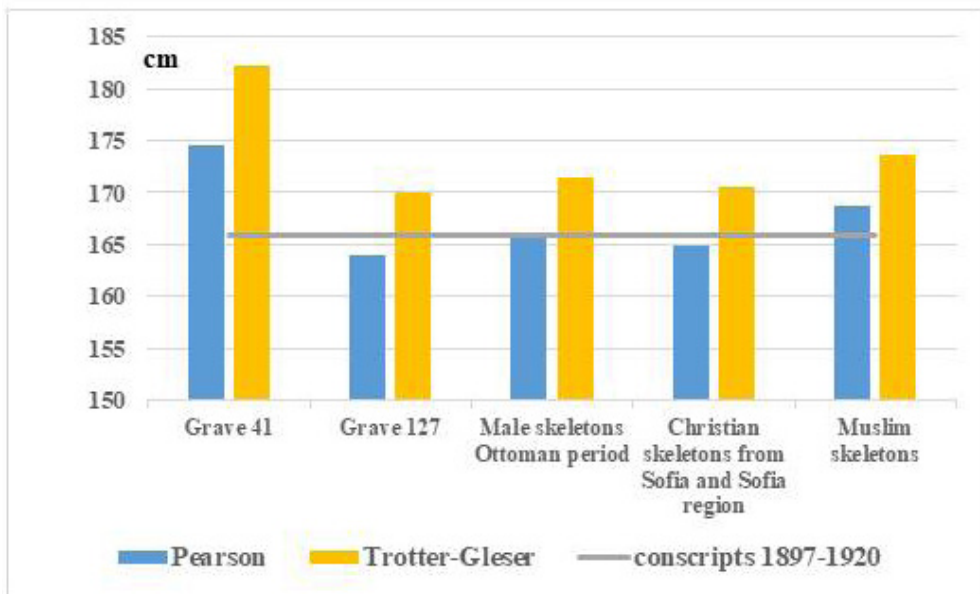


Fig. 5. Comparison of the stature of male skeletons from the necropolis at Turnyane with synchronous skeletal series and with the height of conscripts (1897-1920)

graves No. 23 and No. 107 from the necropolis near the village of Turnyane is below the mean values observed in synchronous female skeletal series, whereas the female buried in grave No. 53 exhibits a greater height than the others, with the statistically significant difference [Fig. 6].

The paleopathological analysis reveals a large number of pathological changes in the dental-jaw system, the cranial, and postcranial skeletons of adolescents and adults [Table 1]:

➤ Porotic hyperostosis (Fig. 7) – In the global scientific literature, a link has long been established between cranial porotic hyperostosis (PH) and iron-deficiency anemias (megaloblastic and hemolytic anemias). A high percentage of this type of pathological bone change is recorded in many ancient populations, which is attributed to nutritional deficiencies, poor sanitary and hygienic conditions, numerous infectious diseases, and various cultural and religious practices during pregnancy and breastfeeding, leading to severe vitamin B group deficiencies in infants and children [18].

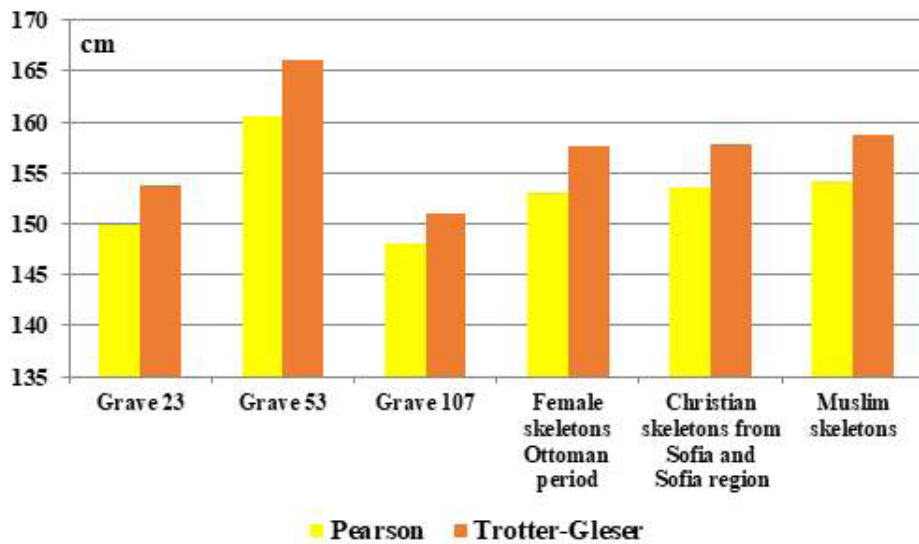


Fig. 6. Comparison of the stature of female skeletons from the necropolis at Turnyane with synchronous skeletal series



Fig. 7. Grave No. 135. Child (7–8 years old). Porotic hyperostosis (PH) on the ectocranial surface of both parietal bones.

➤ Cribra orbitalia (CO) (**Fig. 8**). Pathological porotic bone change of the superior orbital roof as a result of subperiosteal bleeding associated with deficiency of vitamin C and B12 predominately in the childhood. Active forms of CO is a mainly childhood phenomenon. Cribra orbitalia results from multiple nutritional deficiencies associated mainly with anemia (megaloblastic and hemolytic anemias), but also with scurvy, rickets, hemangiomas or trauma [18]. This is a common paleopathological finding in human skulls from archaeological sites;

➤ Serpens endocrania symmetrica (SEM) - periosteal reactions on the endocranial surface of the occipital bones (**Fig. 9**), the bones of the limbs and ribs, as well as bone lesions on the vertebrae. These pathological bone changes are associated in the scientific literature with tuberculosis. Due to the lack of antibiotics in past historical periods, the risk of fatal outcomes resulting from secondary intracranial infections, caused by respiratory viral and bacterial infections, was very high among adolescent individuals [6];



Fig. 8. Grave No. 26. Juvenile individual (14-15 years). Cribra orbitalia (CO)



Fig. 9. Grave No. 47. Child (2-3 years). Serpens endocrania symmetrica (SEM)

➤ Caries and late carious complications, including jaw cysts and ante mortem tooth loss (**Fig. 10**);

➤ Degenerative-dystrophic changes (DJD) in the area of the spine and limbs (**Fig. 11**);



Fig. 10. Grave No. 23. Probably female individual (55-60 years). Cribra orbitalia (CO)



Fig. 11. Grave No. 23. Probably female individual (55-60 years). Ankylosis of thoracic vertebrae

➤ Lateral epicondylitis on the humeral bones, resulting from excessive strain (repetitive movements) on the elbow joints (**Fig. 12**);

Fig. 12. Grave No. 53. Probably female individual (40-44 years). Lateral epicondylitis on the humeral bones





Fig. 13. Grave No. 41. Male individual (45-49 years). SSBO (S1-S2)

➤ Sacral Spina Bifida Occulta (SSBO) – a congenital defect in the development of the spine, in which the spinal cord remains relatively unprotected due to the absence of a bony dorsal wall. In SSBO, the meninges and/or nervous tissue remain beneath the skin. The occurrence of spina bifida occulta in the sacral region, spreading from S1 to S5 (from the first to the fifth sacral vertebrae), is referred to as sacral spina bifida occulta (SSBO). It is a hidden defect that may be indicated by a skin lesion such as a hairy patch, dermal sinus tract, dimple, hemangioma or lipoma. The investigations show that the rarest cases

of SSBO involve a fully open sacral canal and an open canal between S1 and S2 [15], which is also the case with the studied male skeleton from Grave No. 41 (**Fig. 13**).

Conclusions

Preliminary studies of the population near the village of Turnyane show mixed phenotypic traits. Most of the identified morphological bone changes in the studied skeletons were due to nutritional deficiency, various cultural and religious practices during pregnancy and breastfeeding, as well as poor sanitary and hygienic living conditions, which led to infectious diseases, including tuberculosis.

References

1. **Aufderheide, A. C., C. Rodriguez-Martin.** *The Cambridge encyclopedia of human paleopathology.* NY, Cambridge University Press, 1998.
2. **Bass, W.** *Human Osteology: A Laboratory and field manual of human skeleton.* Columbia, Mo, Special publication no. 2 of the Missouri Archaeological Society, 2005.
3. **Brothwell, D.** *Digging up bones.* London, British Museum of Natural History, 1965.
4. **Buikstra, J., D. Ubelaker.** *Standards for data collection from human skeletal remains.* Fayetteville, AK, Arkansas Archaeological Survey, 1994.
5. **Ferembach D., I. Schwidetzky, M. Stloukal.** Recommendations for age and sex diagnoses of skeletons. – *J. Hum. Evol.*, **9**, 1980, 517-549.
6. **Hershkovitz, I., C. M. Greenwald, B. Latimer, L. M. Jellema, S. Wish-Baratz, et al.** Serpens Endocrania Symmetrica (SES): A New Term and a Possible Clue for Identifying Intrathoracic Disease in Skeletal Populations. – *American Journal of Physical Anthropology*, **118**, 2002, 201–216.

7. **Martin, R., K. Saller.** *Lehrbuch der anthropologie in sistematischer Darstellung.* Stuttgart, Gustav Fischer Verlag, 1957.
8. **Maresh, M.M.** Measurements from roentgenograms. – In: *Human growth and development* (Ed. R. W. McCammon.), Springfield IL: C.C.Thomas, 1970, 157–200.
9. **Meindl, R., C. Lovejoy.** Ectocranial suture closure: a revised method for the termination of skeletal age at death based on lateral-anterior sutures. – *Am. J. Phys. Anthropol.*, **68**, 1985, 57-66.
10. **Ortner, D. J, W. G. J. Putschar.** *Identification of pathological conditions in human skeletal remains.* Washington, Smithsonian Institution Press, 1981.
11. **Ortner, D. J.** *Identification of pathological conditions in human skeletal remains. 2nd Edition,* San Diego, Academic Press, 2003.
12. **Pearson, K.** Mathematical contributions to the theory of evolution. V. On the reconstruction of the stature of prehistoric caeces. – *Phil. Trans. Royal Soc. A*, **193**, 1899, 169–244.
13. **Ruff, C. B., W. W. Scott, , A. Y. Liu, 1991.** Articular and diaphyseal remodeling of the proximal femur with changes in body mass in adults. – *Am. J. Phys. Anthropol.*, **86**(3), 397- 413.
14. **Schaefer, M., S. M. Black, L. Scheuer.** *Juvenile osteology: A laboratory and field manual.* San Diego, CA, Academic Press, 2009.
15. **Singh, R.** Classification, causes and clinical implications of sacral spina bifida occulta in Indians. – *Basic Sciences of Medicine*, **2**(1), 2013, 14-20.
16. **Stoev, R.** Body height in recruits in Bulgaria (1897-1920). – *Acta morphologica et anthropologica*, **18**, 2012, 95-101.
17. **Trotter, M., G. Gleser.** Estimation of stature from long bones of American whites and Negroes. – *Am. J. Phys. Anthropol.*, **10**, 1952, 469–514.
18. **Walker, P. L. R. R. Bathurst, R. Richman, T. Gjerdrum, V. A. Andrushko.** The causes of porotic hyperostosis and cribra orbitalia: A reappraisal of the iron-deficiency-anemia hypothesis. – *American Journal of Physical Anthropology*, 2009, 139: 109-125
19. **White, T. D., P. A. Folkens.** *The Human bone manual.* Burlington: Elsevier, 2005.
20. **Alexeev, V. P., G. F. Debetz.** *Craniometry. Methods of anthropological research.* Moscow, Science, 1964 [in Russian].
21. **Alexeev, V.P.** *Osteometry. Methods of anthropological research.* Moscow, Science, 1966 [in Russian].
22. **Atanassova, N.** Comparative characteristics of anthropological indicators of bone remains from the Ottoman period (15th – 19th Century). *PhD thesis*, Bulgarian Academy of Sciences, Sofia, 2018 [in Bulgarian].
23. **Gerasimov, M.** *Reconstruction of the face from the skull: (modern and fossil human).* Moscow, Publishing house AN USSR, 1955 [in Russian].
- 24.0 **Zubov, A.** *Odontology. Methods of anthropological research.* Moscow, Science, 1968 [in Russian].

Review Articles

Advantages and Disadvantages of Virtual Autopsy in the Field of Forensic Medicine

Antoaneta Fasova^{1}, Mirena Sotirova², Teodora Gudelova², Atanasios Topalidis³, Slavi Delchev¹*

¹ *Department of Anatomy, Histology and Embryology, Faculty of Medicine, Medical University-Plovdiv, Bulgaria*

² *Department of Forensic Medicine and Deontology, Faculty of Medicine, Medical University-Plovdiv, Bulgaria*

³ *medical student, Faculty of Medicine, Medical University-Plovdiv, Bulgaria*

*Corresponding author e-mail: antoaneta.fasova@mu-plovdiv.bg

In forensic practice, the methodology of classical autopsy includes external examination of dead body, dissection of organs with identification of macroscopic pathologies and injuries and histopathology. In many forensic cases, the traditional autopsy is less accurate than the virtual one and often may destroy key forensic evidence. Some communities have religious objections to the autopsy and the search for a minimally invasive alternative in forensic practice is increasing. Autopsy is supported by diagnostic imaging techniques, e.g. computed tomography (CT) and magnetic resonance imaging (MRI). Compared to traditional autopsy, they have several advantages: non-invasive, the data can be visualized in situ, stored and fully interpreted at any time in cases of re-autopsy. Computed tomography is more accurate imaging technique for establishing the cause of death, presence of skeletal pathology and pathological abnormalities in fetuses, newborns and infants.

Key words: virtual autopsy, forensic examination, 3D scanning, tomography

Introduction

Traditional autopsy has changed little in the past century, consisting of external examination and evisceration, dissection of the major organs with identification of macroscopic pathologies and injuries, and histopathology if needed [20].

Medical imaging has become an indispensable part of diagnosis and treatment of patients in almost all medical disciplines. The process of a standard autopsy can

damage or destroy evidence of the cause and manner of death due to the elaborate, intense and timely surgical procedure. In light of this unfortunate and common issue, a new technology has been developed to eliminate hands-on autopsies i.e. virtual autopsy, which have a lot of potential applications [1, 3, 10].

3D scanning makes autopsies of decomposed bodies significantly easier, establishing key data that would be difficult to detect during traditional autopsies, such as the angle of entry of a knife or bullet or cases related to medical errors, etc. Advances in radiology, combined with advances in computer technology, have made 3D (three-dimensional) representation of anatomical structures easily accessible using CT and MR [13, 14, 18].

Virtual autopsy is a virtual alternative to a traditional autopsy, conducted with scanning and imaging technology. With virtual autopsy, radiation is used to examine the innards to reach a conclusion about the cause of death. A CT scan or an MRI could be used, in the same way that they are used to scan a living human's body [2, 5, 6, 12].

In Bulgaria, virtual autopsy has not yet been implemented in the departments of Forensic Medicine and Deontology of the Medical Universities. It would be a new approach in Bulgaria, but exists as a practice worldwide. Its introduction as a new innovative method in forensic medical examinations of dead bodies in Bulgaria will lead to more accurate determination of cause of death, description of traumatic injuries and reconstruction of their mechanism.

Benefits of virtual autopsy

Virtual autopsy is a non-invasive method that allows identification of organs damage while preserving their topographic location, eliminating the possibility of iatrogenic damage. Additionally, it allows for repeated forensic analyses of dead body in cases of re-autopsy and exhumation: it requires a much shorter time to perform compared to conventional autopsy, there is no primary contact between the operator and the object for examination (corpse and remains), which will lead to optimization of automatic image analysis. Thus it has the potential to save costs, optimize resource allocation by automating tasks, reduce the risk of infection, as well as development of Burnout syndrome, which is common in forensic medical practice [11, 23, 29, 34].

Advantages of virtual autopsy:

1. Virtual autopsy is a non invasive technique where non-intrusive human autopsies are performed by using a CT scanner or MRI to obtain a detailed view of the body.
2. Virtual autopsy creates digital and permanent records of the body, making it easier for pathologists and clinicians to communicate with each other.
3. Real samples are hard to transport and share, while the digital image of the body can be shared electronically among medical professionals and experts and can be stored for future retrieval and re-examination.
4. Doctors can conduct virtual autopsy remotely. This means that hospitals centres with CT scanners can take advantage of virtual autopsy even though they may not have an in-house pathologist.
5. The legal system can also benefit from this technology as the 3-dimensional images can easily be shown in courtrooms and spare people from having to look at the traditional autopsies' gruesome pictures of the victim's body. The images from a

virtual autopsy can be made interactive, helping the judge and jury understand some technical facts.

6. Virtual autopsy leaves the body intact, so it would not add to the grief of the victim's family. This also overcomes the obstacles presented by religions that forbid cutting of the deceased.

7. Virtual autopsy is also a good method to eliminate cross contamination and infection, as all deceased are scanned in a body bag. It lowers the risk of contaminating pathologists and other medical specialists [34].

8. 3D scanning makes autopsies of decomposed, mummified and partially skeletonized bodies noticeable easier. It also determines key findings that are difficult to discover with traditional autopsy because they can be destroyed.

Disadvantages of virtual autopsy:

1. Virtual autopsy is expensive and includes high equipment and technology costs.

2. Virtual autopsy needs skills and training to deduce from the autopsy results. Lack of experience is a disadvantage [21, 27, 34].

3. Imaging alone cannot diagnose biochemical and toxicological causes, and is poor in the identification of asphyxial deaths. A minimally invasive autopsy service should include careful external examination of the body by a pathologist to identify superficial signs of injury not detected on imaging [20].

Applications of virtual autopsy in forensic practice

Which imaging technique should be used in forensic practice? Forensic pathologists use CT more often because it provides better spatial resolution than MRI and is effective for showing fractures and haemorrhages. Non-forensic and paediatric specialists use MRI because it provides greater detail of soft tissues than does CT. CT provides visualisation of coronary artery calcification that is not apparent with MRI, whereas acute myocardial infarcts might be seen with MRI but not with CT. CT has important practical advantages, being more widely available, less expensive, and quicker to do than MRI. CT could also be combined with angiography, increasing the accuracy of detection of vascular pathologies [9, 20].

Forensic examination, especially of deceased pedestrians in cases of car accidents, is a challenge in determining the position of the body relative to the vehicle based on the morphological characteristics of the identified traumatic injuries. The application of virtual autopsy in these cases successfully allows the identification of bruises, subcortical hematomas on long bones, which is impossible with conventional autopsy. The latter allows localization of the primary contact with motor vehicles. Digital storage of the established results of traumatic injuries of internal organs and bones would allow a detailed analysis of their mechanism of injury with subsequent detailed reconstruction of the car accident [15, 17, 26].

Cases of falls from a height are always accompanied by multiple injuries of the internal organs and bones. In conventional autopsy, these cases are often associated with difficult dissection of the soft tissues around the traumatically damaged bones. This makes it impossible to detect the fracture and/or accurately determine the fracture line and reconstruct the type of fall based on the mechanism of bone damage. With virtual autopsy, this drawback is completely eliminated [7, 16, 30].

In forensic medicine, in cases of drowning, proving viability and determining the length of time the dead body has been in the water, is almost impossible. Several imaging studies have been described that virtual autopsy can help in such cases [4, 16, 20, 25].

The application of virtual autopsy in cases of child mortality is of utmost importance to differentiate the Child abuse syndrome. The detection of Bucket handle fractures of the long bones is one of the main signs proving physical abuse of a child. These microfractures are impossible to detect during a conventional autopsy, which makes this type of autopsy insufficient in such cases [28, 29, 31].

In cases of death from gunshot wounds, forensic analysis is mainly related to determining the entry-exit wound and the wound channel. The application of 3D reconstruction with virtual autopsy allows for accurate determination of direction of passage of the projectile through the body, since the topographical location of the organs is preserved, unlike conventional autopsy [8, 22, 24, 32].

Using a 3D virtual dissection table allows us to examine 3D images of human body using CT or MRI data and could help forensic pathologist to locate vital anatomical structures (e.g. bone fragments, variable positions of anatomical structures, position of foreign bodies, presence of pneumothorax, air embolism or subcutaneous emphysema, etc.). To achieve good image quality in 3D imaging, thin slices (< 1 mm) and the use of correct scanning protocols for specific tissues, organs and pathology are required. Investigators can intuitively zoom in, rotate or crop the visualized body without using a scalpel or destroying the object. This means that the same image can be used multiple times, which is a valuable aspect in forensic autopsies. The idea of interacting with virtual patients is to provide a better understanding of the anatomy of the body, which in turn will contribute to higher autopsy efficiency [19, 33]. The combination of computed tomography and three-dimensional examination with a virtual dissection table in forensic practice is an innovative approach in the search of more successful methods for diagnosing the causes of death. It will provide more in-depth data in detailed reconstruction of traumatic injuries. This, in turn, will contribute to the modernization of forensic medicine and will facilitate the diagnostic process for medical specialists.

In summary, the virtual autopsy approach has the following advantages: allows for objective data archiving without tissue and organ destruction; minimally invasive; provides life-size documentation; preservation of forensic evidence without iatrogenic damage; provides an alternative or additional tool for examination in “difficult body area autopsy” (e.g. face, neck, pelvis); can be used in cultures and situations where autopsy is not tolerated by religion or is rejected by family members (e.g. psychological reasons); provides the ability to examine bodies contaminated with infection, toxic substances, radionuclides or other biological hazards (i.e. bioterrorism); provides 2D and 3D post-processing for visualization of the autopsy by non-attending specialists during the procedure; provides greater clarity in court and creation of digital archives (database for teaching and training).

Conclusions

Virtual autopsy is a necessary addition to the traditional autopsy in forensic medical practice nowadays. Using both methods of investigation in combination could be of great benefit in teaching medical students, residents and PhD students in forensic medicine and imaging diagnostics in order to increase their level of competence and will contribute to knowledge transfer in the field of forensic medicine by creating a database of virtual autopsies for further comparative analysis.

Acknowledgements. This study is financed by the European Union-NextGenerationEU, through the National Recovery and Resilience Plan of the Republic of Bulgaria, project № BG-RRP-2.004-0007-C01.

References

1. **Ahuja, P., N. Ansari.** **Virtopsy: A New era in forensic medico-legal autopsies.** – In: *Autopsy – what do we learn from corpses?* (Ed. K. Dogan), London, IntechOpen Publisher, 2022, 103781.
2. **Badam, R.K., T. Sownetha, D. Babu, S. Waghay, L. Reddy, K. Garlapati, S. Chavva.** **Virtopsy: Touch-free autopsy.** - *J. Forensic Dent. Sci.*, **9**(1), 2017, 42.
3. **Blokker, B., A. Weustink, I. Wagenveld, J. von der Thüsen, A. Pezzato, R. Dammers, J. Bakker, N. Renken, M. den Bakker, F. van Kemenade, G. Krestin, M. Hunink, J. Oosterhuis.** **Conventional autopsy versus minimally invasive autopsy with postmortem MRI, CT, and CT-guided biopsy: Comparison of diagnostic performance.** – *Radiology*, **289**(3) 2018, 658-667
4. **De Boer, H. H., Z. Obertová, E. Cunha, P. Adalian, E. Baccino, T. Fracasso, E. Kranioti, P. Lefèvre, N. Lynnerup, A. Petaros, A. Ross, M. Steyn, C. Cattaneo.** **Strengthening the role of forensic anthropology in personal identification: position statement by the Board of the Forensic Anthropology Society of Europe (FASE).** – *Forensic Sci. Int.*, **315**, 2020, 110456.
5. **Dirnhofer, R., C. Jackowski, P. Vock, K. Potter, M. Thali.** **VIRTOPSY: minimally invasive, imaging-guided virtual autopsy.** – *Radiographics*, **26**(5), 2006, 1305-1333.
6. **Dwivedi, D., D. Das, A. Singh, J. George.** **Virtopsy: An Emerging Tool in Forensic Investigation.** - *Glob. J. Res. Anal.*, **11**, 2022, 182-184.
7. **Engelke, K., O. Museyko, L. Wang, J. Laredo.** **Quantitative analysis of skeletal muscle by computed tomography imaging – State of the art.** – *J. Orthop. Translat.*, **15**, 2018, 91-103.
8. **Fukuda, H., H. Tokue, A. Hayakawa, Y. Kominato, R. Sano.** **Superimposed imaging of knife and stab wound relationships through pre-autopsy and intraautopsy computed tomography integration: a case report.** – *Cureus*, **16**(8), 2024, e66720.
9. **Haque, M.** **Medical professionals’ perspective on virtual autopsy: Comprehensive analysis and validation study with respect to traditional autopsy.** – *Medico Legal Update*, **21**(4), 2021, 278-287.
10. **Herath, J. C., U. R. Herath.** **Are invasive postmortem examinations still the ‘gold standard’ in diagnosing the cause of death?** – *Sri Lanka J. Forensic Med. Sci. Law*, **15**(1), 2024, 34-42.
11. **Jayakrishnan, J., J. Reddy, R. Kumar.** **Role of forensic odontology and anthropology in the identification of human remains.** – *J. Oral Maxillofac. Pathol.*, **25**(3), 2021, 543-547.

12. **Lawson, N. E.** Autopsy V. Virtopsy: A new approach for postmortem forensic examination. – *Honors Projects*, 2022, 851.
13. **Mann, R., D. Hunt.** Non-metric traits and anatomical variants that can mimic trauma in the human skeleton. – *Forensic Sci. Int.*, **301**, 2019, 202-224.
14. **Mentink, M., B. Latten, F. Bakers, C. Muhl, R. Rennenberg, B. Kubat, P. Hofman.** Clinical relevance of unexpected findings of post-mortem computed tomography in hospitalized patients: An observational study. – *Int. J. Environ. Res. Public Health*, **17**(20), 2020, 7572.
15. **Moza, B., D. Mukherjee, M. Singh, V. Pahwa, P. Ujjainia, S. Pathak, A. Saha, A. Srivastava.** Advancements in the imaging techniques for detection of skeletal pathologies: A comprehensive review. – *Tuijin Jishu/Journal of Propulsion Technology*, **45**(1), 2024, 645-663.
16. **O'Donnell, C., M. Iino, K. Mansharan, J. Leditscke, N. Woodford.** Contribution of postmortem multidetector CT scanning to identification of the deceased in a mass disaster: experience gained from the 2009 Victorian bushfires. – *Forensic Sci. Int.*, **205**(1-3), 2011, 15-28.
17. **Plattner, T., M. J. Thali, K. Yen, M. Sonnenschein, C. Stoupis, P. Vock, K. Zwygart-Brügger, T. Kilchör, R. Dirnhofer.** Virtopsy-postmortem multislice computed tomography (MSCT) and magnetic resonance imaging (MRI) in a fatal scuba diving incident. – *J. Forensic Sci.*, **48**, 2003, 1347-1355.
18. **Ramchand, S., J. Tsai.** New imaging techniques for bone. – In: *Osteoporosis. pathophysiology and clinical management*. (Eds. B. Leder, M. Wein). Totowa, USA, Humana Cham Publisher, 2020, 151-167.
19. **Redéen, S., P. Elmhester, R. Larsson, L. Lindfors.** Highlights and potentials when using the visualization table for pre-operative planning and diagnosis in seven surgical and one oncological department – a pilot study at the University Hospital of Linköping. – *Am. J. Med. Stud.*, **2**(3), 2014, 42-45.
20. **Roberts, I. S., R. E. Benamore, E. W. Benbow, S. H. Lee, J. N. Harris, A. Jackson, S. Mallett, T. Patankar, C. Peebles, C. Roobottom, Z. C. Traill.** Post-mortem imaging as an alternative to autopsy in the diagnosis of adult deaths: a validation study. – *Lancet*, **379**, 2012, 136-142.
21. **Sonnemans, L. J. P., B. Kubat, M. Prokop, W. M. Klein.** Can virtual autopsy with postmortem CT improve clinical diagnosis of cause of death? A retrospective observational cohort study in a Dutch tertiary referral centre. – *BMJ. Open*, **8**(3), 2018, e018834.
22. **Tartaglione, T., L. Filograna, S. Roiati, G. Guglielmi, C. Colosimo, L. Bonomo.** Importance of 3D-CT imaging in single-bullet cranioencephalic gunshot wounds. – *Radiol. Med.*, **117**(3), 2012, 461-470.
23. **Thali, M. J., R. Dirnhofer, P. Vock.** *The Virtopsy approach: 3D optical and radiological scanning and reconstruction in forensic medicine*. CRC Press, 2009.
24. **Thali, M. J., W. Schweitzer, K. Yen, P. Vock, C. Ozdoba, E. Spielvogel, R. Dirnhofer.** New horizons in forensic radiology: the 60-second digital autopsy-full-body examination of a gunshot victim by multislice-computed tomography. – *Am. J. Forensic Med. Pathol.*, **24**, 2003, 22-27.
25. **Thali, M. J., K. Yen, W. Schweitzer, P. Vock, C. Ozdoba, R. Dirnhofer.** Into the decomposed body-forensic digital autopsy using multislice-computed tomography. – *Forensic Sci. Int.*, **134**, 2003, 109-114.

26. **Thali, M. J., K. Yen, T. Plattner, W. Schweitzer, P. Vock, C. Ozdoba, R. Dirnhofer.** Charred body: virtual autopsy with multi-slice computed tomography and magnetic resonance imaging. – *J. Forensic Sci.*, **47**, 2002, 1326-1331.
27. **Thali, M. J., K. Yen, W. Schweitzer, P. Vock, C. Boesch, C. Ozdoba, G. Schroth, M. Ith, M. Sonnenschein, T. Doernhoefer, E. Scheurer, T. Plattner, R. Dirnhofer.** Virtopsy, a new imaging horizon in forensic pathology: virtual autopsy by postmortem multislice computed tomography (MSCT) and magnetic resonance imaging (MRI) – a feasibility study. – *J. Forensic Sci.*, **48**, 2003, 386-403.
27. **Thayyil, S., N. Sebire, L. Chitty, A. Wade, W. Chong, O. Olsen, R. S. Gunny, A. C. Offiah, C. M. Owens, D. E. Saunders, R. J. Scott, R. Jones, W. Norman, S. Addison, A. Bainbridge, E. B. Cady, E. De Vita, N. J. Robertson, A. M. Taylor.** Post-mortem MRI versus conventional autopsy in fetuses and children: a prospective validation study. – *Lancet*, **382**, 2013, 223-233.
28. **Vadivel, J. K.** Virtual autopsy. – *International Journal of Forensic Odontology*, **1**, 2016, 14-16.
29. **Vester, M., R. van Rijn, W. Duijst, L. Beenen, M. Clerkx, R. Oostra.** Added value of post-mortem computed tomography (PMCT) to clinical findings for cause of death determination in adult “natural deaths. – *International Journal of Legal Medicine*, **134**, 2020, 1457-1463.
30. **Wagensveld, I. M., M. G. M. Hunink, P. A. Wielopolski, F. J. van Kemenade, G. P. Krestin, Blokker B. M., J. W. Oosterhuis, A. C. Weustinket.** Hospital implementation of minimally invasive autopsy: A prospective cohort study of clinical performance and costs. – *PLoS ONE*, **14**(7), 2019, e0219291.
31. **Wilson, A., A. Holland, T. Sparrow.** Laser scanning of skeletal pathological conditions. – In: *Human remains: another dimension the application of imaging to the study of human remains* (Eds. D. Errickson, T. Thompson), London, Academic Press, 2017, 123-134.
32. Sectra Medical, 2025, Available at <https://medical.sectra.com/>
33. Civil Services Examination & Indian Forest Service Examination preparation, 2012, Available at <https://forumias.com/>

Longevity in the Exhibition „Codes of Identity“ of the National Anthropological Museum at the Institute of Experimental Morphology, Pathology and Anthropology with Museum, Bulgarian Academy of Sciences

Rosen Gatsin

Institute of Experimental Morphology, Pathology and Anthropology with Museum, Bulgarian Academy of Sciences

Corresponding author e-mail: r.gatsin@gmail.com

Longevity is a topic that has always fascinated humankind. Throughout the stages of civilization's development, the average human lifespan has varied. Undoubtedly, the living conditions, environment, food, and advancement of medicine influence life expectancy. Yet, there have always been centenarians, and there is still no definitive answer to the key to reaching a record-breaking age. This study aimed to collect, summarize, and analyze material related to specific Bulgarian families concerning longevity in order to identify the factors that influence it. The exhibition "Codes of Identity" presents Bulgarian longevity via specific settlements and families. A rich photographic archive reflecting the anthropological characteristics of the population has been collected and analyzed. The genealogy of selected families is also presented. In conclusion, the „Human“ is placed at the center of the exhibition. He is the element that Anthropology and Genealogy, and the exhibition shows that the symbiosis between the two disciplines is beneficial and promising.

Key words: National Anthropological Museum, anthropology, genealogy, longevity, centenarian

Introduction

Longevity is a topic that has always intrigued people. In different stages of civilization's development, average life expectancy has varied. Many factors determine these values. Living conditions, environment, nutrition, and the emergence of medicine undeniably influence life expectancy. Yet, the fact remains that centenarians have always existed, and the key to extreme longevity still remains elusive.

The exhibition "Codes of Identity" presents the longevity of Bulgarians through the lens of specific villages and families.

The aim of this study is to collect, summarize, and analyze materials related to specific Bulgarian families and their experiences with longevity, to present the environment in which these families have lived over the years, and to attempt to identify the factors influencing their longevity.

Materials and Methods

A field study was conducted in selected communities and villages: Lik and Kameno Pole, Dzhurovo village, and the town of Ugarchin. A rich photographic archive reflecting the anthropological traits of the population was collected. The genealogy of the selected families was recorded and described.

Results and Discussion

In November 2024, the author's exhibition "*Codes of Identity*" was opened in the temporary exhibition halls of the National Anthropological Museum at the Institute of Experimental Morphology, Pathology, and Anthropology with Museum of the Bulgarian Academy of Sciences. The focus of this exhibition is Bulgarian longevity, supported by specific examples. The exhibition is a result of the author's longstanding interest in the topic of longevity and genealogical connections. During the research process, one focal point of the exhibition emerged quite naturally – the discovery of a tombstone containing information about a man who lived to be 130 years old.

This case came to light after reports from the village of Lik, Mezdra municipality, Vratsa region, that a person of biblical age had died there at the end of the 20th century. In the summer of 2024, a field study was organized in the mentioned area. Indeed, a tombstone was found in the local cemetery near the village of Lik. The inscription reads:

„Here rest father Yoncho – 130 years, son Ivan – 103 years, son Krastyo – 106 years. Their father died in 1906. Erected / Exalted by Geno Krastev.“ (Fig. 1).

An inquiry was made at the Lik village hall, which provided an official document – a death certificate from 1907, known at the time as an “Act of Dying” (Fig. 2). This document confirms the age of Yoncho Tzolov as 130 years. He belonged to the Pelovski family. It became evident that Yoncho outlived both of his centenarian sons and died of illness rather than natural causes. Key contributions to uncovering this story came from his relatives in the Pelovski family: Georgi Pelovski, Diana Pelovska, Georgi Dimitrov, Gergana Nikolova, and Yoncho Pelovski, along with Valentina Misheva, the mayor of Lik. Stone crosses are considered a valuable source of information [2].

The tombstone also reveals that both sons, aged 103 and 106, passed away before their father. Yoncho had another son who also died before him, aged over 90. Interestingly, the tombstone notes who exalted it – Geno Krastev, born in 1873, the great-great-grandson of Yoncho. He was old enough to care for the centenarian. The tombstone is small and was nearly buried, which helped preserve it. It was discovered during excavation for a new grave. The family always knew there was a man who lived to 130.



Fig. 1. Tombstone from the village of Lik, Vratsa Province

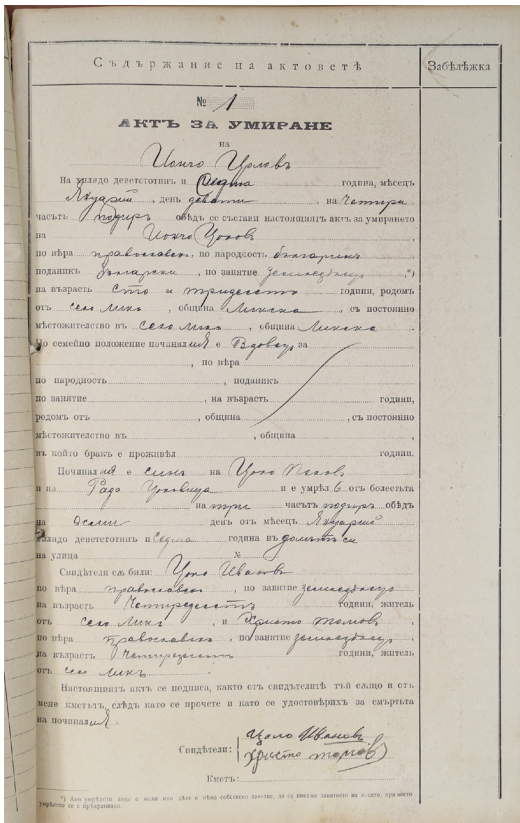


Fig. 2 Death certificate from 1907, known at the time as an “Act of Dying”

According to records, Yoncho Tsolov was a farmer. Documents list his death in 1907, though the tombstone says 1906 – a common discrepancy in that era due to delays in burial for holidays or weather conditions. It is believed that one of the reasons for Yoncho Tsolov’s longevity may be the healing properties of the water in the village of Lik, which is currently under investigation. The cult of water holds an important place in Bulgarian culture [5].

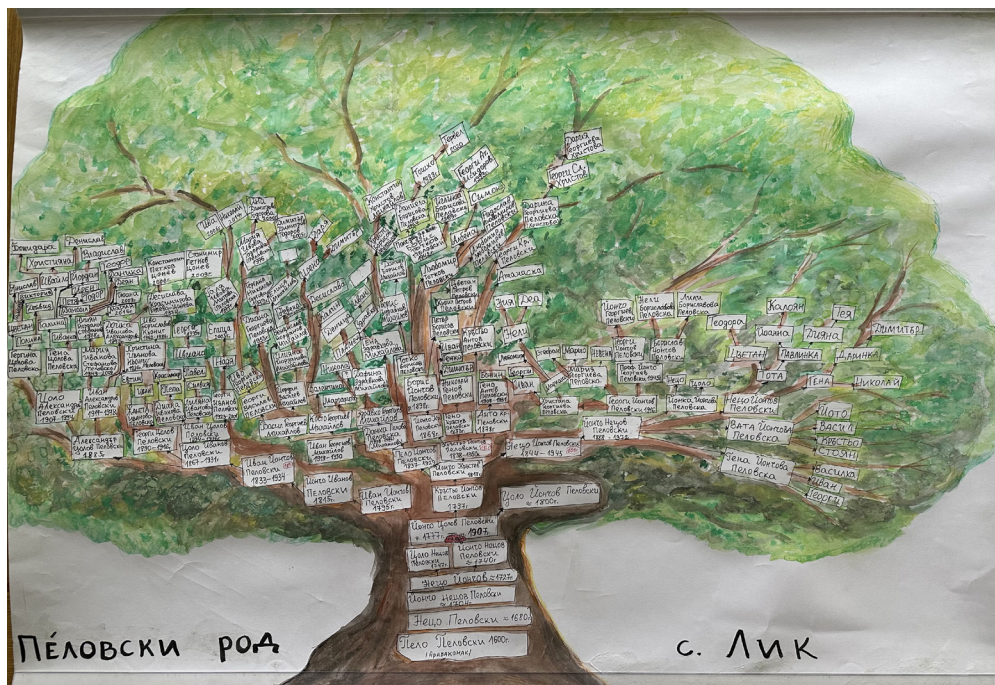


Fig. 3. The Pelovski Family Tree

Research indicates the Pelovski family migrated from today’s Republic of North Macedonia in the early 16th century (Fig. 3). They traveled through the Sofia Valley, likely passing through the Arabakonak (Botevgrad) or Etropole Pass. The reasons for the migration are unknown. They eventually settled in the Etropole region. Their main livelihoods were livestock farming and crafts. Later, they spread into the Vratsa region – villages like Lik, Dolna Beshovitsa, and Kunino – and from Oreshak in the Troyan Balkan to towns like Troyan, Lovech, Debnevo, Shipkovo, Teteven, Glozhene, Golyam Izvor, Dzhurovo, and Vidrare.

The exhibition “Codes of Identity” also features a photo of a Bulgarian believed to have lived 128 years – Krastyo Ilyanov from Pordim. A 1910 postcard reads: „Grandfather Krastyo B. Ilyanov, born in 1785 in Pordim. Lived through the 18th, 19th, and 20th centuries. This photo commemorates his 125th birthday in 1910.“ His story was researched by Lyubomir Bukovski and published in his book “Pleven – Meeting with the Past 1877–1944.” Due to a postcard printed in Germany, we have a photo of this remarkable man (Fig. 4).



Fig. 4. A photo of Krastyo Ilyanov from Pordim that commemorates his 125th birthday in 1910

Krastyo Beshev Ilyanov is believed to be the longest-living Bulgarian, born in 1785 in Pordim, Plevan region. A farmer, known for his work ethic and kind nature, he lived through epidemics, wars, and famine, never leaving his birthplace until his death in 1913 [1].

Another interesting case is Vasilka Bangieva from Pavelsko, who reportedly lived to 125. Later records show that she was born in 1790 and died in 1909, aged 119. She was photographed with her son, over 100 himself, by photographer Krum Savov. The photo was exhibited in Liège in 1905 (**Fig. 5**).

Reaching old age brings a special status and respect [6]. The thread of longevity in the exhibition is also traced through genealogy, the science of family history. From Greek “*genos*” (family) and “*logos*” (science) [10]. Genealogy explores bloodline and kinship terminology. It contributes to understanding biological ancestry using traditional research methods and, when needed, genetic genealogy. The types of kinship in Bulgaria are presented in detail in the book “Brachnik” by Ivan Genadiev from 1887 [3]. The renowned Bulgarian scholar Dimitar Marinov, Director of the Ethnographic Museum, explored the topic of longevity in great detail as early as the late 19th century [7-9]. The beliefs about the human body in the traditional culture of Bulgarians are examined in a very interesting and detailed manner in *Mythology of the Human Body – Anthropological Dictionary* [4].

Greek philosopher Theophrastus (372–287 BC) wrote: „*You ask me about him, since you are interested, let me proceed as genealogists do – I will begin with his parents.*“

Fig. 5. A photo of Vasilka Bangieva from Pavelsko, who lived to 125.



Genealogy reveals detailed family histories and relationships, often uncovering important data missed by traditional sources. An example is the teacher Yordan Hvirlev from the National Revival period. Notes in his personal Bible, preserved to this day, describe valuable contributions to Bulgarian history. Born in 1864 in Elena, he studied at a seminary, taught in Varna, and died in Sofia in 1936, buried in Sofia Central Cemetery.

Several families are presented in the exhibition. The research attempts to trace hereditary diseases, skills, and a genealogical chronology. One example is the family of Eustati Martinov, mayor of Veliko Tarnovo in the early 20th century (**Fig. 6**). Born on March 20, 1857, Martinov descended from several notable families – Priest Stoyko of Elena, Priest Martin of Razpopovtzi, the Aprilov family from Gabrovo, and Hadzhidaskalov from Tryavna. Eustati Martinov was a teacher, lawyer, public figure, and friend of Stefan Stambolov and Aleko Konstantinov.

He became mayor of Tarnovo in 1902. Stambolov once asked him to become a monk to be appointed bishop, but he refused, wanting a family. Lawyer Nikolay Martinov recalls his father was named after Vasyl Aprilov's father – Eustati.

The *Codes of Identity* exhibition raised important societal topics, increased attendance at the National Anthropological Museum, and sparked a tradition of genealogy workshops well-received by the public. These are open to all ages and help participants begin personal genealogical research.

The „*Human*“ is placed at the exhibition's center – the unifying element between Anthropology and Genealogy. The results demonstrate that this coalition is both beneficial and full of potential.



Fig. 6. Photo of Family of Eustati Martinov. From left to right: wife Zhivka (holding grandson Dimitar Abadjiev), Eustati Martinov, daughter Venka, and standing: sons Nikolay and Georgi, and son-in-law Petar Abadjiev

References

1. **Bukovski, L.** Pleven. A Meeting with the Past 1877–1944. Pleven, IVKO, 2006, p. 288.
2. **Enchev, I.** Sofia. Bulgarian Folk Cross, 1994.
3. **Genadiev, Iv.** *Bratchnik: A Book of Kinship and Other Marriage Relations*, Plovdiv, 1887, 320 p
4. **Georgiev, M.** *Mythology of the Human Body – An Anthropological Dictionary*. Professor Marin Drinov Publishing House of BAS, Sofia, 2008.
5. **Mankova, Y.** *The Cult of Water in Bulgarian Folklore Culture*. Vratsa, 1996.
6. **Marinov, D.** *Living Antiquity*. Sofia, 1891.
7. **Marinov, D.** *Living Antiquity*. Ruse, Vols. 2–3, 1892.
8. **Marinov, D.** *Customary Folk Law*. Ruse, 1894.
9. **Marinov, D.** *Selected Works*, Vol. 3, 246 pages, 1981, Science and Art, Sofia
10. **Zapryanova, A.** *Genealogy or How to Study Your Family Lineage*, St. Kliment Ohridski University Press, 2003



Professor Stefan Stefanov Mutafov

(20.03.1925 – 18.01.2010)

It has been one hundred years since the birth of our outstanding Bulgarian anthropologist and neurologist Prof. Stefan Mutafov. Let us remember his life, his academic career and scientific contributions.

Stefan Stefanov Mutafov was born on March 20, 1925 in the town of Popovo in the family of Stefan K. Mutafov and his wife Dochka. His father was a famous merchant, but died in his early fifties while his son was 8 years old.

Stefan Mutafov – Jr., graduated in 1945 simultaneously from two high schools - Sofia Theological Seminary, and the Classical Department of the Male High School in Ruse. In 1952 he graduated in medicine at Higher Medical Institute in Sofia (now Medical University – Sofia).

As a son of prominent merchant and because Stefan Mutafov graduated from theological seminary, he encountered many difficulties in his life and academic career, which he overcame through his intelligence and amazing work capacity.

After Stefan Mutafov graduated from the Medical University he was appointed as a physician in village of Kamenovo (district of Kubrat) and then quickly was promoted in the Chief physician of the hospital in the town of Kubrat. He was the Head of Department of Public Health and Social Care in the town of Silistra (1953-1955). In 1958 Stefan Mutafov became a senior inspector in the District Health Department in the city of Ruse and the Head of Department of Neurology of the three medical and sanitary units in Ruse.

During this period, Stefan Mutafov also completed two specializations at the Institute for Specialization of Medical Doctors in Sofia – in “Organization of Health Care and History of Medicine” (1953) and in “Neurology and Psychoneurology” (1957-1958). Later in 1967 he has got specialization in medical anthropology in German Democratic Republic (1967) and in neuro-defectology and bioanthropology in Switzerland (1972-1973).

Apart from his busy work, Stefan Mutafov conducted anthropological studies on the population of Northeastern Bulgaria from different ethnic groups, which remained unpublished, but preserved in the archive. His work was noticed by Dr. Petar Boev, scientist in ethnical anthropology, who invited him to work at the Institute of Morphology (now Institute of Experimental Morphology, Pathology and Anthropology with Museum) at the Bulgarian Academy of Sciences in Sofia. Thus, in 1961, after a competition, Stefan Mutafov started his scientific career as Assistant Professor in the Institute. In 1969 he successfully defended his PhD dissertation on oligophrenology and later in 1984 – dissertation for Doctor of medical sciences. In 1969 he acquired his first habilitation as Associate Professor in medical anthropology followed by full professorship in applied anthropology (1982). He was Head of the Laboratory of Applied Anthropology and Defectology established by him and later he became Head of the Department of Anthropology in the Institute.

Stefan Mutafov has a great contribution for universities not only in student’s education but in establishing specialized departments. He started to teach students in 1959 as a lecturer in Medical School in Ruse. In 1969 Stefan Mutafov was elected as a part-time lecturer in Sofia University “St. Kliment Ohridski starting with training of students in clinics of oligophrenia. Since 1973, he was Head of the Sector of Defectology at the Department of Pedagogy of the Faculty of Philosophy. In 1975, he was promoted in full-time associate professor in neurology and psychopathology, and in 1986 he became full professor in neurology. In 1987 Prof. Mutafov established in the Sofia University the first Department of Defectology (now Special Pedagogy) in Bulgaria and he was Head of the Department until his retirement in 1991. Soon after his retirement Prof. Mutafov continued his academic activity in Shumen University “Konstantin Preslavski” in the Department of Special Pedagogy and Sociagogy established by him in 1993 at the Faculty of Pedagogy. Since 1996 he worked in Thracian University – Stara Zagora in newly-established Department of Special Pedagogy as well.

Prof. Stefan Mutafov is the author and co-author of over 550 scientific papers of which more than 100 have been published abroad. He is also the author of 35 monographs and 7 university textbooks. He participated in over 250 scientific congresses, conferences and symposia. He is author of 12 inventions and 5 rationalizations, which are in the field of applied anthropology and ergonomics, for which he received the title of “honorary inventor” of Bulgaria. Prof. Mutafov was recognized as one of the greatest anthropologists in Bulgarian scientific societies. His broad scientific output is highly appreciated – in the fields of anthropology, neurology, psychology, pedagogy, defectology, ergonomics, hygiene, cultural studies, history of medicine. Prof. Mutafov is the founder of several research fields in anthropological sciences - applied anthropology, ergonomic anthropology, neuro-anthropology, anthropological standardization biodeflectology.

Bellow I will mention few of his works, emphasizing those that are related to anthropology.

✓ “Anthropometry and somatoscopy” (1959) - a work revealing his early interest in anthropology, while still working in Ruse.

✓ “Anthropometric study of the Bulgarian population” (1976), co-authored with I. Goranov, D. Sepetliev, S. Tornjova, A. Nacheva.

✓ “Psychophysical characteristics of children with anomalies” (1981)

✓ “The human skull in a medical-anthropological aspect” (1984), co-authored with another great Bulgarian anthropologist Prof. Dimitar Kadanov, corresponding member of the Bulgarian Academy of Sciences. The scientific data generated by both scientists on the cranial material from the Military Ossuary in Sofia, were used by the prominent German anthropologist Rösing for comparison with other European populations. Another famous anthropologist Prof. Jelinek highly appreciated the cranial variations discovered by Stefan Mutafov.

✓ “Anthropological and ergonomic characterization of the Bulgarian population” (1985), co-authored with I. Goranov, D. Sepetliev, S. Tornjova, A. Nacheva. This work and the previous one by the same authors (1976), analyzed the results of a large-scale, very well-organized and methodologically relevant study of the Bulgarian population.

✓ “The foot in a medical-anthropological aspect” (1988). The work is largely based on the study of the foot by using devices invented by Prof. Mutafov.

✓ “Pedagogical hygiene” (1991), co-authored with Veska Shosheva.

✓ “Clinical forms of oligophrenia” (1992)

✓ “Medicine in Bulgarian iconography” /1992/

✓ “Anthropology, ergonomics, robotics” (2000).

Prof. Mutafov was a member of several national and international scientific societies. He was member of the New York Academy of Sciences and the Bulgarian National Academy of Medicine.

Prof. Mutafov received honorary awards from the Sofia University (2000) and Shumen University. He was recognized by one of the most prestigious awards – The Order “Sts. Cyril and Methodius” 1st degree”.

Prof. Mutafov will be remembered not only with his bright mind and encyclopedic knowledge but with his civil and purely Christian position. He did not allow himself to make compromise with his own conscience and openly opposed the linking of anthropology with political situations/background in Bulgaria. As a person and scholar he remained humanist and dreamer.

Racho Stoev



Professor Anna Georgieva Boyadjieva-Michailova

(08.05.1925 – 13.10.1997)

It has been one hundred years since the birth of our outstanding Bulgarian scientist, the morphologists and cell anatomists Prof. Anna Georgieva Boyadjieva-Michailova. Let us remember her life and personality as a leader, her scientific career and contributions.

Anna Boyadjieva-Michailova was born on May 8, 1925 in the town of Veliko Tarnovo in the family of the famous gynecologist Prof. Georgi Boyadjiev.

Anna Boyadjieva graduated in medicine in 1950 at Higher Medical Institute in Sofia (now Medical University-Sofia). Since 1955 till 1957 she joined Bulgarian military medical brigade in Korea as a head of bacteriological laboratory. Soon after, Anna Boyadjieva successfully completed specialization in microbiology at the Institute for Specialization of Medical Doctors in Sofia (1958). Her scientific inspiration in electron microscopy is marked by two specializations – in the Charles University in Prague and in the Institute of Biology and Medicine at the German Academy of Sciences in Berlin (1960). Upon her return in Bulgaria, Anna Boyadjieva introduced electron microscopy in the Institute of Morphology (now Institute of Experimental Morphology, Pathology and Anthropology with Museum) at the Bulgarian Academy of Sciences in Sofia. Under the supervision of Acad. Asen I. Hadjiolov, Anna Boyadjieva established the Laboratory of Electron Microscopy which she led for 30 years (1960-1990).

In 1968 Anna Boyadjieva acquired her habilitation as Associate Professor followed by full professorship in 1981 after successfully defended dissertation for Doctor of medical sciences. Prof. Boyadjieva was Scientific Secretary (1972-1986), Deputy Director (1986-1990) of the Institute of Morphology.

Since the first years of her research activity in the Institute, Anna Boyadjieva enthusiastically and persistently applied electron microscopy in cytology and histology. Leading the Electron Microscopy Laboratory for more than 30 years, she actively contributed to its development and establishment as a laboratory for modern ultrastructural studies in Bulgaria. In 1977 she introduced scanning electron microscopy into scientific investigations in the Institute of Morphology. Her great contribution is equipping the Institute with two electron microscopes – transmission (EM Opton 109) and scanning electron microscope (Jeol JSM-35).

Prof. Boyadjieva was a beloved lecturer in electron microscopy at the Faculty of Biology of Sofia University “St. Kliment Ohridski”. As a scientist with national and international recognition, Anna Boyadjieva was devoted to young researchers supporting and encouraging their scientific development in the field of electron microscopy.

Prof. Boyadjieva published more than 100 scientific papers. She is author of 5 inventions, 1 monograph, 1 practicum for electron microscopy.

The remarkable scientific achievements by prof. Boyadjieva are of fundamental importance for elucidation of the mechanisms of gametogenesis and gonadogenesis. Pioneer are her comparative ultrastructural studies on the ovarian cellular populations of different classes of vertebrates. In 1965 Anna Boyadjieva in co-authorship with Asen I. Hadjiolov, Jores Jordanov and Marlena Anastassova-Kristeva described electron microscopic characteristics of Corpus Albani in embryonal chicken ovary. Prof. Boyadjieva introduced ultrastructural histochemistry and developed numerous original methods, some of which were assessed as inventions. She created new methods for observation of isolated cells by scanning electron microscope. Applied contributions by Anna Boyadjieva are of great importance for the development of radiobiology, hybridoma biotechnology, diagnosis and treatment of infertility in domestic animals by assisted reproductive technology.

Prof. Boyadjieva was a member of several national and international scientific societies – International Association of French Speaking Anatomists, Bulgarian Anatomical Society, Union of Scientists in Bulgaria.

She received several honorary awards – from the Government of Korea for her participation in the military medical brigade (1956); the order “Sts. Cyril and Methodius” 2nd degree” for her remarkable contribution for the development of electron microscopy in Bulgaria, a medal from BAS.

Professor Anna Boyadjieva will be remembered with her distinctive features – prominent enthusiastic leader with unique sense of humor, erudition and glamour, nobility and dedication, active public position and humanism.

Nina Atanassova

Author Guidelines

Acta Morphologica et Anthropologica is an open access peer review journal published by Bulgarian Academy of Sciences, Prof. Marin Drinov Publishing House.

Corporate contributors are Bulgarian Academy of Sciences, Institute of Experimental Morphology, Pathology and Anthropology with Museum and Bulgarian Anatomical Society.

Acta Morphologica et Anthropologica is published in English, 4 issues per year.

The journal accepts manuscripts in the following **fields**: experimental morphology, cell biology and pathology, anatomy and anthropology.

Publication types: original articles, short communications, case reports, reviews, Editorial, letters to the Editors.

Acta Morphologica et Anthropologica is the continuation of *Acta cytobiologica et morphologica*

The **aim** of the Journal is to disseminate current interdisciplinary biomedical research and to provide a forum for sharing new scientific knowledge and methodology. The general editorial policy is to optimize the process of issuing and distribution of *Acta Morphologica et Anthropologica* in line with modern standards for scientific periodicals focusing on content, form, and function.

Scope—experimental morphology, cell biology and pathology (neurobiology, immunobiology, tumor biology, environmental biology, reproductive biology, etc.), new methods, anatomy and pathological anatomy, anthropology and paleoanthropology, medical anthropology and physical development.

Acta Morphologica et Anthropologica is published twice a year as one volume with 4 issues. For the first two issues (1-2) the deadline for manuscript submission is March 15th and for the next two issues (3-4), the deadline is September 15th. Electronic version for issues 1-2 is uploaded on the website till June 30th and for issues 3-4 – till December 30th.

Contact details and submission

Manuscript submission is electronical only. The manuscripts should be sent to the Managing Editor's e-mail address ygluhcheva@hotmail.com with copy to iempam@bas.bg

All correspondence, including notification for Editor's decision, requests for revision, is sent by e-mail.

Article structure

Manuscripts should be in English with total length not exceeding 10 standard pages, line-spacing 1.5, justified with 2.5 cm margins. The authors are advised to use Microsoft Word 97-2003, Times New Roman, 12 pt throughout the text. Pages should be numbered at the bottom right corner of the page.

The article should be arranged under the following headings: Introduction, Material and Methods, Results, Discussion, Conclusion, Acknowledgements and References.

Title page – includes:

- **Title** – concise and informative;
- **Author(s)' names and affiliations** – indicate the given name(s) and family name(s) of all authors. Present the authors' affiliation addresses below the names. Indicate all affiliations with a lower-case superscript after the author's name and in front of the appropriate address. Provide the full postal address information for each affiliation, including the country name.
- **Corresponding author** – clearly indicate who will handle the correspondence for refereeing, publication and post-publication. An e-mail should be provided.
- **Abstract** – state briefly the aim of the work, the principal results and major conclusions and should not exceed 150 words. References and uncommon, or non-standard abbreviations should be avoided.
- **Key words** – provide up to 5 key words. Avoid general, plural and multiple concepts. The key words will be used for indexing purposes.

Introduction – state the objectives of the work and provide an adequate background, avoiding a detailed literature survey or summary of the results.

Material and Methods – provide sufficient detail to allow the work to be reproduced. Methods already published should be indicated as a reference: only relevant modifications should be described.

Results – results should be clear and concise.

Discussion – should explore the significance of the results in the work, not repeat them. A combined *Results and Discussion* section is often appropriate. Avoid extensive citation and discussion of published literature.

Conclusions – the main conclusions of the study should be presented in a short section.

Acknowledgements – list here those individuals who provided help during the research and the funding sources.

Units – please use the International System of Units (SI).

Math formulae – please submit math equations as editable text, not as images.

Electronic artwork – number the tables and illustrations according to their sequence in the text. Provide captions for them on a separate page at the end of the manuscript. The proper place of each figure in the text should be indicated in the left margin of the corresponding page. **All illustrations (photos, graphs and diagrams)** should be referred to as “figures” and given in abbreviation “Fig.”, and numbered in Arabic numerals in order of its mentioning in the manuscript. They should be provided in grayscale as JPEG or TIFF format, minimum 300 dpi. The illustrations should be submitted as separate files.

References – they should be listed in alphabetical order, indicated in the text by giving the corresponding numbers in parentheses. The “References” should be typed on a separate sheet. The names of authors should be arranged alphabetically according to family names. In the reference list titles of works, published in languages other than English, should be translated, original language must be indicated at the end of reference (e.g., [in Bulgarian]). Articles

should include the name(s) of author(s), followed by the full title of the article or book cited, the standard abbreviation of the journal (according to British Union Catalogue), the volume number, the year of publication and the pages cited, for books – the city of publication and publisher. In case of more than one author, the initials of the second, third, etc. authors precede their family names. Ideally, the names of all authors should be provided, but the usage of “et al” after the fifth author in long author lists will also be accepted.

For articles: **Davidoff, M. S., R. Middendorff, G. Enikolopov, D. Riethmacher, A. F. Holstein, D. Muller.** Progenitor cells of the testosterone-producing Leydig cells revealed. – *J. Cell Biol.*, **167**, 2004, 935-944.

Book article or chapter: **Rodriguez, C. M., J. L. Kirby, B. T. Hinton.** **The development of the epididymis.** - In: *The Epididymis - from molecules to clinical practice* (Eds. B. Robaire, B. T. Hinton), New York, Kluwer Academic Plenum Publisher, 2002, 251-269.

Electronic books: **Gray, H.** *Anatomy of the human body* (Ed. W.H.Lewis), 20th edition, NY, 2000. Available at <http://www.Bartleby.com>.

PhD thesis: **Padberg, G.** *Facioscapulohumeral diseases.* *PhD thesis*, Leiden University, 1982, 130 p.

Website: National survey schoolchildren report. National Centre of Public Health and Analyses, 2014. Available at <http://ncphp.government.bg/files>

Page charges

Manuscript publication is free of charges.

Ethics in publishing

Before sending the manuscript the authors must make sure that it meets the Ethical guidelines for journal publication of *Acta morphologica et anthropologica*.

Human and animal rights

If the work involves the use of human subjects, the authors should ensure that work has been carried out in accordance with *The Code of Ethics of the World Medical Association* (Declaration of Helsinki). The authors should include a statement in the manuscript that informed consent was obtained for experimentation with human subjects. The privacy rights of human subjects must always be observed.

All animal experiments should comply with the *ARRIVE guidelines* and should be carried out in accordance with the U.K. Animals (Scientific procedures) Act, 1986 and the associated guidelines *EU Directive 2010/63/EU* for animal experiments, or the National Institutes of Health guide for the care and use of Laboratory animals (NIH Publications No. 8023, revised 1978) and the authors should clearly indicate in the manuscript that such guidelines have been followed.

Submission Details

Acta Morphologica et Anthropologica is published twice a year as one volume with 4 issues. For the first two issues (1-2) the deadline for manuscript submission is March 15th and for the next two issues (3-4), the deadline is September 15th. Electronic version for issues 1-2 is uploaded on the website till June 30th and for issues 3-4 – till December 30th.

Manuscript submission is electronic only.

The manuscripts should be sent to the Managing Editor email address ygluhcheva@hotmail.com with copy to iempam@bas.bg

All correspondence, including notification for Editor's decision, requests for revision, is sent by e-mail.

Submission declaration

Submission of the manuscript implies that the work described has not been published previously, is not considered under publication elsewhere, that its publication is approved by all authors, and that if accepted, it will not be published elsewhere in the same form, in English or in any other language, including electronically, without the informed consent of the copyright-holder.

Contributors

The statement that all authors approve the final article should be included in the disclosure.

Copyright

http://www.iempam.bas.bg/journals/acta/Author%20Copyright%20Agreement_last.pdf

Upon acceptance of an article, the authors will be asked to complete a “**Copyright Transfer Agreement**”.

http://www.iempam.bas.bg/journals/acta/Copyright_Transfer_Agreement_Form_AMA.doc

Peer review

Once a manuscript is submitted, the Managing Editor (or the Editor-in-Chief) briefly checks the manuscript for conformance with the journal's Focus, Scope, Policies and style requirements and decide whether it is potentially suitable for publication and can be processed for review, or rejected immediately, or returned to the author for improvement and re-submission.

Manuscripts are peer-reviewed by the Editors, Editorial Board members, and/or external experts before final decisions regarding publication are made. The entire editorial workflow is performed in the following steps:

1. The submitted manuscript is checked in the editorial office whether it is suitable to go through the normal peer review process.
2. If deemed suitable, the manuscript is sent to 2 reviewers for peer-review. The choice of reviewers depends on the subject of the manuscript, the areas of expertise of the reviewers, and their availability.
3. Each reviewer will have 2 weeks to provide evaluation of the manuscript. The Editor may recommend publication, request minor, moderate or major revision, or provide a written critique of why the manuscript should not be published (rejected).
4. In case only one reviewer suggests rejection of the manuscript, the latter is subjected to additional evaluation by a third reviewer.
5. The manuscript will be published in a revised form provided that the authors successfully answer the critics received. The Editor-in-Chief is the final authority on all editorial decisions.

Open Access

This journal provides immediate open access to its content on the principle that making research freely available to the public supports a greater global exchange of knowledge.

After acceptance**Proof correction**

The corresponding author will receive proofs by e-mail in PDF format and will be requested to return it with any corrections within two weeks.

ISSN 1311-8773 (print)
ISSN 2535-0811 (online)

